



**ANAND**

INTERNATIONAL COLLEGE  
OF ENGINEERING

**CONFERENCE PROCEEDINGS**

Dr. Praveen Agarwal.

Dr. Ruzana Pskhu

Dr. Bhavana Mathur. - Editors

---

# Recent Developments in Engineering & Technology-II

**25-26 February, 2022**

**ISBN 978-81-953996-5-9**

## **Recent Developments in Engineering & Technology-II**

**Editor**

**Dr. Praveen Agarwal, Dr. Ruzana Pskhu and Dr. Bhavana Mathur**

## **Recent Developments in Engineering & Technology-II**

© Praveen Agarwal, Dr. Ruzana Pskhu and Dr. Bhavana Mathur

All rights reserved

No part of this publication may be reproduced, stored in a retrieval system or transmitted, in any form or by any means, without prior permission. The views and contents of this book are solely of the authors. Moreover, in the event, the authors have been unable to track any source and if any copyright has been inadvertently infringed, please notify the publisher in written for corrective action.

ISBN: 978-81-953996-5-9

Second Edition: March 2023

Price: 200 INR

Printed and Published by:

Anand International College of Engineering

Near Kanota, Agra Road, Jaipur

Rajasthan: 303012

## Preface

**(ICRDET) International Conference on Recent Developments in Engineering & Technology** is a vast canvas that primarily involves independent innovations in the arena of core engineering and technology. The conference intuitively provides excellent opportunities to the leading Researchers, Mathematicians, Engineers, Scientists and Students from all around the world to bring about high potentiality for the future. This edition is the 3rd (Hybrid) International Conference **(ICRDET-2022)** which was held at Anand International College of Engineering, Jaipur, INDIA is a generalization of engineering concepts that intends to increase research efforts and raise awareness of different problems in and around the society with public wellness solutions. The conference aims to promote quality research by focusing attention on the recent outstanding achievements, future trends and requirements.

For this edition the conference comprised of four technical sessions, some of them scheduled concurrently. The theme, Recent Developments in Engineering & Technology, was divided into two parallel sessions in order to accommodate the large number of presentations. Each theme started with a keynote lecture by an eminent personality in the domain. There are 23 invited speakers (10 International and 7 National) over the globe gave talks on topics of their expertise emphasizing emerging trends in high tech knowledge, featuring the diverse objectives in engineering by holding several session and exchanging views with various emerging information from the world and scope of technology.

This book is organized as follows. The **Chapter 1** “Application of Artificial Neural Network in Prediction of hardness value of Al 6063 reinforced with SiC” discussed about the development of Predictive Model for Metal Matrix Composite using Artificial Neural Network for prediction of hardness value of the developed Al6063 composite reinforced with silicon carbide by using stir casting machine. The results found that trained ANN Model is an efficient tool in predicting the hardness value of the developed composite.

In **Chapter 2** “Dynamical Transmission of SIR Model of COVID-19” created a mathematical model by incorporating a new recovery rate  $\mu$  into the already existing covid-19 SIR model of the human population. Mathematical analysis of the presented model is studied by using stability theory.

Further, in **Chapter 3** is a review focuses on various methods used for printing scaffolds like stereo lithography (SLA), selective laser sintering (SLS), fused deposition modeling (FDM), and binder jetting (BJ). This work also reviews various materials used for the fabrication of scaffolds for tissue engineering.

In **Chapter 4** “Neonatal Monitoring System: Review and Future Directions” focuses on existing biological parameters in incubator, analysis technique used for that, alarm system for attention in real time system and transmission technique for the same and discussed about the need of future, more health parameters that can be added and analyzed for better health prediction of an infant.

In **Chapter 5** “A Review of Applications of Biopolymeric Membranes in Removal of Organic Pollutant and Micro pollutants from Wastewater” discusses about paper consequences of using non-biodegradable membrane and benefits of using nanostructured biodegradable polymeric membranes. The study concluded that biopolymers like cellulose ought to be taken into account, for their complete biodegradability, abundance in nature, cost-effectiveness, and affordability. biopolymers are exceptional is that they are biocompatible, sustainable, nontoxic, and renewable.

In **Chapter 6** “Role of Nano science and nanotechnology in improving the efficiency of solar cell - graphene sheets in solar cell” discussed about advantages and application of graphene as new generation devices that will be lighter, eco- friendly and less expensive.

Further, **Chapter 7** “Fractional Integrals Using Generalized Bessel Function Associated with Generalized Fractional Calculus Operators” discussed Fractional integrals using generalized Bessel function associated with generalized Fractional calculus operators.

In **Chapter 8** “Analyzing Mathematical Models of Tumor Growth and their Applications” Mathematical equations were constructed using ordinary differential equations (ODEs), partial differential equations (PDEs), and discrete modeling features to model the tumor cell's growth rate by dividing the current population's negative logarithm by the carrying capacity.

In **Chapter 9** “Monitoring the co<sub>2</sub> level indoors and determining the need for ventilation” the study indicates that the environment, although naturally ventilated, is not adequately ventilated. Considering that this area is a classroom, this also reduces the learning capacity of students who use the environment. Further it is concluded that CO<sub>2</sub> levels cannot always be maintained at the desired levels for houses with natural ventilation.

In **Chapter 10** “Advancements and future prospects in castings: A comprehensive review of new trends & technologies” study discussed about future research should focus on developing advanced materials, optimizing casting processes, and expanding the capabilities of simulation techniques. By embracing these new trends, the casting industry can achieve enhanced performance, efficiency, and sustainability, driving advancements in various industrial sectors.

In **Chapter 11** “A Review on Recycling Plastic Waste into Sustainable, Valuable and Useful Products” the review article covers some of the options like recycling of plastic waste into diesel fuel, recycling plastic waste into yarn and fiber and also use of plastic waste material as sustainable resource in civil engineering.

In **Chapter 12** “Power Quality Improvement using Active Power Filter” discussed about a hybrid filter which is a combination of series active filter and shunt passive filter. This paper presents the control strategy to regulate the filter in such a way that the harmonics are reduced. The proposed control strategy is simulated in MATLAB SIMULINK.

Further, **Chapter 13**, “Renewable energy sources – a review” the paper discussed about study of different types of renewable sources of India and the possibilities of fulfillment of nations' energy requirement in coming future from different types of renewable sources.

In Chapter 14 “Study of Plasticizer on the Properties of Concrete” discussed about the slump test and compressive strength test. The results show that for the constant water cement ratio, increase of plasticizer dose in Concrete leads to gain of good workability. Moreover, there is also slightly increase in compressive strength than that of normal concrete mix.”

In Chapter 15 “Effects of Marble Slurry and Granite Dust in the Manufacturing of Concrete” discussed about the effect of Marble dust and Granite dust on the mechanical properties of concrete. The main parameter investigated was the cube compressive strength. In this research, M-25 grade concrete mix was prepared using IS method of mix design. Cubic specimens of dimension (150 x 150 x 150) mm were casted for compressive strength test.

In Chapter 16 “Design and Development of a Drone with Video Recording and Weight Lifting Function” paper explores the applications of quadcopters or drones in various scenarios, including search and rescue operations in remote areas, monitoring areas and boundaries, and aerial photography. The paper highlights the advantages of using drones in these contexts, such as their ability to provide a higher perspective for capturing landscapes and their potential for delivering assistance in emergency situations.

At Last, In Chapter 17, “Design and Simulation of C2N based Solar Cell using SCAPS 1D” the study discussed about the use of Scaps-1D simulation to examine the effects of various factors on the C2N-based solar cell. It is found that a large layer thickness of C2N, the ideal thickness of the window layer, and low ambient temperature were crucial to obtaining high-performance solar cells by adjusting the layer thickness and annealing the device at various temperatures.

## CONTENTS

<b>S.no</b>	<b>Title</b>	<b>Authors</b>	<b>Page. no</b>
1	Application of Artificial Neural Network in Prediction of hardness value of Al 6063 reinforced with SiC	<i>Prashant Kumar, Dheeraj Joshi, Bhavana Mathur</i>	1
2	Dynamical Transmission of SIR Model of COVID-19	<i>Attiq ul Rehman , Ram Singh</i>	8
3	Scaffolds for tissue engineering applications: A Review	<i>Venkata Durga Prasad Kadambari, Sanat Agrawal</i>	16
4	Neonatal Monitoring System: Review and Future Directions	<i>Prashant Jani, Dr. Seema Mahajan</i>	36
5	A Review of Applications of Biopolymeric Membranes in Removal of Organic Pollutant and Micro pollutants from Wastewater.	<i>Susmita Sharma, and Sanjana Chugh</i>	40
6	Role of nanoscience and nanotechnology in improving the efficiency of solar cell - graphene sheets in solar cell.	<i>Anil Dhawan ,N. Abarna</i>	48
7	Fractional integral using generalized bessel function associated with generalized fractional calculus operator.	<i>Prakash Singh, Shilpi Jain and Praveen Agarwal</i>	53
8	Analyzing mathematical model of tumor growth and their applications	<i>Aadil Rashid Sheergojri, Pervaiz Iqbal</i>	72
9	Monitoring the co2 level indoors and determining the need for ventilation	<i>Saban PUSAT, Muhammet İkbal TAYYAN</i>	80
10	Advancements and Future Prospects in Castings: A Comprehensive Review of New Trends and Technologies	<i>Prashant Kumar, Bhavana Mathur</i>	88
11	A Review on Recycling Plastic Waste into Sustainable, Valuable and Useful Products	<i>Sanjana Chugh and Susmita Sharma</i>	94
12	Power Quality Improvement using Active Power Filter	<i>Ajit, Seema Agarwal</i>	97
13	Renewable energy sources – a review	<i>ManMahendra Singh Daksh, Shubham Shahi, Vishal Yadav</i>	107
14	Effects of Marble Slurry and Granite Dust in the Manufacturing of Concrete	<i>Shahnawaz Ansari, Sunil R. Meena, Amit Kumawat</i>	114
15	Study Of Plasticizer on the Properties of Concrete	<i>Shiv Kumar S, Meharrudin Ahmad, Juber Khan</i>	119
16	Design And Development of a Drone With Video Recording and Weight Lifting Function	<i>Rohit Saini, Sonu Saini, Prashant Kumar, Bhavana Mathur</i>	124
17	Design and Simulation of C2N based Solar Cell using SCAPS 1D	<i>Vivek Bhojak, Lalit Kumar Lata, Praveen K Jain</i>	130

# Application of Artificial Neural Network in Prediction of hardness value of Al 6063 reinforced with SiC

Prashant Kumar, Dheeraj Joshi, Bhavana Mathur

**Abstract :** This work is based on development of Predictive Model for Metal Matrix Composite using Artificial Neural Network for prediction of hardness value of the developed Al6063 composite reinforced with silicon carbide by using stir casting machine. ANNs are numerical coding that imitates the working style of human brain. For prediction of the data the training of the network is done by using two sets of data called the training data and test data by using feed forward back propagation technique. The Design of experiments was done using Taguchi L 16 orthogonal arrays and 70% of the data was used as training data and 30% of the data was used as test data for checking the developed network. Reinforcement %, Stirring speed and stirring time were taken as the process parameters .The whole work is divided into two parts, in the first part the composite were obtained using L 27 orthogonal arrays and the hardness values of the sample were recorded .In the second part the training of the Artificial Neural Network was done using the training data and finally the network was tested using test data The Predicted value of the the network was compared with the experimental data. After comparing the results it can be said that a well trained ANN Model is an efficient tool in predicting the hardness value of the developed composite.

**Keywords-** Artificial Neural Network (ANN), Metal Matrix Composite (MMC), Stir Casting.

## 1. Introduction

The artificial neural networks concept is based on the working of the human brain. The artificial neural network is based on layers namely the input layer, hidden layer, and output layer [14].The data to be analyzed is taken as input. The input data is multiplied with weight in the input layers and processed in hidden layers by a mathematical function to get the output in the output layer. The ANN concept is popular due to its ability in analyzing small experimental data efficiently. A feed-forward back propagation artificial neural network with a Levenberg-Marquardt training algorithm was employed for the prediction of the Brinell hardness value of the prepared samples. The ANN model was developed with 10 hidden layers with four input parameters and single out. The whole data was divided into a training set and a testing set [1]. Before the prediction of the results, the ANN model was trained with a training set of 5000 epochs. The testing set was further divided into training, validation, and test set by the ANN model. After that, the regression plot is made for training, validation, and test samples. The overall correlation coefficient ( $R$ -value) for all samples was 0.99, which shows a very good correlation between experimental data and network response.

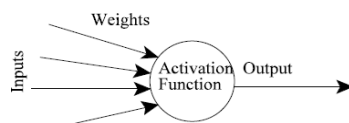


**Fig.1 Basic Working of ANN Model (1)**

Prashant Kumar

Department of Mechanical Engineering, Centre of Excellence in Material Engineering, Anand International College of Engineering, Agra road ,Jaipur)

e-mail: [prashant.kumar@anandice.ac.in](mailto:prashant.kumar@anandice.ac.in)

Research Scholar, Swami Keshvanand Institute of Technology, Management & Gramothan, Jaipur, India

e-mail: [h21001@skit.ac.in](mailto:h21001@skit.ac.in)

Dheeraj Joshi

Department of Mechanical Engineering , Swami Keshvanand Institute of Technology, Management & Gramothan, Jaipur, India

e-mail: [dheeraj.joshi@skit.ac.in](mailto:dheeraj.joshi@skit.ac.in)

BhavanaMathur

Department of Mechanical Engineering, Centre of Excellence in Material Engineering, Anand International College of Engineering, Agra road ,(Jaipur)

e-mail: [bhavana.mathur@anandice.ac.in](mailto:bhavana.mathur@anandice.ac.in)

**P. Agarwal et al. (eds.), Recent Developments in Engineering & Technology-II Feb 25-26, 2022, AICE, Jaipur, India**

## 2. Design of Experiment

For getting the training and test data the experiments were designed according to Taguchi's L-16 orthogonal arrays as shown in Table I. Four different process parameters were taken at four levels.

**Table 1.1 Stir casting parameters and their levels**

		LEVELS				
FACTORS		UNITS	1	2	3	4
Reinforcement wt %	grams	3	6	9	12	
Pouring temperature	Celsius	660	680	700	720	
Stirring time	min	5	10	15	20	
Stirring speed	RPM	200	300	400	500	

The wt % SiC was taken as 3, 6, 9, 12. The pouring temperature was taken 660, 680, 700, 720 ° Celsius. The stirring time was taken as 5, 10, 15, 20 in minutes and finally, the stirring speed was taken 200, 300, 400, 500 RPM. The design matrix is shown below in Table 1.2.

**Table 1.2 Design matrix based on Taguchi's L16 array design of experiment**

STIR CASTING PARAMETERS				
Samples	Reinforcement wt % (grams)	Pouring temperature ( Celsius)	Stirring time (min)	Stirring speed (RPM)
S(1)	3	660	5	200
S(2)	3	680	10	300
S(3)	3	700	15	400
S(4)	3	720	20	500
S(5)	6	660	10	400
S(6)	6	680	5	500
S(7)	6	700	20	200
S(8)	6	720	15	300
S(9)	9	660	15	500
S(10)	9	680	20	400
S(11)	9	700	5	300
S(12)	9	720	10	200
S(13)	12	660	20	300
S(14)	12	680	15	200
S(15)	12	700	10	500
S(16)	12	720	5	400

### 3. Preparation of Samples

The samples were prepared according to Taguchi's L-16 arrays using the stir casting process. The stir casting setup used in this study is a bottom pouring type stir casting machine. The die/mould is split type to obtain a cast of 50 mm OD × 300 mm long (standard).

### 4. Hardness Testing

The hardness testing of various samples was done on the Brinell hardness testing machine .The diameter of the indenter was taken as 10mm and the load applied for each sample was 500kgf with a dwell time of 15 seconds.Before performing the hardness test the specimens were clean and the surface was prepared by using emerypaper of different grades.

**Table 4.1 BHN of different samples**

<b>Stir Casting Parameters</b>					
Samples	Reinforcement wt % (grams)	Pouring Temperature ( Celsius)	Stirring Time (min)	Stirring Speed (RPM)	BHN
S(1)	3	660	5	200	66.26
S(2)	3	680	10	300	64.30
S(3)	3	700	15	400	66.80
S(4)	3	720	20	500	67.50
S(5)	6	660	10	400	68.10
S(6)	6	680	5	500	68.80
S(7)	6	700	20	200	69.40
S(8)	6	720	15	300	69.70
S(9)	9	660	15	500	71.60
S(10)	9	680	20	400	72.80
S(11)	9	700	5	300	72.30
S(12)	9	720	10	200	71.50
S(13)	12	660	20	300	75.50
S(14)	12	680	15	200	76.80
S(15)	12	700	10	500	78.20
S(16)	12	720	5	400	77.30

### 5. Training and Test Sets

Out of the 16 samples, a total of 10 samples were taken for training the network. For training the network the various combination of stir casting parameters as shown in Table 4.1 were taken as input for the network and the experimental hardness values for the 10 samples were taken as the target for the network. After creating the network the network was trained. Out of 16 samples, a total of 5 samples were selected for the test set. Once the network was trained it was tested for getting the predicted value. The training and test set input is shown in Table 5.1 and Table 5.2.

**Table 5.1 The experimental data used to form the Training set**

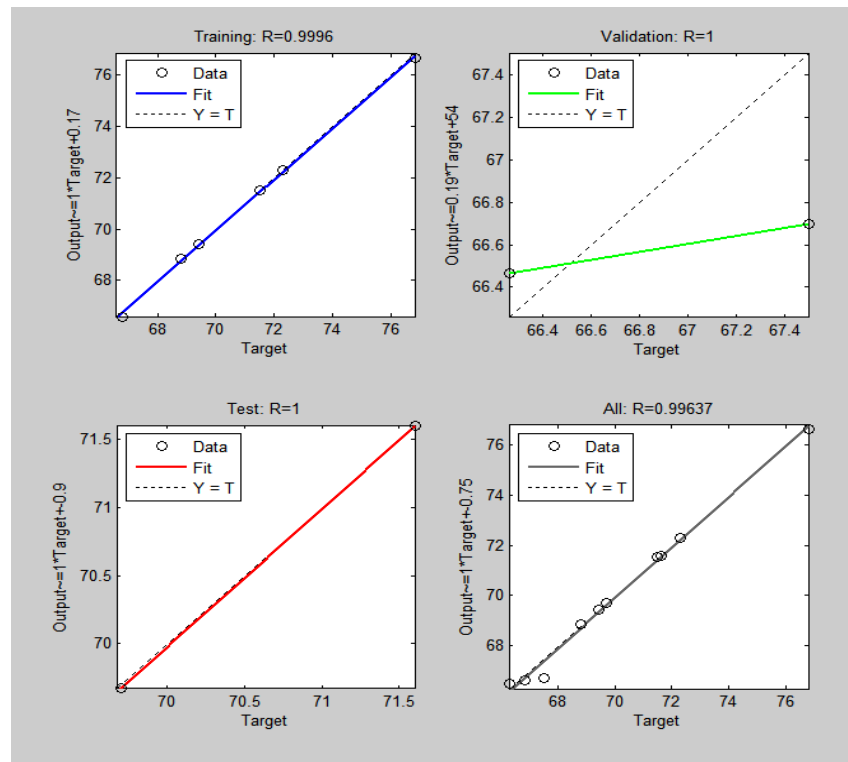
Training Set Input					Target
Samples.	Reinforcement wt % (grams)	Pouring temperature (°Celsius)	Stirring time (min)	Stirring speed (RPM)	BHN
S(1)	3	660	5	200	66.26
S(3)	3	700	15	400	66.80
S(4)	3	720	20	500	67.50
S(6)	6	680	5	500	68.80
S(7)	6	700	20	200	69.40
S(8)	6	720	15	300	69.70
S(9)	9	660	15	500	71.60
S(11)	9	700	5	300	72.30
S(12)	9	720	10	200	71.50
S(14)	12	680	15	200	76.80

**Table 5.2 The experimental data used to form Test Set**

Test Set Input				
Samples.	Reinforcement wt % (grams)	Pouring Temperature ( Celsius)	Stirring Time (min)	Stirring Speed (RPM)
S(2)	3	680	10	300
S(5)	6	660	10	400
S(10)	9	680	20	400
S(13)	12	660	20	300
S(15)	12	700	10	500

### 5.1 Regression Plot

The overall correlation coefficient ( $R$ -value) for all samples was 0.99, which shows a very good correlation between experimental data and network response as shown in fig 5.1.


**Fig.5.1 Regression Plots**

After getting the satisfactory performance and overall correlation coefficient value i.e R-value of 0.99 as shown in Fig.5.1 which a good relationship among the parameters. The ANN developed was applied to the test samples for prediction as shown in table 5.3.

**Table 5.3 ANN Prediction**

Neural Network Output for Training Set		
	Experimental data	Neural Network Prediction
<b>Samples.</b>	BHN	BHN
S(2)	64.30	64.50
S(5)	68.10	68.57
S(10)	72.80	72.14
S(13)	75.50	75.20
S(15)	78.20	78.16

## 6. Conclusions

The following conclusions can be made from the present study.

1. The Artificial Neural network developed was efficient in predicting the Hardness values of the test samples.
2. Finally, it can be concluded that a well-trained Neural Network is efficient in predicting the results.

## References

- [1] K. K. Alaneme and B. J. Bamike, —Characterization of mechanical and wear properties of aluminium based composites reinforced with quarry dust and silicon carbide,|| *Ain Shams Eng. J.*, vol. 9, no. 4, pp. 2815–2821, 2018, doi: 10.1016/j.asej.2017.10.009.
- [2] N. . Kumar, R. Saravanan, and R. Sellamuthu, -Effect of Marble Dust on Microstructure and Mechanical properties of Al-Cu-Ni / Marble Dust Particles Composites .,|| *Int. J. Pure Appl. Math.*, vol. 118, no. 24, pp. 1–12, 2018.
- [3] N. Lokesh, B. Manoj, K. Srikanth, P. V. Kumar, P. K. V. Ramanayya, and M. V. Rao, -Mechanical characterization of stir cast Al 6063 TiO<sub>2</sub>-Cu reinforced hybrid metal matrix composites,|| *Mater. Today Proc.*, vol. 5, no. 9, pp. 18383–18392, 2018, doi: 10.1016/j.matpr.2018.06.178.
- [4] E. Kozeschnik, *Advances in Materials Processing and Manufacturing Applications*. 2020.
- [5] S. Dhanesh, K. S. Kumar, N. K. M. Fayiz, L. Yohannan, and R. Sujith, —Recent developments in hybrid aluminium metal matrix composites: A review,|| *Mater. Today Proc.*, vol. 45, no. xxxx, pp. 1376–1381, 2021, doi: 10.1016/j.matpr.2020.06.325.
- [6] A. Nirala, S. Soren, N. Kumar, V. K. Dwivedi, and D. R. Kaushal, —A comprehensive review on stir cast Al-SiC composite,|| *Mater. Today Proc.*, vol. 21, no. xxxx, pp. 1610–1614, 2020, doi: 10.1016/j.matpr.2019.11.240.
- [7] P. Samal, P. R. Vundavilli, A. Meher, and M. M. Mahapatra, -Recent progress in aluminum metal matrix composites: A review on processing, mechanical and wear properties,|| *J. Manuf. Process.*, vol. 59, no. September, pp. 131–152, 2020, doi: 10.1016/j.jmapro.2020.09.010.
- [8] B. Suresh Babu *et al.*, —Studies on mechanical properties of aluminum based hybrid metal matrix composites,|| *Mater. Today Proc.*, vol. 33, no. xxxx, pp. 1144–1148, 2020, doi: 10.1016/j.matpr.2020.07.342.
- [9] K. Kaviyarasan, J. Pradheep Kumar, S. Karthik Anandh, M. Sivavishnu, and S. Gokul, —Comparison of mechanical properties of Al6063 alloy with ceramic particles,|| *Mater. Today Proc.*, vol. 22, pp. 3067–3074, 2019, doi: 10.1016/j.matpr.2020.03.442.
- [10] S. Madhankumar, R. Balamurugan, S. Rajesh, and K. M. Senthilkumar, —Fabrication of Al6063 alloy, silicon carbide and boron glass powder metal matrix composites in stir casting process and analysis the impact of process variables on mechanical properties,|| *Mater. Today Proc.*, vol. 42, no. xxxx, pp. 529–535, 2020, doi: 10.1016/j.matpr.2020.10.483.
- [11] P. Chakrapani and T. S. A. Suryakumari, -Mechanical properties of aluminium metal matrix composites-A review,|| *Mater. Today Proc.*, vol. 45, no. xxxx, pp. 5960–5964, 2020, doi: 10.1016/j.matpr.2020.09.247.
- [12] P. O. Babalola, C. A. Bolu, A. O. Inegbenebor, and O. Kilanko, -Graphical Representations of Experimental and ANN Predicted Data for Mechanical and Electrical Properties of AlSiC Composite Prepared by Stir Casting Method,|| *IOP Conf. Ser. Mater. Sci. Eng.*, vol. 413, no. 1, 2018, doi: 10.1088/1757-899X/413/1/012063.
- [13] P. Sathyabalan and R. Srimath, —A neural network model for the compressive strength of a hybrid LM6 aluminium alloy composite,|| *Int. J. Recent Technol. Eng.*, vol. 8, no. 2 Special Issue 8, pp. 1652–1654, 2019, doi: 10.35940/ijrte.B1123.0882S819.
- [14] P. Babalola, C. Bolu, and A. Inegbenebor, —Artificial Neural Network Prediction of Aluminium Metal Matrix Composite with Silicon Carbide Particles Developed Using Stir Casting Method,|| *Int. J. Mech. Mechatronics Eng. IJMME-IJENS*, vol. 15, no. 6, pp. 151–158, 2015.
- [15] A. M. Hassan, A. Alrashdan, M. T. Hayajneh, and A. T. Mayyas, -Prediction of density, porosity and hardness in aluminum-copper-based composite materials using artificial neural network,|| *J. Mater. Process. Technol.*, vol. 209, no. 2, pp. 894–899, 2009, doi: 10.1016/j.jmatprotec.2008.02.066.
- [16] S. Poria, P. Sahoo, and G. Sutradhar, -Tribological Characterization of Stir-cast Aluminium-TiB<sub>2</sub> Metal Matrix Composites,|| *Silicon*, vol. 8, no. 4, pp. 591–599, 2016, doi: 10.1007/s12633-016-9437-5.
- [17] K. Trinath, R. Aepuru, A. Biswas, M. Ramalinga Viswanathan, and R. Manu, -Study of self lubrication property of Al/SiC/Graphite hybrid composite during Machining by using artificial neural networks (ANN),|| *Mater. Today Proc.*, vol. 44, pp. 3881–3887, 2021, doi: 10.1016/j.matpr.2020.12.927.
- [18] N. Altinkok and R. Koker, —Use of artificial neural network for prediction of physical properties and tensile strengths in particle reinforced aluminum matrix composites,|| *J. Mater. Sci.*, vol. 40, no. 7, pp. 1767–1770, 2005, doi: 10.1007/s10853-005-0689-5.

## **Application of Artificial Neural Network in Prediction of hardness value of Al 6063 reinforced with SiC**

- [19] N. R. J. Hynes, R. Sankaranarayanan, R. Tharmaraj, C. I. Pruncu, and D. Dispinar, —A comparative study of the mechanical and tribological behaviours of different aluminium matrix–ceramic composites,|| *J. Brazilian Soc. Mech. Sci. Eng.*, vol. 41, no. 8, pp. 1–12, 2019, doi: 10.1007/s40430-019-1831-7.
- [20] R. Koker, N. Altinkok, and A. Demir, -Neural network based prediction of mechanical properties of particulate reinforced metal matrix composites using various training algorithms,|| *Mater. Des.*, vol. 28, no. 2, pp. 616–627, 2007, doi: 10.1016/j.matdes.2005.07.021.
- [21] N. Altinkok, -Use of artificial neural network for prediction of mechanical properties of  $\alpha$ -Al<sub>2</sub>O<sub>3</sub> particulate-reinforced al-si10mg alloy composites prepared by using stir casting process,|| *J. Compos. Mater.*, vol. 40, no. 9, pp. 779–796, 2006, doi: 10.1177/0021998305055547.
- [22] R. Kumar and V. Kumar, —Optimization of process parameter for stir casted AA6063 metal matrix composite on hardness, tensile strength and impact energy,|| *Int. J. Mech. Eng. Technol.*, vol. 8, no. 12, pp. 108–117, 2017.
- [23] S. K. Mishra, A. Brahma, and K. Dutta, -Prediction of mechanical properties of Al-Si-Mg alloy using artificial neural network,|| *Sadhana - Acad. Proc. Eng. Sci.*, vol. 46, no. 3, 2021, doi: 10.1007/s12046-021-01660-x.
- [24] P. D. Srivyas and M. S. Charoo, -Role of Reinforcements on the Mechanical and Tribological Behavior of Aluminum Metal Matrix Composites - A Review,|| *Mater. Today Proc.*, vol. 5, no. 9, pp. 20041–20053, 2018, doi: 10.1016/j.matpr.2018.06.371.
- [25] N. Kaushik and S. Singhal, -Hybrid combination of Taguchi-GRA-PCA for optimization of wear behavior in AA6063/SiCp matrix composite,|| *Prod. Manuf. Res.*, vol. 6, no. 1, pp. 171–189, 2018, doi: 10.1080/21693277.2018.1479666.
- [26] M. O. Bodunrin, K. K. Alaneme, and L. H. Chown, —Aluminium matrix hybrid composites: A review of reinforcement philosophies; Mechanical, corrosion and tribological characteristics,|| *J. Mater. Res. Technol.*, vol. 4, no. 4, pp. 434–445, 2015, doi: 10.1016/j.jmrt.2015.05.003.

# Dynamical Transmission of SIR Model of COVID-19

Attiq ul Rehman , Ram Singh

**Abstract** The four new variants of severe acute respiratory syndrome coronavirus 2 (SARS-CoV-2) have been seen in different nations around the world. These four variants are thought to affect more people than the current covid-19 pandemic. The mathematical model is created by incorporating a new recovery rate  $\mu$  into the already existing covid-19 SIR model of the human population. Mathematical analysis of the presented model is studied by using stability theory. The numerical analysis is carried out by the Runge-Kutta fourth-order method (RK4). Furthermore, the sensitivity analysis is also discussed. The numerical simulation is performed by using MATLAB software. The paper ends with some discussion and a conclusion.

**Keywords:** - Covid-19, Basic Reproduction Number, Stability Analysis, RK4, Sensitivity.

## 1 Introduction

The covid-19 illness is brought out by a SARS-CoV-2 that constitutes a subsidiary narrator of a positive deadly illness and a considerable global health problem. It is a disease that scatters quickly due to its easily accessible transmission pathways, which include respiratory droplets breathed during sneezing, talking, or coughing. The covid-19 disease, which began in the Chinese city of Wuhan, has quickly spread to other countries, with several cases written down around the world. This deadly pandemic started in India in Jan. 2020 and lasted until the 8th of Oct., 2021. There have been at least 33,915,569 confirmed cases with 4,50,127 deaths, reported by the World Health Organization (WHO) [33]. This deadly infection is part of a family that can give rise to diseases, including SARS and the common cold. MERS is a disease, that can give rise to lung damage if left untreated [10,24].

Some people may have only a few symptoms, while others may have none at all. Infected people often experience fevers, coughs, and exhaustion. However, such people may have a loss of flavour or even scent. People who have been infected with the coronavirus may have symptoms 2-14 days after submission. The incubation break is the time between the onset of symptoms and uncovering [31, 35]. When an infected person sneezes, sings, breathes, coughs, or talks, the deadly virus scatters into cold respiratory droplets. These respiratory droplets can land or inhale into someone else's nose, eyes, or mouth. This virus can scatter when a human being is exposed to minor aerosols or droplets that linger in the surrounding for many seconds or minutes, a process known as airborne transmission.

They discovered that weather conditions play a big role in affecting the recurrence charge of covid-19 in India. Theirs offered a preparatory product that the covid-19 epidemic in India could be largely inhibited by increases in temperature and humidity. In Mumbai, India, linkage analysis of climatic parameters with the covid-19 pandemic has been presented [7]. They discovered that the pressure and relative humidity factors have the greatest influence on the active number of covid-19 cases, out of all other relevant things, as determined by the Spearman technique. From 10th of Mar. 2020 to 25th of Aug. 2020, the impact of climatic variables like humidity, temperature, and rainfall on complete covid-19 covering in Pakistan, its administrative units, and provinces have been studied [2]. Covid-19 temperature and instances are positively connected, according to the study of correlation analysis. For the research of covid-19 dynamical scattering processes in mainland China, a mathematical model using a memory-based method has been built [16]. They examined the effectiveness of various estimated model parameters and control estimates using real biological reported data from the National Health Commission (NHC) of the People Republic of China from the 10th of Jan. to the 17th of Feb. 2020.

A compartmental model to represent the development of dangerous illness in a host population, with a focus on coronavirus disease propagation, has been performed [21].

Attiq ul Rehman

Department of Mathematical Sciences, BGSB University, Rajouri, 185234, J&K, India

Email: - attiqrehman24@gmail.com

Ram Singh

Department of Mathematical Sciences, BGSB University, Rajouri, 185234, J&K, India

Email:-drramsinghm@gmail.com

The eye explore the model both analytically and numerically. The SEIR model with a non-linear incidence rate explains covid-19 dynamics within [8]. They looked and used bifurcation analysis to look at the influence of different basic reproduction numbers  $R_0$  on covid-19 dynamical transmission in their research. To understand epidemiological mathematical modelling of infectious diseases, archetypes of diseases are highly fruitful. It aids in the execution of important public health estimates by limiting the scatter of illness. The global impact of the covid-19 pandemic in India in terms of its scattered circumstances has been depicted within [20]. Mathematical modelling of covid-19 transmissions aids commitments about the allotment, epidemic conspiring, and execution of interventions and social distancing estimates by partners and counties responding to the aforementioned epidemic by informing commitments about epidemic conspiring, allotment, execution of interventions, and social distance estimates [11]. Several research have been given to predict the upcoming consequences of covid-19 epidemics around the world [3{6, 13, 14, 17, 22, 25, 32, 34]. A dynamical transmission mathematical model of covid-19 in New York to evaluate the impact of the scattering order on covid-19 infections and deaths [18]. They stressed the need of establishing mask rules in urban communities as quickly as to prevent the reduced mortality and covid-19 scatter in their study. In India, covid-19 reliance on environmental factors and scatter forecasts have been investigated [9]. In their research, the impact of environmental parameters such as relative humidity and temperature on the product of covid-19 chances every day is investigated using statistical approaches such as response surface methodology and Pearson correlation. Even though many researchers have presented studies to build more viable and accurate models for covid-19 disease control and prevention [19, 27]. The paper is arranged as follows. The mathematical model formulation is described in section 2. The analysis in which existence and uniqueness, positivity and boundedness, as well as equilibria and stability are discussed in section 3. The numerical algorithm of RK4 is created in section 4. Sensitivity analysis is performed in section 5. Numerical simulations and discussions are provided in section 6. Finally, the conclusion is drawn in section 7.

## 2 Mathematical Model Formulation

There are many types of rates in different possible classes that are used in mathematical models within epidemiology. The mathematical epidemic models divide any kind of population in this universe into different groups. The classes of epidemiology can be defined over a minimum time by the possible illness states that one can overcome these within a fixed time. These are the main points of epidemiology and have provided a straightforward idea for creating mathematical models. To make a model for the dynamics of the covid-19 pandemic, we have devoted a fresh predetermined mathematical model by taking some ideas from different research papers.

In the proposed pandemic model, we have contained three epidemiological classes of human population namely susceptible  $S(t)$ , infected  $I(t)$ , and recovered class  $R(t)$  with the passage of time  $t$ . In these three aforementioned classes, we have taken different positions in order to mitigate this ongoing havoc pandemic. Therefore, the total covid-19 affected human population around the world is denoted by  $Z(t)$ , and is disposed of by

$$Z(t) = S(t) + I(t) + R(t).$$

So, to explain the dynamical transmission process, the host population is interacting and mixing homogeneously. Moreover, the infection is scattered in the human group due to the interaction of infectious agents and a susceptible host. The state variables and their biological meaning of covid-19 diseases are demonstrated in table 1. Hence, the dynamical transmission mathematical model describes different host population classes in the below ordinary differential equations (ODEs):

$$\begin{aligned} \frac{dS(t)}{dt} &= \Lambda - aS(t)I(t) - d_1 S(t), \\ \frac{dI(t)}{dt} &= aS(t)I(t) - (b + \mu + d_2)I(t), \\ \frac{dR(t)}{dt} &= bI(t) - d_3 R(t), \end{aligned} \tag{2.1}$$

with the positive initial conditions,  $S(0) = S_0 \geq 0$ ,  $I(0) = I_0 \geq 0$  and  $R(0) = R_0 \geq 0$ . The new upcoming rate for the susceptible host population is denoted by  $\Lambda$ . The susceptible human population becomes infected, with the essential contact with infectious humans at the rate  $a$ .  $d_1$  is the natural mortality rate in the case of the susceptible human population,  $d_2$  is the natural death rate in the case of the infectious human population, and likewise  $d_3$  is the natural mortality rate in case of recover human population. All these three aforementioned death rates are going out of their class. In the infectious class, the recovery rate  $b$  is implemented into it and going forward into recovered class  $R(t)$ . Also, we have considered a covid-19 induced death rate in the susceptible host by the rate  $\mu$ . The parametric values of different constants are demonstrated in table 2 with some exact and estimated quantities. The movement among the three compartments is depicted in figure 1.

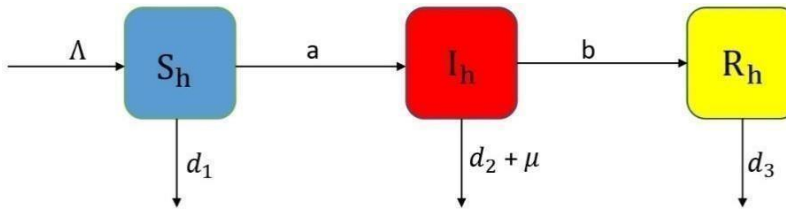


Figure 1: Rate transformational diagram of SIR covid-19 epidemic model.

State Variables	Biological Meaning
$S(t)$	Collection of susceptible hosts
$I(t)$	Collection of infected hosts
$R(t)$	Collection of recovered hosts

Table 1: Biological meaning of the dynamical system (2.1).

Parameter	Meaning	Values	Source
$a$	Transmission rate	0.5	[12]
$b$	Recovery rate	0.11	[12]
$\mu$	Covid-19 induced mortality rate	0.1	Assumed
$d_1$	Susceptible host natural mortality rate	0.6	[12]
$d_2$	Infectious host natural death rate	0.3	Assumed
$d_3$	Recovered host natural death rate	0.2	Assumed

Table 2: The parametric values of the dynamical model (2.1).

### 3 The Analysis

The mathematical analysis of the model is the technical representation of the system. It acts as a relationship between the system and the design model. In the analysis, the behaviour, information, and mappings of the system are translated and defined into the component, architecture, and interface level in the design modeling.

#### Equilibria and Stability

For the evaluation of stability of the model through stability theory, the possible equilibrium points play a key role.

#### Disease Free Equilibrium (DFE)

For the evaluation of equilibrium points, we have set all three classes of SIR model equal to zero. The DFE points are those in which the disease is eliminated from the system totally. The formulation of the DFE is as given below.

$$E_0 = (S_0, I_0, R_0) = \left( \frac{\Lambda}{d_1}, 0, 0 \right).$$

#### Endemic Equilibrium (EE)

The endemic equilibrium points are the points where the disease is still present in the system for the cause of havoc among human beings. These points are proceeded with as follows:

$$E^* = (S^*, I^*, R^*) = \left( \frac{b + \mu + d_2}{a}, \frac{a\Lambda - d_1(b + \mu + d_2)}{a(b + \mu + d)}, \frac{(a\Lambda - d_1(b + \mu + d_2))}{d(b + \mu + d)} \right).$$

#### Basic Reproduction Number

The basic reproduction number  $R_0$  for the SIR covid-19 model is evaluated by using the Next Generation Technique [28]. It is biologically very essential for determining the concentration of infection. Thus, the  $R_0$  is the spectral radius, hence we have

$$R_0 = \sqrt{\frac{a\Lambda}{d_1(b + \mu + d_2)}}.$$

#### 4 Numerical Algorithm

The Runge-Kutta method was found by two well-known German mathematicians, CarlRunge and Wilhelm Kutta. The idea beyond this aforesaid numerical method is to examinealmost Taylor. However, due to derivative calculations, the explanation of gross domesticproduct by Taylor isn't applicable in practical [30]. The RK4 method is the most accurateas compared to the other three RK methods. Thus, the aforementioned numerical methodis often utilized to explain an ODE. The RK4 method has been procced as follows.

$$m_{n+1} = m_n + \frac{1}{6}(j_1 + 2j_2 + 2j_3 + j_4) \quad (4.1)$$

in which

$$\begin{aligned} j_1 &= (p_n, m_n) \\ j_2 &= f(p_n + \frac{1}{2}j_1, m_n + \frac{1}{2}j_1) \\ j_3 &= f(p_n + \frac{1}{2}j_2, m_n + \frac{1}{2}j_2) \\ j_4 &= (p_n + j_3, m_n + j_3). \end{aligned}$$

$$\frac{dS}{dt}(t) = f(t, S(t), I(t), R(t)) = \Lambda - aS(t) - dS(t), \quad (4.2)$$

$$\frac{dI}{dt}(t) = f(t, S(t), I(t), R(t)) = aS(t) - (b + \mu + )t, \quad (4.3)$$

$$\frac{dR}{dt}(t) = f(t, S(t), I(t), R(t)) = bI(t) - dR(t), \quad (4.4)$$

The equation (4.2) - (4.4) is solved using the RK4 method based on (4.1) bysubstitution,so we get

$$S_{(n+1)} = S_n + \frac{1}{6}(j_1 + 2j_2 + 2j_3 + j_4) \quad (4.5)$$

$$I_{(n+1)} = I_n + \frac{1}{6}(k_1 + 2k_2 + 2k_3 + k_4) \quad (4.6)$$

$$R_{(n+1)} = R_n + \frac{1}{6}(l_1 + 2l_2 + 2l_3 + l_4) \quad (4.7)$$

Equation (4.5) - (4.7) is a numerical solution of the proposed mathematical model on thebehaviour of three aforesaid human body cells.

## 5 Sensitivity Analysis

The sensitivity analysis produces how different values of an independent variable effect on a specific dependent variable under a proposed collection of suppositions. The influential lbiological parameters have been identifying and optimizing model behaviour. In the model(2.1), due to without assumptions associated with the forecasting of some biological parametric values, it is powerful to implement the analysis to find the system's animation as changes. With the analytic expression for  $R_0$ , it is reasonable to apply the normalized sensitivity index of the basic reproduction number, that fully depends on three rates  $a, b$ , and  $\mu$ .

$$\frac{\partial R_0}{\partial a} = \frac{1}{2\sqrt{R_0}} \times \frac{a\Lambda}{d_1(b + \mu + d_2)} \quad (5.1)$$

$$\frac{\partial R_0}{\partial b} = -\frac{1}{2\sqrt{R_0}} \times \frac{a\Lambda}{d_1(b + \mu + )^2} \quad (5.2)$$

$$\frac{\partial R_0}{\partial \mu} = -\frac{1}{2\sqrt{R_0}} \times \frac{a\Lambda}{d_1(b + \mu + d_2)^2} \quad (5.3)$$

$$E_a = \frac{a}{2\sqrt{R_0}} \times \frac{a\Lambda}{d_1(b + \mu + d_2)} \quad (5.4)$$

$$E_b = -\frac{1}{2\sqrt{R_0}} \times \frac{a\Lambda}{d_1(b + \mu + )^2} \quad (5.5)$$

$$E_\mu = -\frac{1}{2\sqrt{R_0}} \times \frac{a\Lambda}{d_1(b + \mu + d_2)^2} \quad (5.6)$$

where  $a, b$ , and  $\mu$  are three biological parameters whose sensitivity analysis on basic reproduction number is sought. This sensitivity index gives the upper value in their size, themore sensitive to the parameter. The positivity and negativity signs demonstrate that the  $R_0$  increases or decreases as  $b$ , and  $\mu$ , increases.

## 6 Numerical Simulations and Discussion

In this section, the RK4 is utilized to present the analytic results and to find numerical valuesfor a collection of systems with the help of suitable biological parameters by the MATLABsoftware. The values are given in table 2 along with the initial value. The numerical sciencesare demonstrated graphically in figures 2 to 6.

In figure 2, the Contrast of susceptible host rate with time is shown for different values of covid-19 transmission rate that is  $a = 0.5, 0.7, 0.9$ . It is seen that the population of susceptible host ( $S(t)$ ) mitigates exponentially with the passage of time  $t$  as the values of  $a$  increase. This fact is real in the human population. Figure 3 depicts the Contrast of infected host ( $I(t)$ ) with the passage of time  $t$  for different values of  $b = 0.11, 0.22, 0.33$ . It is understandable from the figure that as we decrease the values of  $b$ , the graphs of infected host also decrease. It means that the recovery rate of  $b$  has generally true with ( $I(t)$ ).

In figure 4, the Contrast of ( $I(t)$ ) with time  $t$  for various values of  $a$  is shown. It is observed that with the increase in the transmission rate  $a$ , the infected host population continuously increases. Figure 5 demonstrates the Contrast of recovered human ( $R(t)$ ) with time  $t$  for the various values of recovery rate  $b$ . It is seen that the recovery rate  $b$  has a good impact on the recovered human population as we increase the values of  $b$ , the population of recovered host ( $R(t)$ ) also increases.

Figure 6 demonstrates the effects of covid-19 induced death rate  $\mu$  on the infected human population ( $I(t)$ ). It is noticed that  $\mu$  has reciprocal effects on ( $I(t)$ ). The graph of infected humans significantly affected by covid-19 induced death rate  $\mu$ . The infected human population first increases initially at  $t = 30$ , but it exponentially decreases afterward.

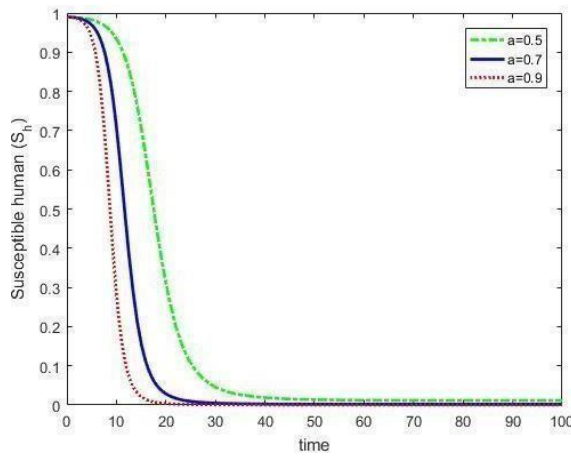


Figure 2: Contrast of  $S(t)$  against  $t$  for  $a = 0.5, 0.7, 0.9$ .

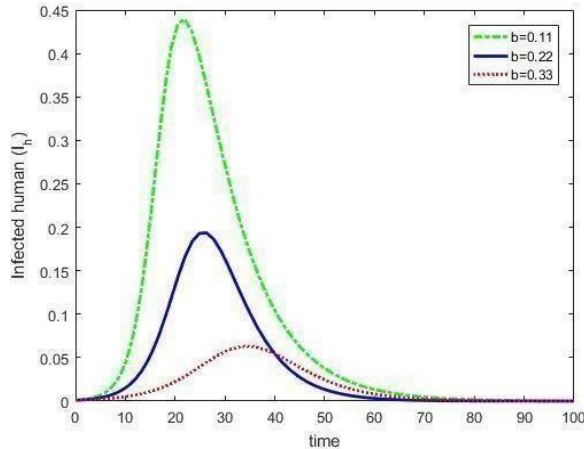
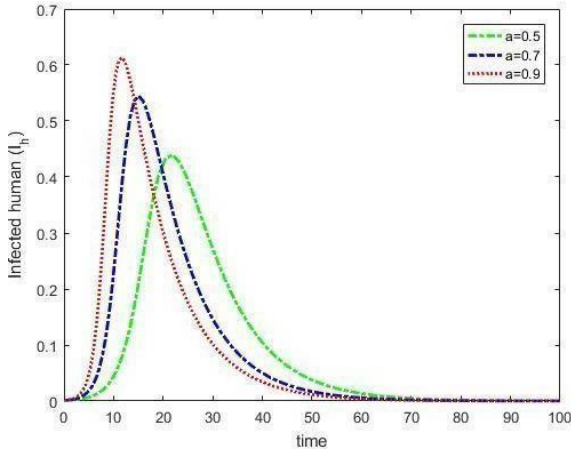
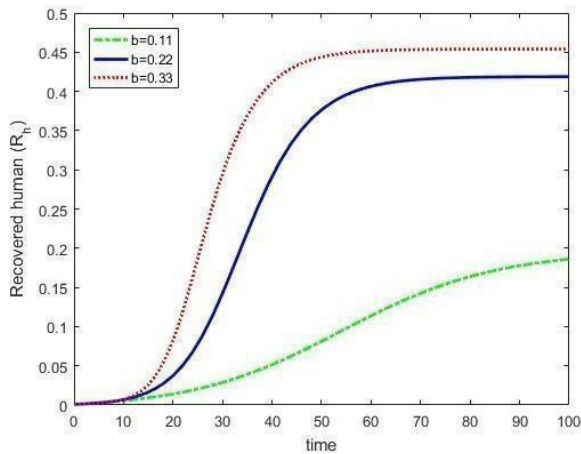
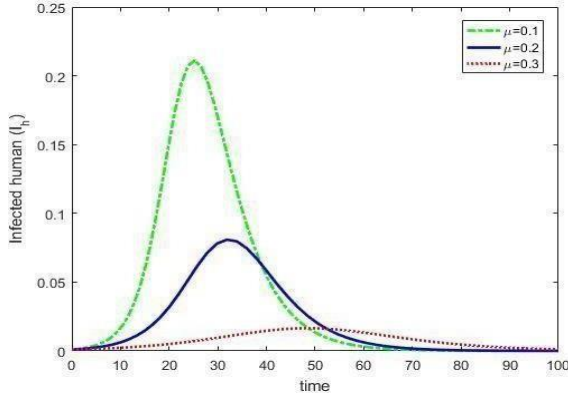


Figure 3: Contrast of  $I(t)$  against  $t$  for  $b = 0.11, 0.22, 0.33$ .

Figure 4: Contrast of  $I(t)$  against  $t$  for  $a = 0.5, 0.7, 0.9$ .Figure 5: Contrast of  $R(t)$  against  $t$  for  $b = 0.11, 0.22, 0.33$ .Figure 6: Contrast of  $I(t)$  against  $t$  for  $a\mu = 0.1, 0.2, 0.3$ .

## 7 Conclusion

Covid-19 is an infectious illness that causes havoc around the world, and its dynamic transmission is a mystery. We considered the dynamics of covid-19 infection mathematically in this investigation. We computed  $R_0$  and discussed stability with some theorems. Figures show the effect of various transmission rates graphically. In the numerical simulation, RK4 is found to have even better outcomes in terms of its solutions. Finally, we conclude that the DFE point is LAS when  $R_0 < 1$ , and unstable if  $R_0 > 1$ . Similarly, the DFE point is GAS when  $R_0 < 1$ , and unstable if  $R_0 > 1$ . Also, the EE point is LAS when  $R_0 > 1$ , and unstable if  $R_0 < 1$ . Likewise, the EE point is GAS when  $R_0 < 1$ , and unstable if  $R_0 > 1$ . Local is checked through the Routh-Hurwitz criteria, and globality is checked through Lyapunov. The upcoming study will incorporate the minimization of medical treatment for covid-19, which has an estimation.

## References

- [1] A. Elazzouzi, A. L. Alaoui, M. Tilioua, et al., Analysis of a SIRI epidemic model with distributed delay and relapse. *Stat Optim Inform Comput* 2019;7(3):1-12.
- [2] A. Raza, M. T. I. Khan, Q. Ali, et al., Association between meteorological indicators and COVID-19 pandemic in Pakistan. *Environ Sci Pollut Res* 2020.
- [3] C. Yang, J. Wang, A mathematical model for the novel coronavirus epidemic in Wuhan, China. *Math. Bio. sci. Eng.* 2020;17(3):2708-24.
- [4] D. Adam, Special report: the simulations driving the world's response to COVID-19. *Nature* 2020;580(7803):316-8.
- [5] D. Pal, D. Ghosh, P. K. Santra, et al., Mathematical analysis of a COVID-19 epidemic model by using data-driven epidemiological parameters of diseases spread in India, <http://dx.doi.org/10.1101/2020.04.25.20079111>.
- [6] F. Ndairou, I. Area, J. J. Nieto, et al., Mathematical modeling of COVID-19 transmission dynamics with a case study of Wuhan. *Chaos Solitons Fractals*. 135(2020) 109846.
- [7] G. Kumar, R. R. Kumar, A correlation study between meteorological parameters and COVID-19 pandemic in Mumbai, India. *Diabetes Metab Syndr: Clin Res Rev* 2020;14(6):1735-42.
- [8] G. Rohith, K. B. Devika, Dynamics and control of COVID-19 pandemic with nonlinear incidence rates. *Nonlinear Dynam* 2020;101:2013-26.
- [9] H. Bherwani, A. Gupta, S. Anjum, et al., Exploring dependence of COVID-19 on environmental factors and spread prediction in India. *Npj Clim Atmos Sci* 2020;3:38.
- [10] <https://mayoclinic.org/diseases/conditions/coronavirus/symptoms-causes/syc/0479963>.
- [11] <https://www.cdc.gov/coronavirus/2019-ncov/covid-data/mathematical-modeling.html>.
- [12] I. Cooper, A. Mondal, C. G. Antonopoulos, A SIR model assumption for the spread of COVID-19 in different communities. *Chaos, Solitons and Fractals*. 139(2020) 110057.
- [13] J. E. Amaro, J. Dudouet, J. N. Orce, Global analysis of the COVID-19 pandemic using simple epidemiological models. *Appl Math Model* 2021;90:995-1008.
- [14] J. K. K. Asamoah, M. A. Owusu, Z. Jin, et al., Global stability and cost-effectiveness analysis of COVID-19 considering the impact of the environment: using data from Ghana. *Chaos Solitons and Fractals*. 140(2020) 110103.
- [15] J. P. LaSalle, The stability of dynamical systems. CBMS-NSF regional conference series in applied mathematics, vol. 25, Philadelphia: SIAM; 1976.
- [16] J. Zu, M. L. Li, Z. F. Li, et al., Transmission patterns of COVID-19 in the mainland of China and the efficacy of different control strategies: a data-and model-driven study. *Infect Dis Poverty* 2020;9:83.
- [17] K. Sarkar, S. Khajanchi, J. J. Nieto, Modeling and forecasting the COVID-19 pandemic in India. *Chaos Solitons and Fractals*. 139(2020) 110049.
- [18] M. Shen, J. Zu, C. K. Fairley, et al., Effects of New York's executive order on facemask use on COVID-19 infections and mortality: A modeling study. *J Urban Health* 2021;98(2021):197-204.
- [19] M. Shen, J. Zu, C. K. Fairley, et al., Projected COVID-19 epidemic in the United States in the context of the effectiveness of a potential vaccine and implications for social distancing and face mask use. *Vaccine* 2021;39(16):2295-302.
- [20] M. J. Borah, B. Hazarika, S. K. Panda, et al., Examining the correlation between the weather conditions and COVID-19 pandemic in India: A mathematical evidence. *Results Phys* 2020;19:103587.
- [21] M. Rafiq, J. E. Macias-Diaz, A. Raza, N. Ahmed, Design of a nonlinear model for the propagation of COVID-19 and its efficient nonstandard computational implementation. *Appl Math Model* 2021;89:1835-46.
- [22] N. P. Jewell, J. A. Lewnard, B. L. Jewell, Predictive mathematical models of the COVID-19 pandemic: underlying principles and value of projections. *JAMA* 2020;323(19):1893-4.
- [23] O. Diekmann, J. A. P. Heesterbeek, M. G. Roberts, The construction of next generation matrices for compartmental epidemic models. *J Roy Soc Inter* 2010;7(47):873-85.
- [24] P. A. Naik, M. Yavuz, S. Qureshi, et al., Modeling and analysis of COVID-19 epidemics with treatment in fractional derivatives using real data from Pakistan. *Eur. Phys. J. Plus* 2020; 135:795.
- [25] P. Samui, J. Mondal, S. Khajanchi, A mathematical model for COVID-19 transmission dynamics with a case study of India. *Chaos Solitons and Fractals*. 140(2020) 110173.
- [26] P. A. Naik, J. Zu, K. M. Owolabi, Modeling the mechanics of viral kinetics under immune control during primary infection of HIV-1 with treatment in fractional order. *Physica A* 2020;545:123816.
- [27] P. A. Naik, J. Zu, M. Ghoreishi, Stability analysis and approximate solution of SIR epidemic model with Crowley-Martin type functional response and Holling type-II treatment rate by using homotopy analysis method. *J Appl Anal Comput* 2020;10(4):1482-515.
- [28] P. V. Driessche, and J. Watmough, Reproduction numbers and sub-threshold endemic equilibria for compartmental models of disease transmission, *Math. Biosci.*, 2002, 180:29-48.

- [29] S. O. Sowole, A. Ibrahim, D. Sangare, et al., Mathematical model for measles disease with control on the susceptible and exposed compartments. *Open J. Math. Anal.* 2020,4(1), 60-75.
- [30] S. Side, A. M. Utami, Sukarana, et al., Numerical solution of SIR model for transmission of tuberculosis by Runge-Kutta method. *IOP Conf. Series: Journal of Physics: Conf. Series* 1040(2018) 0112021.
- [31] S. A. Lauer, K. H. Grantz, Q. Bi, et al., The incubation period of coronavirus disease2019 (Covid-19) from publicly reported confirmed cases: estimation and application. *Ann.Intern. Med.* 2020; 172:577-82.
- [32] S. S. Nadim, J. Chattopadhyay, Occurrence of backward bifurcation and prediction of disease transmission with imperfect lockdown: a case study on COVID-19. *Chaos Solitons and Fractals.* 140(2020) 110163.
- [33] WHO, Coronavirus disease(covid-19); data as received by WHO from national authorities. 13 october 2021.
- [34] X. Rong, L. Yang, H. Chu, et al., Effect of delay in diagnosis on transmission of COVID-19. *Math Biosci Eng* 2020;17(3):2725-40.
- [35] Y. Deng, C. You, Y. Liu, et al., Estimation of incubation period and generation time based on observed length-biased epidemic cohort with censoring for COVID-19 outbreak in China. *Biometrics* 2020. <http://dx.doi.org/10.1111/biom.13325>.
- [36] Z. Shuai, V. P. Driessche, Global stability of infectious disease models using Lyapunov functions. *SIAM J Appl Math* 2013;73(4):1513-32.

# Scaffolds for tissue engineering applications: A Review

Venkata Durga Prasad Kadambari, Sanat Agrawal

**Abstract**—Additive manufacturing (AM) is widely used to produce intrinsic 3D structures with high accuracy. The use of additive manufacturing technique has increased significantly in tissue engineering (TE) over the years. TE is used to repair and regenerate impaired tissues caused by trauma, disease, and injury by fabricating scaffolds. Various materials like polymers, ceramics, and composites provide immense potential for producing scaffolds. The major challenge in manufacturing these bioactive and patient-specific scaffolds has been to control the architecture and the pore size for cell proliferation and adhesion. The traditional techniques are not efficient enough for meeting the requirements of the scaffolds. The AM technology can produce the desired pore distribution and the pore size. Hence, the AM technology is being employed for the development and fabrication of TE scaffolds. This review focuses on various methods used for printing scaffolds like stereolithography (SLA), selective laser sintering (SLS), fused deposition modeling (FDM), and binder jetting (BJ). This work also reviews various materials used for the fabrication of scaffolds for tissue engineering. It discusses the advantages of those materials, and various applications of those materials for TE scaffolds. This work also deals with the effect of scaffold geometry on various scaffold properties like mechanical properties, porosity and proliferation.**Keywords**—additive manufacturing, tissue engineering, scaffolds, porosity

## I. INTRODUCTION

Additive manufacturing (AM) process is an automated process to fabricate part or model efficiently and rapidly by adding material in a layer-by-layer fashion. The ISO/ASTM International defined AM as the process of joining the materials to make objects from three-dimensional CAD data, usually layer upon layer, in contrast to subtractive manufacturing technologies such as conventional machining (ISO/ASTM 2015). The AM process can achieve various advantages like design freedom, no assembly requirement, and minimal wastage because of the approach used for fabrication. Also, compared to conventional manufacturing processes, most AM techniques are less hazardous to the environment. AM has also been known as Rapid Prototyping (RP), 3D Printing (3DP), Layered Manufacturing Technology (LMT), Solid Freeform Fabrication (SFF), tool-less manufacturing, model making, desktop manufacturing, automated fabrication, and Material Ingress Manufacturing (MIM) [1]. It is one of the fast-growing technologies and has gained popularity in the sectors like automobile, aerospace, and biomedical. Fig. 1 shows the percentage-wise breakdown of various

Venkata Durga Prasad Kadambari

Department of Mechanical Engineering National Institute of Technology, Uttarakhand Srinagar (Garhwal), Uttarakhand, India

Email: [prasadkadambari@gmail.com](mailto:prasadkadambari@gmail.com)

Sanat Agrawal

Department of Mechanical Engineering National Institute of Technology, Uttarakhand Srinagar (Garhwal), Uttarakhand, India

Email: [sanata@nituk.ac.in](mailto:sanata@nituk.ac.in)

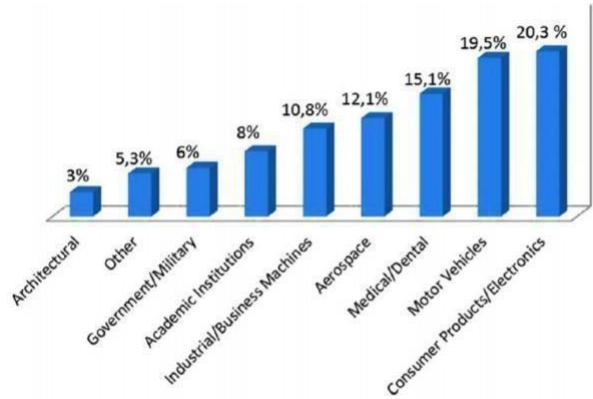


**Fig. 1. Percentage breakdown of industrial sector using AM**

industrial sectors utilizing AM technology [2]. The medical sector stands in third place in percentage use of AM machines among various industrial sectors. In the biomedical sector, the AM technology can be applied for the fabrication of surgical instruments, models for pre-surgical planning, learning models, research testing, custom-made prosthetics, hearing- aids, drug delivery devices, patient-specific implants, and tissue engineering (TE) [3]–[5]. Approximately 230 million major surgical procedures are performed worldwide daily [6]. Most of the surgeries involve reconstruction, repair, or replacement of one or more organs or tissues. TE in combination with AM has emerged as an alternative technique to regenerate the damaged tissues by developing patient-specific implants and organs to maintain the tissue function [7]. The functional organ or tissue manufacturing requires a scaffold, which acts as a framework for tissue regeneration. AM can help in fabricating such scaffolds growing them additively layer-by-layer. This is very appropriate in reconstructive surgery for facial trauma as scaffolds with patient-specific anatomical geometries can be fabricated. Currently, materials that facilitate bone ingrowth are widely used for tissue engineering scaffolds. The most common AM technique for tissue engineering scaffolds is the Fused Deposition Modeling (FDM) process, in which the extrusion of various materials like polymers, hydrogels, and ceramic pastes take place for fabricating a part layer-by-layer. Different AM process is required depending upon the type of material to be used. For thermoplastics, the FDM is used. Fully interconnected pores can be achieved with this additive manufacturing process. This is not possible in conventional techniques such as injection molding. Porosity is vital in scaffold design as it allows blood vessel ingrowth, nutrient diffusion, and oxygen transport which are essential factors for the regeneration of fully functional tissues [8]. [9] introduced four levels of geometry for tissue engineering scaffolds, (1) surface topography, (2) pore size and geometry, (3) porous networks, and (4) macroscopic pore arrangement. The first level relates to the surface feature of approximately 10 µm size, depending on the type of material and the processing method employed. The other three levels of geometry are entirely governed by the geometric placements of the filaments or hatching in each layer of the scaffold. A scaffold is a temporary porous structure having good mechanical integrity. It also assists the new cells in proliferation, adhesion, and differentiation [7]. The traditional methods for scaffold manufacturing include gas foaming, phase separation, electrospinning, solvent casting, and particulate leaching [10]– [13]. The traditional methods have low control over porosity, pore shape and size, pore interconnectivity. [14] first reported the use of additive manufacturing for tissue engineering applications. He produced scaffolds with various filament orientations. Many features of the porous geometry like pore volume fraction (porosity), pore size, pore shape, mechanical properties, and functional gradients of these properties can be controlled by the position and orientation of the filaments. The scaffold geometry can influence biological responses like cell proliferation, cell seeding, and tissue formation [99]. This review identifies the state-of-the-art of designing the scaffold by considering the position and orientation of the filaments and various methods for the fabrication of scaffolds, and the effect of position and orientation on the properties like porosity, mechanical properties, and biological performance of tissue engineering scaffolds produced by material extrusion additive manufacturing.

## II. REQUIREMENTS OF SCAFFOLDS

In this section we will discuss some of the requirements of scaffolds. TE has three essential elements: cells, growth factors, and scaffolds as shown in Fig. 2. Numerous techniques with various materials can fabricate a scaffold. However, there are some essential considerations required to determine the suitability of the technique for TE.

### A. Biocompatibility and biodegradability

A scaffold must be biodegradable so that it combines with the bone in which it is implanted. A biocompatible scaffold is required for cell attachment and proliferation to be successful. The material for the TE scaffold should be non-toxic and non-inflammatory. Else, the healing capacity rate may be reduced

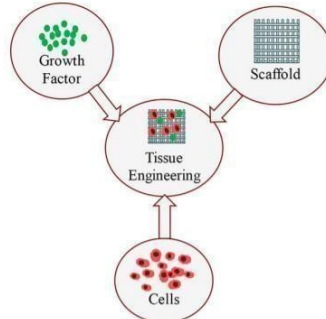


**Fig. 2. TE growth factor, scaffolds and cells**

or it may get rejected from the body. Also, it should allow cells to produce extracellular matrix without damaging human body organs. The degradation of the scaffold should be balanced with the increase in the extra-cellular matrix strength.

### B. Mechanical properties

Tissue scaffolds should have sufficient strength, elasticity, and stiffness to sustain a variety of load applications. It is a challenge for the scaffolds to provide necessary mechanical strength for orthopedic applications like bone and cartilage.

### C. Pore architecture and vascularization

The pore architecture is an important feature of a scaffold as it promotes the cell growth and prevents apoptosis. Mechanical strength of the scaffold should be excellent enough for providing the necessary support to the bone. The scaffolds should also have high porosity, specific structure, and inter-connected pore structure. Pore size and pore interconnectivity are responsible for the fluid mobility in the scaffolds [15]. A pore size of 300  $\mu\text{m}$  can improve the cell proliferation ability of a scaffold [16]. Vascularization also depends on the pore architecture of the scaffold. It facilitates supply of the nutrients to the cells and helps prevent apoptosis [17].

The above properties are interdependent on each other for the design of scaffolds. For attaining required cell proliferation and vascularization, a balance between pore size and mechanical properties of scaffolds should be maintained [18].

## III. TECHNIQUES FOR FABRICATION OF SCAFFOLDS

This section provides an overview of the various techniques used for fabrication of scaffolds. The techniques for additive manufacturing of scaffolds are broadly classified into three domains, namely, powder-based, photosensitive-based, and extrusion based. It is further classified according to the working principle as shown in Fig. 3. Widely used additive manufacturing techniques today are stereolithography (SLA), selective laser sintering (SLS), fused deposition modeling (FDM), binder jetting (BJ).

SLA is the first AM technique developed by Charles Hull in the 1980s, which works on the principle of photopolymerization [19]. The build platform is submerged in a resin tank.

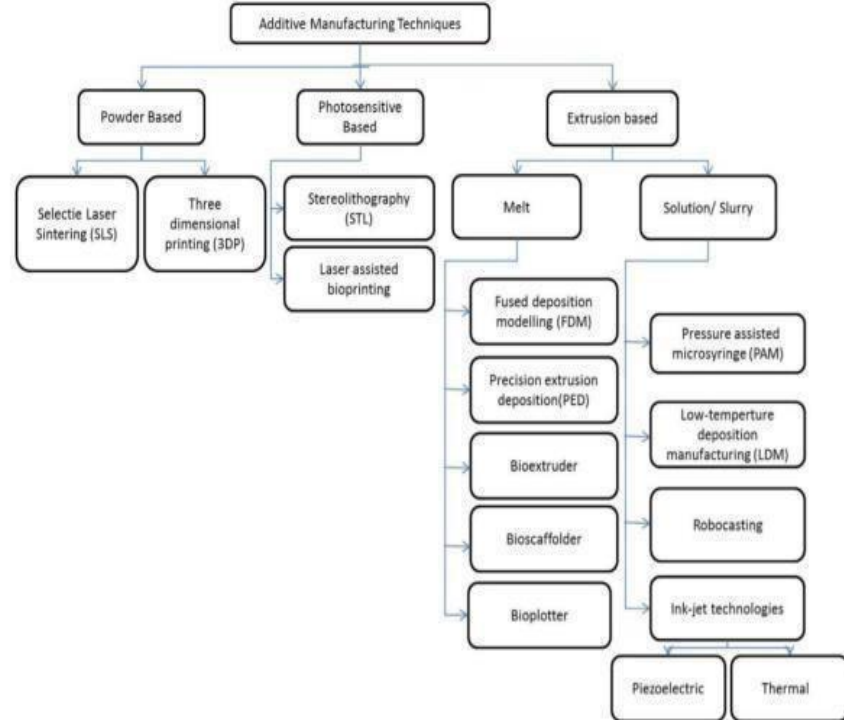


**Fig. 3. Different techniques for AM**

Ultraviolet light emitted from the laser scans the contour of a slice on the liquid resin surface. The part is grown layer-by-layer. The green part is then taken to an oven for completing the curing. Thermal light curing or UV light curing are the post-processing techniques for increasing the strength of the green part [1], [19]. In terms of complexity, flexibility, microfabrication, better control on porosity and other geometric parameters, AM technique is preferable to other conventional manufacturing processes. The AM processes other than SLA have limited resolution [20]. Though SLA is preferred, it has mainly four drawbacks: shrinkage during post-processing, support requirement, polymer materials only, and difficulty in achieving multi-material fabrication [21]. Properties such as the layer thickness and the orientation of the part can affect the mechanical properties of the printed scaffolds [22]. Table I shows the various reported techniques for tissue scaffold fabrication with different materials, process parameters, and their outcomes in terms of mechanical and biological properties using SLA technique. Carl Deckard developed SLS in 1986 in the University of Texas; Austin. It was later commercialized by DTM Corporation. This process is widely popular for its wide range of available materials, including wax, nylon, composites, and metal powders [27]. An Nd-YAG or a CO<sub>2</sub> laser is used in SLS technique for sintering the powder material in a layer-by-layer fashion to fabricate the required 3D object [28]. The bed of the apparatus is filled with powder material up to the brim. The sintering bed moves down once a layer is sintered and another layer of powder is laid on top of it. Laser beam selectively scans the powder bed for sintering the layer. No support material is required in this process. The main advantage of SLS process is that it can fabricate objects with different materials or a combination of materials [29], [30]. By adjusting the process parameters, this technique is very much useful as it provides good user control over microstructure of the created scaffold. Fabrication of ceramic scaffolds is very difficult using this process as the heating and cooling rates of the high temperature laser. This method usually produces scaffolds that are brittle. The dimensional accuracy of the SLS technique is poor and is limited to 150 - 180 μm. A variety of materials can be used in this process except natural polymers as the temperatures generated by the lasers are high. Also, due to thermal distortion shrinkage and warping of the scaffolds can be noticed [31]. Table II presents major findings of the use of SLS in scaffold applications in terms of mechanical and biological properties of various materials with different pore sizes and the respective process parameters. FDM, invented by Scott Crump in 1988, is one of the widely used AM process for TE applications.

Scott Crump had founded Stratasys Inc. USA for commercializing the process. This process is melting the filament of material and depositing it in a layer-by-layer fashion to obtain the required product. Rollers are used to push the filament to the heating element for melting. The molten paste is allowed to flow through a nozzle that can move in the x and y directions. The build platform lowers in the Z-direction and the process is repeated till the required product is fabricated. Dual nozzles can be used in the extruder head for depositing the support material [37]. FDM can fabricate well interconnected porous scaffolds from CAD models.

The main consideration should be kept on the materials of the scaffolds. The materials used should be either can be converted to filaments form or slurry form. Once the materials are finalized this method can fabricate scaffolds with good dimensional accuracy, depending upon the type of extrusion (i.e., wire or grain extrusion) [38]. Table III gives a brief description of the research attempts on FDM techniques for TE applications with different types of materials, parameters, mechanical and biological properties. Binder Jetting (BJ) can also be referred to as 3D powder printing (3DPP) or 3D Printing (3DP). It was developed at Massachusetts Institute of Technology (MIT) in 1990. This process also uses powder as in the SLS process. However, binder is printed onto the powder bed in this process using an inkjet print-head. High flexibility and ample availability of materials (ceramics, polymers, and composites) make the BJ process available for biomedical applications [44]. The shape and size of the particles play a key role in 3D printing applications as it affects the quality of the printing and the resolution of the printed part. Particle size plays a key role in this process. If the particle size is less than 5  $\mu\text{m}$ , it may result in agglomeration of the powder due to van der Waals forces [45] and poor flowability during the process. The particle size of more than 20  $\mu\text{m}$  results in lower internal friction, good flowability, and ability to spread [46]. The optimal powder size of the material is in the range of 15-50  $\mu\text{m}$  [47], [48]. Also, it is found that the binder droplet size also affects the resolution of the product. Table IV gives a brief description of the research attempts on BJ techniques for TE applications with different types of materials, binders, parameters, outcomes along with post processing techniques.

**TABLE I**  
MAJOR FINDINGS OF SLA IN SCAFFOLD APPLICATIONS

Materials	Photoinitiator	Parameters	Outcomes	References
PLGA (polymer)	TPO (1 Wt.%)	I: 9 mWcm <sup>-2</sup> λ: 365 nm	Degradation rate after 4-12 weeks makes it suitable for soft tissues	[23]
PEGDA (polymer)	DAROCUR-1173 and DAROCUR-TPO (0.25 Wt. %)	I: 2.64&14.98 mWcm <sup>-2</sup> λ: 400-410 nm	Basic osteochondral scaffold is manufactured using multi-material SLA and the tensile strength is found to be 19.35 MPa	[24]
GelMA (polymer)	Irgacure 2959 (1%w/v), HMBS (0.1% w/v)	I: 50 mWcm <sup>-2</sup>	GelMA scaffold's thickness was found to assist cell adhesion and proliferation, and during compression test no fracture was observed	[25]
PPF/DEF (polymer)	BAPO (1% w/w)	t: 500 μm; scanning approach P: 280 mW	Increase in scaffold size promoted increase in cell proliferation ability up to 300 μm	[16]
PDLLA (polymer)	Lucirin TPO-L (2 Wt. %)	Scanning approach I: 16 mWcm <sup>-2</sup> t: 25 μm	Cell distribution in gyroid scaffold was more homogenous than other scaffolds	[26]

**TABLE II**  
MAJOR FINDINGS OF SLS IN SCAFFOLD APPLICATIONS

Materials and powder size	Parameters	Mechanical properties	Biological properties	References
PVDF (200 nm) and GO (0.5-3 μm)	P: 2.7 W Vs: 400 mm/s	Max. compressive and tensile strength for PVDF/0.3GO: 9.7 and 33 MPa	After 4 days of cell culture more cells were produced in PVDF/0.3 GO scaffold	[32]
PCL (<100 μm)	P: 3 W d: 150 μm Vs: 10 & 50 mm/s t: 0.15 mm	Elastic modulus of the sinusoidal scaffold: 1944 to 27.3 kPa	Highly flexible scaffold	[33]
HA (1 μm), Silica sol (25 nm) , STPP	P: 7-16 W d: 0.3 mm t: 100-500 μm Vs: 120-550 mm/s	Compressive and bending strength at 1300°C: 43.26 and 1.28 MPa	Cell growth depends on pore structure and surface roughness	[34]
PCL and Gelatin or collagen coating	P: 2 W Vs: 500 mm/s	Scaffolds with gelatin have high elastic modulus	For cell growth, collagen coating is better than gelatin	[35]
PCL pellets (3-5 nm) and HA nanoparticles	P: 6-10 W d: 200 μm Vs: 1200 & 2000 mm/s	Compressive strength decreases with increase in HA%	In vitro study of 20% HA/PCL scaffold shows better cell growth, adhesion and migration within 5-7 days	[36]

**TABLE III**  
MAJOR FINDINGS OF FDM IN SCAFFOLD APPLICATIONS

Materials	Parameters	Mechanical Properties	Biological Properties	References
PCL, PGA structure yarn	T <sub>g</sub> : 100 °C T <sub>b</sub> : 40°C V: 5 mm/s D <sub>n</sub> : 0.5 mm	Tensile strength 79.7 MPa	Reinforced scaffold degraded by 20 times faster than non-reinforced scaffold.	[39]
PLGA, PLCL and TCP	T <sub>g</sub> : 160-195 °C D: 330 μm pore: 325 μm	Water contact angle decreased with the increase in TCP %	The degradation study in PBS solution on TCP scaffold showed that the mass loss is independent of the scaffold architecture.	[40]
PCL and HA	T <sub>g</sub> : 150°C V: 35 mm/s	Max. tensile strength: 23.29 MPa flexural strength: 21.39 MPa	PCL/ HA scaffolds have great potential for bone tissue engineering applications	[41]
PLA	T <sub>g</sub> : 180 °C, V: 40 mm/s, D <sub>n</sub> :0.4mm t:0.1-0.3 mm	FDM generates macropores of range 100-800 μm and gas foam generates pores of range 1-10 μm in the scaffold	FDM and gas foaming process combinations enhanced various biological functions like controlled cell performance in TE generation	[42]
PCL	D <sub>n</sub> : 0.4 mm, t: 0.3mm T <sub>g</sub> : 85°C	For cell growth and functioning porosity is a key factor	Large sized pores did not help the cells to attach the scaffold.	[43]

**TABLE IV**  
MAJOR FINDINGS OF BJ IN SCAFFOLD APPLICATIONS

Materials	Binder	Parameters	Post-processing	Outcomes	References
Tetracalcium phosphate	Phytic acid (IP6)	100 μm 40% porosity	10s immersion in IP6 for 4 times	Compression strength in range of cancellous bone i.e. 4 to 8.5 MPa	[49]
TCP and doped TCP with ZnO	Commercial organic water based (ProMetal)	20 μm	1250°C for 2 h	Cell viability and flexural strength is improved by adding 1-2 Wt% collagen in the binder solution	[50]
TCP	Aqueous-based binder	20 μm	Conventional sintering	Mechanical strength is increased	[51]
HA, TCP and BCP	20 Wt.% dextrin and 2.5 Wt.% saccharose	260 μm	1250°C for 2h	Highest compressive strength in BCP samples and High amount of organic additives implied in low compressive strength	[52]
PLGA	Acetone, deionized water, and ethanol	50% porosity	Leaching and annealing	Implanted scaffold resulted in new bone generation within 24 weeks	[53]
Calcium Phosphate/ PVA(10 Wt.%)	Aqueous solvent	t: 150 μm up to 35% porosity	400°C for 2 hours	Compressive strength of the scaffold is obtained to be 35MPa, in the range of human bone	[54]

#### IV. MATERIALS

There is a wide variety of bio-compatible materials available for fabricating scaffolds using AM. The selection of material and the AM process depends upon the type of scaffold required and its application. This section reviews the materials available for fabricating scaffolds using AM. The European Society of Biomaterials (ESB) gave a definition of biomaterials as —material intended to interface biological systems to evaluate, treat, augment, or replace any tissue, organ or function of the body [7]. Polymers (natural or synthetic), ceramics (bioinert, bioactive, and bioresorbable) and composites are used in AM systems to fabricate TE scaffolds [55]. The materials are selected depending upon the type of tissues such as hard or soft, for regeneration or repair. AM technologies are used for fabrication of scaffolds for soft tissues such as cardio-vascular, cartilage, neural, liver, as well as hard tissues such as bones of the body, cranium, maxilla and mandible [56]– [58]. Development of ceramic omnidirectional bioprinting in cell suspension (COBICS) helped overcome major challenges in generation of bone mimicked tissue engineering constructs mimicking the bone microenvironment. COBICS provided a scope for real-time bone reconstruction in clinical setting [59]. For gene therapy, expression and modulation, biomaterials such as PCL, HAP and PLGA (Poly lactic-co-glycolic-acid) are 3D printed by including gene (DNA, mRNA, miRNA, siRNA etc.) [60]. For treatment of extensive wounds of the skin, researchers provided a novel approach for mobile bioprinting of skin integrated with scanner for management of external wounds [61].

The materials for scaffolds are broadly classified into three main categories as follows:

- Polymeric
- Ceramic
- Metallic

##### A. *Polymeric scaffolds*

Polymeric materials provide more control on physical properties of scaffolds like porosity, pore size, solubility, and biocompatibility. Polymers such as **poly(lactic acid)** (**PLA**), **poly(glycolic acid)** (**PGA**), and **poly(caprolactone)** (**PCL**) are introduced for their excellent mechanical properties. These polymers are for bone tissue engineering materials and can be given various shapes [62]–[66]. Natural polymer scaffolds are comprised of extracellular biomaterials in three classes: 1) **proteins** (collagen, silk, elastin, keratin, gelatin. . .), 2) **polysaccharides** (cellulose, dextran) and 3) **polynucleotides** (DNA, RNA) [64], [67]. Some of the natural polymer materials for bone scaffolds include **collagen (type i, ii, and iii)**, **alginate**, **chitin**, and **chitosan** [68]. These polymeric materials are non-toxic. For osteoconductive properties, extra cellular matrix (ECM) is suggested as it is similar to that of the original tissue. Such scaffolds could be cell-derived or tissue-derived [69]–[72]. Though natural scaffolds provide better properties in terms of biodegradability and biocompatibility, poor mechanical

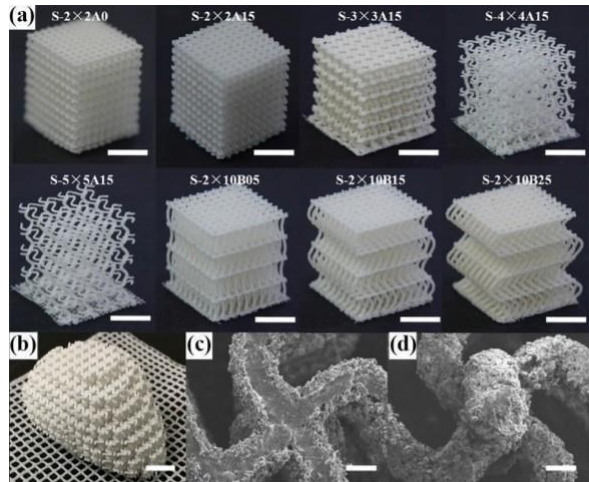


**Fig. 4. PCL scaffolds by SLS process. (a) isometric view of flexible scaffold. (b) patient-specific scaffold. (c) top view of the scaffold. (d) bottom view of the scaffold.** [33]

properties are the major concern when the scaffolds are used for bone implants. Also, these natural polymer scaffolds fail to provide sufficient architectural support and protection for the cells like osteogenic cells. Immunogenic reactions and pathogen transmission may also happen due to a lack of impure content in the natural polymers. There are many synthetic polymers for bone tissue engineering (BTE) like **poly(methyl methacrylate)**, **poly(*e*- c prolactone)**, **poly hydroxyl butyrate**, **polyethylene**, **polypropylene**, **polyurethane**, **poly(ethylene terephthalate)**, **poly(ether ketone)**, and **polyphenol sulfone**. Among these materials, **poly(propylene fumarate)** (PPF) has high compressive strength and controlled degradation time [73], [74]. [75] developed a polymer scaffold of poly(propylene fumer-ate) (PPF)/ Diethyl fumerate (DEF) incorporating the PLGA microsphere loaded with bone morphogenic protein-2 (BMP- 2) using the microstereolithography (micro-SL) technique. The in vitro and in vivo studies showed that the scaffold has great potential to reconstruct the damaged bone tissue. In another research [76] developed a biphasic osteochondral scaffold using light-curable poly(ethylene glycol) diacrylate (PEGDA) hydrogel and betatricalcium phosphate ( $\beta$ -TCP) ceramic suspension. Table V lists various natural polymers available for scaffold fabrication and their properties, applications, and toxicity. [29] reported a bio-composite blend of Hydroxyapatite (HA) and polyether ether ketone (PEEK) using SLS process. An increase in laser power helps in enhancing the compressive strength of the bioactive scaffolds [30]. In another research[78] developed a bone scaffold using nano-HA/ Poly (D, L- Lactide) (PDLLA) composite microspheres. PDLLA has muchfaster degradation rate than poly(L-lactide) (PLLA) because of its amorphous structure. They fabricated the bone scaffold preparation by a low-power SLS technique.

Material	Properties	Application	Toxicity	References
Polylactic acid (PLA)	biocompatible, biodegradable, supports cell adhesion	BTE applications, sinuses and nasal cavity filters	nontoxic, non-inflammatory	[62]
Polyglycolic acid (PGA)	biodegradable, biocompatible	BTE applications	nontoxic, non-inflammatory	[63]
Polyethylene glycol (PEG)	biocompatible, steering cells into scaffolds, osmotic effects in the body	bone regeneration, pharmacy, industrial chemistry, sinuses and nasal cavity filters	nontoxic, FDA approved	[64]
Collagen	biocompatible, degradable	tissue engineering, biomedical applications	nontoxic	
Alignate	ease of chemical modifications, formation of gels, controlled release of tissues	BTE applications	nontoxic	[77]
Chitin	biocompatible, biodegradable	biotechnology and medical applications	nontoxic	[68]

flexible scaffolds in the SLS process for soft tissue applications is a challenge. [33] designed and fabricated various flexible scaffolds with PCL material using SLS technique as shown in the Fig. 4. [79] reported that the yield strength and compressive strength of PCL scaffolds be in the range of 2 to 3.2 MPa and 52 to 67 MPa respectively. Researchers have fabricated composite scaffolds of PCL/TCP for analyzing the effect of the TCP (a ceramic) content on the mechanical and biological properties of the scaffold. [80] reported that 50 weight percentage of TCP in PCL/TCP mixture was possible to use for the fabrication of a composite scaffold. The stiffness was found to decrease with the increase in the macro-porosity. A TCP content of 10 weight-percentages showed weak bone growth in critical-size defects with a low regeneration capacity. [81] used an FDM machine for preparing bone implants for cancellous bone grafts using polypropylene/ tricalcium phosphate PP/TCP materials building several concentric cylinders with different pore sizes radially from segment to segment. The scaffolds were fabricated using a constant lay-down pattern of  $0^\circ$  -  $60^\circ$  -  $120^\circ$  with a varying roadmap (2.03 mm at the center, 1.27 mm at the middle, and 0.51mm at the outer ring) having decreasing porosity and pore size towards the outer part. Experiments showed that the compressive strength decreased as the porosity increased. In vitro analysis revealed that these scaffolds were non-toxic. [82] used poly(vinyl alcohol)/ poly(lactic acid)/ hydroxyapatite bioactive nanocomposites (PVA/PLA/mHA) for fabrication of porous scaffold using FDM. The MTT cytotoxicity tests were conducted along with mechanical and thermal analysis. This research provided that, the composite with PVA/30PLA/20m-HA with 385  $\mu\text{m}$  pore size and 60% porosity had a compressive strength of 7.6 MPa providing adequate strength for tissue engineering applications.

### B. Ceramic scaffolds

The bone tissue consists of about 70% hydroxyapatite (HA) and 30% collagen by weight [83]. Bio-ceramics almost mimic the bone tissue and provide higher osteoblasts adherence and proliferation compared to other materials [84]. Calcium phosphate ceramics (CPCs) are widely studied as they are highly tunable ceramic materials. CPCs are bioactive mate-

rials that possess unique properties such as osteoconductivity and osteoinductivity, making them suitable candidates for the regeneration of bone. Hydroxyapatite, tricalcium phosphate (TCP) and their combinations as biphasic and amorphous calcium phosphate are commonly used CPC for bone tissue engineering applications [85]. It is also observed that the mechanical strength, biocompatibility, and dissolution rates of a scaffold can be modified by adding calcium phosphate [86]. Doping of  $\beta$ -TCP scaffold with  $\text{SiO}_2$  (0.5 wt%) and  $\text{ZnO}$  (0.25 wt%) has been shown to upgrade the compressive strength of the scaffold by 2.5 times [50]. Though the mechanical properties of the ceramic scaffolds are better compared to polymeric scaffolds, they are still inferior to natural bones in terms of tensile and torsional strength. HA has a greater compressive strength (500-1000 MPa) and bending strength (115-200 MPa) compared to cortical bone (100-230 MPa compressive strength and 50-150 MPa bending strength, respectively). However, its fracture strength is significantly less (2-12 MPa). The biocompatibility and osteoconductivity of HA and TCP are better than that of bovine HA scaffolds. Studies by [87] showed that biphasic calcium phosphate (BCP) with varying HA and TCP content has excellent properties in bone regeneration and biocompatibility. Studies by [88] shows the process capability analysis of the binder jetting (BJ) process for the fabrication of calcium sulphate porous scaffolds using the tolerance grading ranging from IT3 to IT10, and the maximum dimensional deviation before and after adjusting the center of the process is found out to be 0.41% to 0.44% respectively. It is also found that the process capability indices  $C_p$  and  $C_{pk}$  obtained are close to the industrial benchmarks (greater than 1 and close to 1.33). Dimensional accuracy is one of the challenging tasks in BJ process. For better dimensional accuracy, care must be taken while considering the shrinkage allowance during printing the scaffold. [89] fabricated a BCP scaffold with a pore size of 300  $\mu\text{m}$  and 96.5% dimensional accuracy for the orbital rim of the skull. In vitro analysis proved that the scaffold resulted in good proliferation, cell viability, and cytocompatibility compared to the pure TCP scaffold.

### C. Metallic scaffolds

Iron (Fe) and magnesium (Mg) based materials such as Fe- RE (rare earth) alloys, pure Fe, Fe-Mn alloys, Fe foam, and Mg-Ca have been used for bone scaffolds [90]–[92]. Fe has 211 GPa elastic modulus, which is higher than Mg (41 GPa) and its alloys (44 GPa), and 316L stainless steel (190 GPa) [93]. Magnesium and its alloys are widely used for bone tissueengineering applications compared to iron due to its wide range of characteristics likebio-resorbability, biodegradability, suitable mechanical properties, non-inflammatory responses, and bone cell activation support. Moreover, the Mg-based implants have shown a superior increase in bone area in comparison with PLA. Furthermore, porous Mg shows better degradation behavior and slower decay of compressive yield strength in stimulated body fluids (SBF) immersion tests [94]. Titanium (Ti) porous scaffolds have also been studied for bone replacement materials. These materials are not biodegradable and do not integrate with biomolecules. Oxidization of Ti ( $TiO_2$ ), modification of surface and combination of chrome-cobalt (Cr-Co) alloys and stainless steel with titanium alloys can improve biocompatibility. Titanium- aluminum-vanadium alloys (ASTM F1472, ASTM F136, ASTM F110) possess better mechanical properties than pure titanium and can be used in joint implants [95]. Tantalum (Ta) is widely used in bone tissue engineering and knee re- placement surgeries [96]–[98]. Metal implants are lightweight, strong, biocompatible, and osteoconductive.

## V. EFFECTS OF SCAFFOLD GEOMETRY ON VARIOUS

### PROPERTIES

In this section the effect of scaffold geometry on the properties of the scaffold are reviewed.

#### A. Effect of scaffold geometry on performance

Properties like porosity, mechanical properties, cell proliferation and biocompatibility are affected by the design of the scaffold. Different geometries of scaffolds can be achieved by changing the orientation of the filament to be printed. Commonly used orientations are  $-0^\circ/90^\circ$  orientation|| where the filament is on alternate layers,  $-0^\circ/60^\circ/120^\circ$  orientation||, where the orientation is changed by  $60^\circ$  for every layer, or a  $-0^\circ/45^\circ/90^\circ/135^\circ$  orientation||, and  $-0^\circ/72^\circ/144^\circ/216^\circ/288^\circ$  orientation||. There are two aspects of filament positioning:

(1) aligned versus staggered filaments and (2) repeated layers. In the first aspect, the filament layers are laid directly on the top of one layer or staggered in an alternate manner by offsetting their horizontal position. In the second aspect, several identical layers are laid on the lower layer before changing the orientation of the filament [99, 100, 101, 102].

#### B. Effect of scaffold geometry on porosity

Domingos [103] conducted a detailed study on the porosity of PCL scaffolds. Various scaffolds are fabricated by varying deposition speed, layer thickness, and melt-chamber temperature. It was observed that the porosity of the scaffolds ranged from 49% to 77% and the pore size from 579  $\mu m$  to 711

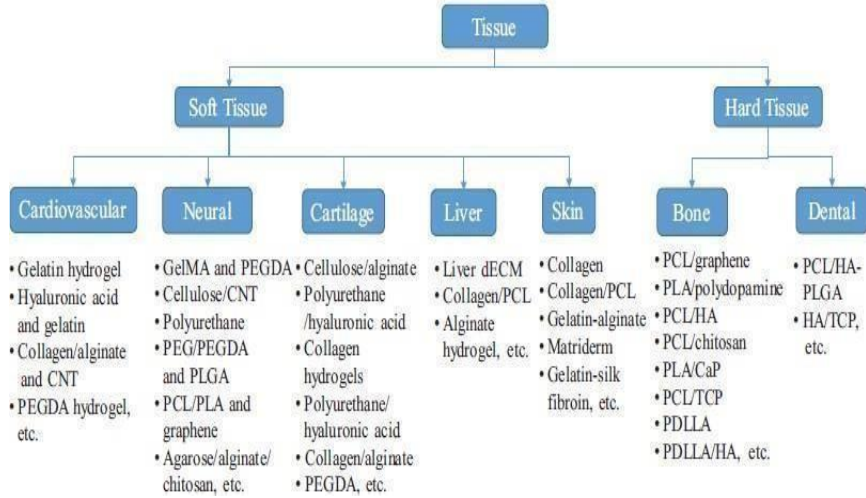


**Fig. 5. Biomaterials used for scaffold manufacturing**

μm, whereas the pore height is observed from 83 μm to 340 μm. Another research conducted by [104] also investigated the effect of process parameters on PCL scaffold. They fabricated scaffolds with porosity ranging from 10% to 60%. Pores on the external surface have some effect on the material properties of the scaffold, but with a minimal effect. [105] proposed that the scaffold porosity can still be maintained by changing the filament orientation direction. It also stated that excessive deposition of the scaffold material could be controlled by changing the filament orientation by 45° near to the edge of it.

### C. Effect of scaffold geometry on mechanical properties

The position and orientation of the filaments can have minor or major impact on the mechanical properties of the scaffold. However, the scaffold porosity is one of the key factors affecting its mechanical properties, as mechanical properties are inversely related to the scaffold geometry. [103] proved that a minor change in the porosity affects the mechanical properties of the scaffold to a high level. Research by [106] and [104], developed models for relating mechanical properties to porosity and observed results similar to [100]. Studies by [107], [108], [109], [110] found that with the reduction of the scaffold's porosity, there is a more significant improvement of the mechanical properties. If the alignment of the scaffold is changed, the mechanical properties also change. Studies by [101], [111] showed that if the filaments of the scaffold are staggered, the elastic modulus is lowered by 40-50% in comparison to the scaffolds with aligned filaments. The FEA analysis performed based on the mechanism on which the scaffolds collapse for the staggered and aligned filaments is shown in Fig.6 [112]. The filament orientation of the scaffold is also one of the factors that affect the mechanical properties of the scaffolds. Studies by [100], [113], [114] found that the scaffold orientation other than 0°/45°/90°/135° showed poor mechanical properties. The scaffolds with orientation 0°/90° and 0°/60°/120° will cross over the same point in every layer, which helps form a column of polymer from top to bottom of the scaffold which results in high elastic modulus. The various orientations of the filaments are shown in the figure 7. [14] proved experimentally that the scaffolds with orientation of the filaments 0°/60°/120° have the modulus stiffness greater than that of the

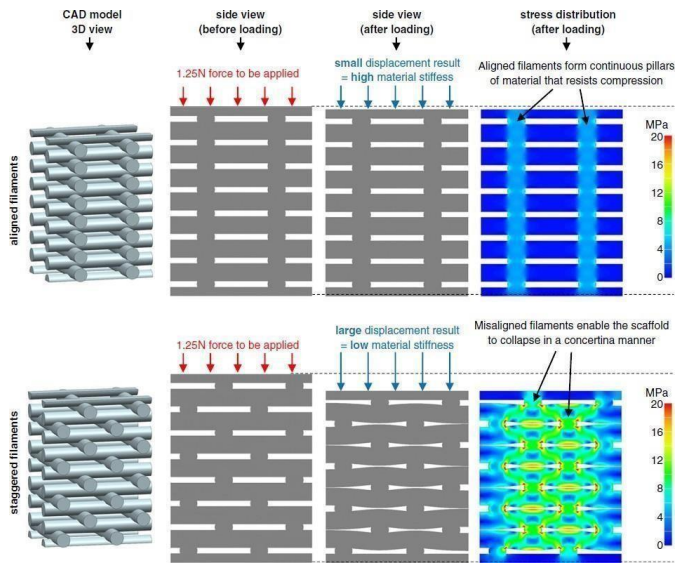


**Fig. 6. FEA of scaffolds with various filament arrangements. [112]**

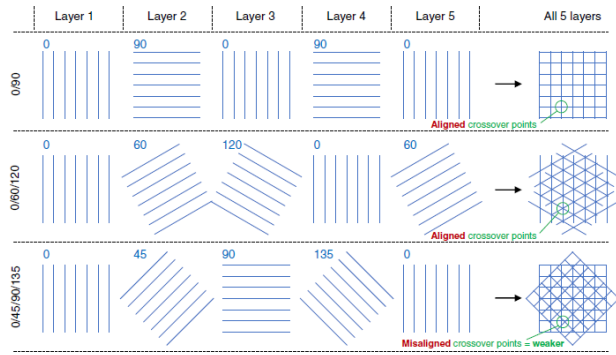


**Fig. 7. Orientation of filaments in scaffolds. [112]**

$0^\circ/72^\circ/144^\circ/216^\circ/288^\circ$  oriented scaffold. Statistical analysis confirmed that the five-angle scaffolds had significantly lower stiffness and 1% offset yield strengths under compression loading than those with a three-angle pattern. Studies from [113] proved that if the scaffold has more than two repeated layers can have the modulus less than that of the scaffold with alternating layers, they stated that the structure was weak as there are longer pores in the compression axis lead to the weaker section of the scaffold. If the orientation is  $0^\circ/90^\circ$ , the scaffold has similar moduli up to three repeated layers. Varying the number of repeated layers has more impact on the pore size of the scaffold [105]. [101] also examined scaffolds with one and two repeating layers, but direct comparison of the scaffolds was difficult as the filament alignment was altered.

#### D. Effect on proliferation

Pore size is one factor that affects cell seeding and proliferation in scaffolds [115]–[117]. The same for this was demonstrated by [118] for human adipose-derived stem cells (hASCs) by adjusting the filament size in the scaffold and found that uniform cell seeding is achieved with a pore size of 800  $\mu\text{m}$  for PCL scaffolds. The study by [16] found that for proliferation the ideal pore size should be in the range of 350  $\mu\text{m}$ . [100] found that for more significant proliferation, the pore size of the scaffold should be in the range of 245 to 433  $\mu\text{m}$ .

## VI. CLINICAL STUDIES

Osteopore International Pte Ltd, Singapore provides PCL- based 3D printing scaffolds that are clinically approved under current good manufacturing practices (cGMP) facilities according to the patient's requirement ([www.osteopore.com](http://www.osteopore.com)). Various organizations have approved the use of scaffolds in the United States (FDA 510), Europe (CE mark), Singapore (HSA), Korea (KFDA), India (CDSCO) [119]. [120] have stated that the orbital fracture reconstruction using a bioresorbable implant is performed on 94 patients and 98 orbits over ten years (2005-2014) by obtaining written consent from all the patients under the Declaration of Helsinki (DoH) by the World Medical Association, version 1989 along with the approval of institutes review board. CT images of the implants between 15 and 24 months in all the patients showed complete resorption of implants and new

bone formation, which made it clear that bioresorbable implants were safe and clinically effective.

TABLE V  
VARIOUS POLYMER MATERIALS FOR SCAFFOLD

## VII. CONCLUSIONS AND FUTURE SCOPE

The role of AM in TE is growing in a great pace with the aim to meet the required patient-specific implants and scaffolds for replacement and surgeries. The materials used for this process should be biocompatible and biodegradable. A scaffold may require a multi-material fabrication capability in the AM technique used. The AM technique used for scaffold fabrication should possess high dimensional accuracy, low production cost, high resolution etc.

AM techniques, being additive in nature, does not recognize complexity. They can relate complex shapes with great ease and accuracy. The capabilities of AM machines provide easy control over various properties like pore architecture, pore size and interconnectivity. The SLA process has the dimensional accuracy and highest resolution compared to other techniques. However, the availability of biodegradable photopolymers is low. The FDM process is affordable and simple. However, the material available to the FDM systems should be in the form of filament. Therefore, this process is restricted to thermoplastic materials. The FDM process combined with the gas foaming process generates both micropores and macropores in the scaffold and enhances several biological functions. The SLS process provides good resolution for the scaffold, but is expensive. Due to the high intensity of laser, the photopolymer may degrade and post-processing is required to remove the unused material powder. The BJ process is inexpensive and low temperature process. However, the parts fabricated from this possess has a low mechanical strength. More work should be conducted on scaffold fabrication using AM processes to provide better accuracy and good mechanical strength. Current research studies have considered a relatively narrow range of scaffold geometries.

Many of the scaffold fabrication methods deposit filaments of uniform thickness in a repeated or alternating manner over sequential layers. This is because most of the bioprinting software packages have similar capabilities. There is a large scope for improving the deposition techniques for creating scaffold structure that mimic the native tissues. Selection of biomaterials, fabrication processes, mechanical properties and post-processing techniques should be properly performed, to reduce the effects after fabrication. Novel scaffold fabrication methods such as magnetic scaffolds and cell-laden hydrogel-based scaffolds can enhance implant fixation, stability, healing of tissue, and promote bone repair and regeneration. There is a scope of improving the ability of the bioinks to be printed so that they represent the tissue architecture for restoring the organ functioning. Drug delivery is a key function for TE scaffold to promote the cell and tissue growth by delivering required biomolecules and there is ample scope for further research in this area.

## REFERENCES

- [1] I. Gibson, D. W. Rosen, B. Stucker, and M. Khorasani, *Additive manufacturing technologies*. Springer, 2021, vol. 17.
- [2] H. Bikas, P. Stavropoulos, and G. Chryssolouris, —Additive manufacturing methods and modelling approaches: a critical review,|| *The International Journal of Advanced Manufacturing Technology*, vol. 83,no. 1-4, pp. 389–405, 2016.
- [3] N. Genina, J. Holländer, H. Jukarainen, E. Maikila, J. Salonen, and N. Sandler, -Ethylene vinyl acetate (eva) as a new drug carrier for 3d printed medical drug delivery devices,|| *European Journal of Pharmaceutical Sciences*, vol. 90, pp. 53–63, 2016.
- [4] K. Phan, A. Sgro, M. M. Maharaj, P. D'Urso, and R. J. Mobbs, —Application of a 3d custom printed patient specific spinal implant for c1/2 arthrodesis,|| *Journal of Spine Surgery*, vol. 2, no. 4, p. 314, 2016.
- [5] A. Shafiee and A. Atala, -Printing technologies for medical applications,|| *Trends in molecular medicine*, vol. 22, no. 3, pp. 254–265, 2016.
- [6] T. G. Weiser, S. E. Regenbogen, K. D. Thompson, A. B. Haynes, S. R. Lipsitz, W. R. Berry, and A. A. Gawande, -An estimation of the global volume of surgery: a modelling strategy based on available data,|| *The Lancet*, vol. 372, no. 9633, pp. 139–144, 2008.
- [7] F. J. O'brien, -Biomaterials & scaffolds for tissue engineering,|| *Materi- als today*, vol. 14, no. 3, pp. 88–95, 2011.
- [8] Q. L. Loh and C. Choong, —Three-dimensional scaffolds for tissue engineering applications: role of porosity and pore size,|| 2013.
- [9] M. I. Garibaldi and S. M. Best, -Effect of ceramic scaffold architectural parameters on biological response,|| *Frontiers in bioengineering and biotechnology*, vol. 3, p. 151, 2015.
- [10] S. Gautam, A. K. Dinda, and N. C. Mishra, —Fabrication and char- acterization of pcl/gelatin composite nanofibrous scaffold for tissue engineering applications by electrospinning method,|| *Materials Science and Engineering: C*, vol. 33, no. 3, pp. 1228–1235, 2013.
- [11] Y. S. Nam and T. G. Park, -Porous biodegradable polymeric scaffolds prepared by thermally induced phase separation,|| *Journal of Biomed- ical Materials Research: An Official Journal of The Society for Bio- materials, The Japanese Society for Biomaterials, and The Australian Society for Biomaterials and the Korean Society for Biomaterials*, vol. 47, no. 1, pp. 8–17, 1999.
- [12] Y. S. Nam, J. J. Yoon, and T. G. Park, -A novel fabrication method of macroporous biodegradable polymer scaffolds using gas foaming salt as a porogen additive,|| *Journal of Biomedical Materials Research: An Official Journal of The Society for Biomaterials, The Japanese Society for Biomaterials, and The Australian Society for Biomaterials and the Korean Society for Biomaterials*, vol. 53, no. 1, pp. 1–7, 2000.
- [13] D. Sin, X. Miao, G. Liu, F. Wei, G. Chadwick, C. Yan, and T. Friis, -Polyurethane (pu) scaffolds prepared by solvent casting/particulate leaching (scpl) combined with centrifugation,|| *Materials Science and Engineering: C*, vol. 30, no. 1, pp. 78–85, 2010.
- [14] D. W. Hutmacher, T. Schantz, I. Zein, K. W. Ng, S. H. Teoh, and K. C. Tan, -Mechanical properties and cell cultural response of polycaprolac- tone scaffolds designed and fabricated via fused deposition modeling,|| *Journal of Biomedical Materials Research: An Official Journal of The Society for Biomaterials, The Japanese Society for Biomaterials, and The Australian Society for Biomaterials and the Korean Society for Biomaterials*, vol. 55, no. 2, pp. 203–216, 2001.
- [15] F. J. O'Brien, B. A. Harley, M. A. Waller, I. V. Yannas, L. J. Gibson, and P. J. Prendergast, -The effect of pore size on permeability and cell attachment in collagen scaffolds for tissue engineering,|| *Technology and Health Care*, vol. 15, no. 1, pp. 3–17, 2007.
- [16] J. W. Lee, G. Ahn, J. Y. Kim, and D.-W. Cho, -Evaluating cell proliferation based on internal pore size and 3d scaffold architecture fabricated using solid freeform fabrication technology,|| *Journal of Materials Science: Materials in Medicine*, vol. 21, no. 12, pp. 3195– 3205, 2010.
- [17] E. A. Phelps and A. J. Garcí'a, -Engineering more than a cell: vascularization strategies in tissue engineering,|| *Current opinion in biotechnology*, vol. 21, no. 5, pp. 704–709, 2010.
- [18] X. Tan, Y. Tan, C. Chow, S. Tor, and W. Yeong, -Metallic powder-bed based 3d printing of cellular scaffolds for orthopaedic implants: A state- of-the-art review on manufacturing, topological design, mechanical properties and biocompatibility,|| *Materials Science and Engineering: C*, vol. 76, pp. 1328–1343, 2017.

- [19] P. J. Bartolo and I. Gibson, —History of stereolithography,|| in *Stereolithography*. Springer, 2011, pp. 37–56.
- [20] S.-H. Park, D.-Y. Yang, and K.-S. Lee, —Two-photon stereolithography for realizing ultraprecise three-dimensional nano/microdevices,|| *Laser & Photonics Reviews*, vol. 3, no. 1-2, pp. 1–11, 2009.
- [21] C. Mota, D. Puppi, F. Chiellini, and E. Chiellini, —Additive manufacturing techniques for the production of tissue engineering constructs,|| *Journal of tissue engineering and regenerative medicine*, vol. 9, no. 3, pp. 174–190, 2015.
- [22] Z. Feng, Y. Li, L. Hao, Y. Yang, T. Tang, D. Tang, and W. Xiong, —Graphene-reinforced biodegradable resin composites for stereolithographic 3d printing of bone structure scaffolds,|| *Journal of Nanomaterials*, vol. 2019, 2019.
- [23] E. M. Wilts, A. Gula, C. Davis, N. Chartrain, C. B. Williams, and T. E. Long, —Vat photopolymerization of liquid, biodegradable plga-based oligomers as tissue scaffolds,|| *European Polymer Journal*, vol. 130, p. 109693, 2020.
- [24] Y. Wu and R. L. Clark, —Electrohydrodynamic atomization: a versatile process for preparing materials for biomedical applications,|| *Journal of Biomaterials Science, Polymer Edition*, vol. 19, no. 5, pp. 573–601, 2008.
- [25] R. Gauvin, Y.-C. Chen, J. W. Lee, P. Soman, P. Zorlutuna, J. W. Nichol, H. Bae, S. Chen, and A. Khademhosseini, —Microfabrication of complex porous tissue engineering scaffolds using 3d projection stereolithography,|| *Biomaterials*, vol. 33, no. 15, pp. 3824–3834, 2012.
- [26] F. P. Melchels, K. Bertoldi, R. Gabbielli, A. H. Velders, J. Feijen, and D. W. Grijpma, —Mathematically defined tissue engineering scaffold architectures prepared by stereolithography,|| *Biomaterials*, vol. 31, no. 27, pp. 6909–6916, 2010.
- [27] I. Gibson and D. Shi, —Material properties and fabrication parameters in selective laser sintering process,|| *Rapid prototyping journal*, 1997.
- [28] J.-P. Kruth, P. Mercelis, J. Van Vaerenbergh, L. Froyen, and M. Romouts, —Binding mechanisms in selective laser sintering and selective laser melting,|| *Rapid prototyping journal*, 2005.
- [29] K. Tan, C. Chua, K. Leong, C. Cheah, P. Cheang, M. A. Bakar, and S. Cha, —Scaffold development using selective laser sintering of polyetheretherketone-hydroxyapatite biocomposite blends,|| *Biomaterials*, vol. 24, no. 18, pp. 3115–3123, 2003.
- [30] K. C. Kolan, M. C. Leu, G. E. Hilmas, and M. Velez, —Effect of material, process parameters, and simulated body fluids on mechanical properties of 13-93 bioactive glass porous constructs made by selective laser sintering,|| *Journal of the mechanical behavior of biomedical materials*, vol. 13, pp. 14–24, 2012.
- [31] P. Rider, Z. P. Kacarovic, S. Alkildani, S. Retnasingh, R. Schmittler, and M. Barbeck, —Additive manufacturing for guided bone regeneration: A perspective for alveolar ridge augmentation,|| *International journal of molecular sciences*, vol. 19, no. 11, p. 3308, 2018.
- [32] C. Shuai, Z. Zeng, Y. Yang, F. Qi, S. Peng, W. Yang, C. He, G. Wang, and G. Qian, —Graphene oxide assists polyvinylidene fluoride scaffold to reconstruct electrical microenvironment of bone tissue,|| *Materials & Design*, vol. 190, p. 108564, 2020.
- [33] Z. Meng, J. He, Z. Cai, F. Wang, J. Zhang, L. Wang, R. Ling, and D. Li, —Design and additive manufacturing of flexible polycaprolactone scaffolds with highly-tunable mechanical properties for soft tissue engineering,|| *Materials & Design*, vol. 189, p. 108508, 2020.
- [34] F.-H. Liu, —Synthesis of biomedical composite scaffolds by laser sintering: Mechanical properties and in vitro bioactivity evaluation,|| *Applied Surface Science*, vol. 297, pp. 1–8, 2014.
- [35] C.-H. Chen, M.-Y. Lee, V. B.-H. Shyu, Y.-C. Chen, C.-T. Chen, and J.-P. Chen, —Surface modification of polycaprolactone scaffolds fabricated via selective laser sintering for cartilage tissue engineering,|| *Materials Science and Engineering: C*, vol. 40, pp. 389–397, 2014.
- [36] Y. Du, H. Liu, J. Shuang, J. Wang, J. Ma, and S. Zhang, —Microsphere-based selective laser sintering for building macroporous bone scaffoldswith controlled microstructure and excellent biocompatibility,|| *Colloids and Surfaces B: Biointerfaces*, vol. 135, pp. 81–89, 2015.
- [37] A. Houben, J. Van Hoorick, J. Van Erps, H. Thienpont, S. Van Vlierberghe, and P. Dubrule, —Indirect rapid prototyping: opening up unprecedented opportunities in scaffold design and applications,|| *Annals of biomedical engineering*, vol. 45, no. 1, pp. 58–83, 2017.
- [38] M.-W. Sa, B.-N. B. Nguyen, R. A. Moriarty, T. Kamalitdinov, J. P. Fisher, and J. Y. Kim, —Fabrication and evaluation of 3d printed bcp scaffolds reinforced with zro2 for bone tissue applications,|| *Biotechnology and bioengineering*, vol. 115, no. 4, pp. 989–999, 2018.

- [39] S. K. Hedayati, A. H. Behravesh, S. Hasannia, A. B. Saed, and B. Akhoundi, -3d printed pcl scaffold reinforced with continuous biodegradable fiber yarn: A study on mechanical and cell viability properties,|| *Polymer Testing*, vol. 83, p. 106347, 2020.
- [40] E. Walejewska, J. Idaszek, M. Heljak, A. Chlenda, E. Choinska, V. Hasirci, and W. Swieszkowski, -The effect of introduction of filament shift on degradation behaviour of plga-and plcl-based scaf- folds fabricated via additive manufacturing,|| *Polymer Degradationand Stability*, vol. 171, p. 109030, 2020.
- [41] Z. Jiao, B. Luo, S. Xiang, H. Ma, Y. Yu, and W. Yang, —3d printing of ha/pcl composite tissue engineering scaffolds,|| *Advanced Industrial and Engineering Polymer Research*, vol. 2, no. 4, pp. 196–202, 2019.
- [42] C. Zhou, K. Yang, K. Wang, X. Pei, Z. Dong, Y. Hong, and X. Zhang, —Combination of fused deposition modeling and gas foaming technique to fabricated hierarchical macro/microporous polymer scaffolds,|| *Ma- terials & Design*, vol. 109, pp. 415–424, 2016.
- [43] G.-P. Ariadna, R. Marc, P. Teresa, and C. Joaquim, —Optimization of poli (e-caprolactone) scaffolds suitable for 3d cancer cell culture,|| *Procedia Cirp*, vol. 49, pp. 61–66, 2016.
- [44] A. Butscher, M. Bochner, S. Hofmann, L. Gauckler, and R. Müller, —Structural and material approaches to bone tissue engineering in powder-based three-dimensional printing,|| *Acta biomaterialia*, vol. 7, no. 3, pp. 907–920, 2011.
- [45] H. Chen, Q. Wei, S. Wen, Z. Li, and Y. Shi, -Flow behavior of powder particles in layering process of selective laser melting: Numerical modeling and experimental verification based on discrete element method,|| *International Journal of Machine Tools and Manufacture*, vol. 123, pp. 146–159, 2017.
- [46] B. Utela, D. Storti, R. Anderson, and M. Ganter, —A review of process development steps for new material systems in three dimensional printing (3dp),|| *Journal of Manufacturing Processes*, vol. 10, no. 2, pp. 96–104, 2008.
- [47] A. Butscher, M. Bohner, C. Roth, A. Ernstberger, R. Heuberger, N. Doebelin, P. R. von Rohr, and R. Müller, -Printability of calcium phosphate powders for three-dimensional printing of tissue engineering scaffolds,|| *Acta biomaterialia*, vol. 8, no. 1, pp. 373–385, 2012.
- [48] Z. Zhou, F. Buchanan, C. Mitchell, and N. Dunne, -Printability of calcium phosphate: calcium sulfate powders for the application of tissue engineered bone scaffolds using the 3d printing technique,|| *Materials Science and Engineering: C*, vol. 38, pp. 1–10, 2014.
- [49] S. Mandal, S. Meininger, U. Gbureck, and B. Basu, -3d powder printed tetracalcium phosphate scaffold with phytic acid binder: Fabrication, microstructure and in situ x-ray tomography analysis of compressive failure,|| *Journal of Materials Science: Materials in Medicine*, vol. 29, no. 3, pp. 1–18, 2018.
- [50] G. A. Fielding, A. Bandyopadhyay, and S. Bose, -Effects of silica and zinc oxide doping on mechanical and biological properties of 3d printed tricalcium phosphate tissue engineering scaffolds,|| *Dental Materials*, vol. 28, no. 2, pp. 113–122, 2012.
- [51] S. Tarafder, V. K. Balla, N. M. Davies, A. Bandyopadhyay, and S. Bose, -Microwave-sintered 3d printed tricalcium phosphate scaffolds for bone tissue engineering,|| *Journal of tissue engineering and regenerative medicine*, vol. 7, no. 8, pp. 631–641, 2013.
- [52] H. Seitz, U. Deisinger, B. Leukers, R. Detsch, and G. Ziegler, -Different calcium phosphate granules for 3-d printing of bone tissue engineering scaffolds,|| *Advanced Engineering Materials*, vol. 11, no. 5, pp. B41–B46, 2009.
- [53] Z. Ge, X. Tian, B. C. Heng, V. Fan, J. F. Yeo, and T. Cao, -Histological evaluation of osteogenesis of 3d-printed poly-lactic-co-glycolic acid (plga) scaffolds in a rabbit model,|| *Biomedical materials*, vol. 4, no. 2, p. 021001, 2009.
- [54] Y. Shanjani, J. A. De Croos, R. M. Pilliar, R. A. Kandel, and E. Toyserkani, -Solid freeform fabrication and characterization of porous calcium polyphosphate structures for tissue engineering purposes,|| *Journal of Biomedical Materials Research Part B: Applied Biomaterials*, vol. 93, no. 2, pp. 510–519, 2010.
- [55] P. De Aza, A. De Aza, and S. De Aza, -Crystalline bioceramic materials,|| *Bol. Soc. Esp. Ceram*, vol. 44, no. 3, pp. 135–145, 2005.
- [56] S. Maity, -Use of nanostructured materials in soft tissue engineering,|| in *Nanobiomaterials*. Elsevier, 2018, pp. 465–480.
- [57] J. Venkatesan, S. Anil, and S. S. Murugan, -3d bioprinted alginate-based biomaterials for bone tissue engineering,|| 2020.  
—Bioactive materials for soft tissue repair,|| *Frontiers in Bioengineering and Biotechnology*, vol. 9, p. 94, 2021.
- [58] S. Romanazzo, T. G. Molley, S. Nemec, K. Lin, R. Sheikh, J. J. Gooding, B. Wan, Q. Li, K. A. Kilian, and I. Roohani, -Synthetic bone-like structures through omnidirectional ceramic bioprinting in cell suspensions,|| *Advanced Functional Materials*, vol. 31, no. 13, p. 2008216, 2021.
- [59] P. Shende and R. Trivedi, -3d printed bioconstructs: regenerative modulation for genetic expression,|| *Stem Cell Reviews and Reports*, pp. 1–12, 2021.
- [60] M. Albanna, K. W. Binder, S. V. Murphy, J. Kim, S. A. Qasem, W. Zhao, J. Tan, I. B. El-Amin, D. D. Dice, J. Marco *et al.*, -In situ bioprinting of autologous skin cells accelerates wound healing of extensive excisional full-thickness wounds,|| *Scientific reports*, vol. 9, no. 1, pp. 1–15, 2019.
- [61] P. X. Ma, -Scaffolds for tissue fabrication,|| *Materials today*, vol. 7, no. 5, pp. 30–40, 2004.
- [62] J. D. Kretlow and A. G. Mikos, -Mineralization of synthetic polymer scaffolds for bone tissue engineering,|| *Tissue engineering*, vol. 13, no. 5, pp. 927–938, 2007.
- [63] A. Moradi, A. Dalilottojari, B. Pingguan-Murphy, and I. Djordjevic, -Fabrication and characterization of elastomeric scaffolds comprised of a citric acid-based polyester/hydroxyapatite microcomposite,|| *Ma- terials & Design*, vol. 50, pp. 446–450, 2013.

- [64] S. Ali Akbari Ghavimi, M. H. Ebrahimzadeh, M. Solati Hashjin, and N. A. Abu Osman, -Polycaprolactone/starch composite: Fabrication, structure, properties, and applications,|| *Journal of biomedical materials research Part A*, vol. 103, no. 7, pp. 2482–2498, 2015.
- [65] D. W. Hutmacher, -Scaffolds in tissue engineering bone and cartilage,|| *Biomaterials*, vol. 21, no. 24, pp. 2529–2543, 2000.
- [66] A. Moradi, -Development of bovine cartilage extracellular matrix as a potential scaffold for chondrogenic induction of human dermal fibroblasts,|| Ph.D. dissertation, University of Malaya, 2015.
- [67] C. Wu, Y. Zhou, W. Fan, P. Han, J. Chang, J. Yuen, M. Zhang, and Y. Xiao, -Hypoxia-mimicking mesoporous bioactive glass scaffolds with controllable cobalt ion release for bone tissue engineering,|| *Biomaterials*, vol. 33, no. 7, pp. 2076–2085, 2012.
- [68] M. Pei, J. Li, M. Shoukry, and Y. Zhang, -A review of decellularized stem cell matrix: a novel cell expansion system for cartilage tissue engineering,|| *Eur Cell Mater*, vol. 22, no. 333, p. 43, 2011.
- [69] Y. Qiang, P. Jiang, S.-B. Lu, Q.-Y. Guo, Z. Bin, L. Zhang, A.-y. Wang, W.-J. Xu, X. Qun, Y.-c. HU *et al.*, -Evaluation of an extracellular matrix-derived acellular biphasic scaffold/cell construct in the repair of a large articular high-load-bearing osteochondral defect in a canine model,|| *Chinese medical journal*, vol. 124, no. 23, pp. 3930–3938, 2011.
- [70] S. Koob, N. Torio-Padron, G. B. Stark, C. Hannig, Z. Stankovic, and G. Finkenzeller, -Bone formation and neovascularization mediated by mesenchymal stem cells and endothelial cells in critical-sized calvarial defects,|| *Tissue Engineering Part A*, vol. 17, no. 3-4, pp. 311–321, 2011.
- [71] S. Cowley and L. Anderson, -Hernias through donor sites for iliac-bone grafts,|| *JBJS*, vol. 65, no. 7, pp. 1023–1025, 1983.
- [72] K. Drzwińska, J. Kleczewska, M. Krasiński, B. Łapińska, and J. Sokołowski, -The influence of amorphous calcium phosphate addition on mechanical properties of the experimental light-cured dental composite,|| *Dental and Medical Problems*, vol. 53, no. 1, pp. 34–40, 2016.
- [73] J. Roether, A. R. Boccaccini, L. Hench, V. Maquet, S. Gautier, and R. Jérôme, -Development and in vitro characterization of novel biresorbable and bioactive composite materials based on polylactide foams and bioglass® for tissue engineering applications,|| *Biomaterials*, vol. 23, no. 18, pp. 3871–3878, 2002.
- [74] J. W. Lee, K. S. Kang, S. H. Lee, J.-Y. Kim, B.-K. Lee, and D.-W. Cho, -Bone regeneration using a microstereolithography-produced cross-linked poly (propylene fumarate)/diethyl fumarate photopolymer 3d scaffold incorporating bmp-2 loaded plga microspheres,|| *Biomaterials*, vol. 32, no. 3, pp. 744–752, 2011.
- [75] X. Wu, Q. Lian, D. Li, and Z. Jin, -Biphasic osteochondral scaffold fabrication using multi-material mask projection stereolithography,|| *Rapid Prototyping Journal*, 2019.
- [76] A. Moradi, F. Ataollahi, K. Sayar, S. Pramanik, P.-P. Chong, A. A. Khalil, T. Kamarul, and B. Pingguan-Murphy, -Chondrogenic potential of physically treated bovine cartilage matrix derived porous scaffolds

- on human dermal fibroblast cells,|| *Journal of biomedical materials research Part A*, vol. 104, no. 1, pp. 245–256, 2016.
- [77] K. Lin, J. Liu, J.-M. Wu, Y. Sun, F. Li, Y. Zhou, and Y. Shi, —Selective laser sintered nano-ha/pdlla composite microspheres for bone scaffoldsapplications,|| *Rapid Prototyping Journal*, 2020.
- [78] J. M. Williams, A. Adewunmi, R. M. Schek, C. L. Flanagan, P. H. Krebsbach, S. E. Feinberg, S. J. Hollister, and S. Das, —Bone tissue engineering using polycaprolactone scaffolds fabricated via selective laser sintering,|| *Biomaterials*, vol. 26, no. 23, pp. 4817–4827, 2005.
- [79] S. Lohfeld, S. Cahill, V. Barroon, P. McHugh, L. Duerksen, L. Kreja, C. Bausewein, and A. Ignatius, —Fabrication, mechanical and in vivo performance of polycaprolactone/tricalcium phosphate composite scaf-folds,|| *Acta biomaterialia*, vol. 8, no. 9, pp. 3446–3456, 2012.
- [80] S. J. Kalita, S. Bose, H. L. Hosick, and A. Bandyopadhyay, —Develop- ment of controlled porosity polymer-ceramic composite scaffolds via fused deposition modeling,|| *Materials Science and Engineering: C*, vol. 23, no. 5, pp. 611–620, 2003.
- [81] J. Wu, N. Chen, F. Bai, and Q. Wang, —Preparation of poly (vinyl alcohol)/poly (lactic acid)/hydroxyapatite bioactive nanocomposites forfused deposition modeling,|| *Polymer Composites*, vol. 39, pp. E508–E518, 2018.
- [82] R. M. Biltz and E. D. Pellegrino, —The chemical anatomy of bone: I. a comparative study of bone composition in sixteen vertebrates,|| *JBJS*, vol. 51, no. 3, pp. 456–466, 1969.
- [83] P. Ducheyne and Q. Qiu, —Bioactive ceramics: the effect of surface reactivity on bone formation and bone cell function,|| *Biomaterials*, vol. 20, no. 23-24, pp. 2287–2303, 1999.
- [84] S. Samavedi, A. R. Whittington, and A. S. Goldstein, —Calcium phosphate ceramics in bone tissue engineering: a review of properties and their influence on cell behavior,|| *Acta biomaterialia*, vol. 9, no. 9, pp. 8037–8045, 2013.
- [85] S. Bose, M. Roy, and A. Bandyopadhyay, —Recent advances in bone tissue engineering scaffolds,|| *Trends in biotechnology*, vol. 30, no. 10, pp. 546–554, 2012.
- [86] T. L. Arinzeh, T. Tran, J. Mcalary, and G. Daculsi, —A comparative study of biphasic calcium phosphate ceramics for human mesenchymalstem-cell-induced bone formation,|| *Biomaterials*, vol. 26, no. 17, pp. 3631–3638, 2005.
- [87] Y. K. Modi and K. K. Sahu, —Process capability analysis of binder jetting 3d printing process for fabrication of calcium sulphate based porous bone scaffolds,|| *Australian Journal of Mechanical Engineering*, pp. 1–9, 2020.
- [88] M. Castilho, C. Moseke, A. Ewald, U. Gbureck, J. Groll, I. Pires, J. Teßmar, and E. Vorndran, —Direct 3d powder printing of biphasic calcium phosphate scaffolds for substitution of complex bone defects,|| *Biofabrication*, vol. 6, no. 1, p. 015006, 2014.
- [89] P. Quadbeck, R. Hauser, K. Kümmel, G. Stanké, G. Stephani, B. Niess, S. Roßbläser, and B. Wegener, —Pm bio materials : Iron based cellular metals for degradable synthetic bone replacement,|| in *European Congressand Exhibition on Powder Metallurgy. European PM Conference Proceedings*. The European Powder Metallurgy Association, 2010, p. 1.
- [90] Z. Li, X. Gu, S. Lou, and Y. Zheng, —The development of binary mg–ca alloys for use as biodegradable materials within bone,|| *Biomaterials*, vol. 29, no. 10, pp. 1329–1344, 2008.
- [91] F. Witte, V. Kaese, H. Haferkamp, E. Switzer, A. Meyer-Lindenberg, C. Wirth, and H. Windhagen, —In vivo corrosion of four magnesium alloys and the associated bone response,|| *Biomaterials*, vol. 26, no. 17, pp. 3557–3563, 2005.
- [92] M. P. Staiger, A. M. Pietak, J. Huadmai, and G. Dias, —Magnesium and its alloys as orthopedic biomaterials: a review,|| *Biomaterials*, vol. 27, no. 9, pp. 1728–1734, 2006.
- [93] G. B. Stroganov, E. M. Savitsky, N. M. Tikhova, V. F. Terekhova, M. V. Volkov, K. M. Sivash, and V. S. Borodkin, —Magnesium-base alloy for use in bone surgery,|| Aug. 29 1972, uS Patent 3,687,135.
- [94] J. Jansen, J. Vehof, P. Ruhe, H. Kroese-Deutman, Y. Kuboki, H. Takita, E. Hedberg, and A. Mikos, —Growth factor-loaded scaffolds for bone engineering,|| *Journal of Controlled Release*, vol. 101, no. 1-3, pp. 127–136, 2005.
- [95] J. E. Adams, M. E. Zobitz, J. S. Reach Jr, K.-N. An, D. G. Lewallen, and S. P. Steinmann, —Canine carpal joint fusion: a model for four- corner arthrodesis using a porous tantalum implant,|| *The Journal of hand surgery*, vol. 30, no. 6, pp. 1128–1135, 2005.

- [96] Y. Okazaki, —A new ti–15zr–4nb–4ta alloy for medical applications,|| *Current Opinion in Solid State and Materials Science*, vol. 5, no. 1, pp. 45–53, 2001.
- [97] J. Bobyn, G. Stackpool, S. Hacking, M. Tanzer, and J. Krygier, —Characteristics of bone ingrowth and interface mechanics of a new porous tantalum biomaterial,|| *The Journal of bone and joint surgery. British volume*, vol. 81, no. 5, pp. 907–914, 1999.
- [98] J. M. Sobral, S. G. Caridade, R. A. Sousa, J. F. Mano, and R. L. Reis, -Three-dimensional plotted scaffolds with controlled pore size gradients: effect of scaffold geometry on mechanical performance and cell seeding efficiency,|| *Acta biomaterialia*, vol. 7, no. 3, pp. 1009– 1018, 2011.
- [99] M. Domingos, F. Intranuovo, T. Russo, R. De Santis, A. Gloria, L. Am- brosio, J. Ciurana, and P. Bartolo, -The first systematic analysis of 3d rapid prototyped poly ( $\epsilon$ -caprolactone) scaffolds manufactured through biocell printing: the effect of pore size and geometry on compressive mechanical behaviour and in vitro hmsc viability,|| *Biofabrication*, vol. 5, no. 4, p. 045004, 2013.
- [100] T. Serra, J. A. Planell, and M. Navarro, -High-resolution pla-based composite scaffolds via 3-d printing technology,|| *Acta biomaterialia*, vol. 9, no. 3, pp. 5521–5530, 2013.
- [101] S.-I. Roohani-Esfahani, P. Newman, and H. Zreiqat, -Design and fab- rication of 3d printed scaffolds with a mechanical strength comparable to cortical bone to repair large bone defects,|| *Scientific reports*, vol. 6, no. 1, pp. 1–8, 2016.
- [102] M. Domingos, F. Chiellini, A. Gloria, L. Ambrosio, P. Bartolo, and E. Chiellini, -Effect of process parameters on the morphological and mechanical properties of 3d bioextruded poly ( $\epsilon$ -caprolactone) scaffolds,|| *Rapid Prototyping Journal*, 2012.
- [103] J. E. Trachtenberg, P. M. Mountzaris, J. S. Miller, M. Wettergreen, F. K. Kasper, and A. G. Mikos, -Open-source three-dimensional printing of biodegradable polymer scaffolds for tissue engineering,|| *Journal of biomedical materials research Part A*, vol. 102, no. 12, pp. 4326–4335, 2014.
- [104] L. Ruiz-Cantu, A. Gleadall, C. Faris, J. Segal, K. Shakesheff, and J. Yang, -Characterisation of the surface structure of 3d printed scaffolds for cell infiltration and surgical suturing,|| *Biofabrication*, vol. 8, no. 1, p. 015016, 2016.
- [105] J. de Ciurana, L. Sereno, and È. Vallès, -Selecting process para m eters in rerap additive manufacturing system for pla scaffolds manufacture,|| *Procedia Cirp*, vol. 5, pp. 152–157, 2013.
- [106] M. Too, K. Leong, C. Chua, C. Cheah, and S. Ho, -Feasibility of tissue engineering scaffold fabrication using fused deposition modelling,|| in *The Seventh Australian and New Zealand Intelligent Information Systems Conference, 2001*. IEEE, 2001, pp. 433–438.
- [107] M. Too, K. Leong, C. Chua, Z. Du, S. Yang, C. Cheah, and S. L. Ho, -Investigation of 3d non-random porous structures by fused deposition modelling,|| *The International Journal of Advanced Manufacturing Technology*, vol. 19, no. 3, pp. 217–223, 2002.
- [108] K. C. Ang, K. F. Leong, C. K. Chua, and M. Chandrasekaran, -Investi- gation of the mechanical properties and porosity relationships in fused deposition modelling-fabricated porous structures,|| *Rapid Prototyping Journal*, 2006.
- [109] I. Zein, D. W. Hutmacher, K. C. Tan, and S. H. Teoh, —Fused depo- sition modeling of novel scaffold architectures for tissue engineering applications,|| *Biomaterials*, vol. 23, no. 4, pp. 1169–1185, 2002.
- [110] J. Korpela, A. Kokkari, H. Korhonen, M. Malin, T. Närhi, and J. Sep p a la, -B i o d e g r a d a b l e a n d b i o c a t i v e p o r o u s s c a f f o l d s t r u c t u r e s p r e p a r e d u s i n g f u s e d d e p o s i t i o n m o d e l i n g ,|| *Journal of Biomedical Materials Research Part B: Applied Biomaterials*, vol. 101, no. 4, pp. 610–619, 2013.
- [111] A. Gleadall, D. Visscher, J. Yang, D. Thomas, and J. Segal, -Review of additive manufactured tissue engineering scaffolds: relationship between geometry and performance,|| *Burns & trauma*, vol. 6, 2018.
- [112] L. Moroni, J. De Wijn, and C. Van Blitterswijk, -3d fiber-deposited scaffolds for tissue engineering: influence of pores geometry and architecture on dynamic mechanical properties,|| *Biomaterials*, vol. 27, no. 7, pp. 974–985, 2006.
- [113] B. Tellis, J. Szivek, C. Bliss, D. Margolis, R. Vaidyanathan, and P. Calvert, -Trabecular scaffolds created using micro ct guided fused deposition modeling,|| *Materials Science and Engineering: C*, vol. 28, no. 1, pp. 171–178, 2008.
- [114] J. E. Dennis, S. E. Haynesworth, R. G. Young, and A. I. Caplan, -Osteogenesis in marrow-derived mesenchymal cell porous ceramic

# **Neonatal Monitoring System: Review and Future Directions**

**Prashant Jani, Dr. Seema Mahajan**

**Abstract :**A lots of premature babies' loss their lives due to Improper monitoring inside the neonatal Incubator worldwide. An Incubator is an electrical equipment in which any premature infant kept and monitored on certain bio-logical parameters and these parameters ensure baby's safety rate as well as death rate too. For monitoring these parameters health centers use some sensors which are directly connected with infant and represent it on display. Any irregularity and abnormal activity will be detected via alarm. In this Survey, we are focusing on existing biological parameters in incubator, analysis technique used for that, alarm system for attention in real time system and transmission technique for the same.

**Keywords:** IoT, Incubator, Neonate, Premature Baby

## **1. Introduction:**

The recent emerging in IoT technology for numerous applications [1, 2] crushes the traditional sensing of adjoining environments. It is developing very rapidly and attractive a major source for discussion of communication among different sensors including dream sensors over smart devices such as smartphones, smart cities etc. The neonatal period is the most vulnerable period for child survival and a critical phase for later development [3]. Maintaining a normal body temperature (BT) is thus a critical function for the survival of the newborn baby (NB). However, especially for preterm, lowbirth weight, and sick NBs, utensils for temperature instruction may easily be stunned, leading to hypothermia, cold stress, metabolic deterioration, and, ultimately, death [4]. Improving temperature solidity for sick and preterm infants, thus, continues to be an area of precedence in the neonatal intensive care unit (NICU).

A cool incubator system has been projected in [5] that continuously monitors and sends the measurements to the cloud. The system involves of Arduino controller, several sensors, Wi-Fi connection, and cloud storing and processing system. A wireless smart sensor system has been proposed in [6] for infant incubator system to remotely screen the infants utilizing different sensors, ZigBee wireless protocol and IEEE 1451 communication edge. Currently, Most of NICU are well-resourced with progressive machines and devices to monitor which are designed for the special condition of the infants. Some of the checking equipment often used in NICU are cardiorespiratory monitor, blood pressure monitor, temperature, pulse oximeter, transcutaneous oxygen and carbon-di-oxide monitor, Ultrasound, X-Ray, etc. With Internet of Things, medical occupation has listed and technologists are trying to merge the various situation together to build a strong monitoring system. Connecting things to internet with standard rules and suitable architectural variations expedites continuous health monitoring for all day and any place. In this context several incubator monitoring classification for neonatal care are argued in literature review.

## **2. Literature Review:**

There are so many factors that should have to be considered in baby's nourishment and specially health centers and NICU has to monitored some parameters as far as baby's health concerned. Few of them are listed here:

Prashant Jani  
Department of Computer Science, Indus University, Gujarat, INDIA  
E-mail:- janiprashant9@gmail.com

Dr. Seema Mahajan  
Department of Computer Science, Indus University, Gujarat, INDIA  
E-mail :- ce.hod@indusuni.ac.in

**Table 1: Literature Review**

Sr. No.	1	2	3	4	5
Investigator	[7]	[8]	[9]	[10]	[11]
Input Parameters Used	Temperature, Humidity	Body Temperature	Temperature, Heart beat	Temperature, Pulse rate	weight, temperature, and head circumference.
Findings of the study	This paper that would enable the medical specialist to monitor and control temperature and humidity of incubator.	In this Paper, Author using Arduino, temperature sensor, monitoring or controlling the Temperature of the baby's body.	Raspberry Pi is used for monitoring and controlling the whole system. LCD is used to display humidity, temperature, heart beat and respiration of neonatal.	The Neonatal Health Monitoring System is a tool that can measure, display and record human features such as body temperature, pulse rate and other health-related criteria.	A Growth parameters that parents often pay attention and monitoring for their infants are weight and temperature to determine the health condition of the infant.

#### Various Parameters for infant monitoring in incubator:

After reviewing existing study, here are some parameters that has to be monitored by every NICU through IoT are listed below:

##### 1. Infant Body Temperature

Constantly taking infant's body temperature and giving notification if any abnormal activity detected.

##### 2. Pulse Rate

Through Pulse sensor it returns infant's heart rate continuously and it is monitored on display.

##### 3. Infant Body Weight

Body weight of the premature plays a vital role in early days because it helps to predict or understand the overall wealth progress of an infant

##### 4. Infant Humidity

Real time monitoring system is used to measure a humidity of an infant.

##### 5. Incubator Temperature

This temperature is purely depending and set after infant's body temperature measured. Generally, NICU kept it around 82-86 Degree F.

##### 6. Blood Oxygen Level

It can be read by small probe putting in newborn's hand or foot and generally, it can be kept 95% to 98%.

##### 7. Sound Recognition

Through sound recognition sensor NICU can recognize the infant's sound response and detection ability.

### **3. Analysis technologies Used:**

Incubators all over the globe were made using different technologies. These technologies are responsible for data storage, data transmission.

#### a) Wireless Transmission

In this system [11] The skin temperature of child, temperature and humidity of the incubator, Oxygen and Carbon-di- Oxide concentration in incubator weight, heartbeat, Blood pressure and oxygen saturation are monitored. All these are conveyed to computer via network (internet). Infant Folks can spot their infant's nursing situation in their office or family by the network. A processer is official to browse and download the vision-frequency picture and monitoring data. Author [12] has designed a method to display the new-born infant's biological data remotely outside NICU. It is finished by providing a modest mobile application where data can be supervised live. To create communication between vital sign monitor and the remote server Wi-Fi and 3G used.

#### b) Wireless PLC System

Author Eugene T. Puzio [13] has intended an incubator wherever the Temperature and humidity of the incubator and Skin temperature of infant is dignified. The Mechanisms used are Blue light lamps, Ventilation holes, controller, display screen, control buttons and buzzer with PLC system and Wireless Transmission module.

#### c) Cloud Storage Based Technology

Cloud computing uses Virtual Machine storage or an application in its place of building computer substructures. An improved system designed by Mr. Soukaina Brangui [14] the author monitors the temperature and weight data in real-time. Cloud server is used to store the data. A variety of data being uploaded on cloud like Weight, Pulse rate, Temperature. Alarm or notification also has been generated using cloud server.

#### d) Bluetooth technology

Wei Chen [15] has deliberate system with wireless transmission technology. BlueSMiRF and Arduino pro mini were used. An infant jacket is considered for the baby to monitor in non-invasively. The system data are conveyed and traditional from multiple sensors within specific range. For this system temperature sensor and display LCD were used.

#### e) Respiratory sensor using fiber optics technology

Author Arika Dhia [16] has created a design of respiratory sensor using fiber optics technology for this incubator presentation. This sensor functions based on the light intensity change due to the thorax movement. This movement is happened during the respiration. The data is handled in Arduino Uno microcontroller and it is measured real time and showed in LCD.

#### f) Fuzzy Inference System

In 2019, Authors [17] introduces the optimization of the egg incubator system using fuzzy inference and based on Internet of Things (IoT). So the egg hatching system is more steady when it warms up the temperature at the incubator and can be measured via the internet network. The results gained by running IoT-based incubator system on the 38 OC set point, system are successively optimally.

### **4. Abnormal neonatal Activity detection:**

Mostly, Incubator system were designed to read the data and monitor the data. If any abnormal activity happen in between it indicates notifications using alarm detection system. Different types of alert system used for indication. If any irregularity occurs, alarm is directed through Short-Message Transmitting module (SMS) to hospital staff's phone. In this system [18] Real time monitoring of temperature and humidity of the incubator is measured. The Modules used are WIFI, Camera, Battery, Micro Controller, Captive touch screen. In some abnormal situation data is also reported on family members mobile phone too using Internet via Arduino. Some image based algorithm constantly sending Neonatal images to decided cell phones or computers for monitoring purpose. Any of the parameters falls down or goes to beyond limits then alarm ringed on doctor's or respective NICU staff members phone or device.

## **Conclusion & Future Scope:**

A design of incubator is most important thing as far as infant's health concerned. So design must be well structured and efficient enough. The system design must be affordable and effective manner. All the parameters and technologies used inside incubator must be worked efficiently to maintain infant's health records.

In future, more health parameters can be added and analyzed for better health prediction of an infant. Also, any classification technique will be applied on infant's data for health prediction.

## **References:**

- [1] S. Khan, K. Muhammad, S. Mumtaz, S. W. Baik, and V. H. C. de Albuquerque, "Energy-efficient deep CNN for smoke detection in foggy IoT environment," IEEE Internet of Things Journal, (2019)
- [2] T. Hussain, K. Muhammad, J. Del Ser, S. W. Baik, and V. H. C. de Albuquerque, "Intelligent Embedded Vision for Summarization of Multi-View Videos in IIoT," IEEE Transactions on Industrial Informatics (2019)
- [3] D. Askin, "The high-risk newborn and family. Wong's nursing care of infants and children, 6th ed., Hockenberry MJ, and Wilson D. St. Louis: Mosby," ed: Elsevier (2007)
- [4] A. R. Laptook and M. Watkinson, "Temperature management in the delivery room," (in eng), Semin Fetal Neonatal Med, vol. 13, no. 6, pp. 383-91, (Dec 2008)
- [5] D Sivamani, R Sagayaraj, R Jai Ganesh and A. Nazar Ali. —Smart incubator using internet of things.|| International Journal for Modern Trends in Science and Technology, Vol. 4, no. 9, pp 23-27, (2018)
- [6] Wu, Guoguang, and Shangwen Chen. -Design of wireless smart sensor module for infant incubator test.|| In 2016 5th International Conference on Measurement, Instrumentation and Automation (ICMIA 2016). Atlantis Press, (2016)
- [7] Shehla Inam, Muhammad Farrukh Qureshi, Faisal Amin, Muhammad Akmal, Muhammad Ziaur Rehman —Android based Internet Accessible Infant Incubator.|| IEEE 978-1-7281-2334-9/19, (2019)
- [8] Megha Koli , Purvi Ladge, Bhavpriya Prasad, Ronak Boria, Prof. Nazahat J. Balur|| INTELLIGENT BABY INCUBATOR|| Proceedings of the 2nd International conference on Electronics, Communication and Aerospace Technology (ICECA, 2018)
- [9] Pravin Kshirsagar, Varsha More, Vaibhav Hendre, Pranav Chippalkatti and Krishan Paliwal -IOT Based Baby Incubator for Clinicl ICCCE , (2019)
- [10] Sheril Amira O.1, Nor Asmira H.1, Tengku Nadzlin T. I.2, Mohd Helmy A. W.1,Omar A.H.3, Muhammad Shukri A.2 & Ahmad Alabqari M.R. -Neonatal Health Monitoring System with IOT Application|| Journal of Physics: Conference Series, JICETS (2019)
- [11] -Network monitoring device for nursing baby||;2006-06-14; Patent no:CN200960246Y
- [12] Robert Greer, Chris Olivier., -Remote Real-Time Monitoring and Analysis of Neonatal Graduate Infants||,
- [13] Anthony McClain, 364 Shadetree La., -Incubator system with monitoring and communication capabilities||; (Jun. 25, 2002)
- [14] —Cloud-based monitoring system and risk management for premature new-borns||, José Ilton de Oliveira Filho and Otacilio da Mota Almeida Electrical Engineering Department Federal University of Piauí Teresina, Brazil
- [15] Wei Chen, Son Tung Nguyen, Roland Coops., -Wireless Transmission Design for Health Monitoring at Neonatal Intensive Care Units||; Department of Industrial design, Eindhoven University of Technology, Den Dolech 2,5612 AZ, The Netherlands.
- [16] Arika Dhia, Kresna Devara., -Design of Fiber Optic Based Respiratory Sensor for New-born Incubator Application||, API Conference Proceedings 1933,040018 (2018)
- [17] Renny Rakhmawati, Irianto, Farid Dwi Murdianto, Atabik Luthfi, Aviv Yuniar Rahman -Thermal Optimization on Incubator using Fuzzy Inference System based IoT|| 978-1-5386-8448-1/19 (2019)

# **A Review of Applications of Biopolymeric Membranes in Removal of Organic Pollutant and Micro pollutants from Wastewater.**

**Susmita Sharma, and Sanjana Chugh**

**Abstract:** This paper presents a detailed analysis of biopolymeric membrane applications in the removal of micropollutants from wastewater. In this paper consequences of using non-biodegradable membrane and benefits of using nanostructured biodegradable polymeric membranes have been discussed. When compared to non-biodegradable polymers and degradable biopolymers, these biopolymer materials have the following advantages: renewability, biocompatibility, biodegradability, and cost-effectiveness. Modifications to biopolymeric membranes have also been thoroughly discussed. Recent improvements in the use of nanofillers to stabilize and improve the performance of biopolymeric membranes in the removal of organic pollutants have been considered. Biopolymeric membranes are used in removal of Organic colours (methyl blue, Congo red, azo dyes), crude oil, hexane, medicinal compounds such as tetracycline and micropollutants. The characteristics of biopolymeric membranes were also discussed.

**Keywords:** micropollutants; water treatment; biodegradable; biopolymer; polymeric membrane

## **1. Introduction**

The treated effluents from waste water treatment plants (WWTPs) have been discovered to frequently include contaminants that are organic micropollutants [1]. Concerns concerning the harmful consequences of micropollutants have been raised by certain studies. Therefore, improved technology for the cleanup of organic micro contaminants should be developed. Due to their extended half-lives and inability to degrade, the majority of polymeric membranes may be detrimental to the environment. The use of biopolymers in membrane technology applications is covered in this review study. In order to properly treat water contaminated with organic micropollutants, this paper evaluates all newly published membrane filtration-based approaches.

Biopolymers are synthetic polymers that come from living things rather than fossil fuels, like plants and bacteria [3]. These biopolymers are both artificial and organic [4]. The synthetic biopolymers can be chemically generated from synthetic monomers or modified from natural polymers. Natural biopolymers, on the other hand, are derived from natural sources [4,5]. Cellulose, starch, chitosan, collagen, fibrinogen, chitin, alginate, and carrageenan are among the biopolymers derived from natural sources. [4,5,6]. When used as membranes for water treatment, biopolymers' hydrophilicity improves membrane fouling resistance and water permeability [7,10]. It is preferable made possible by the hydrophilic functional groups that a thin layer of water can form on membrane surfaces. Foulants cannot settle because of this preferred development on the hydrophilic membrane surfaces. This phenomenon thus lessens membrane fouling [10]. Additionally, cellulose has a contact angle range of 20° to 30° and is quite hydrophilic. Fundamentally, the presence of hydroxyl functional groups is what causes the cellulose to be hydrophilic. Hydrogen interactions between these hydroxyl functional groups and water allow for the preferential attachment of water molecules, which increases water permeability [7].

---

Susmita Sharma

Anand International College of Engineering, Jaipur (Raj).

EmailAddress:Susmita.sharma@anandice.ac.in

Department of Applied Science

Sanjana Chugh

Anand International College of Engineering, Jaipur (Raj).

EmailAddress:Sanjana.chugh@anandice.ac.in

Department of Applied Science

## **A Review of Applications of Biopolymeric Membranes in Removal of Organic Pollutant and Micro pollutants from Wastewater**

Additionally, biopolymers are taken seriously because of their capacity to break down after being dumped in landfills [4]. Fortunately, the biodegradation of biopolymers does not produce any hazardous byproducts. Humus, carbon dioxide, biomass, and methane are examples of known by-products. Therefore, using biopolymers in water treatment applications becomes wise [8]. Numerous scholars have created numerous strategies for wastewater treatment remediation. These technologies include membrane technology, adsorption, filtering, and advanced oxidation processes such ozonation, photocatalysis, and biodegradation [11,12]. These technologies must, however, be extremely effective, efficient, and cost-effective [13]. Because membranes have shown to be successful at purifying wastewater and pose no environmental risk, they are preferable to traditional water treatment methods [14]. A membrane serves as a barrier during separation, permitting water molecules to pass through while blocking the passage of contaminants [15]. Non-biodegradable polymeric membranes have been made using a wide range of polymers. Notably, non-biodegradable materials are used to synthesis and construct the majority of commercial membranes. Polyvinylidene fluoride (PVDF), polysulfone (PSf), polyethersulfone (PES), polyphenylsulfone, polypropylene, polyvinyl alcohol, polystyrene, and poly(1,5-diaminonaphthalene) are examples of commonly used non-biodegradable polymers[10,16,17,18]. The majority of synthetic polymers used in membrane manufacture are non-biodegradable and have hydrophobic qualities, which makes them vulnerable to membrane fouling and reduces water permeability once micropollutant foulants are formed on the membrane surfaces. As a result, there will be a greater requirement for routine membrane cleaning, which will raise the cost of maintaining the membrane system [10,16,17,20]. Biopolymers, on the other hand, are biodegradable, compostable, cost-effective, non-toxic, biocompatible, and hydrophilic [21,24]. Additionally, hydrophilic materials greatly increase the rejection capacity and effectiveness of biopolymer membranes, because biopolymers are known to be hydrophilic. Therefore, because they are ecologically safe, biopolymers can replace the potentially harmful and non-biodegradable polymers employed as an alternative in the production of membranes [21,22,25,26]. The efficient development of removal and neutralisation techniques for organic micro contaminants is widely desired [27]. Because of their inherent simplicity and effectiveness, even at high pollutant concentrations, membrane filtration methods, for instance, have been taken into consideration. Additionally, they produce very little solid waste. Additionally, membranes frequently eliminate almost all varieties of salts, minerals, and colours [28].

As a result, membrane technology offers good potential for treating organic pollution [29]. Ultrafiltration (UF), nanofiltration (NF), forward osmosis (RO), and reverse osmosis (FO) membranes are some of the several membrane technologies. Numerous micro pollutant pollutants can be eliminated with these membrane methods. For instance, reverse osmosis and nanofiltration membranes are frequently used to remediate micropollutants and have shown some efficacy in remediating micropollutants [27,30]. For the retention of multivalent ions and organic molecules at relatively low operation pressure, NF membranes have been utilised [29]. However, even at low concentrations, RO membranes can remove micropollutants and monovalent salts from water. Due to their versatility, polymeric membranes are frequently used in the manufacture of membranes. To achieve maximal water permeability and micropollutant rejection performances, membrane fabrication processing parameters are developed and put into practise [31]. As a result, by adjusting the contact time parameters, water source type, micropollutant concentrations, and membrane construction elements, it is possible to experimentally manipulate the removal efficiencies of these polymeric membranes [2]. Over time, these non-biodegradable and non-renewable polymers could affect the environment. This is due to the fact that after their service half-life, they are often disposed of in landfills and sometimes end up in aquatic environments. These materials are occasionally burned, which causes secondary pollution like global warming [16,32]. As a result, environmental contamination and landfill capacity are both at an all-time high. Therefore, putting non-biodegradable membrane materials on top of the pressure from environmental contamination is harmful. In order to prevent secondary contamination, it is necessary to create fully biodegradable materials that may quickly disintegrate totally after usage. Starch, pollutants, cellulose, chitosan, alginate, and proteins are examples of natural biopolymers that have been utilised in the filtration of water [5]. Such polymers have been created from garbage and transformed into useful products like cellulose, which has reduced waste [8].

## **2. Biopolymer membrane in water treatment**

Due to the incredible qualities of biopolymers, using natural polymers for membrane synthesis, fabrication, and production to create fully biodegradable membrane materials becomes perfect and alluring [33]. The creation of membranes for the purification of water has utilised pure biopolymers. You can use these biopolymers and biomembranes as adsorbents. For instance, cellulose biopolymers and its derivatives are being made into ultra-,

nano-, and osmotic membranes to be used for water filtering. The removal of pollutants including colours [5,7,9,32], microbes [7,36], heavy metals and salts [5,7,37], medicines [7,30], pesticides, and oil/grease [7,32] is notable usage of these membranes. However, The features and performance aspects of biopolymers still need to be improved. [8].Chlorophenoxyacetic acid herbicides were eliminated from water by Pandiarajan et al. [38] using orange peel-activated carbon and adsorption-desorption technology. As a result, this bio-sourced activated carbon effectively adsorbs herbicides containing chlorophenoxyacetic acid from water. Membranes can be adapted from these biopolymers. For instance, due to their abundance of polysaccharides, cellulose polymers have been widely used in water treatment membrane applications. As a result, the polymers are practical and have applications in the manufacture of textiles, paper, pharmaceuticals, and membrane technology [7,39]. Blend membranes, nanofibrous membranes, mixed matrix membranes, imprinted membranes, and thin film composite membranes are a few examples of the several biopolymer-based membrane types that can be created [7]. For the elimination of cationic contaminants by metal chelation, Janesh et al. [40] created all biopolymer-based membranes based on chitin-glucan, chitosan-glucan, and chitin-glucan with cellulose. Additionally, Abdellah et al. [41] employed membranes made of cellulose mixed with catechins to remove DMF through solvent permeation. The membrane had a molecular weight limit of  $500 \text{ g mol}^{-1}$  and a high DMF permeability of  $1.2 \text{ L m}^{-2} \text{ h}^{-1} \text{ bar}$ . The difficulty with employing biopolymers to make membranes, such as cellulose, is that they are insoluble in ordinary solvents. But N-methyl-morpholine-N-oxide can be used to dissolve cellulose (NMMO). Additionally, there are other dual-solvent systems that can be used to dissolve cellulose, including ammonium fluorides/dimethyl sulfoxide, hydrazine/thiocyanate, N-methylmorpholine-N-oxide (NMMO), and dimethyl sulfoxide/lithium chloride (LiCl) [7,23,32,42]. (DMSO). Fortunately, cellulose mixes well with other biopolymers, which enables scientists to develop novel bio-based products. In contrast to functionalized or modified biopolymers, however, pure biopolymers have a restricted potential for adsorption [7]. Therefore, biopolymer modification is still the best option for enhancing adsorption-desorption capabilities, biopolymer compatibility, and solvent solubilities.

#### 4.1. Development in Biopolymer Preparation and Functionalization for Water Treatment

Mechanical instability is generally a drawback and restriction of biopolymers in water treatment applications [16,43]. Due to the high pressures involved in water filtration, biopolymers' weak mechanical characteristics limit their usage in this process. The biopolymeric membranes can thus rupture [43]. These qualities can, however, be improved through modification procedures [8]. As a result, the adjustments enhance not only the mechanical stability but also the water permeability, antifouling, and self-cleaning capabilities of the resulting membranes [1]. In order to achieve the best separation performance, including increased flux, swelling capacity, penetration, and better selectivity, additional research has been done to understand the impact of blending different types of synthetic or natural polymers with biopolymers [7]. New functional groups must be added to biopolymers in order to increase their adsorptive-desorptive attraction for organic pollutants like cationic dyes, as shown in Scheme 1 using cellulose as an example. Due to their greater affinity for micropollutants, functional groups like sulphur, amine, and hydroxyl as well as carboxylic groups are introduced in this process. Notably, ligands with these functional groups can improve modified membrane selectivity and play a substantial role in the adsorption-desorption of pollutants [9]. Through electrostatic attraction, ion exchange, van der Waals forces, and hydrogen bonds, the hydroxyl group on the backbone of cellulose also interacts with charged contaminants such as salts and heavy metals [37].

Numerous reactions have been used to add new functions to the cellulose, the building block of biopolymers. For instance, hydroxyl group modification throughout the cellulose chain is one way to modify cellulose [5,8,44,45]. Cationization, phosphorylation, (2,2,6,6-tetramethyl-piperidin-1-yl)oxyl (TEMPO) oxidation, etherification, grafting, carboxymethylation, sulfoethylation, sulfonation, aminoguanidine, ozonation, thiolation, esterification, acetylation, and amination are all methods that can be used to carry out these modifications. The hydroxyl group of cellulose's proton is replaced by functional groups in the mechanisms of these reactions, improving the membrane's physico-chemical characteristics [46]. In order to create carboxymethyl cellulose (CMC), cellulose nanofibrils (CNF), and bacterial cellulose (BC) membranes, Male et al. [9] modified cellulose with various functions. Thus, azo and anthraquinone dyes were effectively removed from wastewater by these modified membranes. The anthraquinone dye was completely removed by the CMC and CNF membranes. All of these altered biopolymeric membranes, however, had ineffective removal rates for azo dyes. Due to their substantial adsorption capability, biopolymers are helpful in the removal of harmful contaminants. Most crucially, as described in Table 2, the biopolymers can be altered or mixed into different derivatives to have the appropriate qualities advantageous for water treatment.

**A Review of Applications of Biopolymeric Membranes in Removal of Organic Pollutant and Micro pollutants from Wastewater**

**Table 1.Uses of Biopolymeric Membrane in Water Treatment**

S. No	Type of membrane	Material	Pollutant Treated	Performance	References
1	NF membranes	Cellulose acetate blended with Nicotiana tabacum ash and Fe0 nanoparticles. (ACA@Fe0)	Congo Red (CR), Methyl Blue (MB), Methyl Orange (MO), 4-Nitrophenyl phosphate (4NP)	CR, MB, MO dyes were reduced using the ACA compared to ACA@Fe0; however, the 4NP was reduced using the ACA@Fe0	11
		ZIF-8/chitosan/ Polyvinyl alcohol	RG dye	142.85mg g <sup>-1</sup> of dye was adsorbed	47
		Bacterial cellulose with MOFs	Nitrobenzene	Water permeation of 10.85 L m <sup>-2</sup> h <sup>-1</sup> psi <sup>-1</sup> rejection of nitrobenzene (68.6%)	48
		Chitosan with oxidized starch and silica	Blue 71 and Red 31	Good thermal stability and swelling properties. Adsorption capacity increased as the pH increased	49
		Hyper-crosslinked cyclodextrin membranes	MB, Safranin O, rhodamine B, MO, methyl red, CR, rose bengal, and direct red 80	adsorption capacity of above 180 mg g <sup>-1</sup>	50
	Cross-linked -cyclodextrin	steroid hormone: estradiol	removal efficiency of 75% after only 180 min and reaching the saturation after 5 h with 80% removal		51
	UF nanofibrous membrane	Cellulose nanofibril (CNF), Carboxymethylated cellulose (CMC), Bacterial cellulose (BC)	Anthraquinone dye Azo dye	100% rejection of anthraquinone dye with CNF and CMC membranes and 24.3% rejection	9

				with BC. Less than 10% rejection was observed on azo dye on all membranes	
		La(OH) <sub>3</sub> @cellulose	Oils: Hexane, cyclohexane, toluene, pump oil, crude oil, petroleum ether; Dyes: CR, MB, MO	High water flux ( $5897.7 \text{ L m}^{-2} \text{ h}^{-1}$ ), which is 2 times greater than cellulose membranes. Above 90% rejection of oils was observed. 91.2% of CR was adsorbed effectively, whereas MB and MO were not adsorbed. Membrane was selective to CR. CR was adsorbed from a CR/MO mixture	23
		Deacylated cellulose/acetate with polydopamine (DA@PDA)	MB	88.15 mg/g was adsorbed, which is about 9 times higher than the adsorption observed on DA.	26
	TFC membrane	Cellulose/polydopamine	MgSO <sub>4</sub>	Stable membranes with a rejection capacity of up to 75.6% and water flux of $25.06 \text{ L m}^{-2} \text{ h}^{-1}$ at a pressure of 0.4 MPa was reported	22
		Filter paper coated with activated cellulose (cotton)	MB	98% rejection at lower concentrations (5–10 ppm), 89% rejection at 20 ppm 78% rejection at 100 ppm	32

## A Review of Applications of Biopolymeric Membranes in Removal of Organic Pollutant and Micro pollutants from Wastewater

		Catechin/cellulose	Amido black dye (617 g/mol)	92% rejection of dye was reported	41
--	--	--------------------	-----------------------------	-----------------------------------	----

The performance and characteristic efficiencies of the biopolymeric membranes can be improved by including nanomaterials into the biopolymer matrix in addition to modifying the biopolymers [16,43]. Due to this, a variety of modification techniques have been investigated in an effort to functionalize biopolymeric membranes and introduce functions and features. As an illustration, nanoparticles were surface grafted, coated, and doped onto biopolymers [1]. Additionally, biopolymeric membranes have accepted the integration of nanofillers. The characteristics of the biopolymeric membranes can be affected by the sizes and types of the nanofillers. Membranes 2021, 11, 798 15 of 28 functions and features, changing the nanofiller surface area to volume ratio enhances the membrane's functionalities such as catalytic activity, adhesion qualities, electrical resistivity, and chemical reactivity [19,43]. Additionally, biopolymeric membranes have accepted the integration of nanofillers. The characteristics of the biopolymeric membranes can be affected by the sizes and types of the nanofillers. Notably, adjusting the nanofiller's surface area to volume ratio enhances the membrane's catalytic activity, adhesion capabilities, electrical resistivity, and chemical reactivity [19,43], which has an effect on the membrane's efficiency as shown in the example.

When inserted into biopolymeric membranes, nanofillers can provide new functions, enhancing their thermal and mechanical capabilities, hydrophilicity, porosity, antibacterial and antioxidant properties, photocatalytic properties, adsorption-desorption properties, and barrier properties.

The problems with solubility and mechanical strength of biopolymeric membranes are the main obstacles to their development, scalability, and market entry. Because biopolymers are insoluble in common solvents, manufacturing membranes will be expensive [34, 95]. Additionally, compared to their nonbiodegradable counterparts, biopolymeric membranes are mechanically weak, necessitating the blending, crosslinking, and addition of nanofillers [52]. Even yet, there isn't much information available on the upcycling and recycling of biopolymer membranes after they've been used to purify water. Therefore, in order for biopolymers to be used to their full potential in adsorptive and membrane technology applications, researchers still need to overcome the issues of their solubility and mechanical strength. In an effort to use them in the purification of wet-process phosphoric acid, Khaless et al. [53] proved the feasibility of recycling membranes. In an effort to use them in the purification of phosphoric acid produced by a wet process, they established the feasibility of reusing membranes. They demonstrated the feasibility of recycling used reverse osmosis (RO) membranes in this work. The RO membranes were stripped using NaOH, KMnO<sub>4</sub>, and KMnO<sub>4</sub>/NaOH before being converted into microfiltration (MF) membranes. Compared to the KMnO<sub>4</sub>-regenerated membranes, which exhibited a 61% rejection of organic matter and a 54% rejection of suspended particles, the MF treated with NaOH were able to reject 61% of organic matter and 70% of suspended particles. According to reports, all of the regenerate membranes outperformed the wasted RO membranes in terms of permeance and flow. The permeability of the previously used membrane was less than 1 L m<sup>-2</sup> h<sup>-1</sup> bar<sup>-1</sup>, but the permeabilities of the regenerated membranes made from NaOH, KMnO<sub>4</sub>, and KMnO<sub>4</sub>/NaOH were 40 L m<sup>-2</sup> h<sup>-1</sup>, 45 L m<sup>-2</sup> h<sup>-1</sup>, and 43 L m<sup>-2</sup> h<sup>-1</sup> bar<sup>-1</sup>, respectively. After 7 days, the membrane permeability remained mostly unchanged. Last but not least, for NaOH-, KMnO<sub>4</sub>-, and the regenerated membranes, the wet- process phosphoric acid flow was 43 L m<sup>-2</sup> h<sup>-1</sup>, 54 L m<sup>-2</sup> h<sup>-1</sup>, and 53 L m<sup>-2</sup> h<sup>-1</sup>, respectively. membranes treated with KMnO<sub>4</sub>/NaOH

The flux did not vary much either, changing after 7 days of use on the different membranes into 44 L m<sup>-2</sup> h<sup>-1</sup>, 56 L m<sup>-2</sup> h<sup>-1</sup>, and 51 L m<sup>-2</sup> h<sup>-1</sup>, respectively. Dai et al[56] .'s recycling of old biopolymers for the creation of highly permeable, thin-film composite membranes is another innovation. In order to create high-permeance, thin-film composite polyamide membranes, Dai et al. employed biopolymers that had already been used. In this study, clogged microfiltration membranes were reused to create interfacial polymerization (IP) thin-film composite membranes out of polyamide (PA).

The thin film composite membranes had a 95% rejection of Na<sub>2</sub>SO<sub>4</sub> and an average water permeability of 30 L<sup>-1</sup> m<sup>-2</sup> h<sup>-1</sup> bar. Additionally, some scientists [54,55] have shown that biopolymers can degrade. As an illustration, Fenyvesi et al. [55] showed how cyclodextrin degrades in soil and discovered more than 90% disintegration after 178 days. Despite all these encouraging breakdown results, there is currently little interest in and activity surrounding the adoption of biopolymers for various water treatment applications. Therefore, given appropriate circumstances like temperature and moisture, the biopolymeric membranes can be used as compost after use. Therefore, additional

efforts should be made to thoroughly examine the rate of biopolymer degradation to add value after usage in compost formation.

## Conclusions

Both terrestrial and aquatic habitats are at risk from organic micropollutants. Therefore, preventing the short- and long-term hazardous effects of the organic micropollutants requires the development of effective, sustainable, and technologically affordable membrane-based filtration systems. To prevent secondary contamination, biodegradable polymeric materials should be taken into account since synthetic polymeric membranes, which are currently employed to build water treatment membranes, are not biodegradable. As a result, biopolymers like cellulose ought to be taken into account, especially given their complete biodegradability, abundance in nature, cost-effectiveness, and affordability. The main reason why natural biopolymers are exceptional is that they are biocompatible, sustainable, nontoxic, and renewable. Because biopolymers are mechanically weaker than nonbiodegradable membranes and are insoluble in typical organic solvents, the mixing process has only seen a small number of applications. Therefore, additional study should be done to address this constraint. Additionally, the functionalization of the biopolymers and the incorporation of nanoparticles should be taken into account. The antifouling, pH-resistance, and stability of biopolymeric membranes under a range of operating pressures and temperatures without affecting the water flux and rejection capacities have seen only modest optimization to date. To establish realistically feasible direct biopolymeric membrane filtering processes, more research in this area is necessary.

## References

- [1] Aljohny, B.O.; Ahmad, Z.; Shah, S.A.; Anwar, Y.; Khan, S.A. Cellulose Acetate Composite Films Fabricated with Zero-Valent Iron Nanoparticles and Its Use in the Degradation of Persistent Organic Pollutants. *Appl. Organomet. Chem.* 2020, 34, 1–13.
- [2] Yao, Q.; Fan, B.; Xiong, Y.; Jin, C.; Sun, Q.; Sheng, C. 3d Assembly Based on 2d Structure of Cellulose Nanofibril/Graphene Oxide Hybrid Aerogel for Adsorptive Removal of Antibiotics in Water. *Sci. Rep.* 2017, 7, 1–13. *Membranes* 2021, 11, 798 21 of 27
- [3] Maalige, N.; Aruchamy, K.; Polishetti, V.; Halakarni, M.; Mahto, A.; Mondal, D.; Kotrappanavar, N.S. Restructuring Thin Film Composite Membrane Interfaces Using Biopolymer as a Sustainable Alternative to Prevent Organic Fouling. *Carbohydr. Polym.* 2021, 254, 1–12.
- [4] Xu, L.; Zhou, Z.; Graham, N.J.; Liu, M.; Yu, W. Enhancing Ultrafiltration Performance by Gravity-Driven Up- Flow Slow Biofilter Pre-Treatment to Remove Natural Organic Matters and Biopolymer Foulants. *Water Res.* 2021, 195, 1–12.
- [5] Asif, M.B.; Zhang, Z. Ceramic Membrane Technology for Water and Wastewater Treatment: A Critical Review of Performance, Full-Scale Applications, Membrane Fouling and Prospects. *Chem. Eng. J.* 2021, 418, 129481.
- [6] Arsuaga, J.M.; Sotto, A.; Del Rosario, G.; Martínez, A.; Molina, S.; Teli, S.B.; De Abajo, J. Influence of the Type, Size, and Distribution of Metal Oxide Particles on the Properties of Nanocomposite Ultrafiltration Membranes. *J. Membr. Sci.* 2013, 428, 131–141.
- [7] Arockiasamy, D.L.; Alhoshan, M.; Alam, J.; Muthumareeswaran, M.; Figoli, A.; Kumar, S.A. Separation of Proteins and Antifouling Properties of Polyphenylsulfone Based Mixed Matrix Hollow Fiber Membranes. *Sep. Purif. Technol.* 2017, 174, 529–543.
- [8] Saleh, T.A.; Parthasarathy, P.; Irfan, M. Advanced Functional Polymer Nanocomposites and Their Use in Water Ultra-Purification. *Trends Environ. Anal. Chem.* 2019, 24, 1–11.
- [9] Ahmad, K. Study of Different Polymer Nanocomposites and Their Pollutant Removal Efficiency. *Polymer* 2021, 217, 1–23.
- [10] Esfahani, M.R.; Aktij, S.A.; Dabaghian, Z.; Firouzjaei, M.D.; Rahimpour, A.; Eke, J.; Escobar, I.C.; Abolhassani, M.; Greenlee, L.F.; Esfahani, A.R. Nanocomposite Membranes for Water Separation and Purification: Fabrication, Modification, and Applications. *Sep. Purif. Technol.* 2019, 213, 465–499.
- [11] Tarchoun, A.F.; Trache, D.; Klapötke, T.M.; Krumm, B.; Kofen, M. Synthesis and Characterization of New InSensitive and High-Energy Dense Cellulosic Biopolymers. *Fuel* 2021, 292, 1–12.
- [12] Wang, D.; Yuan, H.; Chen, Y.; Ni, Y.; Huang, L.; Mondal, A.K.; Lin, S.; Huang, F.; Zhang, H. A Cellulose-Based Nanofiltration Membrane with a Stable Three-Layer Structure for the Treatment of Drinking Water. *Cellulose* 2020, 27, 8237–8253.
- [13] Ao, C.; Zhao, J.; Xia, T.; Huang, B.; Wang, Q.; Gai, J.; Chen, Z.; Zhang, W.; Lu, C. Multifunctional

## A Review of Applications of Biopolymeric Membranes in Removal of Organic Pollutant and Micro pollutants from Wastewater

- La(OH)3 @ Cellulose Nanofibrous Membranes for Efficient Oil/Water Separation and Selective Removal of Dyes. *Sep. Purif. Technol.* **2021**, 254, 1–10.
- [14] George, J.; Sabapathi, S. Cellulose Nanocrystals: Synthesis, Functional Properties, and Applications. *Nanotechnol. Sci. Appl.* **2015**, 8, 45.
- [15] Sudhakar, Y.; Selvakumar, M.; Bhat, D.K. Biopolymer Electrolytes: Fundamentals and Applications in EnergyStorage; Elsevier: Amsterdam, The Netherlands, 2018; pp. 1–34.
- [16] Cheng, J.; Zhan, C.; Wu, J.; Cui, Z.; Si, J.; Wang, Q.; Peng, X.; Turng, L.-S. Highly Efficient Removal of Methylene Blue Dye from an Aqueous Solution Using Cellulose Acetate Nanofibrous Membranes Modified by Polydopamine. *ACS Omega* **2020**, 5, 5389–5400.
- [17] Tröger, R.; Klöckner, P.; Ahrens, L.; Wiberg, K. Micropollutants in Drinking Water from Source to Tap- Method Development and Application of a Multiresidue Screening Method. *Sci. Total Environ.* **2018**, 627, 1404–1432.
- [18] Crini, G.; Lichtfouse, E. Advantages and Disadvantages of Techniques Used for Wastewater Treatment. *Environ. Chem. Lett.* **2019**, 17, 145–155.
- [19] Zhao, S.; Ba, C.; Yao, Y.; Zheng, W.; Economy, J.; Wang, P. Removal of Antibiotics Using Polyethylenimine Cross-Linked Nanofiltration Membranes: Relating Membrane Performance to Surface Charge Characteristics. *Chem. Eng. J.* **2018**, 335, 101–109.
- [20] Pandele, A.M.; Iovu, H.; Orbeci, C.; Tuncel, C.; Miculescu, F.; Nicolescu, A.; Deleanu, C.; Voicu, S.I. Surface Modified Cellulose Acetate Membranes for the Reactive Retention of Tetracycline. *Sep. Purif. Technol.* **2020**, 249, 1–9.
- [21] Warsinger, D.M.; Chakraborty, S.; Tow, E.W.; Plumlee, M.H.; Bellona, C.; Loutatidou, S.; Karimi, L.; Mikelonis, A.M.; Achilli, A.; Ghassemi, A. A Review of Polymeric Membranes and Processes for Potable Water Reuse. *Prog. Polym. Sci.* **2018**, 81, 209–237.
- [22] Ao, C.; Zhao, J.; Li, Q.; Zhang, J.; Huang, B.; Wang, Q.; Gai, J.; Chen, Z.; Zhang, W.; Lu, C. Biodegradable All-Cellulose Composite Membranes for Simultaneous Oil/Water Separation and Dye Removal from Water. *Carbohydr. Polym.* **2020**, 250, 1–11. *Membranes* **2021**, 11, 798 22 of 27
- [23] Moore, C.J. Synthetic Polymers in the Marine Environment: A Rapidly Increasing, Long-Term Threat. *Environ. Res.* **2008**, 108, 131–139.
- [24] Rathi, B.S.; Kumar, P.S.; Vo, D.-V.N. Critical Review on Hazardous Pollutants in Water Environment: Occurrence, Monitoring, Fate, Removal Technologies and Risk Assessment. *Sci. Total Environ.* **2021**, 797, 1–22.
- [25] Mehariya, S.; Marino, T.; Casella, P.; Iovine, A.; Leone, G.P.; Musmarra, D.; Molino, A. Biorefinery for Agro-Industrial Waste into Value-Added Biopolymers: Production and Applications of the chapter. In *Biorefineries: A Step TowardsRenewable and Clean Energy*; Springer: Berlin/Heidelberg, Germany, 2020; pp. 1–19. *Membranes* **2021**, 11, 798 24 of 27
- [26] Saedi, S.; Shokri, M.; Rhim, J.-W. Preparation of Carrageenan-Based Nanocomposite Films Incorporated with Functionalized Halloysite Using Agnp and Sodium Dodecyl Sulfate. *Food Hydrocoll.* **2020**, 106, 1–9.
- [27] Razak, M.R.; Yusof, N.A.; Aris, A.Z.; Nasir, H.M.; Haron, M.J.; Ibrahim, N.A.; Johari, I.S.; Kamaruzaman, S. Phosphoric Acid Modified Kenaf Fiber (K-PA) as Green Adsorbent for the Removal of Copper (Ii) Ions Towards Industrial Waste Water Effluents. *React. Funct. Polym.* **2020**, 147, 104–466.
- [28] Pandiarajan, A.; Kamaraj, R.; Vasudevan, S.; Vasudevan, S. OPAC (Orange Peel Activated Carbon) Derived from Waste Orange Peel for the Adsorption of Chlorophenoxyacetic Acid Herbicides from Water: Adsorption Isotherm, Kinetic Modelling and Thermodynamic Studies. *Bioresour. Technol.* **2018**, 261, 329–341.
- [29] Peng, B.; Yao, Z.; Wang, X.; Crombeen, M.; Sweeney, D.G.; Tam, K.C. Cellulose-Based Materials in Wastewater Treatment of Petroleum Industry. *Green Energy Environ.* **2020**, 5, 37–49.
- [30] Janesch, J.; Jones, M.; Bacher, M.; Kontturi, E.; Bismarck, A.; Mautner, A. Mushroom-Derived Chitosan-Glucan Nanopaper Filters

# Role of nanoscience and nanotechnology in improving the efficiency of solar cell - graphene sheets in solar cell.

Anil Dhawan ,N. Abarna

## Abstract

Nanomaterials play a vital role in the applications of Nanotechnology in the field of fabrication-such as information technology, energy resources, health and medical therapies. As our reliance upon sustainable power source turns out to be clearer, the requirement for proficient solar based cells turns out to be more critical, particularly when they are one of the most straightforward and least expensive approaches to produce clean vitality. As a rule, Solar cells are not excessively effective. Ongoing advances in graphene - based sun powered cells have seen the reflectance of sunlight based beams diminished by 20%, which gives potential proficiency increments up to 20%. These are at present a wide range of varieties of graphene-based sun based cells being explored today. This guide gives a far reaching review into the technique which is being examined and thereof accomplishing a decent productivity.

Keywords: Nanotechnology, Photovoltaic cells, Graphene Solar cells, Roll-Roll process, Parylene.

## 1. Introduction

Nanotechnology helps in design and manufacturing of thin film PV cells. With the help of nanostructures and materials like Silicon and Titanium oxide efficient solar cells can be made. In order to avoid the cost barrier of conventional solar cells the research suggests the use of nanotechnology. The many possible applications of nanotechnology make efficient photovoltaic cells. Photovoltaic solar cells made of organic compounds offer a variety of benefits. They are lighter and more flexible than heavy ones, so they are easier to transport, including remote areas without a central grid. Over the past decades, researchers have made significant advances in the design of organic solar cells, but they have consistently encountered a dilemma: finding suitable materials for electrodes that carry current from cell to cell. In nature it is rare to find materials that conduct electricity and are optically transparent. Conductive indium tin oxide (ITO) is used in most organic solar panels with transparent non-conductive glass layer as transparent electrodes because it is conductive, but it is rigid and brittle, so when the organic solar cell bends, the ITO electrode cracking occurs. It can be overcome by using graphene. It can be easily combined in some layers and combined with its excellent electrical, optical, mechanical and thermal properties. Yingjie Ma LinjieZhi [4] says that the graphene exhibits low sheet resistance with approximately 90-100% high optical transparency. It is a very thin material, in which atomically thick carbon atoms are arranged in a hexagonal lattice, and this is the least expensive material. It is brawny material than diamond and has more tensile strength than steel. Graphene is an excellent 2D material that is flexible with good light absorption, good conductivity of electricity and rubber optical transparency. A Single layer of graphene shows an optical transparency of 97.7% whereas, a 3-layered graphene exhibits around 90.8% optical transparency and the addition of each layer corresponds to a 2.3% decrease in optical transparency. The essential guideline of graphene-based sun powered cells isn't not quite the same as current silicon sun oriented cells, where materials are supplanted by graphene subsidiaries. Many studies focus on graphene as an alternative to ITO on the transparent electrodes of OPVs. Others are looking for ways to use graphene to improve the overall performance of photovoltaic devices, mainly OPVs, as well as electrodes, active layers, interface layers and electron receivers.

---

Anil Dhawan

Department of Physics, School of Basic & Applied Sciences,  
Anand International College of Engineering, Jaipur-303012;  
[anil.dhawan@anandice.ac.in](mailto:anil.dhawan@anandice.ac.in)

N. Abarna

PG Student, Department of Physics, Sri Sarada College for Women (Autonomous),  
Affiliated to Periyar University, Salem, India- 630016;  
[abarnanagarajan19@gmail.com](mailto:abarnanagarajan19@gmail.com)

## **Role of nanoscience and nanotechnology in improving the efficiency of solar cell - graphene sheets in solar cell.**

Graphene makes solar cells more efficient, which is also exposed to a certain area of infrared sunlight. Each moving photon absorbs a freely moving electron, which absorbs only a fraction of the energy and heats the remaining crystal lattice as thermal energy, while graphene has the ability to overcome this problem, and is suitable for tuneability and adaptability. The solar cell uses graphene as an excellent conductor, but is not good at collecting the electricity generated inside the solar cell. Therefore, researchers are looking for suitable ways to replace graphene for this purpose, as many graphene-based solar cells have been reported to operate in different parts of the cell. M.S. Shamsudin [2] says that it can be used as a photosynthetic material as it can stimulate and adjust its band spacing and band position via chemical action. There are several methods for making graphene sheets such as CVD, Mechanical Exfoliation, Epitaxial Development on SiC, Chemical and Liquid Peeling. Yuanhong Xu and Jingquan Liu [5] researchers say that of these techniques, CVD-graphene has the potential to produce flexible and transparent electrodes with large and high electrical conductivity. Maryam Saeed , Yousef Alshammari et.al [6] researchers say that due to the high temperature catalytic development of CVD-graphene (1000 C) it is inevitable to replace graphene to form graphene based electrodes on flexible substrates. Graphene for photovoltaic devices also has other attractive properties: -For example, graphene is incorporated into integrated polymers to enhance exitone deformation. Martin Grolms [3] researcher says that the most widely adopted approach for fabrication of graphene electrodes are Polymer-assisted transfer techniques. PEDOT:PSS, poly(methyl methacrylate) (PMMA), ethylene vinyl acetate (EVA), poly(dimethyl siloxane) (PDMS), silicone-coated poly(ethylene terephthalate) (PET), thermal release tape (TRT), etc., are conductive polymers are easy to used for to roll-to-roll production and flexible devices. During the transfer process they act as support layers by sticking tightly to the graphene monolayer and protecting it from damage. In this proposed work, we are going to analyse about Roll-to-Roll Transfer and Doping of CVD-Graphene Using Parylene in solar cells.

## **2. Literature review**

In an article by Paul Bazylewski, Arash Akbari-Sharbafet.al[1], an application is designed based on vertical graphenenano hills (VGNH) which in turn grown without the influence of catalyst. In order to analyse the electrical properties the photovoltaic device is compared with bare silicon. The ultimate aim of this experiment is to fabricate large area devices thereof optimizing the thickness of VGNH and surface texturing is done so as to overcome the crucial problem of high reflectivity of silicon. A low reflectivity of thick layers of VGNH is achieved which will be beneficial for high photocurrent. Finally, the conversion efficiency of 10.97% is achieved in this experiment.

In an article by Minas M. Stylianakis, DimitriosKonioset.al[2] has discussed about an efficient technique, which is used to enhance the efficiency of graphene design in their paper. Two set of devices were fabricated based on flat and pyramidal structures of Si and the photovoltaic properties of graphene/Si heterojunction solar cell were compared. For producing pyramidal skeleton, chemical dissolution of Si wafers was carried out. A technique named as Electrophoretic deposition is used to transfer the Reducedgraphene oxide on the pyramidal Si. After this step the evidence of graphene layer is studied using Raman spectroscopy and other techniques includes XRD and atomic force microscopy analysis which thereof enhanced the interface area. That enhanced surface area of this sample promotes its antireflective behaviour which is proved with the help of reflectance spectroscopy by which the optical properties of the graphene is improved as well. Hence, the current voltage characteristics showed that the efficiency is improved.

In an article by Tahira Mahmood, Madeeha Aslam et.al [3] they approach for the development of two terminal solar cells is discovered instead of four terminal architecture which reduced the plant costs. However, it is very difficult to process monolithically the solar cells directly onto the micrometer – sized texturing on the front surface because it limits both high – temperature and solution processing on the top cells. In order to overcome this problem they have developed a mechanically stacked two terminal tandem solar cell with sub-cells which is independently fabricated, optimized and subsequently coupled by contacting the back electrode of the top cell with the texturized and metalized front contact of the bottom cell. Thus the tandem device demonstrates 26.3% efficiency over an active area of 1.43 cm<sup>2</sup>.

In an article by ParisaFallahazad , NimaNaderiet.al[4] has discussed about electrical and mechanical properties of graphene. It is the material which could act as an ideal low – cost alternative material for the effective replacement of materials used in organic optoelectronic applications. The enhanced electrical conductivity of graphene when combined with its high transparency is used as an alternative in organic solar cells. In this article, they have given an outline of the latest exploration progress in the utilization of arrangement – prepared graphene based movies, for example, artificially changed over graphene, thermally and photograph synthetically diminished graphene oxide, composite decreased graphene oxide – carbon nanotubes.

In an article by Malik Abdul Rehman, SanjibBaran Roy et.al [5] has discussed about the properties like electronic, thermal and optical properties of graphene – based materials depend strongly on the fabrication method. The metals like Co and Ni which will interact strongly with graphene may form strong chemical bond with graphene which will alter the band structure near the dirac point. Metals which interacts weekly with graphene such as Au and Cu induces shift in graphene Fermi energy which results in doping without alteration to the graphene band structure. The size and distribution of metal nanopraticles can be controlled by the deposition and nucleation condition such as annealing temperature and time, deposition rate. Whereas under ideal conditions, self-assembled arrays of nanoparticles can be obtained on graphene-based films for future use.

Enrico Lamanna,<sup>1</sup> Fabio Matteocci<sup>et.al</sup>[6] One of the most leading sources of renewable energy source is the solar energy, which is inexhaustible and abundantly available. Sun based cells that convert sunlight based energy straightforwardly into power are drawing extensive consideration as a potential turnkey answer for address these difficulties. Several approaches have been made in this aspect. In this paper the use of graphene nanocomposites has been explored as an electrode material in DSSCs and PSCs and played a significant role in increasing the chare transport, reducing charge recombination and this enhancing the performance of the solar cells.

### 3. Proposed work

Chemical vapour deposition (CVD) is the most common method for polymer-assisted transfer techniques, and is currently the most widely accepted approach to the production of graphene sheets. The foil surface glazes to form a honeycomb structure by exposing the copper foil to methane gas at a temperature above 1000 deg C which acts as a supporting layer by firmly sticking to graphene monolayer and securing it. Converting a monolayer graphene from copper plates to substrates is challenging and may result in a web of tears, wrinkles and imperfections on the sheets, which reduces the electrical conductivity of the film. The commercialization and scaling of the graphene roll-to-roll (R2R) transfer process is an important step. But by using the emerging technology large area graphene can be produced and they are transformed into any substrate that is needed and it will not affect the electrical property and mechanical property of original graphene.

**Figure 1:** Schematic of R2R transfer setup for graphene with lamination and delamination units.

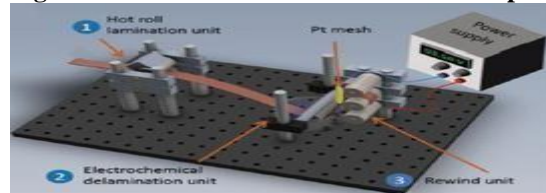


**Figure 2: Fabrication process of graphene electrode.**

In this process, not only the roll-to-roll transfer process of graphene using CVD-parylene developed, but also parylene used as an ultra-thin substrate to simultaneously produce air-stable organic photovoltaics with high conductivity. The process involves an intermediate -buffer|| layer of material, which acts as an aid to success. It allows the ultrathin graphene sheet less than nanometers (in billions of meters) thick can be easily lifted from its substrate, allowing for rapid roll-to-roll production. The buffer layer is made of a Parylene a polymer material. Like graphene, parylene is also made with CVD, which simplifies the manufacturing process and scaling. A lamination process between graphene and a flexible polymer substrate is more advantageous than replacing graphene directly on polymeric flexible substrates, thus minimizing gaps, tears, and image damage. The compound was then laminated in ethylene vinyl acetate (EVA) and poly (ethylene terephthalate). The roll-first-roll transfer technique is used for the release of graphene from its own copper

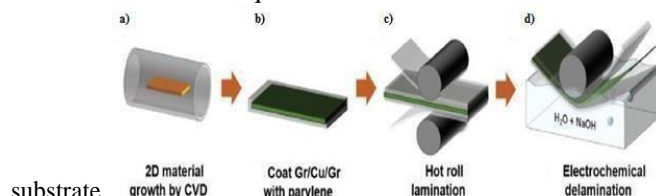


**Figure 3:a)** Growth of graphene in CVD furnace on both sides ofCu foil (orange), b) CVD growth of parylene on graphene/Cu stack (green color), c) lamination process of parylene/graphene/Cu stack by EVA/PET substrates by hot rolling, and d) electrochemical delamination process of graphene/parylene/EVA/PET stack from the Cu foil in both sides.

In this process, a layer of parylene, a polymer used as a moisture and conductivity barrier is placed on the graphene / copper (Q) films grown by chemical vapour deposition (CVD).The electrical and mechanical properties of the graphene which do not affected by a large area graphene sheet can now be reliably

## Role of nanoscience and nanotechnology in improving the efficiency of solar cell - graphene sheets in solar cell.

manufactured. Experiments show that of the three types of parylene present, one of which has the highest chlorine atoms is suitable for this use.

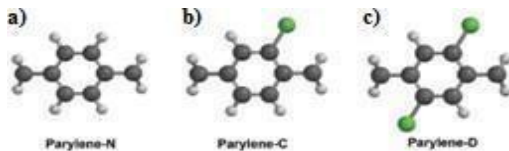


**Figure 4:** Molecular structures of different types of parylene a) N, b) C, and c) D. The dark grey balls represent C atoms, the light grey ones represent H atoms, while the green ones represent Cl atoms.

**Figure: 1,2,3,4 are taken from Synergistic Roll-to-Roll Transfer and Doping of CVD-Graphene Using Parylene for Ambient-Stable and Ultra-Lightweight Photovoltaics.**

Using polyethylene-C, high adhesion of poly phenols with graphene can improve the conductivity of graphene, resulting in fewer defects in the modified graphene. Conventional polymers resulting in less damage during transfer but parylene has a better adhesion of graphene it provides a double benefit as an interface layer in the R2R transfer of graphene. The layers are sanded together, providing a kind of "doping" to the graphene, further enhancing the nuclear proximity of the chlorine-rich parylene, finally providing the most reliable and unusual approach to improving the conductivity of the large area graphene.

### 4. Results and discussion

A roll-to-roll transfer technique is used for the release of the graphene from its native copper substrate. In this process, a layer of parylene is deposited on graphene/copper (Cu) foils grown by chemical vapor deposition method (CVD). MIT researchers [1] develop new roll-to-roll manufacturing process for high quality large sheets Graphene, the team says, could lead to ultra-lightweight, flexible solar cells and a new type of lighting Devices and other thin-film electronics. MIT Researchers [1] test results shows that parylene provides a double benefit as an interface layer in the R2R transfer. It has a better adhesion to graphene than other conventional polymers which results in less damage during the transfer thereof improving the conductivity. They obtained an ultra-lightweight device with a PCE of 5.86% and a power per weight of 6.46 W g<sup>-1</sup> using a graphene/parylene C electrode, which is completely stable in air without any encapsulation. This device is comparable with the PCE of ITO/PET based OSC (6.12%) which gives higher power per weight. With a lightweight parylene substrate and



an atomically thin graphene electrode (combination of parylene C/graphene), offer airstable OSCs with high power per weight. Roll to Roll process is a Novel technique to transfer graphene directly on polymeric flexible substrates which in turn reduce the occurrence of breaks, tears and film damage. This is the major

advantage to use CVD- graphene with parylene in the roll to roll process. It will result a flexible high quality graphene as a transparent electrode.

### Conclusion

The main reason of using the graphene is because of low cost, flexible and highly efficient photovoltaic device and also transparent and conductive electrodes in solar cells. By increasing the layers present in graphene the conductivity can be improved. Some further improvements are- conductivity of graphene over a large area and to propose a better practice for commercialization with better adhesion with graphene to reduce the potential defects caused by R2R transfer process. Due to the high carrier mobility, low resistance and transmission and the unique properties of the 2D network, graphene-based products are considered to be used in PV devices instead of the usual conventional ones. For the accomplishment of the practical application graphene-based material is used. The production methods of graphene (i.e. CVD, roll-to-roll transfer) as the most adjustable, controllable and compatible techniques for making graphene have summarized in this review. Because graphene properties are essentially responsible for its fabrication process, prudent methods are essential for target applications. In particular, high-conductivity graphene is suitable for TCEs in flexible PV devices and is suitable for handling metal oxides, alloys and polymers that can be used as interlayer materials for selective component and electrode. Therefore, by considering the properties thoughtfully, graphene can suppress existing conventional products at a comparable cost. Graphene, a conductive electrode is acting as a substitute for Commercial ITO. Graphene-based materials have the ability to select charges in solar cell buffer layers and act as transport components. Furthermore, the low air stability and atmospheric degradation of photovoltaic devices can be enhanced by the combination of graphene with its standard high-saturation 2D system. The mass

production of continuous large-scale graphene requires the development of a reliable growth system. The key issue is the integration of graphene-based materials into high-yield functional devices. The integration of separation and purification processes is used to control the properties during device fabrication. Despite the chemical and / or physical functions, band energy tuning and size control of graphene sheets must develop a simple, accurate, and reproducible operating system to create graphene novel derivatives with controllable properties for a wide range of applications. This will lead to new generation devices that will be lighter, eco-friendly and less expensive.

### Acknowledgments

The author would like to extend their deepest gratitude and gratefulness to the management at AnandICE and colleagues for providing with the right ways of thinking and concepts of this research.

### References

- [1] Tavakoli, Mohammad & Azzellino, Giovanni & Hempel,et.al.(2020).Advanced Functional Materials.30.2001924.10.1002/adfm.202001924.
- [2] Mohammad Shamsuddin Ahmed, Young-Bae Kim et.al.. Sci Rep 7, 43279 (2017).
- [3] Khodagholy, Dion & Doublet, Thomas & Gurfinkel, Moshe & Quilichini, et.al.. (2011) Advanced materials 23.H268-72.10.1002/adma.201102378.
- [4] Ma, Yingjie & Zhi, Linjie. (2018).3.1800199. 10.1002/smtd.201800199.
- [5] Xu, Yuanhong & Liu, Jingquan. (2016). 12. 10.1002/smll.201502988.
- [6] Saeed, Maryam & Alshammari, Yousef & A. Majeed, Shereen,et.al.. (2020).
- [7] D. Prochowicz, R. Runjhun, M. M. Tavakoli, P. Yadav, et.al..Chem. Mater. 2019, 31, 1620.
- [8] G. Soavi, G. Wang, H. Rostami, D. G. Purdie, D. De Fazio, T. Ma, B. Luo, J. Wang, A. K. Ott,et.al.. Nat.Nanotechnol.2018, 13, 583.
- [9] M. M. Tavakoli, H. Aashuri, A. Simchi, Z. Fan, Phys. Chem. Chem.Phys. 2015, 17, 24412.
- [10] B. S. Jessen, L. Gammelgaard, M. R. Thomsen, D. M. Mackenzie, ,et.al. Nat. Nanotechnol. 2019, 14,340.
- [11] M. M. Tavakoli, H. Aashuri, A. Simchi, S. Kalytchuk, Z. Fan, J. Phys.Chem. C 2015, 119, 18886.
- [12] Y. Lin, J. Chen, M. M. Tavakoli, Y. Gao, Y. Zhu, D. Zhang, M. Kam,Z. He, Z. Fan, Adv. Mater. 2019, 31, 1804285.
- [13] S. H. Bae, X. Zhou, S. Kim, Y. S. Lee, S. S. Cruz, Y. Kim,J. H. Park, Proc. Natl.et.al. Acad. Sci. USA 2017, 114, 4082.
- [14] YuanhongXu, Jingquan Liu Materials, 10.1002/adma.202004356, 33, 5, (2020).
- [15] Y. Liu, Y. Huang, X. Duan, Nature 2019, 567, 323.

# FRACTIONAL INTEGRALS USING GENERALIZED BESSEL FUNCTION ASSOCIATED WITH GENERALIZED FRACTIONAL CALCULUS OPERATORS

Prakash Singh, Shilpi Jain and Praveen Agarwal

**Abstract:** Many infinite integrals involving the product of several Bessel functions have been obtained. Choi and Agarwal have described two integrals involving the generalized Bessel function  $(z)$  which is represented by Galué [1]. Using the same method, in this chapter, we present two generalized integral formulas involving the product of generalized Bessel function of  $(z)$ , which are expressed in terms of the generalized Lauricella series due to Srivastava and Daoust. Some interesting special cases of our main results are also considered.

**Keywords-** Gamma function; Generalized hypergeometric function  ${}_pF_q$ ; Generalized (Wright) hypergeometric functions  ${}_p\Psi_q$ ; Generalized Lauricella series in several variables; cosine and sine trigonometric functions; Bessel function of the first kind; Oberhettinger's integral formula; Generalized Bessel function..

## 1. Introduction and Preliminaries

Here we aim at presenting two generalized integral formulas, which are expressed in terms of the generalized Lauricella functions (1.3), by inserting the product of Bessel function of the first kind (1.1) with suitable arguments into the integrand of (1.11). Some interesting special cases of our main results are also considered.

For our purpose, we begin by recalling some known functions and earlier works. The Bessel function of the first kind  $(z)$  is defined for  $z \in \mathbb{C} \setminus \{0\}$  and  $\nu \in \mathbb{C}$  with  $\Re(\nu) > -1$  by the following series (see, for example, [11, p. 217, Entry 10.2.2] and [19, p. 40, Eq. (8)]):

$$(z) = \sum_{k=0}^{\infty} \frac{(-1)^{\binom{\nu+2k}{2}}}{k! \Gamma(\nu+k+1)}, \quad (1.1)$$

where  $\mathbb{C}$  denotes the set of complex numbers and  $\Gamma(z)$  is the familiar Gamma function (see [14, Section 1.1]).

P.Singh: Research Scholar, Department of Mathematics, Poornima University, Jaipur, India  
2018phdprakash6673@poornima.edu.in, prakashsingh705@gmail.com

S. Jain: Department of Mathematics, Poornima University, Jaipur-303012, India  
shilpi.jain@poornima.org

P. Agarwal: Department of Mathematics, Anand International College of Engineering, Jaipur-303012, India  
[goyal.praveen2011@gmail.com](mailto:goyal.praveen2011@gmail.com)

Value [1] generalized Bessel function which is represented by

$$J(v) = \sum_{k=0}^{\infty} \frac{(-1)^k v^{2k}}{k! \Gamma(v+k+1)}, \quad (v > 0, |z| < \infty, |\arg z| < \pi). \quad (1.2)$$

An interesting further several-variable-generalization of the generalized Lauricella series (see, for example, [17, p. 36, Eq. (19)]) is defined by (cf. Srivastava and Daoust [15, p. 454]; see also [17, p. 37])

$$\begin{aligned}
& \stackrel{\text{def}}{=} (1); \dots; B(n) \\
& \quad \vdots \\
& \quad A^{(1)}; \dots; B^{(n)}([a]; \theta^{(1)}, \dots, \theta^{(n)}) \\
F \underset{C:D}{\cdot} (1; \dots; z^{(n)}) &= F \underset{C:D}{\cdot} (1; \dots; z^{(n)}) \\
& \quad [c]; \psi^{(1)}, \dots, \psi^{(n)} \\
& \quad ) D \qquad \qquad \qquad ) D
\end{aligned}$$

(1)

$$\begin{aligned}
& [(b)^{(1)}; \phi^{(1)}]; \dots; [(b)^{(n)}; \phi^{(n)}]; \\
& [(d)^{(1)}; \delta^{(1)}]; \dots; [(d)^{(n)}; \delta^{(n)}]; z_1, \dots, z_n \\
& \quad k_1 \quad k_n \qquad \qquad \qquad 1 \qquad n \\
& = \sum_{k_1, \dots, k_n=0}^{\infty} \Omega(k_1, \dots, k_n) \frac{z_1^{k_1}}{k_1!} \dots \frac{z_n^{k_n}}{k_n!}, \qquad (1.3)
\end{aligned}$$

where, for convenience,

$$\Omega(k_1, \dots, k_n) = \frac{\prod_{j=1}^{kn} (a_j)^{(1)} \prod_{j=1}^{(1)} (1) \prod_{j=1}^{k_1 \phi_j^{(1)}} (1) \dots \prod_{j=1}^{B(n)} (b^{(n)})_j}{\prod_{j=1}^{(c)} (1) \prod_{j=1}^{D(n)} j \prod_{j=1}^{d(n)} (n)_j}, \quad (1.4)$$

the coefficients

$$\{ \theta^{(m)}(j = 1, \dots, A); \phi^{(m)}(j = 1, \dots, B^{(m)}); \psi^{(m)}(j = 1, \dots, C); \delta^{(m)}_j \\ (j = 1, \dots, D^{(m)}); \quad \forall m \in \{1, \dots, n\} \quad (1.5)$$

are real and positive, and (a) abbreviates the array of  $A$  parameters  $a_1, \dots, a_A$ , ( $b^{(m)}$ ) abbreviates the array of  $B^{(m)}$  parameters

$$\forall m \in \{1, \dots, n\},$$

with similar interpretations for  $(c)$  and  $(d^{(m)})$  ( $m = 1, \dots, n$ ); *et cetera*. The multiple series (??) converges absolutely either

$$1. \quad \Delta_i > 0 \quad (i = 1, \dots, n), \quad \forall z_1, \dots, z_n \in \mathbb{C},$$

or

$$1. \quad \Delta_i = 0 (i = 1, \dots, n), \quad \forall z_1, \dots, z_n \in \mathbb{C}, |z_i| < \varrho_i (i = 1, \dots, n).$$

The multiple series (1.3) is divergent when  $\Delta_i < 0$  ( $i = 1, \dots, n$ ) except for the trivial case  $z_1 = 0, \dots, z_n = 0$ . Here

$$\Delta \equiv 1 + \sum_i \psi_j^{(i)} + \sum_{j=1}^{(i)} \delta_j^{(i)} - \sum_{j=1}^{(i)} \frac{A}{j} - \sum_{j=1}^{(i)} \frac{(i)}{j} \quad (i = 1, \dots, n), \quad (1.6)$$

$$\varrho_i = \min_{\substack{\mu_1, \dots, \\ \geq 0}} \{E_i\} (i = 1, \dots, n), \quad (1.7)$$

with

$$= \left( \frac{1}{\phi_j} \right)^{1+\sum_{j=1}^n \delta_j} \cdot \frac{\prod_{j=1}^n \left( \sum_{i=1}^m \mu_i \theta^{(i)} \right)^{\delta_j}}{\prod_{i=1}^m \left( \prod_{j=1}^n (\phi^{(i)})_j \right)^{\delta_i}}. \quad (1.8)$$

functions of one and two variables, respectively (see, for example, [17, pp. 39-40]). For the sake of completeness, we recall the familiar generalized hypergeometric series  ${}_pF_q$  defined by (see [14, Section 1.5])

$${}_pF_q \left[ \begin{matrix} \alpha_1, \dots, \alpha_p; \\ \beta_1, \dots, \beta_q; \end{matrix} z \right] = \sum_{n=0}^{\infty} \frac{(\alpha_1)\cdots(\alpha_p)_n}{(\beta_1)\cdots(\beta_q)_n} z^n n! \quad (1.9)$$

where  $(\lambda)_n$  is the Pochhammer symbol defined (for  $\lambda \in \mathbb{C}$ ) by (see [14, p. 2 and pp. 4-6]):

$$(\lambda)_n := \begin{cases} 1 & (n = 0) \\ (\lambda + 1) \dots (\lambda + n - 1) & (n \in \mathbb{N} := \{1, 2, 3, \dots\}) \end{cases} = \frac{\Gamma(\lambda+n)}{\Gamma(\lambda)} \quad (1.10)$$

and  $\mathbb{Z}^-$  denotes the set of nonpositive integers.

We also need to recall the following Oberhettinger's integral formula [12]:

$$\int_0^\infty x^{\mu-1} \left( x + a + \frac{x^2}{2} + 2ax \right)^{-\lambda} dx = 2\lambda a^{-\lambda} \int_0^{\lambda} \frac{\Gamma(2\mu)\Gamma(\lambda-\mu)}{2} \frac{r^{2\mu-1}}{\Gamma(1+\lambda+\mu)} dr, \quad (1.11)$$

provided  $0 < R(\mu) < R(\lambda)$ .

Now we discuss generalized Erdelyi- Kober fractional integral operators defined by

$$I_{y+\alpha}^{\beta}(f(t)) = \frac{t^{\beta}(y+\alpha)}{\Gamma(\alpha)} \int_0^t \frac{(t^\beta - r^\beta)^{\alpha-1}}{(t-r)^{\beta-\alpha-1}} f(r) d(r) \quad (1.12)$$

There are some cases if we change in the parameters Case-1

$$\text{if } \eta = 0, \alpha = 1 \text{ and } \beta = 1 \text{ then } I^0(f(t)) = t^0 \int_0^t (t-r)^{-1} f(r) d(r) \quad (1.13)$$

Case-2

if  $\eta = 0$  and  $\beta = 1$  then operator reduce to Riemann-Liouville integral

$$(f(t)) = t^\alpha I^0(f(t)) = \frac{1}{\Gamma(\alpha)} \int_0^t (t-r)^{\alpha-1} f(r) d(r) \quad (1.14)$$

Case-3

if  $\eta = 0, \alpha = 1$  and  $\beta = 1$  then operator reduce to Hardy-Littlewood integral operator

$$L((t)) = I^0(t) = \frac{1}{t} \int_0^1 r f(r) d(r) \quad (1.15)$$

Case-4

if  $\beta = 1$  then operator reduce to Kober and Erdelyi integral operator

$$I^{y,\alpha}(f(t)) = I^{y,\alpha}(f(t)) = \frac{t^{-(y+\alpha)}}{\Gamma(\alpha)} \int_0^t (t-r)^{\alpha-1} f(r) d(r) \quad (1.16)$$

## Case-5

if  $\beta = 2$  then operator reduce to Sneddon integral operator

$$I_y^{\alpha}(f(t)) = I^{y,\alpha}(f(t)) = \frac{2t^{-2(y+\alpha)}}{(t^2 - r^2)^{\alpha-1} r^{2y+1}} r(r) \quad (1.17)$$

Case-6

if  $\beta = 2$  and  $\eta = -1/2$ ,  $\alpha \pm i\alpha + 1/2$  then operator reduce to Uspensky integral transformation

$$(f(t)) = \frac{I}{\Gamma(\alpha+1/2)} \int_0^t (1-t)^{\alpha} f(t) dt$$

we can also see the power representation of operator as

$$t^\lambda = \frac{1}{\frac{\Gamma(1+y+\beta)}{(1+\alpha+y+\frac{\beta}{\lambda})}} \quad (1.18)$$

## 2 Main Results

We establish two generalized integral formulas, which are expressed in terms of the generalized Lauricella functions (1.3), by inserting the product of Bessel function of the first kind (??), with suitable arguments into the integrand of (1.1).

**Theorem 2.1** The following integral formula holds true: For  $\lambda, \mu, v_j \in \mathbb{C}$  with  $\Re(v_j) > -1$ ,  $0 < \Re(\mu) < R(\lambda + v_j)$  ( $j = 1, \dots, n$ ) and  $x > 0$ ,

$$\int_0^\infty x^{\mu-1} \left( x + \frac{y}{x} \right)^n \frac{2^{-\lambda}}{(2x)^{\mu-\lambda}} \prod_{j=1}^n \frac{y_j}{(x+a+\sqrt{x^2+2})^{v_j}} = \frac{\Gamma(2\mu)\Gamma(1+\lambda+\sum_{j=1}^n v_j)\Gamma(\lambda-\mu+\sum_{j=1}^n \frac{n}{v_j})}{\Gamma(\lambda+\sum_{j=1}^n v_j)\Gamma(1+\lambda+\mu+\sum_{j=1}^n)} \times$$

$$F^{2:0;\dots;0}_{2:1;\dots;n} [ [1+\lambda+\sum_{j=1}^n v_j; 2, \dots, 2], [\lambda-\mu+\sum_{j=1}^n v_j; 2, \dots, 2];$$

$$[1+\lambda+\mu+\sum_{j=1}^n v_j; 2, \dots, 2], [\lambda+\sum_{j=1}^n v_j; 2, \dots, 2];$$

$$; ; -\frac{y^{2^{j=1}}}{y^2}, \dots, -\frac{y^2}{y^2}] (2.1)$$

$$[v_1+1: 1] \quad [vn+1: 2] \quad \frac{4a}{2} \quad \frac{4a^2}{4a^2}$$

*Proof.* For convenience, let the left-hand side of the assertion (2.1) be denoted by  $f$ . By applying (1.1) to the integrand of (2.1) and then interchanging the order of integral sign and summation, which is verified by uniform convergence of the involved series under the given conditions, we get

**f** =

$$\begin{aligned}
 & \int_0^\infty x^{\mu-1} (x+a+\sqrt{x^2+2ax})^{-\lambda} \\
 & \times \sum_{k_1=0}^n (-1)^{k_1} \frac{y_1}{k_1! \Gamma(\nu_1 + k_1)} \cdots \sum_{k_n=0}^n (-1)^{k_n} \frac{(y_n)^{k_n}}{k_n! \Gamma(\nu_n + k_n)} dx \\
 \text{and} \quad & 0
 \end{aligned}$$

$$\begin{aligned}
 f = & \sum_{k_1, \dots, k_n=0}^\infty \frac{(-1)^{k_1} (y/2)^{k_1}}{k_1! \Gamma(\nu_1 + 1) (\nu_1 + 1)_k} \cdots \frac{(-1)^{k_n} (y_n/2)^{k_n}}{k_n! \Gamma(\nu_n + 1) (\nu_n + 1)_k} \\
 & \times \int_0^{-\lambda - \nu_1 - \dots - \nu_n - 2k_1 - \dots - 2k_n} x^{\mu-1} (x+a+\sqrt{x^2+2ax}) dx. \tag{2.2}
 \end{aligned}$$

In view of the conditions given in Theorem 1, since

$\Re(\nu_j) > -1, 0 < R(\mu) < R(\lambda + \nu_j) \leq \Re(\lambda + \nu_j + 2k_j) 12mm (k \in \mathbb{N}_0 := \mathbb{N} \cup \{0\} \text{ and } j = 1, \dots, n)$ , we can apply the integral formula (1.11) to the integral in (2.5) and obtain the following expression:

$$\begin{aligned}
 & 2^{1-\mu} a^{\mu-\lambda} \sum_{k_1, \dots, k_n=0}^\infty \frac{(-1)^{k_1} (y_1/2)^{k_1}}{k_1! \Gamma(\nu_1 + 1) (\nu_1 + 1)_k} \cdots \frac{(-1)^{k_n} (y_n/2)^{k_n}}{k_n! \Gamma(\nu_n + 1) (\nu_n + 1)_k} \\
 & \times \frac{\Gamma(2\mu) \Gamma(\lambda - \mu + \nu_1 + \dots + \nu_n + 2k_1 + \dots + 2k_n)}{\Gamma(1 + \lambda + \mu + \nu_1 + \dots + \nu_n + 2k_1 + \dots + 2k_n)} \times (\lambda + \nu_1 + \dots + \nu_n + 2k_1 + \dots + 2k_n)^{-(\nu_1 + \dots + \nu_n + 2k_1 + \dots + 2k_n)}.
 \end{aligned}$$

We know that  $\nu_1 + \dots + \nu_n + 2k_1 + \dots + 2k_n = \frac{\Gamma(1+\lambda+\nu_1+\dots+\nu_n+2k_1+\dots+2k_n)}{\Gamma(\lambda+\nu_1+\dots+\nu_n+2k_1+\dots+2k_n)}$ ,

then we have

$$\begin{aligned}
 f = & 2^{1-\mu} a^{\mu-\lambda} \sum_{k_1, \dots, k_n=0}^\infty \frac{(-1)^{k_1} (y/2)^{k_1}}{k_1! \Gamma(\nu_1 + 1) (\nu_1 + 1)_k} \cdots \frac{(-1)^{k_n} (y_n/2)^{k_n}}{k_n! \Gamma(\nu_n + 1) (\nu_n + 1)_k} \\
 & \times \frac{\Gamma(2\mu) \Gamma(\lambda - \mu + \nu_1 + \dots + \nu_n + 2k_1 + \dots + 2k_n)}{\Gamma(1 + \lambda + \mu + \nu_1 + \dots + \nu_n + 2k_1 + \dots + 2k_n)} \frac{1}{n} \\
 & \times \frac{\Gamma(1 + \lambda + \nu_1 + \dots + \nu_n + 2k_1 + \dots + 2k_n)}{\Gamma(\lambda + \nu_1 + \dots + \nu_n + 2k_1 + \dots + 2k_n)} a^{-(\nu_1 + \dots + \nu_n + 2k_1 + \dots + 2k_n)}.
 \end{aligned}$$

Therefore we find that

$$\begin{aligned}
 & {}_2F_1 \left( \begin{matrix} -\mu, \mu-\lambda \\ a \end{matrix} ; \frac{\frac{y_j}{2} y}{2a} \right) \frac{\Gamma(2\mu)\Gamma(\lambda-\mu+\sum_{j=1}^n v_j)\Gamma(1+\lambda+\sum_{j=1}^n v_j)}{\Gamma(v_j+1)\Gamma(1+\lambda+\mu+\sum_{j=1}^n v_j)\Gamma(\lambda+\sum_{j=1}^n v_j)} \times \\
 & \frac{\sum_{k_1+\dots+k_n}^{\infty} \frac{\Gamma(v_j+1)}{(\lambda-\mu+\sum_{j=1}^n v_j)^{2k_1+\dots+2k_n}}}{(1+\sum_{j=1}^n v_j)^{2k_1+\dots+2k_n}} \times \\
 & \frac{(1+\lambda+\mu+\sum_{j=1}^n v_j)2k_1+\dots+2k_n}{(-y^2/4a^2)^{1/2}} \frac{1}{(v_1+1)k_1 \dots (v_n+1)} \frac{1}{k_1!} \dots \frac{1}{k_n!} \\
 & = 0 \quad \frac{(-y^2/4a^2)^{1/2}}{(2k_1+\dots+2k_n)!} \frac{1}{k_1!} \dots \frac{1}{k_n!}. \tag{2.3}
 \end{aligned}$$

Finally, we interpret the multiple series in (2.3) as a special case of the general hypergeometric series in several variables defined by (1.3). We are thus led to the assertion (2.1).

**Theorem 2.2** *The following integral formula holds true: For  $\lambda, \mu, v_j \in \mathbb{C}$  with  $\Re(v_j) > -1$ ,  $0 < \Re(\mu) < R(\lambda + v_j)$  ( $j = 1, \dots, n$ ) and  $x > 0$ ,*

$$\begin{aligned}
 & \int_0^\infty \frac{x^{\mu-1}}{x+a+\sqrt{x^2+2ax}} e^{-\lambda} \prod_{j=1}^n \frac{x y_j}{(x+a+\sqrt{x^2+2ax})^{v_j}} dx = \\
 & {}_2F_1 \left( \begin{matrix} -\mu, \mu-\lambda \\ 4 \end{matrix} ; \frac{y}{4} \right) \frac{\Gamma(\lambda-\mu)\Gamma(1+\lambda+\sum_{j=1}^n v_j)\Gamma(2\mu+2\sum_{j=1}^n v_j)}{\Gamma(\lambda+\sum_{j=1}^n v_j)\Gamma(1+\lambda+\mu+2\sum_{j=1}^n v_j)} \times \\
 & F^{2:0;\dots;0}_{[2:1;\dots;n] \quad [1+\lambda+\sum_{j=1}^n v_j:2,\dots,2], \quad [2\mu+2\sum_{j=1}^n v_j:4,\dots,4]:} \frac{1}{\prod_{j=1}^n (v_1+1) \dots (v_n+1)}; \dots; \frac{1}{\prod_{j=1}^n (v_1+1) \dots (v_n+1)} \\
 & [1+\lambda+\mu+2\sum_{j=1}^n v_j:4,\dots,4], \quad [\lambda+\sum_{j=1}^n v_j:2,\dots,2]: \quad \frac{y_1^2}{16}, \dots, \frac{y_n^2}{16} \tag{2.4}
 \end{aligned}$$

*Proof.* For convenience, let the left-hand side of the assertion (2.4) be denoted by . By applying (1.1) to the integrand of (2.4) and then interchanging the order of integral sign and summation, which is verified by uniform convergence of the involved series under the given conditions, we get

$$\begin{aligned}
 & \int_0^\infty x^{\mu-1} (x+a+\sqrt{x^2+2ax})^{-\lambda} f(x) dx = \\
 & \times \sum_{k_1=0}^{\infty} (-1)^{k_1} \frac{k_1!}{(2(x+a+\sqrt{x^2+2ax}))^{1+2k_1}} \dots \sum_{k_n=0}^{\infty} (-1)^{k_n} \frac{k_n!}{(2(x+a+\sqrt{x^2+2ax}))^{1+2k_n}} \frac{1}{k_1! \Gamma(v_1+1) \dots k_n! \Gamma(v_n+1)} dx
 \end{aligned}$$

and

$$\begin{aligned}
 f = & \sum_{k_1, \dots, k_n=0}^{\infty} \frac{(-1)^1 (y/2)^1 + 2k_1}{k_1! \Gamma(\nu_1 + 1)(\nu_1 + 1)_{k_1}} \cdots \frac{(-1)^n (y_n/n)^n + 2k_n}{k_n! \Gamma(\nu_n + 1)(\nu_n + 1)_{k_n}} \\
 & \times \int_0^{\infty} x^{\mu + \nu_1 + \dots + \nu_n + 2k_1 + \dots + 2k_n - 1} (x + a \\
 & \quad + \sqrt{x^2 + 2ax})^{2k_1 + \dots + 2k_n} dx. \tag{2.5}
 \end{aligned}$$

In view of the conditions given in Theorem 1, since

$\Re(\nu_j) > -1, 0 < R(\mu) < R(\lambda + \nu_j) \leq \Re(\lambda + \nu_j + 2k_j) (k \in \mathbb{N}_0 := \mathbb{N} \cup \{0\} \text{ and } j = 1, \dots, n)$ ,

we can apply the integral formula (1.11) to the integral in (2.5) and obtain the following expression:

$$\begin{aligned}
 f = & \sum_{k_1, \dots, k_n=0}^{\infty} \frac{(-1)^1 (y/2)^1 + 2k_1}{k_1! \Gamma(\nu_1 + 1)(\nu_1 + 1)_{k_1}} \cdots \frac{(-1)^n (y_n/n)^n + 2k_n}{k_n! \Gamma(\nu_n + 1)(\nu_n + 1)_{k_n}} \\
 & \times \frac{\Gamma(2(\mu + \nu_1 + \dots + \nu_n + 2k_1 + \dots + 2k_n)) \Gamma(\lambda - \mu)}{\Gamma(1 + \lambda + \mu + 2\nu_1 + \dots + 2\nu_n + 4k_1 + \dots + 4k_n)} \times (\lambda + \nu_1 + \dots + \nu_n + 2k_1 + \dots + 2k_n)_{(1/2)(\nu_1 + \dots + \nu_n + 2k_1 + \dots + 2k_n)}.
 \end{aligned}$$

We know that  $\nu_1 + \dots + \nu_n + 2k_1 + \dots + 2k_n = \frac{\Gamma(1 + \lambda + \nu_1 + \dots + \nu_n + 2k_1 + \dots + 2k_n)}{\Gamma(\lambda + \nu_1 + \dots + \nu_n + 2k_1 + \dots + 2k_n)}$

then we have

$$\begin{aligned}
 f = & 2^{1-\mu} a^{\mu-\lambda} \sum_{k_1, \dots, k_n=0}^{\infty} \frac{(-1)^1 (y/2)^1 + 2k_1}{k_1! \Gamma(\nu_1 + 1)(\nu_1 + 1)_{k_1}} \cdots \frac{(-1)^n (y_n/n)^n + 2k_n}{k_n! \Gamma(\nu_n + 1)(\nu_n + 1)_{k_n}} \times \\
 & \frac{\Gamma(2(\mu + \nu_1 + \dots + \nu_n + 2k_1 + \dots + 2k_n)) \Gamma(\lambda - \mu) \Gamma(1 + \lambda + \mu + 2\nu_1 + \dots + 2\nu_n + 4k_1 + \dots + 4k_n)}{\Gamma(\lambda + \nu_1 + \dots + \nu_n + 2k_1 + \dots + 2k_n)} \times \\
 & \times \frac{\Gamma(1 + \lambda + \nu_1 + \dots + \nu_n + 2k_1 + \dots + 2k_n)}{\Gamma(\lambda + \nu_1 + \dots + \nu_n + 2k_1 + \dots + 2k_n)} (1/2)(\nu_1 + \dots + \nu_n + 2k_1 + \dots + 2k_n).
 \end{aligned}$$

Therefore we find that

$$\begin{aligned}
 f = & 2^{1-\mu} a^{\mu-\lambda} \prod_{j=1}^n \frac{(y_j/v_j)^v}{\Gamma(v_j+1)} \frac{\Gamma(2(\mu + \sum_{j=1}^n v_j)) \Gamma(\lambda - \mu)}{\Gamma(1 + \lambda + \sum_{j=1}^n v_j)} \times \\
 & \times \frac{\Gamma(1 + \lambda + \mu + \sum_{j=1}^n 2v_j) \Gamma(\lambda + \sum_{j=1}^n v_j)}{\Gamma(1 + \lambda + \mu + \sum_{j=1}^n 2v_j)} \times \\
 & \times \frac{(2 + \sum_{n,j=1}^{\infty} 2)}{k_1 + \dots + 4k_n} \frac{\Gamma(2k_1 + \dots + 2k_n)}{(\lambda + \sum_{j=1}^n v_j) 2k_1 + \dots + 2k_n} \times \\
 & \times \frac{1}{k_1, \dots, k_n = 0} \frac{1}{j=1} \frac{1}{n} \frac{1}{j=1} \frac{1}{n}.
 \end{aligned}$$

$$(2.6) \quad \frac{1}{(v_1 + 1)_{k_1} \cdots (v_n + 1)_n} \frac{(-y^2/16)^1}{k_1!} \cdots \frac{(-y^2/16)^n}{k_n!}.$$

Finally, we interpret the multiple series in (2.6) as a special case of the general hypergeometric series in several variables defined by (1.3). We are thus led to the assertion (2.1).

**Remark 1.** It is easily seen that if we set  $n = 1$  in (2.1) and (2.4) we can arrive at the Equation (2.1) and (2.2) in Choi and Praveen [6].

**Theorem 2.3**

$$y, \quad I \quad \left\{ \prod_{i=1}^n \frac{J(z)}{v_i} \right\} = \\ z^{v_1+\dots+v_n} \frac{\Gamma(\beta + \beta\alpha + \beta\eta + v_1 + \dots + v_m)}{\Gamma(\beta + \beta\eta + v_1 + \dots + v_m)} \times \sum_{k_1, \dots, k_m=0}^{\infty} \frac{z^{k_1+\dots+k_m}}{k_1! \cdots k_m!} \times \\ (\rightarrow) \quad \frac{F^{1:0,\dots,0}_{1:1,\dots,1} [\beta + \beta\eta + v_1 \dots + v_m; 2, \dots, 2]:[\beta + \beta\alpha + \beta\eta + v_1 + \dots + v_m]}{[v_1:1] \cdots [v_m:1]} \quad (2.7)$$

*Proof.* let left hand side of (2.7) is  $\iota$  then, we can write:

$$\iota = I^y \left\{ \prod_{i=1}^n \frac{J(z)}{v_i} \right\} \quad (2.8)$$

Now using equation (1.2), we can get

$$\iota = I^y \left\{ \sum_{\substack{i=1 \\ k=0}}^m \frac{(-1)^k \frac{z^{vi+2ki}}{2}}{k_i! \Gamma(v_i + i k_i + 1)} \right\}$$

now solving the above equation we can find

$$\iota = I^y \left\{ \sum_{\substack{\alpha \\ \beta \\ k_1, \dots, k_m=0}}^{\infty} \frac{(-1)^{k_1+\dots+k_m} \frac{z^{v_1+\dots+v_m+2k_1+\dots+2k_m}}{2}}{k_1! \cdots k_m! \Gamma(v_1 + 1 k_1 + 1) \cdots \Gamma(v_m + m k_m + 1)} \right\} \quad (2.9)$$

Now arranging the term, we get

$$\iota = \sum_{k_1, \dots, k_m=0}^{\infty} \frac{(-1)^{1+\dots+k}}{k_1! \cdots k_m! \Gamma(v_1 + 1 k_1 + 1) \cdots \Gamma(v_m + m k_m + 1)} \frac{y}{\beta} \quad (2.10)$$

Now using equation , we get

$$\iota = \sum_{\substack{k_1 \\ \dots \\ k_m=0}}^{\infty} \frac{(-1)^{1+\dots+k_m}}{k_1! \cdots k_m! \Gamma(v_1 + 1 k_1 + 1) \cdots \Gamma(v_m + m k_m + 1)} \times$$

$$\frac{\Gamma(1+\dots+1)}{1+\dots+21+\dots+2} \quad \square 1+\dots+21+\dots+2 \quad (2)$$

$$\frac{1+\dots+1}{1+\dots+21+\dots+2}$$

(2.11)

Now arranging the coefficient terms and multiply and divide by  $\Gamma(+_1 + \dots + )$ ,  hen we get our desire result [Equation.

### 3. Special Cases

In this section, we derive certain new integral formulas for the cosine and sine functions involving in the integrands of (2.1) and (2.4). To do this, we recall the following known formula (see, for example, [8, p. 79, Eq. (15)]):

$${}_1 \int_{-1/2}^0 \frac{2}{\sqrt{1-x^2}} \cos x dx. \quad (3.1)$$

Setting  $_1 = \dots = -_2$  in (2.1) and (2.4), and applying the expression in (3.1) to the resulting identities, we obtain two integral formulas stated in Corollary 1 and Corollary 2 below.

**Corollary 3.1** *Let the condition of Theorem 1 be satisfied. Then the following integral formula holds true.*

$$\begin{aligned} & \square \int_{-1}^{\infty} \frac{2(\alpha + \beta \sqrt{1-x^2})}{\sqrt{1-x^2}} \cos \left( \frac{\alpha x + \beta \sqrt{1-x^2}}{1+x^2} \right) dx = \\ & = 1 \cdot \frac{\Gamma(1+\alpha-\beta)}{\Gamma(\alpha)\Gamma(1-\alpha)} \frac{\Gamma(1+\beta-\alpha)}{\Gamma(\beta)\Gamma(1-\beta)} \\ & = 1 \cdot \frac{1}{\Gamma(-\beta)\Gamma(1+\beta-\alpha)} \frac{2}{\Gamma(\alpha)} \frac{1}{\Gamma(1-\alpha)} \frac{1}{\Gamma(\beta)} \frac{2}{\Gamma(1-\beta)} \\ & = 1 \cdot \frac{1}{2} \frac{[1+\frac{-}{2}; 2, \dots, 2], [-\frac{-}{2}; 2, \dots, 2]}{[1+\frac{-}{2}; 2, \dots, 2], [-\frac{-}{2}; 2, \dots, 2]} y^2 \\ & \quad [1/2; 1], \dots, [1/2; 1] ; -\frac{1}{4}, \dots, -\frac{1}{4^2}] \\ & \quad (3.2) \end{aligned}$$

*Proof.* let L.H.S. of (??) is F, then we can write

$$\begin{aligned}
 F &= \int_0^{\infty} (x+a \\
 &\quad - \frac{2(x+a+\sqrt{x^2+2ax})}{\pi y_j} \cos(\frac{j}{x+a+\sqrt{x^2+2ax}}) dx \\
 &\quad + \sqrt{x^2+2ax}) \sum_{j=1}^{\infty} \{ \sqrt{\frac{y_j}{2(x+a+\sqrt{x^2+2ax})}} \cos(\frac{j}{x+a+\sqrt{x^2+2ax}}) \} dx
 \end{aligned} \tag{3.3}$$

Now using (3.2), we can write above equation as

$$\begin{aligned}
 F &= \int_0^{\infty} x^{\mu-1} (x+a+\sqrt{x^2+2ax})^{-\lambda} \times \\
 &\quad I \sum_{k_1=0}^{\infty} \frac{(-1)^1 \left( \frac{y_1}{2(x+a+\sqrt{x^2+2ax})} \right)^{\frac{1}{2}}}{\Gamma(-\frac{1}{2}+k_1+1)} \cdots \sum_{k_n=0}^{\infty} \frac{(-1)^n \left( \frac{y_n}{2(x+a+\sqrt{x^2+2ax})} \right)^{\frac{n}{2}}}{\Gamma(-\frac{1}{2}+k_n+1)} I dx \\
 &\quad h
 \end{aligned} \tag{3.4}$$

Take constant term outside of integral, we get

$$\begin{aligned}
 F &= \sum_{k_1, \dots, k_n=0}^{\infty} \frac{(-1)^{k_1+\dots+k_n}}{k_1! \cdots k_n!} \frac{\frac{y_1}{2}^{-\frac{1}{2}+2k_1} \cdots \frac{y_n}{2}^{-\frac{1}{2}+2k_n}}{\Gamma(-\frac{1}{2}+k_1+1) \cdots \Gamma(-\frac{1}{2}+k_n+1)} \times \\
 &\quad \int_0^{\infty} x^{\mu-1} \left( \frac{x+a+\sqrt{x^2+2ax}}{\sqrt{x^2+2ax}} \right)^{-(\lambda-\frac{1}{2}+2k_1+\dots+2k_n)} dx
 \end{aligned} \tag{3.5}$$

Now using (3.1), we get

$$\begin{aligned}
 F &= \sum_{k_1, \dots, k_n=0}^{\infty} \frac{(-1)^{k_1+\dots+k_n}}{k_1! \cdots k_n!} \frac{\prod_{j=1}^n \frac{y_j}{2}^{-\frac{1}{2}+2k_j}}{\prod_{j=1}^n \Gamma(-\frac{1}{2}+k_j+1)} 2(\lambda - \frac{n}{2} + 2k_1 + \dots + 2k_n) \times (\lambda - \frac{n}{2} + \\
 &\quad 2k_1 + \dots + 2k_n) \frac{a}{2^n} \frac{\Gamma(1+\lambda+\mu-\frac{n}{2}+\frac{2}{2}+\frac{2}{1}+\dots+\frac{2}{n})}{\Gamma(\lambda+\mu-\frac{n}{2}+\frac{2}{2}+\frac{2}{1}+\dots+\frac{2}{n})}
 \end{aligned} \tag{3.6}$$

after little simplification of constant terms and using

$$\Gamma(1+\lambda-\frac{n}{2}+2k_1+\dots+2k_n)$$

$$\lambda - \frac{n}{2} + \frac{2}{1} + \dots + 2k_n = \frac{n}{\Gamma(\lambda - \frac{n}{2} + \frac{2}{2} + \frac{2}{1} + \dots + 2)}$$

, we get

$$\begin{aligned}
 F &= 2^{(1-\mu+2)(\mu-\lambda+2)} \frac{n!}{n!} \frac{1}{(G_{\sqrt{y}})_n} \sum_{k_1, \dots, k_n=0}^{\infty} \frac{\prod_{j=1}^n \left(\frac{-y_j}{2}\right)^{k_j}}{k_1! k_2! \dots k_n! (-\frac{1}{2} + k_j + 1)} \times \\
 &\quad \frac{\Gamma(2\mu) \Gamma(1 + \lambda - \frac{n}{2} + 2k_1 + \dots + 2) \Gamma(\lambda - \mu - \frac{n}{2} + 2k_1 + \dots + 2)_n}{\Gamma(\lambda - n + 2k_1 + \dots + 2k_n) \Gamma(1 + \lambda + \mu - \frac{n}{2} + 2k_1 + \dots + 2k_n)} \\
 &\tag{3.7}
 \end{aligned}$$

Now Multiply and divide by  $\Gamma(1 + \lambda - n/2)$ ,  $\Gamma(\lambda - \mu - n/2)$ ,  $\Gamma(\lambda - n/2)$ ,  $\Gamma(1 + \lambda - \mu - n/2)$  and  $(\Gamma(\frac{1}{2}))^n$ , we get

$$\begin{aligned}
 F &= 2^{(1-\mu+2)(\mu-\lambda+2)} \frac{n!}{n!} \frac{1}{(G_{\sqrt{y}})_n} \frac{n \Gamma(2\mu) \Gamma(1 + \lambda - \frac{n}{2}) \Gamma(\lambda - \mu - \frac{n}{2})}{\Gamma(\lambda - \frac{n}{2}) \Gamma(1 + \lambda + \mu - \frac{n}{2})} \times \\
 &\quad \sum_{\substack{j=0 \\ 1 \leq j \leq n}}^{\infty} \frac{\prod_{k=0}^n \left(\frac{-y_j}{2}\right)^{k_j}}{(1/2)_j} \frac{(\lambda \pm \frac{n}{2})_{2k_1+\dots+2k_n} (\lambda - \mu - \frac{n}{2})_{2k_1+\dots+2k_n}}{z^{2k_1+\dots+2k_n} (1 + \lambda + \mu - \frac{n}{2})_{2k_1+\dots+2k_n}} \\
 &\tag{3.8}
 \end{aligned}$$

Now using (1.3), we can easily write R.H.S. of (3.2).

**Corollary 3.2** Let the condition of Theorem 2 be satisfied . Then the following integral formula holds true.

$$\begin{aligned}
 &\int_0^{-1} (x+a \\
 &+ \sqrt{x^2 + 2ax})^{-\frac{1}{2}} \left\{ \sqrt{\frac{2(x+a+\sqrt{x^2+2ax})}{\pi x y}} \cos \left( \frac{xy}{x+a+\sqrt{x^2+2ax}} \right) \right\} dx = \\
 &\quad 2^{1-\mu+n} a^{\mu-\lambda} \frac{G_{\sqrt{y}}}{\sqrt{y}} \frac{\Gamma(\lambda-\mu)\Gamma(1+\lambda-\frac{1}{2}n)\Gamma(2\mu-n)}{\Gamma(\lambda-\frac{1}{2}n)\Gamma(1+\lambda+\mu-n)} \\
 &\quad F_{2:1,\dots,1}^{2:0,\dots,0} [[1+\lambda-\frac{1}{2}n:2,\dots,2],[2\mu-n:4,\dots,4]:[ \\
 &\quad \dots,1+\lambda+\mu-n:4,\dots,4,[\lambda]]_-, \dots, [n:2,\dots,2]: \\
 &\quad \dots, \dots, \dots, -\frac{1}{2}, \dots, -\frac{y_n}{2}]; \\
 &\quad [1/2:1] \quad [1/2:1] \quad 16 \quad 16 \\
 &\tag{3.9}
 \end{aligned}$$

*Proof.* let L.H.S. of (3.9) is  $F_1$ , the we can write

F1

$$= \int_0^\infty \frac{1}{(x+a)} - \frac{\frac{2(x+a+\sqrt{x^2+2ax})}{\pi j}}{\left\{ \sqrt{\frac{xy}{x+a+\sqrt{x^2+2ax}}} \cos\left(\frac{xy}{x+a+\sqrt{x^2+2ax}}\right) \right\}} dx \quad (3.10)$$

Now using (3.1), we can write above equation as

$$\begin{aligned} & F1 \\ & = \int_0^\infty x^{\mu-1} (x+a+\sqrt{x^2+2ax})^{-\lambda} \\ & \quad \times \prod_{k=1}^n \frac{(-1)^k \left( \frac{xy_1}{2(x+a+\sqrt{x^2+2ax})} \right)^{-\frac{1}{2}+2k}}{1 \cdot \frac{1}{2} \cdot \frac{1}{1+k}} \cdots \prod_{k=n}^\infty \frac{(-1)^k \left( \frac{xy_n}{2(x+a+\sqrt{x^2+2ax})} \right)^{-\frac{1}{2}+2kn}}{k \cdot \frac{1}{n} \cdot \frac{1}{2} \cdot \frac{1}{n+k-1}} I \\ & \quad h ) \end{aligned} \quad (3.11)$$

Take constant term outside of integral, we get

$$\begin{aligned} F1 &= \sum_{k_1, \dots, k_n=0}^\infty \frac{(-1)^{k_1+ \dots + k_n}}{1 \cdot \frac{1}{2} \cdot \frac{1}{n}} \frac{(2)_2 \cdots (2)_2}{\Gamma(-\frac{1}{2}+k_1+1) \cdots \Gamma(-\frac{1}{2}+k_n+1)} \frac{y_1 \cdots y_n}{2} \frac{1}{-(\lambda-\frac{1}{2}+2k_1+ \dots + 2k_n)} \\ &\quad \times \int_0^\infty x^{\mu-n+2k_1+ \dots + 2k_n-1} (x+a+\sqrt{x^2+2ax})^{-\lambda} dx \end{aligned} \quad (3.12)$$

Now using (1.11), we get

$$\begin{aligned} F1 &= \sum_{k_1, \dots, k_n=0}^\infty \frac{(-1)^{k_1+ \dots + k_n}}{k_1! \cdots k_n!} \prod_{j=1}^n \frac{y_j}{\Gamma(-\frac{n}{2}+j)} \frac{1}{2(\lambda-\frac{n}{2}+1+ \dots + 2)_n} \times \\ &\quad a(\lambda-n-\frac{n}{2}+2k_1+ \dots + 2k_n) \left( \frac{a}{2} \right)^{\mu-\frac{n}{2}+2+ \dots + 2k_n} \frac{\Gamma(2\mu-2+4k_1+ \dots + 4k_n)}{\Gamma(1+\lambda+\mu-2+4k_1+ \dots + 4k_n)} \Gamma(\lambda-\mu) \\ & \quad (3.13) \end{aligned}$$

after little simplification of constant terms and using

$$\frac{\Gamma(1+\lambda-\frac{n}{2}+2k_1+ \dots + 2k_n)}{\Gamma(\lambda-\frac{n}{2}+2k_1+ \dots + 2k_n)} = \frac{1}{\frac{1}{2} \cdots \frac{1}{n}}$$

, we get

$$F_1 = 2^{(1-\mu+n)} (\mu-\lambda) \left( \frac{1}{\Gamma(\lambda - \frac{n}{2} + \frac{1}{2} + \dots + \frac{k}{2})} \right) \sum_{j=1}^n \frac{\prod_{k=0}^n \frac{(-y_j)^{kj}}{4a^2}}{\Gamma(1+\lambda - \frac{k}{2} + \dots + \frac{2k}{2} + \dots + \frac{n}{2})} \times$$

$$\frac{\prod_{k=0}^n \frac{k!}{2^k} \Gamma(-\frac{1}{2} + kj + 1)}{\Gamma(1+\lambda + \mu - n + k) \Gamma(n+4k)} \quad (3.14)$$

Now Multiply and divide by  $\Gamma(2\mu - n)$ ,  $\Gamma(1 + \lambda - n/2)$ ,  $\Gamma(\lambda - n/2)$ ,  $\Gamma(1 + \lambda + \mu - n)$  and  $(\Gamma(\frac{1}{2}))^n$ , we get

$$F_1 = 2^{(1-\mu+n)} a(\mu-\lambda) \left( \prod_{j=1}^n \frac{1}{\sqrt{y_j}} \right) \frac{\prod_{k=0}^n \frac{(-y_j)^{kj}}{4a^2}}{\prod_{k=0}^n \frac{k!}{2^k} \frac{\Gamma(2\mu-n)}{\Gamma(\lambda-\frac{n}{2})} \frac{\Gamma(1+\lambda-\frac{n}{2})}{\Gamma(\lambda-\mu)}} \times$$

$$\frac{\prod_{k=0}^n \frac{(-y_j)^{kj}}{4a^2} \frac{(1/2+k)^{2k+1} \dots + 2kn}{2^{2k+1} \dots + 2kn}}{\prod_{k=0}^n \frac{(1/2+k)^{2k+1} \dots + 2kn}{2^{2k+1} \dots + 2kn} \frac{(2\mu-n)4k_1 \dots + 4kn}{(1+\lambda+\mu-n)4k_1 \dots + 4kn}} \quad (3.15)$$

Now using (1.3), we can easily write R.H.S. of (3.9).

**Remark 2.** It is easily seen that if we set  $n = 1$  in (3.2) and (3.9) we can arrive at the Equation(3.2) and (3.3) in Choi and Praveen [6].

Now recall the following formula (see, for example, [8, p. 79, Eq. (14)]):

$$J_{1/2}(z) = \sqrt{\frac{\pi}{2}} z \sin z. \quad (3.16)$$

Just as in finding the formulas (3.2) and (3.9), setting  $v_1 = \dots = v_n = \frac{1}{2}$  in (2.1) and (2.4), and

applying the expression in (3.16) to the resulting identities, we get two integral formulas asserted in Corollary 3 and Corollary 4 below.

**Corollary 3.3** Let the condition of Theorem 1 be satisfied. Then the following integral formula holds true.

$$\int_0^\infty \frac{x^{\mu-1} (x+a+\sqrt{x^2+2ax})^{-\lambda}}{x^n} \prod_{j=1}^n \frac{\sin(x+a+\sqrt{\frac{1}{2}2ax})}{\Gamma(2\mu)\Gamma(1+\lambda+\frac{1}{2}n)\Gamma(\lambda-\mu+\frac{1}{2}n)} dx =$$

$$2^{1-\mu+2} a^{\mu-\lambda+2} \frac{(\Gamma(\sqrt{y_j}))^n}{\prod_{j=1}^n \frac{1}{2}} \frac{2}{\Gamma(\lambda+\frac{1}{2}n)\Gamma(1+\lambda+\mu+\frac{1}{2}n)} \cdot$$

$$F^{2:0;\dots;0}_{2:1;\dots;1} \left[ [1+\lambda \mp \frac{1}{2}n:2,\dots,2], [\lambda-\mu+\frac{1}{2}\bar{n}:2,\dots,2] \right]$$

$$\left[ [1+\lambda+\mu+\frac{1}{2}n:2,\dots,2], [\frac{1}{2}+\frac{n}{2}:2,\dots,2] \right]$$

$$\frac{\frac{-1}{2}; \dots; \frac{-1}{2}}{\frac{1}{2}; \dots; \frac{1}{2}} ; \frac{1}{4a^2} ; \dots ; \frac{1}{4a^2} ] \cdot$$

$$(3.17)$$

*Proof.* let L.H.S. of (3.17) is F<sub>2</sub>, the we can write

$$\begin{aligned}
 & F_2 \\
 &= \int_0^\infty \frac{(x+a)}{\sqrt{x^2+2ax}} - \sum_{j=1}^{\infty} \left\{ \sqrt{\frac{2(x+a+\sqrt{x^2+2ax})}{\pi j}} \sin \left( \frac{jy}{x+a+\sqrt{x^2+2ax}} \right) \right\} dx
 \end{aligned} \tag{3.18}$$

Now using (3.16), we can write above equation as

$$\begin{aligned}
 F_2 &= \int_0^\infty x^{\mu-1} \frac{(x+a+\sqrt{x^2+2ax})^{-\lambda}}{1+2k_1} \times \frac{1}{1+2kn} \\
 &\quad (-1)^1 \left( \frac{y_1}{1} \right)^2 \cdots (-1)^n \left( \frac{y_n}{n} \right)^2 \\
 &\quad \prod_{k_1=0}^{\infty} \frac{2(x+a+\sqrt{x^2+2ax})}{1 \Gamma(\frac{1}{2} + k_1 + 1)} \cdots \prod_{k_n=0}^{\infty} \frac{2(x+a+\sqrt{x^2+2ax})}{n \Gamma(\frac{1}{2} + k_n + 1)} dx
 \end{aligned} \tag{3.19}$$

Take constant term outside of integral, we get

$$\begin{aligned}
 F_2 &= \sum_{k_1, \dots, k_n=0}^{\infty} \frac{(y_1)^{1+2k_1}}{k_1! \cdots k_n!} \frac{(-1)^{\frac{1}{2} \sum_{j=1}^{k_1} j}}{\Gamma(-k_1+1) \cdots \Gamma(-k_n+1)} \times \\
 &\quad \int_0^\infty (x+a+\sqrt{x^2+2ax})^{-(\lambda+2k_1+\cdots+2kn)} dx
 \end{aligned} \tag{3.20}$$

Now using (1.11), we get

$$\begin{aligned}
 F_2 &= \sum_{k_1, \dots, k_n=0}^{\infty} \frac{(-1)^{\frac{1}{2} \sum_{j=1}^{k_1} j}}{k_1! \cdots k_n!} \frac{n!}{n} \frac{1}{\prod_{j=1}^{k_1} (\frac{1}{2} + k_1 + j)^2} \frac{1}{2(\lambda + \frac{n}{2} + 2k_1 + \cdots + 2kn)} \times \\
 &\quad \frac{\prod_{j=1}^{k_1} \Gamma(\frac{1}{2} + k_1 + j)}{\mu \Gamma(2\mu) \Gamma(\lambda - \mu + \frac{n}{2} + \frac{1}{2} + \cdots + 2)} \\
 &\quad \frac{(\lambda + \frac{n}{2} + 2k_1 + \cdots + 2kn)^{\alpha}}{\alpha! (2)^{\frac{n}{2}}} \frac{1}{\Gamma(1 + \lambda + \mu + \frac{n}{2} + 2k_1 + \cdots + 2)}
 \end{aligned} \tag{3.21}$$

After little simplification of constant terms and using

$$\lambda + \frac{n}{2} + \frac{1}{2} + \cdots + 2k = \frac{n}{n} = \frac{\Gamma(1 + \lambda + \frac{n}{2} + 2k + \cdots + 2)}{\Gamma(\lambda + \frac{1}{2} + \frac{1}{2} + \cdots + 2)} \frac{n}{n}$$

, we get

$$\begin{aligned}
 F_2 = & 2^{(1-\mu+2)(\mu-\lambda+2)} (G \sqrt{y_j}) \sum_{j=1}^{\infty} \frac{n}{k! \Gamma(\frac{1}{2} + k + 1)} \times \\
 & \frac{\prod_{j=1}^{n-1} \frac{-y_j}{2^j}}{\Gamma(\lambda + \frac{n}{2} + 2k + \dots + \frac{1}{2})} \frac{\Gamma(1+\lambda+\mu+\frac{n}{2}+2k+\dots+2)}{\Gamma(1+\lambda+\mu+\frac{n}{2})} \frac{n}{n} \\
 & \frac{\Gamma(2\mu)\Gamma(1+\lambda+\frac{n}{2})}{\Gamma(\lambda+\frac{n}{2}+2k+\dots+\frac{1}{2})} \frac{n}{n} \frac{n}{n} \quad (3.22)
 \end{aligned}$$

Now Multiply and divide by  $\Gamma(1+\lambda+n/2)$ ,  $\Gamma(\lambda-\mu+n/2)$ ,  $\Gamma(\lambda+n/2)$ ,  $\Gamma(1+\lambda-\mu+n/2)$  and  $(\Gamma(\frac{3}{2}))^n$ , we get

$$\begin{aligned}
 F_2 = & 2^{\frac{(1-\mu+\lambda)}{2} n} (G \sqrt{y_j}) \frac{\Gamma(2\mu)\Gamma(1+\lambda+\frac{n}{2})\Gamma(\lambda-\mu+\frac{n}{2})}{\Gamma(\lambda+\frac{n}{2})\Gamma(1+\lambda+\mu+\frac{n}{2})} \times \\
 & \frac{\prod_{j=1}^n \frac{(-y_j)^k}{4a^2}}{\prod_{j=1}^n \frac{k!}{j}} \frac{(1+n\lambda+\frac{n}{2})_{2k} 1+\dots+2kn (\lambda-\mu+\frac{n}{2})_{2k} 1+\dots+2kn}{(1+\lambda+\mu+\frac{n^2}{2})_{2k} 1+\dots+2kn} \\
 & \frac{1}{(3/2)^n} \quad j \quad (3.23)
 \end{aligned}$$

Now using (1.3), we can easily write R.H.S. of (3.17).

**Corollary 3.4** Let the condition of Theorem 2 be satisfied . Then the following integral formula holds true.

$$\begin{aligned}
 & \int_0^\infty (x+a \sqrt{x^2+2ax})^{-\frac{1}{2}} \left\{ \sum_{j=1}^{\infty} \frac{\pi x y_j}{n} \sin \left( \frac{x y_j}{x+a+\sqrt{x^2+2ax}} \right) \right\} dx = \\
 & 2^{1-\mu} a^{\mu-\lambda} (G \sqrt{y_j}) \sum_{j=1}^n \frac{\Gamma(\lambda-\mu)\Gamma(1+\lambda+\frac{1}{2}n)\Gamma(2\mu+n)}{\Gamma(\lambda+\frac{1}{2}n)\Gamma(1+\lambda+\mu+n)} \\
 & F^{2:0,\dots,0}_{2:1,\dots,1} \left[ [1+\lambda+\frac{n}{2}:2,\dots,2], [2\mu+n:4,\dots,4]; \right. \\
 & \left. -\frac{1}{1+\lambda+\mu+n:4,\dots,4}, [\lambda+\frac{1}{2}:2,-\frac{1}{2}n:2,\dots,2] \right] \\
 & \frac{1}{[3/2:1]}; \dots; \frac{1}{[3/2:1]} ; -\frac{1}{16}, \dots, -\frac{n}{16} \right] \quad (3.24)
 \end{aligned}$$

*Proof.* let L.H.S. of (3.24) is  $F_3$ , the we can write

F3

$$\begin{aligned}
 &= \int_0^\infty (x+a) \frac{-}{+} \\
 &\quad + \sqrt{x^2 + 2ax} \frac{-}{+} \sum_{j=1}^{\infty} \left\{ \sqrt{\frac{2(x+a+\sqrt{x^2+2ax})}{\pi j}} \sin \left( \frac{xy}{x+a+\sqrt{x^2+2ax}} \right) \right\} dx \\
 &\quad (3.25)
 \end{aligned}$$

Now using (3.16), we can write above equation as

$$\begin{aligned}
 &F3 = \int_0^\infty x^{\mu-1} (x+a+\sqrt{x^2+2ax})^{-\lambda} \times \\
 &\quad \frac{1}{xy_1} \frac{1}{2} \frac{1}{2+2k_1} \dots \frac{1}{2+2kn} \\
 &\quad \frac{(-1)}{1! \Gamma(\frac{1}{2} + k_1 + 1)} \dots \frac{(-1)}{n! \Gamma(\frac{1}{2} + k_n + 1)} I^{dx} \\
 &\quad h \quad k_1=0 \quad 1 \quad 2 \quad 1 \quad n \quad \frac{1}{2} \quad n \\
 &\quad (3.26)
 \end{aligned}$$

Take constant term outside of integral, we get

$$\begin{aligned}
 &F3 = \sum_{\substack{1 \leq k_1 \leq k_2 \dots k_n = 0}}^{\infty} \frac{(-1)^{k_1+k_2+\dots+k_n}}{1! 2! \dots n!} \frac{\frac{y_1}{2}^{1+2k_1} \dots \frac{y_n}{2}^{1+2k_n}}{\Gamma(\frac{1}{2} + k_1 + 1) \dots \Gamma(\frac{1}{2} + k_n + 1)} \times \\
 &\quad \int_0^\infty x^{\frac{\mu+n+2k_1+\dots+2kn-1}{2}} \frac{1}{(x+a+\sqrt{x^2+2ax})^{-(\lambda+\frac{n}{2}+2k_1+\dots+2kn)}} dx \\
 &\quad (3.27)
 \end{aligned}$$

Now using (1.11), we get

$$\begin{aligned}
 &F3 = \sum_{k_1, \dots, k_n=0}^{\infty} \frac{(-1)^{k_1+k_2+\dots+k_n}}{1! 2! \dots n!} \frac{n! \prod_{j=1}^n (\frac{1}{2} + 2kj)}{\prod_{j=1}^n \Gamma(\frac{1}{2} + k_j + 1)} \frac{2(\lambda + \frac{n}{2} + 2k_1 + \dots + 2kn)}{2} \times \\
 &\quad a^{\frac{\mu+n+2k_1+\dots+2kn}{2}} \frac{\Gamma(2\mu+2)}{\Gamma(1+\lambda+\mu+2)} \frac{\Gamma(2k_1+4k_2+\dots+4k_n)}{\Gamma(1+4k_1+\dots+4k_n)} \frac{\Gamma(\lambda-\mu)}{n!} \\
 &\quad (2) \quad (3.28)
 \end{aligned}$$

after little simplification of constant terms adding +

$$\begin{aligned}
 &\lambda + \frac{n}{2} + \frac{2k_1}{2} + \dots + \frac{2k_n}{2} = \frac{2k_1 + \dots + 2k_n}{2} \\
 &\frac{2}{2} \quad 1 \quad n \quad \frac{1}{2} \quad 1 \quad n \\
 &\frac{n-2}{2} \quad \frac{1}{1} \quad n
 \end{aligned}$$

, we get

$$\begin{aligned}
 F_3 = & 2(1-\mu+n)(\mu-\lambda) \left( \sum_{j=1}^n \frac{\prod_{j=1}^n (\frac{-y_j}{4a^2})^{kj}}{\Gamma(2\mu+n+4k+\dots+k)} \right) \times \\
 & \frac{\Gamma(1+\lambda+\frac{n}{2}+2k+\dots+k) \Gamma(\lambda-\mu)}{\Gamma(\lambda+\frac{n}{2}+1) \Gamma(1+\lambda+\mu+n+k) \Gamma(1+\dots+4k+n)} \\
 (3.29) \quad & \text{Now Multiply and divide by } \Gamma(2\mu+n), \Gamma(1+\lambda+n/2), \Gamma(\lambda+n/2), \Gamma(1+\lambda+\mu+n) \\
 & \text{and } (\Gamma(\frac{3}{2}))^n, \text{ we get}
 \end{aligned}$$

$$\begin{aligned}
 F_3 = & 2(1-\mu+n)(\mu-\lambda) \left( G \sum_{j=1}^n \frac{\Gamma(2\mu+n)\Gamma(1+\lambda+\frac{n}{2})\Gamma(\lambda-\mu)}{\Gamma(\lambda+n)\Gamma(1+\lambda+\mu+\frac{n}{2})} \right) \times \\
 & \sum_{j=0}^{\infty} \frac{\prod_{j=1}^n (\frac{-y_j}{4a^2})^{kj} (1+\lambda+\frac{n}{2})_{2k} (2\mu+n)_{4k} \dots (1+\lambda+\mu+n)_{4k}}{(kj!)_{2k} (3/2)_j} \quad (3.30)
 \end{aligned}$$

Now using (1.3), we can easily write R.H.S. of (3.24).

**Remark 3.** It is easily seen that if we set  $n = 1$  in (3.17) and (3.24) we can arrive at the Equation (3.7) and (3.8) in Choi and Praveen [6].

#### 4. Conclusion

Bessel functions are very important special functions. Bessel functions of the first kind ( $y$ ) are oscillatory and could be used as generalizations of trigonometric functions. For large

argument ( $y \geq 1$ ) the function  $\sqrt[2]{Jv(y) \pi_i y^s}$  well approximated by the trigonometric function  $\cos(y - \frac{\pi}{2} - \frac{\pi}{4})$ . For Example: Special cases of infinite integrals of the type

$$\int_0^{\infty} (x+a+\sqrt{x^2+2ax})^{-\lambda} G Jv \left( \sum_{j=1}^n \frac{y^{2j}}{j} \frac{dx}{x+a+\sqrt{x^2+2ax}} \right) \quad (4.1)$$

involving the product of Bessel function of the first kind  $Jv(y)$ , had been researched by a many of authors with different arguments. For  $n=3$ , the infinite integrals with different argument was evaluated independently by Bailey [4]p.45, Eq.(6.1), using different methods and discussed a many of special cases of their main integral involving the product of three Bessel functions. Therefore, the results presented in this chapter are easily converted in forms of the known or new integrals after some suitable parametric replacement. We are also trying to find possible applications of those results presented.

## References

- [1] Abramowitz, M.;Stegun,I.A. Handbook of mathematical functions with formulas,graphs, andmathematical tables.Washington, DC: US Government Printing Office; 1964.
- [2] Andrews, G.E.;Askey, R. ;Roy, R. Special functions. Volume 71 of Encyclopedia ofMathematics and Its Applications.Cambridge: Cambridge University Press; 1999.
- [3] Ali, S. On some new unified integrals. *Adv. Comput. Math. Appl.* 1(3),151-153,
- [4] Bailey, W.N. Some infinite integrals involving Bessel functions,*Proc.LondonMath.Soc.*(2) 40,37-48,1936.
- [5] Brychkov, Y. A. *Handbook of Special Functions, Derivatives, Integrals, Series andOtherFormulas*,CRC Press, Taylor & Francis Group, Boca Raton, London, and New York, 2008.
- [6] Choi, J. ; Agarwal, P. Certain unified integrals associated with Bessel functions,appear inBoundary Value Problems, 2013.
- [7] Erdélyi, A.; Magnus, W.; Oberhettinger, F.; Tricomi, F. G. *Higher TranscendentalFunctions*,Vol. **II** McGraw-Hill Book Company, New York, Toronto, and Gray, A.; Mathews, G.B. A treatise on Bessel functions and their applications to physics. 2nded., prepared by A. Gray and T.M. MacRobert. London: Macmillan;1922.  
Y.L.Luke, Integrals of Bessel functions. NewYork: McGraw-Hill; 1962.
- Olver, F. W. L.; Lozier, D. W.; Boisvert, R. F.; Clark, C. W. *NIST Handbook ofMathematical Functions*, Cambridge University Press, 2010.
- Oberhettinger, F. *Tables of Mellin Transforms*, Springer-Verlag, New York, 1974.
- Rice, S.O. On contour integrals for the product of two Bessel functions,*Quart. J.Math.Oxford Ser.*6,52-64,1935.

Srivastava, H.; Choi, M. J. *Zeta and q-Zeta Functions and Associated Series and Integrals*, Elsevier Science Publishers, Amsterdam, London and New York, 2012.

[8] Srivastava, H.M.; Exton, H. A generalization of the Weber-Schafheitlin integral. *J.Reine Angew.*

[9] Srivastava, H. M.; Karlsson, P. W. *Multiple Gaussian Hypergeometric Series*, Halsted Press (Ellis Horwood Limited, Chichester), John Wiley and Sons, New York, Chichester, Brisbane and Toronto, 1985.

[10] Wang, Z.X.; Guo, D.R. Special functions. Singapore: World Scientific; 1989. Watson, G. N. *A Treatise on the Theory of Bessel Functions*, Cambridge Mathematical Library edition, Cambridge University Press, 1995, Reprinted 1996.

Whittaker, E.T.; Watson, G.N. *A course of modern analysis*. 4th ed. Cambridge: Cambridge University Press; 1927.

# Analyzing Mathematical Model of Tumor Growth And Their Applications

Aadil Rashid Sheergojri, Pervaiz Iqbal

**Abstract** Cancer is a spontaneous, organic change marked by genetic alterations that lead to tumor growth, clinical progression, immune evasion, and the evolution of chemoresistance. Mathematical models of tumor growth have been reviewed in this paper. Mathematical equations were constructed using ordinary differential equations (ODEs), partial differential equations (PDEs), and discrete modeling features to model the tumor cell's growth rate. The stochastic Gompertz model is better suited for evaluating experimental results than the stochastic logistic model. Also, PDEs estimate the long-term change in the total tumor cell population, and the discrete models analyze actions at the scale of individual cells over continuum models. A summary of the major study problems is given, and a rationale is provided for the conclusion.

**Keywords-** Cancer, tumor growth, mathematical modeling, ordinary differential equations, partial differential equation and discrete models

## 1. Introduction

Cancer is the world's second leading cause of mortality worldwide, with low and middle-income nations accounting for 70% of cancer deaths. However, nothing is known about the evolutionary mechanisms governing its lifespan and demise [1]. Over 13 million people are expected to have some form of illness by 2030. While advances in treating cancer such as surgery, chemotherapy, immunotherapy, and radiation have been made, much remains unclear about how cancer cells are generated, spread, and eliminated [2]. Throughout the tumor process, cancer cells develop many hallmark changes. Cells are the fundamental and operational components of life in the human body. Developing new cells is achievable through dividing, growing, differentiating, or dying. Cells follow a natural mechanism that develops more rapidly, allowing an individual to expand, especially during the early stages of our lives [3, 4].

Cancer modeling encompasses various mathematical formalisms categorized based on size, method, or spatial structure integration. Significant advances have been made in the mathematical modeling of tumor progression. The simplest models only consider the number of tumor cells, resulting in a variable whose temporal evolution is investigated. More complex models include several quantities (for example, the number of tumor cells or other types of cells) that are still dependent on time [5, 6].

Mathematical, biological modeling has a strong record since it allows for the analysis and simulation of complicated biological dynamic systems at a cheap cost [7]. As a highly diverse illness, tumors grow in diverse body organs and tissues, and malignancies derived from the same tissue can be classified into illness categories based on variations in genetic data [8, 9]. Mathematical models have been constructed to comprehend the dynamic nature of cancer cell growth. Mathematical models aid in predicting tumor size and optimizing medical interventions [10].

Mathematical models have been used to investigate and prevent cancer in various ways. Models are also used to study how tumor originates and spread. They improve or even customize ongoing medication protocols, forecast the efficacy of novel medicines or combinations of multiple medications, and provide insight into drug resistance development. While models offer enormous promise to enhance cancer therapy research and execution, they will only achieve this potential if they produce accurate predictions [11- 15].

A model of tumor development serves as the foundation for any mathematical model used to investigate cancer therapy. This study emphasizes tumor development models using ordinary differential equations (ODEs). Various ODE models have been developed to describe tumor development, frequently used to anticipate the success of cancer therapies. However, the decision of a growth strategy is frequently influenced by the simplicity of mathematical analysis or whether it gives the best model for tumor growth [16, 17]. Seven deterministic ODE models have been used to characterize the behavior of cancer cell growth and proliferation, including exponential, Mendelsohn, logistic, linear, surface, Gompertz, and Bertalanffy. In reality, parametric

Aadil Rashid Sheergojri

Department of Mathematics and Actuarial Science, B. S. Abdur Rahman Crescent Institute of Science and Technology, Chennai-INDIA

E-mail: aadilrashid1996@gmail.com

Pervaiz Iqbal

Department of Mathematics and Actuarial Science, B. S. Abdur Rahman Crescent Institute of Science and Technology, Chennai-INDIA

E-mail: pervaizmaths@gmail.com

P. Agarwal et al. (eds.), Recent Developments in Engineering & Technology-II Feb 25-26, 2022, AICE, Jaipur, India

methods fail to explain the dynamic process of cancer cell growth. In this situation, studies have been conducted to extend the deterministic logistic and Gompertz models to their probabilistic counterparts [18-20].

Modeling is increasingly interested in the relationship between innate immunity and carcinoma (cancer). Differential equations are the most significant area of modern mathematics in modeling, and they reside at the intersection of mathematical analysis. In biomedical sciences, the concept of differential equations (ODE/PDE) is an incredible resource. Mathematicians have benefited greatly from applying mathematical logic to the discoveries of technology, economics, biology, and other disciplines. We'll examine various modeling techniques and explore their ability to validate and estimate malignancy genetics. The study of several ODE growth models in both deterministic and stochastic forms is reviewed in this work. Also, partial differential equation models (PDEs) and discrete models concepts have been examined in this study.

## 2. Methodology

Many of the models reviewed here were developed during the earlier stages of tumor development research, which focused on developing equations describing cancer cell proliferation. The parametric or deterministic models have been extensively used for tumor cell growth. These models describe the variation in tumor volume, V, across time, 't' to anticipate tumor development. Also, PDE models are used to estimate the long-term change in the total tumor cell population and discrete models are used to analyze actions at the scale of individual cells over continuum models.

### Ordinary Differential Equation Models

These models are important for understanding complicated procedures in biological sciences. Numerous methodologies, including continuity and dynamic modeling, are used to study these models, but most typically computational methods. A tumor's volume can be difficult to estimate because of the constant passage of time. Cells in a tumor can develop, remain dormant, or die. Thus, expressing the proportion of infected tumor cells as a matter of necessity is exceedingly difficult. It is, however, quite simple to describe the projected damage to cell numbers as the time passes.

### Exponential Model

Cells divide consistently into the initial phases of tumor development, producing two identical daughter cells every cycle. The exponential model, in which growth is proportionate to the population, perfectly depicts the initial phases of tumor progression. The tumor's growth rate is represented by the proportional constant, r. This model was frequently used in early tumor development trajectory assessment and looks fairly influential in determining growth prospects. However, this model is rendered unusable in the final phases when vasculature and nutrition deprivation becomes a factor, so this model's extension is required [13, 20-22]. The exponential model equation is given by

$$\frac{dV}{dt} = rV \quad (1)$$

Where  $r$  the proportionality constant or the proliferative rate of tumor cells and  $V$  is tumor cell concentration. The solution of equation (1) is  $V = V_0 e^{rt}$ , where  $V_0$  is the volume of tumor at time  $t = 0$ .

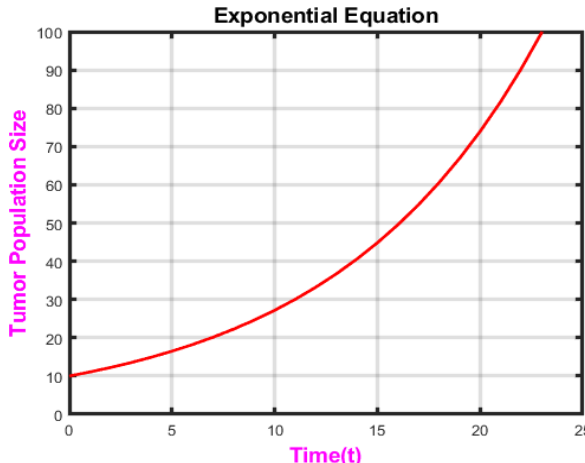


Fig. 2.1.1 In this case, the exponential tumor population growth is defined when we take  $V = 10$ ,  $r = 0.1$  and  $t \in [0, 25]$ .

### Mendelsohn Model

As a special case of equation (1), introduced by Mendelsohn, where the growth rate of tumor is proportional to the volume raised to the power K, which takes any value. The Mendelsohn model equation is given by

$$\frac{dV}{dt} = rV^K \quad (2)$$

If  $K = 1$ , the solution is the above exponential growth curve, but for  $K \neq 1$  the solution of equation (2) is given by  $V = ((1 - K)(rt + C))^{1-K}$ . Where  $C$  is a constant related to the initial condition [15, 21].

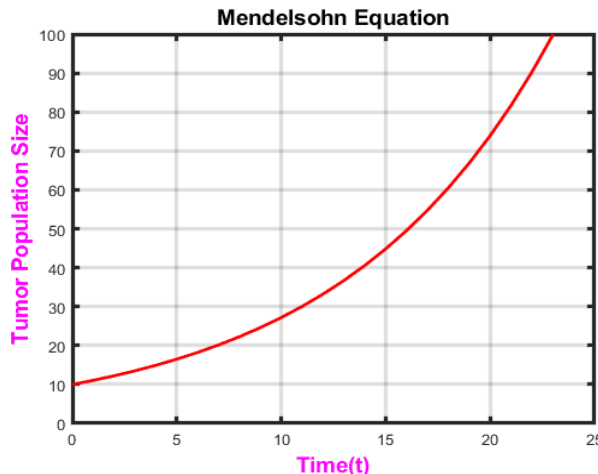


Fig. 2.1.2 In this case, the Mendelsohn tumor population growth is defined when we take  $V = 10, r = 0.1, K = 1$  and  $t \in [0, 25]$

### Logistic Model

The logistic (Verhulst) growth model begins as an exponential growth model, but as time progresses, it asymptotically reaches the limiting cellular carrying capacity  $K$ . The model equation is given by

$$\frac{dV}{dt} = rV(1 - \frac{V}{K}) \quad (3)$$

Where  $K$  is the carrying capacity parameter, expresses a maximum reachable size due to the competition between the cells. Since then, it has been a staple of biomathematics, effectively dealing with many systems biology, from microbial pathogens to algae and mammals. The solution of equation (3) is given by  $V = \frac{V_0 e^{rt}}{1 + \frac{V_0}{K} e^{rt}}$  [15, 21, 22].

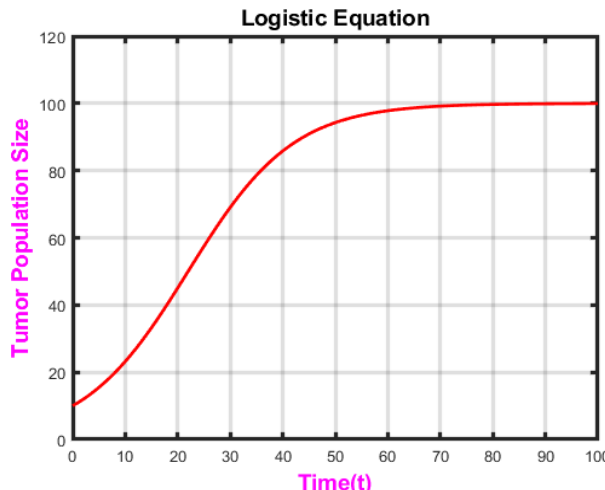


Fig. 2.1.3 In this case, the logistic tumor population growth is defined when we take  $V = 10, r = 0.1, K = 100$  and  $t \in [0, 100]$ .

### Linear Model

The linear model indicates that growth begins exponentially and becomes fairly static. The initial exponential growth rate is supplied by  $r/K$  in this model, whereas the latter constant growth rate is given by  $r$ . The model was first used to study the development of cancer cell clusters in initial studies [21, 22-24]. The model equation is given by

$$\frac{dV}{dt} = \frac{rV}{V+K} \quad (4)$$

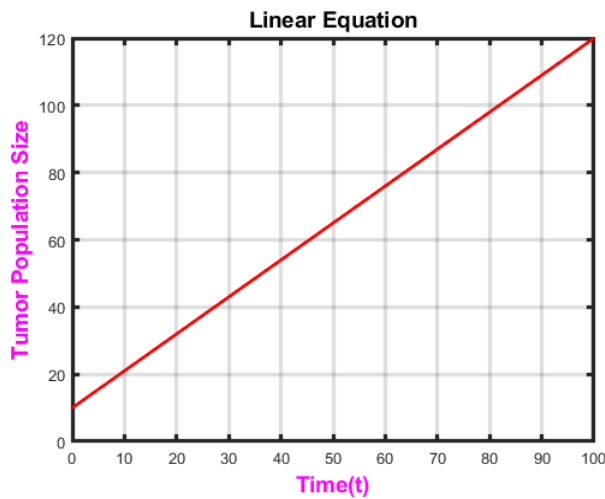


Fig. 2.1.4 In this case, the linear tumor population growth is defined when we take  $V = 10, r = 0.1, K = 1$  and  $t \in [0, 100]$ .

### 2.1.5 Surface Model

The surface model suggests that just a thin layer of cells at the tumor's interface divides, whereas cells inside solid tumors do not divide and remain mitotically dormant. Here, the exponential growth at first, with surface growth taking control as time progresses. The model equation is given as

$$\frac{dV}{dt} = \frac{-rV}{(V+K)^3} \quad (5)$$

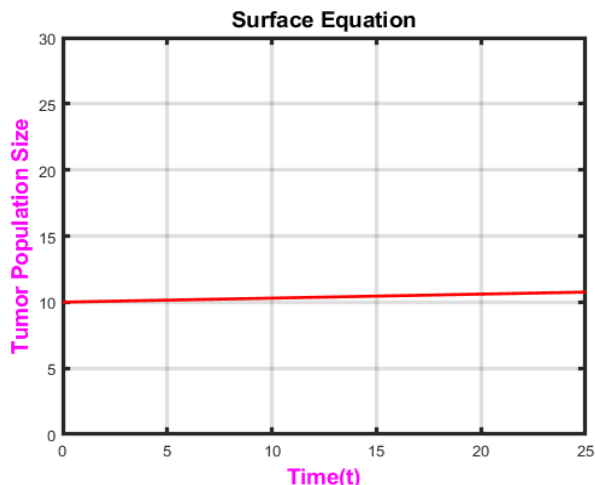


Fig. 2.1.5 In this case, the surface tumor population growth is defined when we take  $V = 10, r = 0.1, K = 1$  and  $t \in [0, 25]$ .

### Gompertz Model

One of the most widely used sigmoid models for modeling growth data and other data is the Gompertz model, perhaps second only to the logistic model. Numerous variable growth rate functions have been considered in tumor growth. Gompertz growth has been shown to reproduce cell proliferation that slows with population size, making it ideal for monitoring tumor development slowing as tumor size increases. The growth rate is determined by dividing the current population's negative logarithm by the carrying capacity. The Gompertz model equation is given by

$$\frac{dV}{dt} = -rV \log\left(\frac{V}{K}\right) e^{-rt} \quad (6)$$

The dynamics of  $V$  over time are defined by the Gompertz model. In this context, a significant query that frequently arises in research is when  $V$  approaches a particular interest value. The solution of equation (6) is given by  $V = Ke^{-ln(\frac{K}{V})}e^{-rt}$  [24-26].

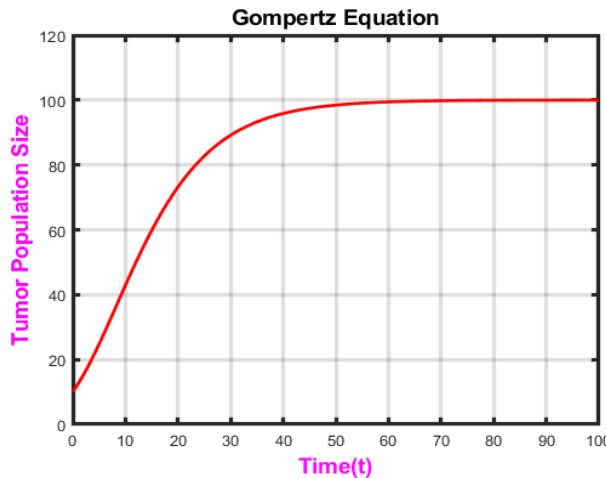


**Fig. 2.1.6** In this case, the Gompertz tumor population growth is defined when we take  $V = 10$ ,  $r = 0.1$ ,  $K = 100$  and  $t \in [0, 100]$ .

#### Bertalanffy Model

The Bertalanffy equation was presented as a model for organism growth in 1949 by Ludwig von Bertalanffy. The biological concepts of anabolism and catabolism, or growth and destruction, formulate the equation. The Bertalanffy model may be written as an ordinary differential equation with two constant coefficients,  $r$ , and  $K$ , representing the population growth rate and the population's "natural" mortality rate [22, 27, 28]. The following equation can represent the Bertalanffy population model

$$\frac{dV}{dt} = rV^{\frac{2}{3}} - KV \quad (7)$$

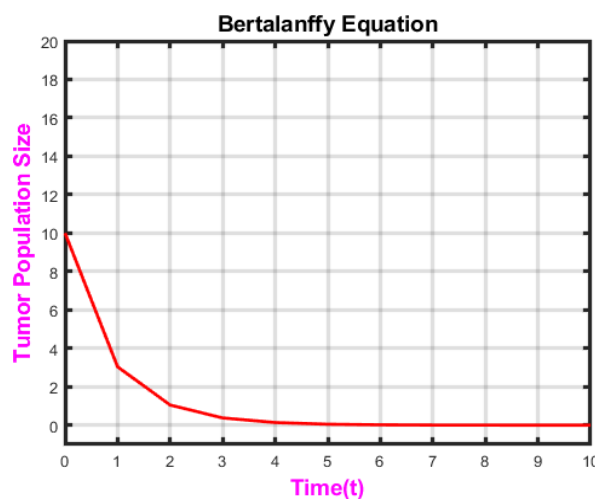


**Fig. 2.1.7** In this case, the Bertalanffy tumor population growth is defined when we take  $V = 10$ ,  $r = 0.1$ ,  $K = 1$  and  $t \in [0, 10]$ .

All models discussed above have limitations in predicting the latter stages of tumor progression and cannot forecast long-term tumor growth rates. The Gompertz model has been proven to offer the greatest fit for clinical and experimental evidence. As a result, modeling the tumor development process using deterministic models is insufficient to represent the real pattern of tumor progression, and these models must be extended to their stochastic equivalent.

In addition to the models mentioned above, several stochastic models of solid tumor growth were reviewed in this paper. The stochastic model has long been regarded as the basis of tumor heterogeneity research. Compared to their deterministic counterparts, stochastic models are more realistic and allow for formulating and resolving issues of considerable practical relevance.

#### Stochastic Logistic Model

In some stochastic logistic models, the stochastic differential equations for the class of conversion probability density functions were reduced to their corresponding Fokker-Plank equations. The stochastic logistic equation randomizes the population growth parameter [29, 30]. Here the Weiner process is perturbed in the deterministic logistic model, and so the model equation is given as

$$\frac{dV}{dt} = (rV - KV) + (\sigma) \quad (8)$$

Where  $\sigma > 0$  is the diffusion coefficient, and  $(t)$  is a Wiener process with a Gaussian zero-mean distribution.

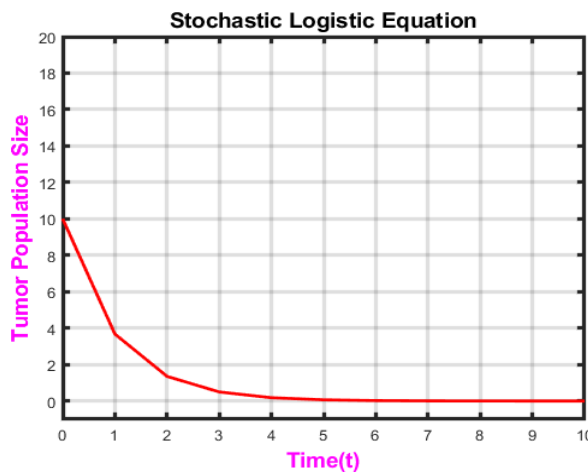


Fig. 2.1.8 In this case, the stochastic logistic tumor population growth is defined when we take  $V = 10, r = 0.1, K = 1$  and  $t \in [0, 10]$ .

### Stochastic Gompertz Model

A stochastic model comparable to the Gompertz system was presented to integrate the significant fluctuations produced by external effects. A few years ago, a stochastic version of the Gompertz law was proposed to account for random fluctuations in parameter estimations. The stochastic Gompertz tumor cell growth method has recently been developed to include cell fission and death at predetermined frequencies. The generalized system has been expressed as a functional Fokker-Planck equation (FPE) [31-33]. Here the Weiner process is perturbed in the Gompertz deterministic model, and so the model equation is given as

$$\frac{dV}{dt} = (rV - KV \ln V) + (\sigma t) \quad (9)$$

Where  $\sigma > 0$  denotes the diffusion coefficient,  $(t)$  denotes a Wiener cycle with a Gaussian zero-mean distribution, and the  $dt$  variance is supplied by the time increase  $t$ . This mathematical model offers a strong estimate and describes the uncontrolled factors that induce cancer cell growth with a low root mean square error(RMSE) [31].

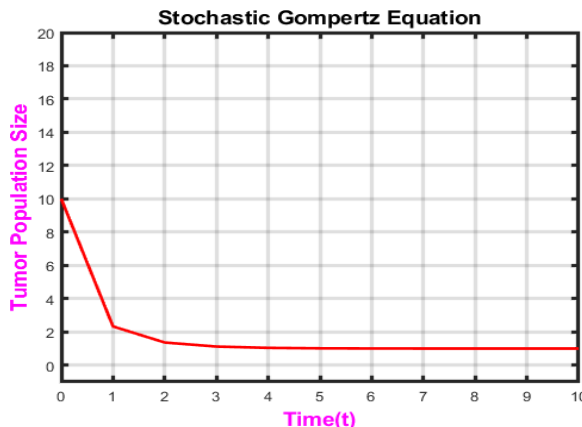


Fig. 2.1.9 In this case, the stochastic Gompertz tumor population growth is defined when we take  $V = 10, r = 0.1, K = 1$  and  $t \in [0, 10]$ .

### 3. Partial Differential Equation Models

A major drawback of using an ordinary differential equation technique to estimate the long-term change in the total tumor cell population is that no temporal information is provided to the equations. To put it another way, patients don't die because of the overall quantity of tumor cells in their bodies, but rather because cancerous tumors penetrate the organ and propagate (metastasize) across the body to produce subsequent tumors. These tumors that have spread throughout the body are the most common cause of death for cancer patients. Cancer invasion and metastatic progression are critical and spatiotemporal phenomena that may be modeled using partial differential equation (PDE) methods. For simulating the spatiotemporal development of cancer cells, we employ a structure of PDEs, which goes like this:

$$\frac{\partial N}{\partial t} = \nabla \cdot D_N (1 - P) \nabla N + \sigma N(1 - N) \quad (10)$$

Where  $D_N$  represents the (steady) dynamic viscosity,  $\sigma$  represents the tumor cell's metastatic potential, and  $P$  represents healthy host tissue.

A partial differential equation model describes the unique dissemination of a transcription disease within a tumor and its influence on tumor development. Also, comparable circumstances for tumor elimination using three different intra-tumoral viral injections: homogeneous, central, and peripheral injections have been developed, and an immunological response, which has enhanced this PDE model [34, 35]. Green's function was used to convert the linked partial differential equations (PDEs) into implied integral values, making numerical methods easier to manage arbitrarily defined PDE variables.

#### 4. Discrete Models

A discrete model of tumor cell penetration (now encompassing development at a discrete level) developed from the conventional PDE model and a highly nonlinear method of tumor invasions concentrating on the function of haptotaxis. Due to this model's numerical simulations, researchers discovered tumors could spread beyond a surgically "perceptible border" of diseased tissue. Stochastic events and probabilities in invasion systems were first addressed in this study. Independent cancer cells can infiltrate healthy cells at a deeper depth than expected by a stochastic PDE model because of their mathematical properties. The ability to analyze actions at the scale of individual cells is one benefit discrete models have over continuum models. Like alterations and other morphological features, significant moments can be considered by employing discrete models. Modeling physiological occurrences through processes of ordinary differential equations and then linking them to cell-level characteristics have been made possible by the advent of discrete models [36, 37]. These "dynamical features" are the result of this progress.

#### 5. Discussion and conclusion

A growing variety of mathematical models have been utilized in tumor research in the past few decades. We've included case studies of how they've been built and used to demonstrate how appropriate statistical models may mimic different biochemical interactions. The role of the ODE and PDE tumor development models is addressed, and the quantitative discrepancies in their predictions of clinically significant values. The mathematical models of tumor growth are reviewed in this work. When the population difference is low relative to the average, deterministic growth models may reflect larger populations; nevertheless, when the population being modeled is low, the intrinsic variability of the birth and death process causes substantial variances. Deterministic models can extend their stochastic counterparts by utilizing the Wiener process to disturb the most relevant factors that reflect external aggression. Among the deterministic exponential, Mendelsohn, logistic, linear, surface, Gompertz, and Bertalanffy models, the logistic and Gompertz models are best suited to experimental and clinical evidence of the tumor development phase, and the exponential and Bertalanffy models are suitable for determining the early stages of tumor progression [2, 17, 37]. PDE models estimate the long-term change in the total tumor cell population. Also, discrete models analyze actions at the scale of individual cells over continuum models, which results in dynamic features. Cancer invasion and metastatic progression are critical and spatiotemporal phenomena that maybe modeled using PDE methods.

The Wiener approach disturbs the intrinsic growth rate parameter, so stochastic logistic and stochastic Gompertz mathematical models arise. Research comparing the predicted efficiency of the stochastic logistic and Gompertz models shows that the Gompertz model has poor root mean square error (RMSE) values. This demonstrates that a stochastic Gompertz model is more suited for comparing experimental findings than a stochastic logistic model. Simulating the discrete model's outcomes is possible because the model parameters in the discrete model are closely tied to the continuous model's output [31, 32]. The discrete analyses validate the continuous model's hypothesis that reactions to the potential gradient of signal transduction and response to a potential gradient of substrate-bound antibodies are required to create a powerful vascular system. As described in this review article, the advantages of a model-based approach can be extremely beneficial to further refining.

#### Acknowledgements

The author wishes deeply thankful to their beloved parents, who fulfilled whatever he needed and gave their never-ending love and encouragement, which helped him in his research to attain the destination without any trouble.

#### References

- [1] H. Sung et al.: "Global cancer statistics 2020: GLOBOCAN estimates of incidence and mortality worldwide for 36 cancers in 185 countries," CA Cancer J. Clin., vol. 71, no. 3, pp. 209–249, 2021.
- [2] P. Unni and P. Seshaiyer.: "Mathematical modeling, analysis, and simulation of tumor dynamics with drug interventions," Comput. Math. Methods Med., vol. 2019, p. 4079298, 2019.
- [3] S. Stamouli, "Mathematical modeling of normal and cancer prostate signaling pathways," 2015.
- [4] A. R. Sheergojri, P. Iqbal, A. M. Ilyas.: "Cancer growth inhibition using predictive mathematical models of signaling pathways," Int. J. Stat. Med. Res., vol. 10, pp. 132–135, 2021.
- [5] L. G. de Pillis, W. Gu, and A. E. Radunskaya.: "Mixed immunotherapy and chemotherapy of tumors: modeling, applications and biological interpretations," J. Theor. Biol., vol. 238, no. 4, pp. 841–862, 2006.
- [6] P. Román-Román and F. Torres-Ruiz.: "Inferring the effect of therapies on tumor growth by using diffusion processes," J. Theor. Biol., vol. 314, pp. 34–56, 2012.

- [7] P. Iqbal, R. Khaliq, and A. R. Sheergojri.: "Mathematical approach in colitis-related colon cancer genomics: Inflammatory bowel disease (IBD)," in Diagnostic and Treatment Methods for Ulcerative Colitis and Colitis-Associated Cancer, IGI Global, 2021, pp. 170–200.
- [8] P. D. P. Pharoah, A. M. Dunning, B. A. J. Ponder, and D. F. Easton.: "Association studies for finding cancer-susceptibility genetic variants," *Nat. Rev. Cancer*, vol. 4, no. 11, pp. 850–860, 2004.
- [9] C. Mader.: "The biology of cancer," *The Yale Journal of Biology and Medicine*, vol. 80, no. 2, p. 91, 2007.
- [10] Z. Agur and S. Vuk-Pavlović.: "Mathematical modeling in immunotherapy of cancer: personalizing clinical trials," *Mol. Ther.*, vol. 20, no. 1, pp. 1–2, 2012.
- [11] W. C. Summers.: "Dynamics of tumor growth: a mathematical model," *growth*, vol. 30, no. 3, pp. 333–338, 1966.
- [12] X. Huang, J. Ning, and A. S. Wahed.: "Optimization of individualized dynamic treatment regimes for recurrent diseases," *Stat. Med.*, vol. 33, no. 14, pp. 2363–2378, 2014.
- [13] A. K. Laird.: "Dynamics of tumor growth," *Br. J. Cancer*, vol. 13, no. 3, pp. 490–502, 1964.
- [14] Z. Wang and T. S. Deisboeck.: "Mathematical modeling in cancer drug discovery," *Drug Discov. Today*, vol. 19, no. 2, pp. 145–150, 2014.
- [15] J. Foo and F. Michor.: "Evolution of acquired resistance to anti-cancer therapy," *J. Theor. Biol.*, vol. 355, pp. 10–20, 2014.
- [16] P. Gerlee.: "The model muddle: in search of tumor growth laws," *Cancer Res.*, vol. 73, no. 8, pp. 2407–2411, 2013.
- [17] J. R. Usher.: "Some mathematical models for cancer chemotherapy," *Comput. Math. Appl.*, vol. 28, no. 9, pp. 73–80, 1994.
- [18] B. Werner, D. Dingli, and A. Traulsen.: "A deterministic model for the occurrence and dynamics of multiple mutations in hierarchically organized tissues," *J. R. Soc. Interface*, vol. 10, no. 85, p. 20130349, 2013.
- [19] A. Di Crescenzo and S. Spina.: "Analysis of a growth model inspired by Gompertz and Korf laws, and an analogous birth-death process," *Math. Biosci.*, vol. 282, pp. 121–134, 2016.
- [20] S. Tabassum, N. B. Rosli, and M. S. A. Binti Mazalan.: "Mathematical modeling of cancer growth process: A review," *J. Phys. Conf. Ser.*, vol. 1366, no. 1, p. 012018, 2019.
- [21] L. A. Dethlefsen, J. M. S. Prewitt, and M. L. Mendelsohn.: "Analysis of Tumor Growth Curves2," *J. Natl. Cancer Inst.*, vol. 40, no. 2, pp. 389–405, 1968.
- [22] H. Murphy, H. Jaafari, and H. M. Dobrovolny.: "Differences in predictions of ODE models of tumor growth: a cautionary example," *BMC Cancer*, vol. 16, no. 1, p. 163, 2016.
- [23] N. C. Atuegwu et al.: "Parameterizing the logistic model of tumor growth by DW-MRI and DCE-MRI data to predict treatment response and changes in breast cancer cellularity during neoadjuvant chemotherapy," *Transl. Oncol.*, vol. 6, no. 3, pp. 256–264, 2013.
- [24] J. F. Nieves and M. R. Ubriaco.: "Linear model of tumor growth in a changing environment," *arXiv [q-bio.PE]*, 2006.
- [25] C. P. Winsor.: "The Gompertz curve as a growth curve," *Proc. Natl. Acad. Sci. U. S. A.*, vol. 18, no. 1, pp. 1–8, 1932.
- [26] C. Vaghi et al.: "Population modeling of tumor growth curves and the reduced Gompertz model improve prediction of the age of experimental tumors," *PLoS Comput. Biol.*, vol. 16, no. 2, p. e1007178, 2020.
- [27] S. Benzekry et al.: "Classical mathematical models for description and prediction of experimental tumor growth," *PLoS Comput. Biol.*, vol. 10, no. 8, p. e1003800, 2014.
- [28] L. Bertalanffy.: "Problems of organic growth," *Nature*, vol. 163, no. 4135, pp. 156–158, 1949.
- [29] L. A. Liotta, G. M. Saidel, and J. Kleinerman.: "Stochastic model of metastases formation," *Biometrics*, vol. 32, no. 3, pp. 535–550, 1976.
- [30] R. Wette, I. N. Katz, and E. Y. Rodin.: "Stochastic processes for solid tumor kinetics II. Diffusion-regulated growth," *Math. Biosci.*, vol. 21, no. 3–4, pp. 311–338, 1974.
- [31] C. F. Lo.: "Stochastic Gompertz model of tumour cell growth," *J. Theor. Biol.*, vol. 248, no. 2, pp. 317–321, 2007.
- [32] P. Kink.: "Some analysis of a stochastic logistic growth model," *Stoch. Anal. Appl.*, vol. 36, no. 2, pp. 240–256, 2018.
- [33] A. R. Sheergojri, P. Iqbal, R. Khaliq, and L. Shafi.: "Deterministic and Stochastic Tumor Growth Models: A Review," *J. Huazhong Univ. Sci. Technol.*, vol. 1671, p. 4512.
- [34] Friedman and H. V. Jain.: "A partial differential equation model of metastasized prostatic cancer," *Math. Biosci. Eng.*, vol. 10, no. 3, pp. 591–608, 2013.
- [35] T. F. Chan, J. Shen, and L. Vese.: "Variational PDE Models in Image Processing," *Ams.org*. [Online]. Available: <https://www.ams.org/journals/notices/200301/fea-shen-03.pdf>. [Accessed: 05-Feb-2022].
- [36] A. R. Anderson and M. A. Chaplain.: "Continuous and discrete mathematical models of tumor-induced angiogenesis," *Bull. Math. Biol.*, vol. 60, no. 5, pp. 857–899, 1998.
- [37] P. Macklin, M. E. Edgerton, V. Cristini, and J. Lowengrub.: "Discrete cell modeling," in *Multiscale Modeling of Cancer*, Cambridge: Cambridge University Press, 2010, pp. 88–122.

# **Monitoring the co2 level indoors and determining the need for ventilation**

**Şaban PUSAT, Muhammet İkbal TAYYAN**

## **Abstract**

Along with the pandemic process that has been effective all over the world, the duration of indoor environment use has increased significantly. In parallel, the spread of viruses in the environment and the transmission of them to humans began to emerge as a serious problem. In this study, analyses and evaluations were made about air quality and the need for ventilation depending on the CO<sub>2</sub> level for indoor spaces. In this context, long-term CO<sub>2</sub> measurements were made in different indoor areas. The obtained data were used to analyze the state of virus spread in closed spaces and, accordingly, to determine the need for ventilation. It has been revealed by the study that the natural ventilation applied in closed spaces that cannot have a ventilation system does not work very much and that there is a serious need for ventilation both in terms of health and cleanliness.

**Keywords:** Carbon dioxide, Air Quality, Covid19, Ventilation, Efficiency

## **1. INTRODUCTION**

With the pandemic period, the amount of time people spend indoors has increased. Although there are different styles and conditions in each country, exits are prohibited or restricted. It is known that with the increase in the time spent indoors, the circulation of viruses between people increases. The rates of virus spread vary depending on the number of people living indoors. The quality of inhaled air in working and living environments in today's conditions depends on the percentage of moisture and oxygen contained in it, as well as the amount of various other gases and harmful microorganisms. Indoor air quality has a direct impact on comfort, convenience, learning ability, productivity and health.

---

**Şaban PUSAT,**

Yildiz Technical University, [spusat@yildiz.edu.tr](mailto:spusat@yildiz.edu.tr)

**Muhammet İkbal TAYYAN**

Yildiz Technical University, [mikbaltayyan@gmail.com](mailto:mikbaltayyan@gmail.com)

The main gas that reduces air quality is carbon dioxide (CO<sub>2</sub>). CO<sub>2</sub> directly reduces productivity when it is found to be higher than a certain standard value in the environment. The maximum amount of CO<sub>2</sub> in a closed environment, specified in ASHRAE 62.1-2016, is indicated as 1000 ppm. The thermal comfort of a person decreases when the ambient air content approaches this value [1]. Maintaining air quality at a certain level in indoor environments is not economically possible with existing systems that mix and use indoor and outdoor air. In these systems, using only outdoor air goes beyond the purpose of making the machine in terms of energy saving [2]. On the other hand, HEPA filters used during the filtration process cannot ensure the retention of microbes harmful to health. At the particle level, various microorganisms, especially Covid19, pass through the HEPA filters of ventilation systems and constantly move in the environment, increasing the infectiousness. HEPA filters can hold particles of 0.3 μm and above, but the Covid19 virus has a size of about 0.1 μm [3-4].

In order to ensure that the existing ventilation systems work at the desired level, as well as to ensure that the harmful contents contained in the air in the space are removed from the environment, ventilation systems must utilize air quality measurement systems to keep indoor air quality. With the increasing importance of disease-causing elements, it has been determined that CO<sub>2</sub> levels should be maintained within the specified levels [6].

In this study, the results of carbon dioxide measurements performed at different locations are given. The selected indoor spaces have been designated as schools, dwellings and offices. Measurements were taken at different times and time-dependent indoor CO<sub>2</sub> changes were examined. Depending on the measurements made, it is evaluated to what degree of ventilation is needed.

## 2. MEASUREMENTS AND EVALUATION

Within the scope of the study, indoor air quality of indoor spaces with different characteristics and use cases was examined. The CO<sub>2</sub> level was monitored for air quality. The time-dependent change of CO<sub>2</sub> level was examined and the need for ventilation was evaluated. Some characteristics of the indoor spaces examined within the scope of the study are presented in Table 1.

As can be seen, measurements were made for 2 offices, 2 classrooms and 2 dwellings. Offices only have mechanical ventilation systems. Therefore, there is a situation of natural ventilation for schools and residential buildings. The number of people for all spaces varies depending on the time. However, approximate values have been given to provide information about the spaces.

**Table 1. Specifications of the spaces**

Space	Area (m <sup>2</sup> )	Specification	Number of People	Location
<b>Office 1</b>	500	Co-Working Space	>5 persons	Istanbul/Esenler
<b>Office 2</b>	30	Small Space	5 persons	Istanbul/Esenler
<b>Dwelling 1</b>	90	Apartment House	4 persons	Istanbul/Pendik
<b>Dwelling 1</b>	90	Apartment House	2 persons	Istanbul/Pendik
<b>Classroom 1</b>	45	Primary School Classroom	16 persons	Istanbul/Pendik
<b>Classroom 2</b>	45	Primary School Classroom	16 persons	Istanbul/Pendik

The space called Office 1 has an area of 500 m<sup>2</sup> and is characterized as a shared work area. The number of people in Office 1 is very high, but it varies a lot. The number of people in Office 1 can be up to 20. Office 1 does not have any window that opens to the outside environment. However, the office has an entrance door that opens to the outside environment.

Office 2 has an area of 30 m<sup>2</sup> and is characterized as a small office. The number of people is about 5, but it varies throughout the day. The office does not have a window that opens to the outdoor environment. The entrance door of the office opens to a shared environment.

2 houses have been subjected to inspection. The dwellings are located in the same apartment building, but the number of people living is different. Measurements were also made in 2 different classrooms located in a primary school. The classrooms have a capacity of 15 students and have an area of 45 m<sup>2</sup>.

The results of the CO<sub>2</sub> levels measured at intervals of 5 seconds between 07:00 and 22:00 on 19.03.2021 and 02.04.2021 for Office 1 are presented in Figure 1. The CO<sub>2</sub> level in an environment should not exceed 1000 ppm according to ASHRAE standards. It is observed that the measurement values vary in the range of 550-715 ppm. Having a mechanical ventilation system, it can keep the level of CO<sub>2</sub> in the environment below the upper limit of the standards.

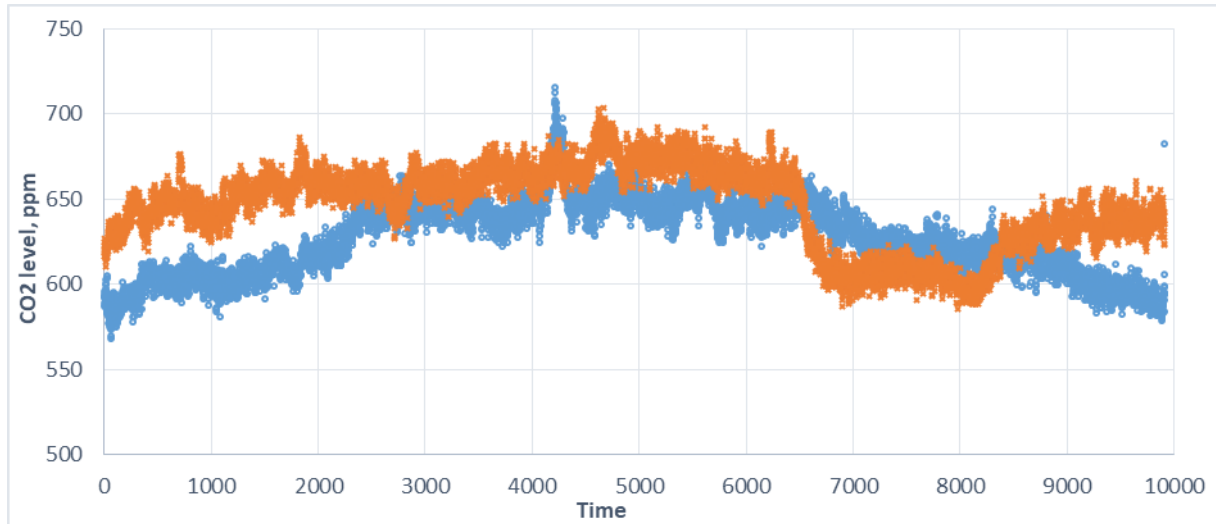


**Figure 1. Measurements in Office 1 for 2 different days**

The CO<sub>2</sub> levels measured at intervals of 5 seconds between 08:00 and 22:00 on 19.03.2021 and 02.04.2021 for a mechanically ventilated Office 2 without a window for 5 people are presented in Figure 2. It is observed that the measurement values vary in the range of 580-890 ppm. In this chart, it is seen that both the peak and bottom points are not far from each other and remain within the standard values compared to the ventilation situations seen in naturally ventilated areas. The main reason for this is that the air balance of this environment is achieved not by natural ventilation, but by regular mechanical ventilation. The CO<sub>2</sub> level in the space remains below the 900 ppm level.

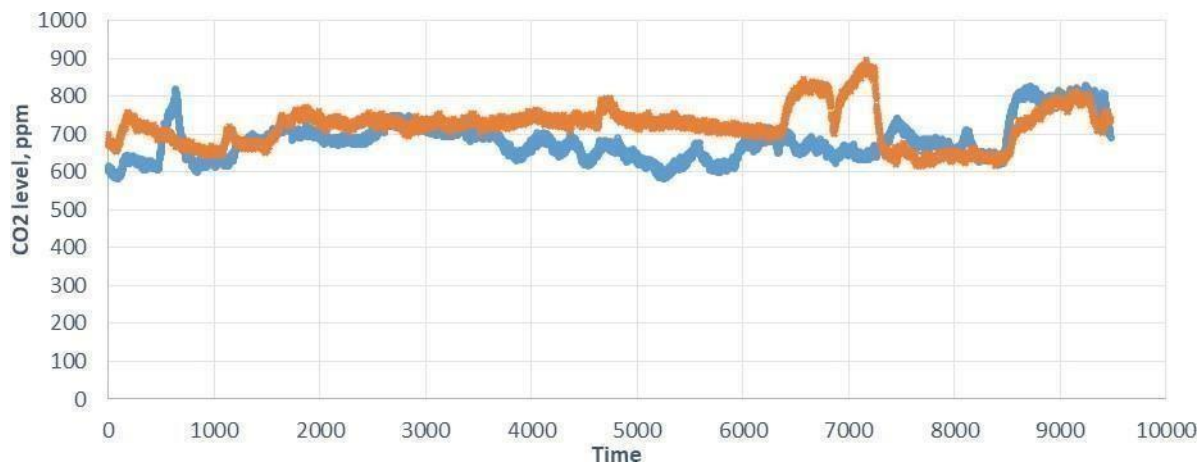


**Figure 2. Measurements in Office 2 for 2 different days**

The CO<sub>2</sub> levels measured at 5-second intervals in a Dwelling 1 between 23.01.2021 and 03.02.2021 are presented in Figure 3. The sensor is in the middle of the house and has received continuous data. It is seen that the measurement values are up to 2000 ppm levels. As can be

seen from this measurement, the amount of CO<sub>2</sub> rises above the limit necessary for human health at certain times of the day. Even in some instantaneous measurements, the value has even exceeded the upper limit of measurement, 2000 ppm. It is observed that the ambient natural ventilation is insufficient.

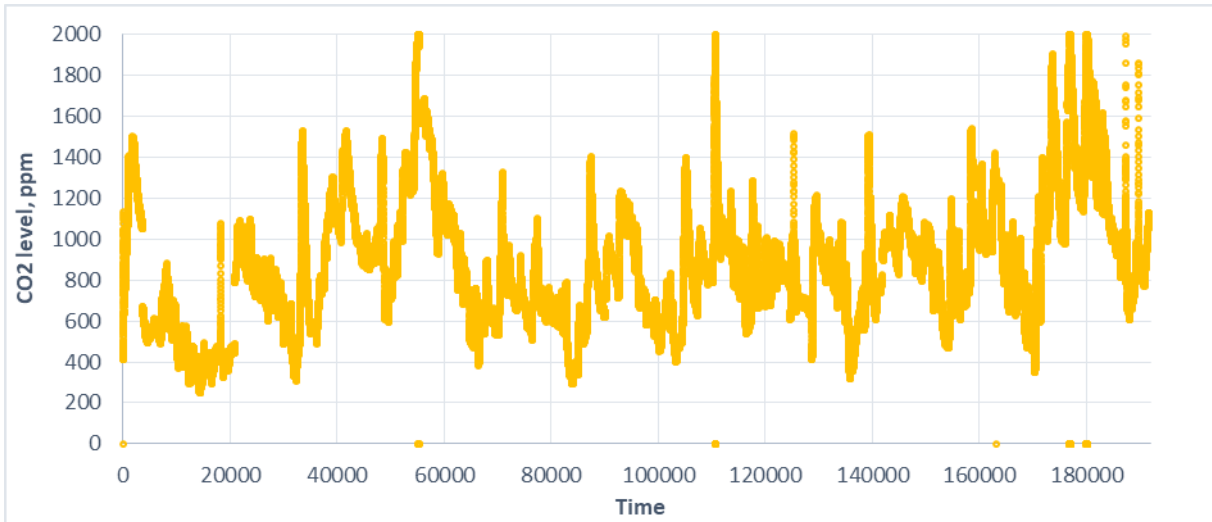


**Figure 3. Measurements in Dwelling 1**

The CO<sub>2</sub> levels measured for Dwelling 2 at intervals of 5 seconds from 04.04.2021 to 04.05.2021 are presented in Figure 4. The sensor is in the middle of the house and has received continuous data. The house in which these data were taken is a naturally ventilated environment with a higher ratio of m<sup>2</sup>/person compared to Dwelling 1. Although the results obtained showed values of 400 ppm due to natural ventilation, the values of 1000 ppm were also seen for a long time.

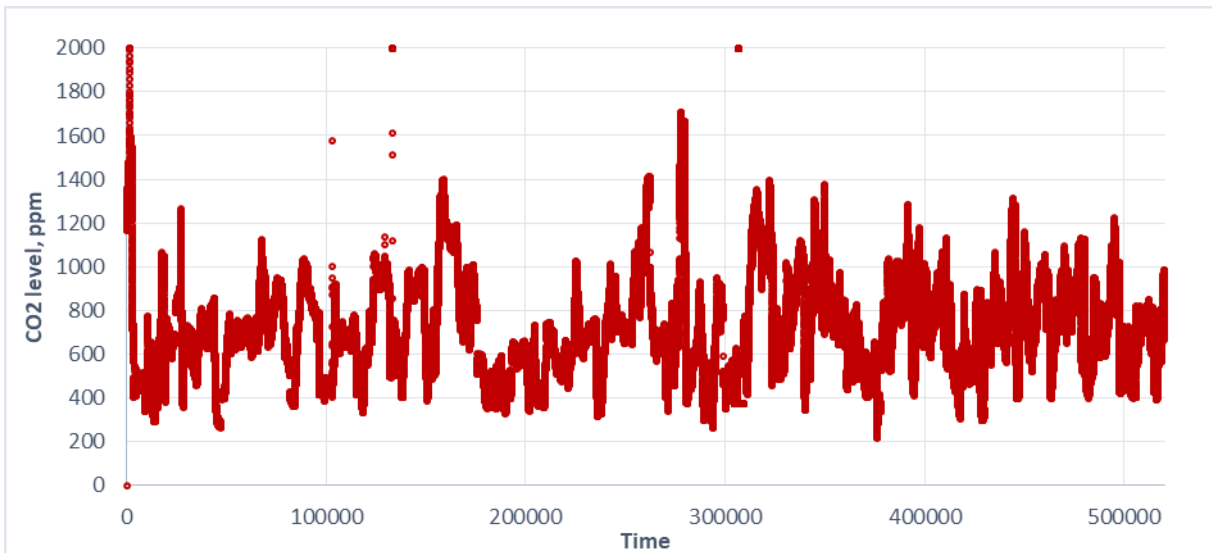


**Figure 4. Measurements in Dwelling 2**

As can be seen from the results gathered from the dwellings that are ventilated only with natural ventilation, a fairly large difference values were obtained between the bottom and peak points. Although natural ventilation can improve air quality in the desired direction, it is insufficient when the ventilation situation disappears and the CO<sub>2</sub> pollution reaches disturbing levels.

The CO<sub>2</sub> levels measured at intervals of 5 seconds between 12:45 to 17:00 from 08.03.2021 to 30.03.2021 in Classroom 1 are presented in Figure 5. As can be seen from the measurement results, the measurements fell below the standard upper limit by a small amount and sometimes exceeded the upper value of the measuring device. The measurement outputs are generally concentrated between 1000-1500 ppm.

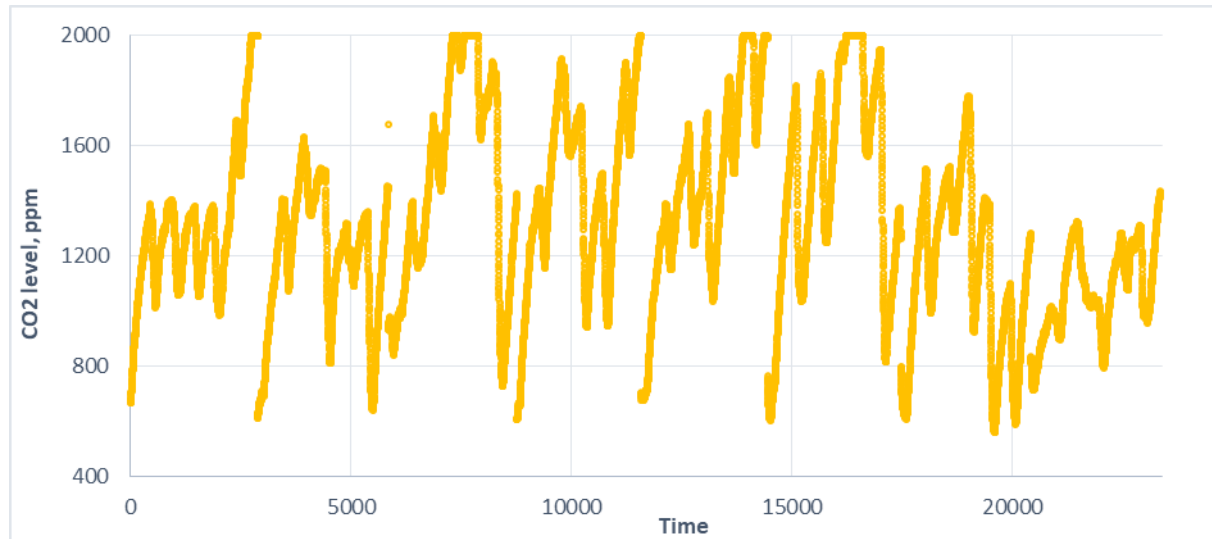


**Figure 5. Measurements in Classroom 1**

The CO<sub>2</sub> levels measured at intervals of 5 seconds between 12:45 to 17:00 from 08.03.2021 to 30.03.2021 in Classroom 2 are presented in Figure 6. As can be seen from the received data, the CO<sub>2</sub> values in the environment are mostly significantly higher than the 1000 ppm value, which is the standard upper limit. The amount of CO<sub>2</sub> was generally measured between 1000- 1500 ppm. This indicates that the environment, although naturally ventilated, is not adequately ventilated. Considering that this area is a classroom, this also reduces the learning capacity of students who use the environment.

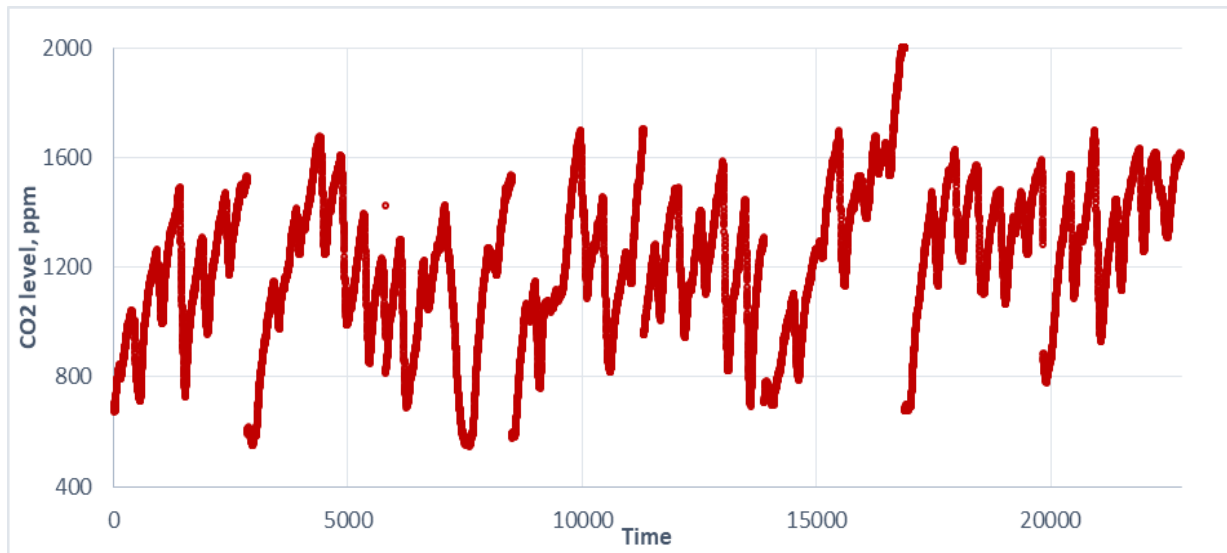


**Figure 6. Measurements in Classroom 2**

A ventilation system beyond natural ventilation is needed because educational and learning activities will be carried out for students in school environments as well. However, this necessity is not suitable for the use of a complex channel and transmission elements such as an air handling unit within the scope of school conditions. For this reason, it is necessary to work on a ventilation system that can balance the CO<sub>2</sub> level in education environments.

## CONCLUSION

In this study, CO<sub>2</sub> measurements were made for 3 different usage spaces: office, dwelling and classroom. The evaluations of the measurements were determined as follows:

- It has been determined that CO<sub>2</sub> levels occur at the desired range for 2 different office environments that have mechanical ventilation. It has been evaluated that mechanical ventilation can provide a good environment for offices.
- It has been determined that CO<sub>2</sub> levels cannot always be maintained at the desired levels for houses with natural ventilation. It has been evaluated that measurement systems showing the CO<sub>2</sub> level and warning in cases where it is high can be applied for houses.
- It has been evaluated that CO<sub>2</sub> levels are very high due to the high number of people in the unit area for schools with natural ventilation. It is believed that this situation poses a very big problem for educational institutions. It has been evaluated that special ventilation systems should be developed for schools.

## **Acknowledgement**

This work has been supported by Yildiz Technical University Scientific Research Projects Coordination Unit under project number FYL-2020-4073.

## **References**

- [1] Ayesha Asif, Muhammad Zeeshan, «Indoor temperature, relative humidity and CO<sub>2</sub> monitoring and air exchange rates simulation utilizing system dynamics tools for naturally ventilated classrooms», Building and Environment, Sayı 180, 2020.
- [2] Zakia Afroz, Gary Higgins, G.M. Shafiullah, Tania Urmee, -Evaluation of real-life demand-controlled ventilation from the perception of indoor air quality with probable implications¶, Energy & Buildings, Sayı:219, 2020.
- [3] Jamaji C. Nwanaji-Enwerem, Joseph G. Allen, Paloma I. Beamer, —Another invisible enemy indoors: COVID-19, human health, the home, and United States indoor air policy¶, Journal of Exposure Science & Environmental Epidemiology, Sayı: 30:773-775, 2020.
- [4] Arsen K. Melikov, -COVID-19: Reduction of airborne transmission needs paradigm shift in ventilation¶, Building and Environment, Sayı: 186, 2020.
- [5] Nan Ma, Dorit Aviv, Hongshan Guo, William W. Braham, —Measuring the right factors: A review of variables and models for thermal comfort and indoor air quality¶, Renewable and Sustainable Energy Reviews, Sayı: 135, 2021.

# **Advancements and Future Prospects in Castings: A Comprehensive Review of New Trends and Technologies**

**Prashant Kumar, Bhavana Mathur**

**Abstract :** This review paper examines the latest trends in castings, encompassing advanced materials, innovative casting processes, digitalization and simulation techniques, integration with Industry 4.0, and sustainable practices. The adoption of advanced materials, including aluminum alloys, titanium alloys, and metal matrix composites, has shown promising results in enhancing the mechanical properties of castings. Innovative casting processes such as investment casting, lost foam casting, squeeze casting, and additive manufacturing (3D printing) offer opportunities for producing complex geometries and improving casting quality. The integration of digitalization and simulation techniques enables design optimization, defect prediction, and process efficiency improvement. The application of Industry 4.0 principles and smart technologies enhances productivity, quality control, and traceability in casting operations. Embracing sustainable practices, such as the use of recyclable materials, energy-efficient processes, and the adoption of circular economy principles, promotes environmental sustainability in casting production. However, challenges remain, including process optimization, material selection, and skilled personnel requirements. Future research should focus on developing advanced materials, optimizing casting processes, and expanding the capabilities of simulation techniques. By embracing these new trends, the casting industry can achieve enhanced performance, efficiency, and sustainability, driving advancements in various industrial sectors

**Keywords:** *Castings, Advanced materials, Casting processes, Digitalization, Simulation, Industry 4.0, Sustainability.*

## **1. Introduction**

The field of castings plays a vital role in various industries, including automotive, aerospace, and manufacturing. Over the years, advancements in materials, processes, and technologies have led to the emergence of new trends in the casting industry. These trends have not only improved the performance and efficiency of castings but have also addressed sustainability concerns. Understanding these new trends and their implications is crucial for researchers, engineers, and industry professionals. This comprehensive review aims to explore the latest advancements in castings and provide insights into their applications, benefits, and challenges. The review will cover various aspects, including advanced materials used in casting processes, innovative casting techniques, the integration of digitalization and simulation, the impact of Industry 4.0 on casting facilities, and sustainable practices in the casting industry. By examining these new trends, we can gain a better understanding of the current state of the field and identify areas for future research and development. The review paper will begin by discussing the significance of advanced materials in casting processes. This section will highlight the use of materials such as aluminum alloys, titanium alloys, and metal matrix composites, along with the incorporation of nanomaterials to enhance mechanical properties. It will also address the challenges associated with the adoption of these materials. Subsequently, the review will delve into advanced casting processes that have gained prominence in recent years. It will explore techniques such as investment casting, lost foam casting, squeeze casting, and additive manufacturing (3D printing), analyzing their advantages, limitations, and applications in different industries. The digitalization and simulation of casting processes will be the focus of the next section. It will discuss the role of computer-aided design (CAD) and simulation software in optimizing casting designs, predicting defects, and improving overall efficiency. The section will also touch upon virtual casting simulations and their impact on process optimization.

Prashant Kumar

Department of Mechanical Engineering, Centre of Excellence in Material Engineering, Anand International College of Engineering, Agra road ,(Jaipur)

e-mail: [prashant.kumar@anandice.ac.in](mailto:prashant.kumar@anandice.ac.in)

Research Scholar ,Swami Keshvanand Institute of Technology, Management &Gramothan, Jaipur, Indiae-mail: [h21001@skit.ac.in](mailto:h21001@skit.ac.in)

Bhavana Mathur

Department of Mechanical Engineering , Anand InternationalCollege of Engineering, Agra road ,(Jaipur) [bhavana.mathur @anandice.ac.in](mailto:bhavana.mathur @anandice.ac.in)

Furthermore, the integration of Industry 4.0 principles and smart technologies in casting facilities will be examined. This section will explore how automation, robotics, artificial intelligence, and real-time monitoring systems have transformed casting operations, leading to enhanced productivity, quality control, and traceability. The review will also highlight the increasing importance of sustainable casting practices. It will discuss eco-friendly foundry practices, energy-efficient processes, waste reduction strategies, and the concept of the circular economy in casting industries. Finally, the review will conclude by summarizing the key findings and emphasizing the significance of these new trends in the casting industry. It will underscore the need for further research and development to overcome challenges and maximize the potential benefits of these advancements. By exploring the new trends and technologies in castings, this review paper aims to contribute to the knowledge and understanding of researchers, practitioners, and industry professionals. It provides a comprehensive overview of the current state of the field and sets the stage for future advancements in casting processes and materials.

## 2. Advanced Materials for Castings

Recent studies have highlighted the significance of advanced materials in modern casting processes. Aluminum alloys have gained popularity due to their lightweight nature and excellent mechanical properties (Smith et al., 2018). Titanium alloys are also being increasingly used for casting applications, offering high strength-to-weight ratios and corrosion resistance (Zhang et al., 2020). Metal matrix composites, such as aluminum-silicon carbide composites, have demonstrated enhanced wear resistance and thermal properties (Sharma et al., 2019). Furthermore, the incorporation of nanomaterials, such as carbon nanotubes and graphene, has shown promising results in improving the mechanical properties of castings (Li et al., 2017).



**Figure 2.1: Advance materials for casting**

## 3. Advanced Casting Processes

In recent years, several innovative casting processes have emerged, revolutionizing the industry. Investment casting, also known as the lost-wax process, enables the production of intricate and complex geometries with high dimensional accuracy (Garg et al., 2016). Lost foam casting, another advanced technique, allows for the production of near-net shape castings with reduced material waste (Balasubramanian et al., 2019). Squeeze casting, combining elements of casting and forging, offers improved mechanical properties and reduced porosity in castings (Flemings, 2010). Additive manufacturing, particularly 3D printing, has also gained attention in casting applications, enabling the production of complex geometries and customized components (Gibson et al., 2015).



**Figure 3.1: Advance casting process**

#### **4. Digitalization and Casting Simulation**

The digitalization of casting processes has brought about significant advancements in design optimization and defect prediction. Computer-aided design (CAD) software allows for the creation of complex casting geometries, streamlining the design process (Chen et al., 2018). Computer-aided engineering (CAE) tools and simulation software aid in predicting potential defects, such as porosity and shrinkage, optimizing casting designs, and reducing the need for costly physical prototypes (Duc et al., 2017). Virtual casting simulations have proven effective in optimizing process parameters, reducing scrap rates, and improving casting quality (Ganesan et al., 2020).

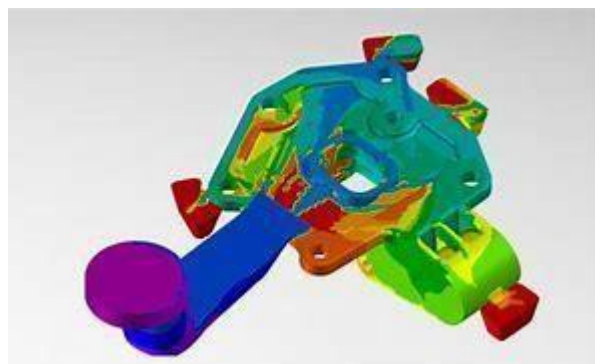


**Figure 4.1: Casting simulation**

#### **5. Industry 4.0 and Smart Casting**

The integration of casting processes with Industry 4.0 principles and smart technologies has resulted in improved productivity, quality control, and traceability. Automation and robotics have enabled efficient and consistent casting production, reducing human errors and enhancing overall efficiency (Zhou et al., 2020). Artificial intelligence and machine learning algorithms are being applied to casting data analysis, aiding in defect detection and process optimization (Garg et al., 2021). The use of sensors and real-time monitoring systems ensures process reliability and enables predictive maintenance, reducing downtime and improving overall equipment effectiveness (Ong et al., 2019).



**Figure 5.1: Industry 4.0**

## 6. Sustainable Casting Practices

Sustainability has become a key focus in the casting industry. Sustainability has become a key focus in the casting industry, leading to the development of eco-friendly practices. The use of recyclable materials, such as scrap metal and alloys, reduces the environmental impact of casting processes (Gupta et al., 2018). Energy-efficient practices, including the adoption of induction melting furnaces and optimized heat treatment processes, contribute to reduced energy consumption (Jindal et al., 2021). Additionally, waste reduction strategies, such as sand reclamation systems and the utilization of biodegradable binders, promote a more sustainable approach to casting production (Mallikarjuna et al., 2017). The concept of the circular economy has also gained traction, encouraging the reuse and recycling of casting materials and by-products (Kumar et al., 2019).

## 7. Challenges and Future Directions

While new trends in castings offer numerous benefits, they also present certain challenges. The adoption of advanced materials may require additional process optimization and compatibility studies (Li et al., 2017). Advanced casting processes, such as additive manufacturing, face challenges in terms of material selection, process repeatability, and quality control (Gibson et al., 2015). Digitalization and simulation techniques require skilled personnel and adequate computational resources for accurate predictions (Duc et al., 2017). Additionally, the integration of Industry 4.0 technologies demands substantial investments in equipment and infrastructure (Zhou et al., 2020). Overcoming these challenges will be crucial in realizing the full potential of these new trends in castings. To address these challenges and further advance the field of castings, future research should focus on developing novel materials with improved properties and process compatibility (Zhang et al., 2020). Further optimization of casting processes, particularly additive manufacturing, will be vital for increasing productivity and quality control (Gibson et al., 2015). Expanding the capabilities of simulation software and modeling techniques will aid in accurate defect prediction and process optimization (Ganesan et al., 2020). Moreover, the implementation of sustainable practices and the circular economy should be explored further to minimize the environmental impact of casting production (Kumar et al., 2019).

## 8. Conclusion

This literature review has examined the new trends in castings, including advanced materials, innovative casting processes, digitalization and simulation techniques, integration with Industry 4.0, and sustainable practices. The findings highlight the potential benefits and challenges associated with these trends, emphasizing the need for further research and development. By embracing these new trends, the casting industry can achieve enhanced performance, efficiency, and sustainability, ultimately driving advancements in various industrial sectors.

The following conclusions can be stated:

1. Advanced materials, such as aluminum alloys, titanium alloys, and metal matrix composites, have shown significant potential in improving the mechanical properties and performance of castings.
2. Innovative casting processes, including investment casting, lost foam casting, squeeze casting, and additive manufacturing, offer opportunities for producing complex geometries, reducing material waste, and enhancing casting quality.
3. The integration of digitalization and simulation techniques in casting processes enables design optimization, defect prediction, and process efficiency improvement.
4. The application of Industry 4.0 principles and smart technologies, including automation, robotics, artificial intelligence, and real-time monitoring systems, enhances productivity, quality control, and traceability in casting operations.
5. Sustainable casting practices, such as the use of recyclable materials, energy-efficient processes, waste reduction strategies, and the adoption of circular economy principles, contribute to minimizing the environmental impact of casting production.
6. While these new trends in castings offer numerous benefits, challenges remain, including process optimization, material selection, quality control, skilled personnel, and infrastructure requirements.
7. Future research should focus on developing advanced materials with improved properties and compatibility for casting processes.
8. Further optimization of casting processes, particularly in additive manufacturing, is crucial to enhance productivity, repeatability, and quality control.
9. Continued advancements in digitalization and simulation techniques will enable more accurate defect prediction, process optimization, and reduced reliance on physical prototypes.
10. The integration of Industry 4.0 technologies should be pursued further to leverage the full potential of smart casting facilities, including real-time monitoring, predictive maintenance, and data-driven decision-making.
11. Emphasizing sustainable practices and the circular economy in casting industries will be essential for reducing environmental impact and promoting long-term sustainability.

Hence, the new trends in castings offer exciting opportunities for improved performance, efficiency, and sustainability in various industries. By addressing the challenges and furthering research in these areas, the casting industry can unlock its full potential and drive advancements in manufacturing processes.

## References

- [1] Smith, R., Belen, R., & Smith, C. (2018). Advancements in aluminum alloy castings for automotive applications. *Journal of Materials Engineering and Performance*, 27(9), 4395-4409.
- [2] Zhang, J., Zhang, Y., & Cui, X. (2020). Recent progress in titanium alloy casting technologies: A review. *Metals*, 10(4), 532.
- [3] Sharma, R., Nair, S., & Gupta, M. (2019). Metal matrix composites: A comprehensive review. *Materials Today: Proceedings*, 9(2), 283-291.
- [4] Li, D., Ma, C., & Li, Z. (2017). A review on the incorporation of nanoparticles into molten metal for the preparation of metal matrix nanocomposites via casting. *Journal of Nanomaterials*, 2017, 6578796.
- [5] Garg, M., Sharma, A., & Dixit, A. (2016). Investment casting: A review. *International Journal of Engineering Research and General Science*, 4(2), 118-124.
- [6] Balasubramanian, K., Sivarupan, T., & Nagarajan, S. (2019). A comprehensive review on lost foam casting. *Materials Today: Proceedings*, 17, 1559-1567.
- [7] Flemings, M. C. (2010). Squeeze casting: The concept and process. *Metallurgical and Materials Transactions A*,

- [8] Gibson, I., Rosen, D. W., & Stucker, B. (2015). Additive manufacturing technologies: 3D printing, rapid prototyping, and direct digital manufacturing. Springer.
- [9] Chen, X., Chen, X., & Hu, L. (2018). Application of computer-aided design in casting technology. *Journal of Physics: Conference Series*, 1049(1), 012006.
- [10] Duc, T. T., Nguyen, D. K., & Vu, V. L. (2017). Simulation and optimization of casting processes: A review. *Advances in Mechanical Engineering*, 9(4), 1687814017699267.

# A Review on Recycling Plastic Waste into Sustainable, Valuable and Useful Products

Sanjana Chugh, Susmita Sharma

**Abstract** Use of plastic materials increases day by day since its invention in the 20th Century. It has changed our lives, bringing many benefits and also huge damage to environment. Plastic wastes are non-biodegradable and can stay in the ecosystem for many decades. It can go through aging processes resulting from physical, chemical, and biological actions with the potential to harm habitats and weaken the life-supporting environment. This review article covers some of the options like recycling of plastic waste into diesel fuel, recycling plastic waste into yarn and fiber and also use of plastic waste material as sustainable resource in civil engineering.

**Keywords-** Sustainable, non-biodegradable, recycling.

## 1. Introduction

As per Central Pollution Control Board( CPCB) Report (2019-20) Plastic Waste generation in India is 9315 TPD (34+ Lakh tones). Estimated Plastic Waste Generation in India is 3.3 trillion grams per year (based on per capita). Plastics have become a crucial part of lifestyle, and the global plastic production has increased immensely during the past 50 years(1). It is a fact that plastics will never degrade and remains on landscape for several years. The disposal of plastic in landfill sites is also highly problematic, with these sites often seeing plastic wastes being decomposed into microplastics before being released to underground rivers or soil via the leachate. Plastics also take an exceptionally long time to degrade, if at. A plastic material is any of a substantial gathering of materials comprising entirely or in part of mixes of carbon with oxygen, hydrogen, nitrogen, and other natural or inorganic components which, while strong in the completed state, at some phase in its make is made fluid, and along these lines equipped for being framed into different shapes,most normally through the application.

This review paper is based on the review of literature which gives the idea to recycle plastic waste into fuel, yarn and also plastic waste material into construction material.

## 2. Recycling Plastic into Fuel

Plastics are usually organic polymers of high molecular mass [1]. Plastics are used in many products due to their low cost, ease of manufacture and many other features. The use of plastics in modern life is widespread and constantly increasing and cannot be avoided, resulting in an increase in the production of plastics worldwide from various industries and households. Around 100 million tons of plastic are manufactured in the world to meet global demands, so the production and consumption of plastic is a big threat to the environment. Many processes, such as landfilling, mechanical recycling, and biological recycling are used to recycle the amount of plastic produced, which can take many years. So, a new recycling process is used, and waste plastics are researched to fuel a value-added product and decompose the process, called pyrolysis.

Pyrolysis is the process of thermal decomposition of plastics in an inert atmosphere and at a high temperature. In this process the chemical composition of plastics is converted to hydrocarbon compounds and is an irreversible process. The use and application of the pyrolysis process is that they can be used to convert waste plastics into useful oils or safely disposable materials.

Chanashetty and Patil [2] have investigated fuel from waste plastic; they used condenser and reactor for pyrolysis process. They found this method is suitable for large plastic seas problems and helping fuel storage by means of products as diesel, kerosene, and lubricant oil. In this investigation, they used the waste plastic as rigid film, sheet plastic, and expanded foam materials.

Pyrolysis is a process of heating of material in the absence of oxygen and can also be defined as the controlled burning of plastic waste into fuel. There are two types of pyrolysis process: Thermal and catalytic pyrolysis.

Sanjana Chugh  
Department of Chemistry, Anand International College of Engineering, Jaipur

Susmita Sharma  
Department of Chemistry, Anand International College of Engineering, Jaipur

The process of pyrolysis which is carried out in the presence of catalyst is known as catalytic pyrolysis and the process which is carried out normally without the help of any catalyst is known as thermal pyrolysis.

Although, there are many ways of plastic waste management like recycling, land filling, depolymerization etc. which can be used for the disposal of the plastic waste but pyrolysis is a process which can not only solve our problem of the disposal of waste plastic but also find a substitute for the fuel. The other reason for choosing this pyrolysis process is that the properties of the fuel obtained by pyrolysis are merely same as that of the natural extracted fuel.

Mathur et al. [3] investigated extraction of pyrolysis oil from waste plastic where pyrolysis process is using, and the waste plastic inlet is all the types of plastic and outputs are waste oil and diesel fuel.

Yadav et al (4) concluded that burning 1 kg of plastic can easily yield 600 to 750 ml of diesel fuel. They observed that by turning plastic into fuel, we can reduce atmospheric CO<sub>2</sub> emissions by 80% and burn 1 kg of plastic in the open atmosphere to produce up to 3 kg of CO<sub>2</sub>, thus solving both problems.

Pyrolysis is clean and very effective means of removing the debris that we have left behind over the last several decades. By converting plastics to fuel, we solve two issues, one of the large plastic seas, and the other of the fuel shortage.[5]

### **3. Recycling Plastic into Yarn**

Economic and population growth and industrialization in the world together cause an increase in the amount of plastic waste. Plastic pollution is the accumulation of plastic objects and particles (e.g. plastic bottles, bags and microbeads) in the Earth's environment that adversely affects wildlife, wildlife habitat, and humans [6]. . For this purpose, plastic waste policies should be developed and waste management studies should also be carried out, especially in the field of recycling these plastic wastes, because of long decomposition time of these wastes in the environment causing landfill and water logging problem [7, 8]. The development of polyester fiber from recycled bottles is really a matter of re-channeling the utilization of the chemical -polyethylene terephthalate|| which is additionally the chemical ingredient in PET bottles. Plastic bottle wastes are going to be supplied by recycle collectors. Workers of the yarn manufacturer will need to separate the colored bottles from the clear ones.

The sorted PET bottles are going to be sterilized clean, dried and crushed into small chips still separating the clear PET bottle chips from colored PET bottle chips. Once the chips are ready they're going to undergo heating which will enable them to pass to the spinneret until they find yourself being wound up like yarn threads in spools. The fibers are drawn into smooth strings, then go through a crimping machine which can give the polyester yarns the fluffy wooly texture. The crimped polyester yarns are going to be dried and baled and can need to pass internal control before they're considered fit selling.

### **4. Recycling Plastic into Civil Construction material**

In terms of civil engineering application, recycling of plastic waste as cementitious based materials, such as cement mixtures or concrete mixture appear as better option for alternative plastic waste disposal. This is due to its economic and ecological advantages which can substitute or replace certain portion of aggregate in concrete mix[9]. In this raw plastic is melted and form into a continuous profile allowing production for various construction material. This process causes no harm to any form of life or environment and helps in avoiding the use of other harmful methods such as landfills, burning in an incinerator, etc. Nzambi Matee from Nairobi, Kenya is the inventor of the plastic brick. The bricks consist of mixture of sand and plastics. The sand and plastic are mixed at very high temperatures and are then compressed into bricks. The cost of bricks is also very low since it is made from waste. The researcher believes the world should reevaluate its relationship with plastic and learn to use plastic waste in a sustainable way. Construction is one effective way to do this. -In addition to removing the plastic from the environment, we are putting it into a fixed application.

## 5. Conclusion

The conversion of plastic waste into value added products like fuel, yarn, building construction materials etc. is reviewed in this paper. Plastic waste, which can be a source of detrimental problems to terrestrial and marine ecosystems, can be thermochemically converted into valuable products, such as gasoline, diesel, and wax. The reuse and recycle of plastic waste is able to achieve its main aim of reducing the plastic waste throughout the globe. Plastic is almost irreplaceable in many applications due to its, strength, low cost, light weight nature, and corrosion resistance. All of these activities contribute to reducing plastic waste in the environment and moving us toward a circular economy that unlocks the value of our garbage. It's a big endeavour, but it's one that can be accomplished with a lot of help.

## References

- [1] <https://en.wikipedia.org/wiki/Plastic>.
- [2] Chanashetty VB, Patil BM (2015) Int J Emerg Technol 6(2):121–128.
- [3] Mathur K, Shubham C, Sunadh H, Aditya P (2016) Extraction of pyrolysis oil from wasteplastics. Int Res J Eng Techno.1
- [4] Ram Jatan Yadav, Shivam Solanki, Sarthak Saharna, Jonty Bhardwaj, Ramvijay International Journal of Recent Technology and Engineering (IJRTE) ISSN: 2277-3878 (Online), Volume-9 Issue-1, May 2020.
- [5] Vijaykumar B. Chanashetty\* and B.M. Patil\*International Journal on Emerging Technologies(Special Issue on NCRIET-2015) 6(2): 121-128(2015)
- [6] <https://get-green-now.com/environmental-impact-plastic-bottled-water/> (visited on 4 November 2019).
- [7] "Plastic pollution". Encyclopædia Britannica. Retrieved 1 August 2019 PET Bottle Recycling for Sustainable Textiles.
- [8] Tayyar AE, Üstün S. Usage of recycled PET. Pamukkale University. Journal of Engineering Sciences 2010; 16:53-62.
- [9] Yin, S., et al., Use of macro plastic fibres in concrete: a review. Construction and Building Materials, 2015. 93: p. 180-188.

# Power Quality Improvement using Active Power Filter

**Ajit, Seema Agarwal**

**Abstract-** Nowadays with the advancement of technology, the demand for electrical power is increasing at an exponential rate. Many consumer appliances demand consistent quality power for their operation. The performance of the end-user equipment depends heavily on the quality of power supplied to it. But the quality of power delivered to the end-user is affected by various external and internal factors such as voltage and frequency variations, faults, outages, etc. These power quality problems reduce the lifespan and efficiency of the equipment. Thus, these problems should be minimized to enhance the performance of the consumer equipment and also to enhance the overall performance of the system. The main effect caused by these problems is the production of harmonics. This results in the overheating of the equipment, insulation failure and over speeding of induction motors, etc. The solution for eliminating these problems is to filter the harmonics from the system. For this purpose, there are many filter topologies present within the paper. A hybrid filter has been studied in this paper which is a combination of series active filter and shunt passive filter. This paper presents the control strategy to regulate the filter in such a way that the harmonics are reduced. The proposed control strategy is simulated in MATLAB SIMULINK and therefore the results are presented.

**Keywords-** Active power filter, Harmonic, Power Quality.

## 1. Introduction

Electrical energy is the most effective and popular sort of energy; therefore, modern society depends on the electrical supply. Life can't be imagined without electricity. At an equivalent time, the standard of the electrical power supply plays an important role in the efficient functioning of user equipment. The term power quality became most prominent within both the power sector and the electrical power supply company, therefore the end-users are concerned about it [1].

The standard of power delivered to the consumers depends on the voltage and frequency ranges. If there is any deviation within the voltage and frequency of the electrical power delivered from that of the standard values, then the quality of power delivered is affected. Nowadays with the advancement in technology, there is a drastic improvement within semiconductor devices. With this development and advantages, the semi-conductor devices got a permanent place within the power sector helping to ease the control of the overall system. Moreover, in an electrical power system, most of the loads are semiconductor-based equipment. But semi-conducting devices are non-linear and draw non-linear current from the source. And semiconductor devices are also involved in power conversion, which can be either AC to DC or DC to AC. This power conversion contains a lot of switching operations which can introduce discontinuity within the current. This discontinuity and non-linearity produce harmonics in the power system which ultimately affects the quality of power delivered to the user. So to maintain the quality of power delivered, the harmonics should be eliminated. Thus, a device named filter is employed which eliminates the harmonics also filters are used to remove the problems caused by harmonics.

There are several filter topologies such as active, passive, and hybrid. Traditionally, passive filters are used, but they depend heavily on system parameters. They also have resonance problems with system impedance and are suitable for filtering out harmonics at a particular frequency. Therefore, to overcome the problems of passive filters, active filters are used, but it is found that active filters are facing some drawbacks when used to improve power quality such as high converter ratings are required, high cost as compared to passive filter, larger size, and increased losses. Therefore, to overcome these shortcomings, a hybrid power filter is proposed which is a combination of active and passive filters [3]. This paper discusses how combining both active and passive filters is an economical solution for improving power quality. The theory proposed in this paper has been validated by simulating it in a MATLAB SIMULINK environment. The proposed control strategy is simulated for unbalanced load conditions.

## 2. Power Quality

Power quality is usually defined as the ability of the power grid to supply clean and steady power flows in the form of a consistently available power supply. Electric current must have a pure sinusoidal wave form and must remain within specified voltage and frequency tolerances.

### 2.1 Power Quality Problems

The quality of power is affected when there is any variation in the voltage, current or frequency [6]. The common problems that affect the sensitivity of the equipment are - power surges, transients, frequency variation, electrical line noise, brownouts or blackouts, power system faults and improper grounding affect. The main effect caused by

these problems is the production of harmonics. The presence of harmonics degrades the power quality and may damage the end user equipment. These harmonics causes the heating of underground cables, insulation failure, reduces the lifespan of the equipment, increases the losses etc.

## 2.2 Solutions to Power Quality Problems

The most effective solution to enhance the power quality is the use of filters to reduce the harmonics. The fundamental idea of employing a filter is shown in Fig. 2.1, where the filter injects a compensating current that compensates the harmonics in load current. There are different filter topologies within the literature such as active, passive, hybrid. The passive power filters are used to filter a specific order harmonics and has the problem of parallel resonance. Another solution is the use of Active Power Filter (APF). There are different kinds of APF like series APF, shunt APF. The shunt APF is expensive and is not used for large systems. The series APF works as a harmonic isolator which reduces the negative-sequence voltage [2]. There is another filter topology which is a combination of passive filter and APF referred as Hybrid Filter.

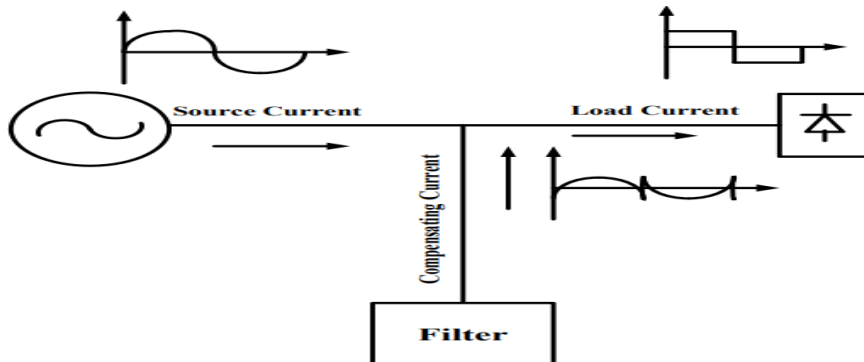


**Fig. 2.1 Basic Operation of Filter**

## 3. Filter Classification

Filters are classified into three basic types. They are active filter, passive filter and hybrid filter. Each type has its own sub classification. Fig. 3.1 shows the detailed classification of the filters.

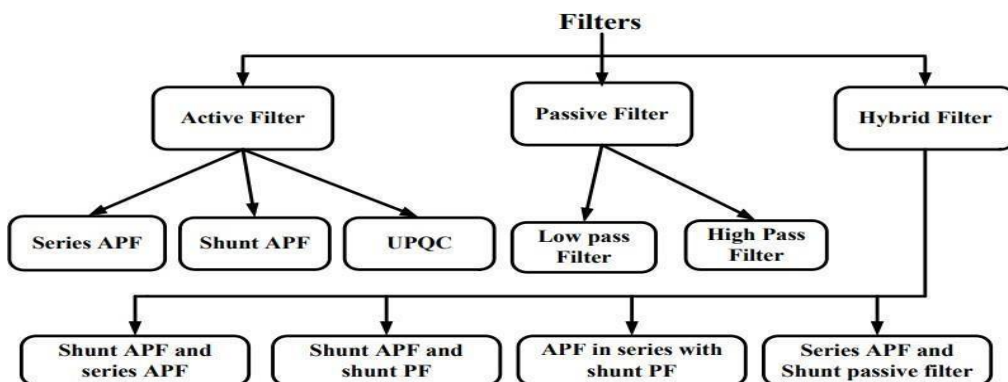


**Fig. 3.1 Classification of Filters**

### 3.1 Passive Filter

These filters contain passive elements like- capacitor, inductor and resistor. These filters are mostly used because of their low cost and ease of control. Passive filters provide reactive power in addition to filtering out harmonics. The performance of these filters depends on the system impedance. These filters are again classified into two types- low pass and high pass. But there are some disadvantages with passive filter, like - the filter characteristic has a strong dependence on the system impedance, the possibility of overload in the passive filter due to the harmonic current circulation generating from power electronic loads, the change of the load impedance can detune the filter, so it is not suitable for variable loads. The problem of series and/or parallel resonances can be originated which causes unstable operation, limited operation, that is used to eliminate either a particular order or fewer harmonics and component aging. Due to these disadvantages, the passive filters cannot provide an effective solution to enhance the quality of the power system. Thus, active power filters are employed to overcome these drawbacks.

### 3.2 Active Filter

To overcome the drawback of passive filter, active compensation known as Active Power Filter (APF) is used. APF is a voltage source inverter (VSI) that injects compensating current or voltage depending on the network configuration. It was proposed around 1970. But the recent advancement in power electronics technology [2], along with the theory of instantaneous active and reactive power which was presented in 1983, APFs are an up-to-date

solution with fast switching devices, low power loss, and fast digital processing equipment at an affordable cost. Depending on the circuit configuration and function, APF's are divided into three types – shunt active power filter, series active power filter, and unified power quality conditioner (UPQC).

### 3.3 Hybrid Filter

Active power filters are a better solution for improving power quality but they require a higher converter rating. So to overcome this drawback, hybrid filters are designed. The hybrid filter is a combination of both active and passive filters. These filters have the advantage of both active and passive filters. There are different types of hybrid filters depending on the circuit combination and arrangement. These are –

- Shunt APF and Series APF
- Shunt APF and Shunt Passive Filter
- APF in series with Shunt Passive Filter
- Series APF with Shunt Passive Filter

## 4. Design of Hybrid Filter

Filters are used to reduce the harmonics and improve the power quality. The filter attached to the system must be effectively controlled so that its response characteristics are desired. Among all the different available filter configurations, a hybrid power filter with series APF and a parallel passive filter is used in this paper. The control circuit of the series-connected APF is designed in such a way that the voltage injected by the APF, which compensates harmonics and also enhances the performance of the shunt-connected passive filter. The control strategy of the hybrid power filter is explained in detail in this paper. The series APF is realized as a voltage source inverter (VSI) used to improve power quality [8]. It can be a three-phase VSI or three single-phase VSI can also be used. VSI is connected in series with the source impedance through a coupling transformer. The circuit diagram is shown in Fig. 4.1. A capacitor is used at the input of the VSI to provide constant input voltage to VSI. A passivefilter is also connected at the PCC (Point of Common Coupling). This filter is used to eliminate higher-order harmonics [9] [10]. In certain cases, there may be two or more LC branches used to eliminate specific order harmonics (especially 5th and 7th). Also, a ripple filter is used in series with VSI. The filter parameters are selectedin such a way that they do not exceed the transformer burden. Thus, with an efficient control strategy, APF compensates for voltage imbalance and distortion. The control strategy is designed in such a way that the series APF acts as a balanced resistive load on the overall system with the passive filter. In a four-wire system, the harmonic currents circulating in the neutral wire are also reduced due to the series APF.

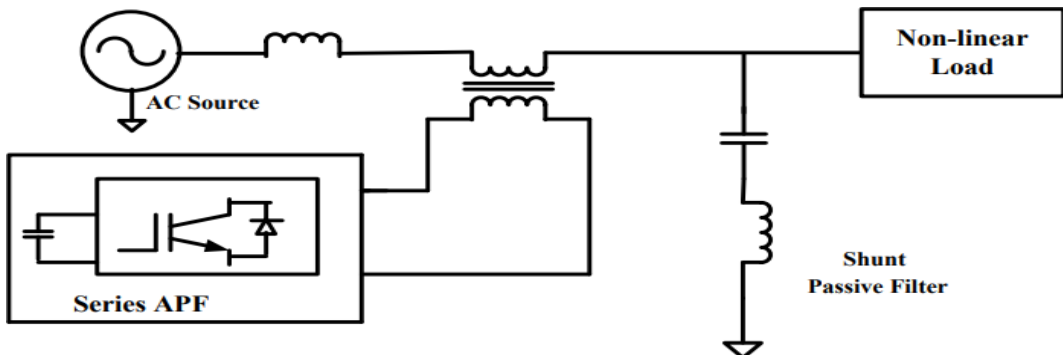


**Fig. 4.1 Basic configuration of hybrid filter**

## 5. Simulation and Results

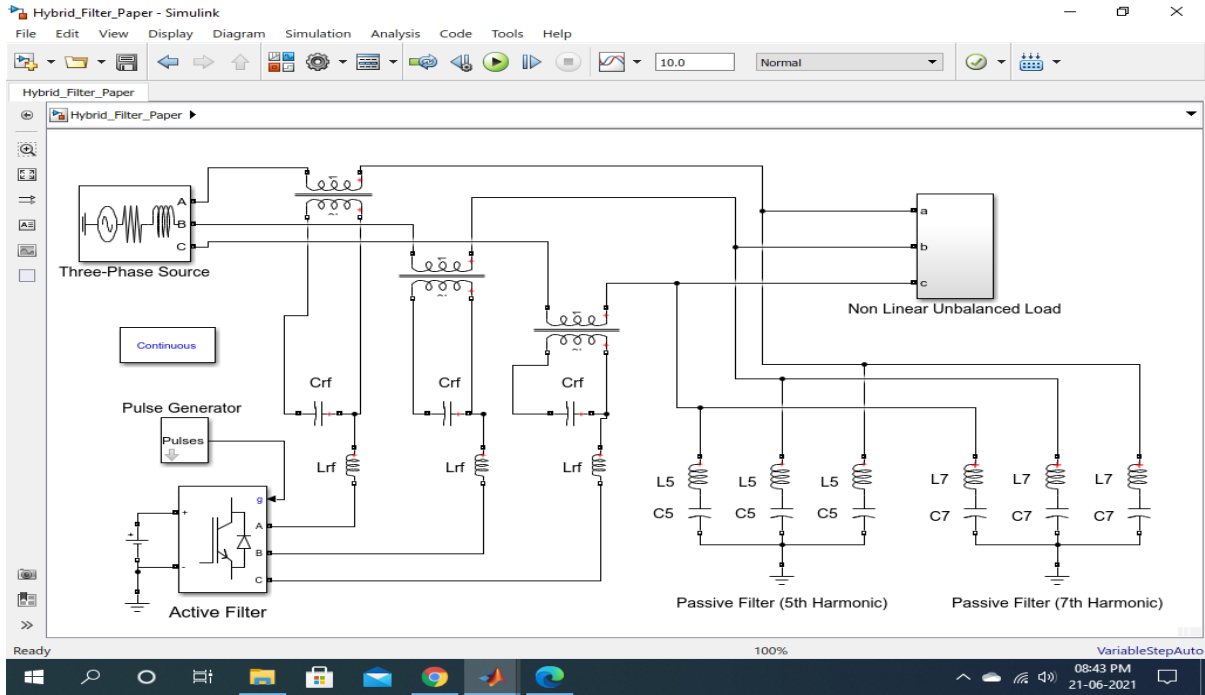


**Fig.-5.1 Simulation Diagram with non-linear unbalanced load**

The proposed control strategy is simulated with a non-linear unbalanced load shown in Fig 5.1 and the performance of the system is observed. The system data is given in Table – 5.1.

**Table 5.1 System Parameters**

System Parameter	Val ue
Voltage	100 V
Switching Frequency	20 KHz
Source Inductance	5.8 mH
Source Resistance	3.6 $\Omega$
Turns Ratio of Coupling Transformer	1:1

The series APF is connected through a coupling transformer whose turn's ratio is 1:1. A passive filter is connected at PCC to eliminate fifth and seventh-order harmonics. Ripple filter is also connected at the output of the VSI (Voltage Source Inverter). The values of these filters are given in Table – 5.2.

**Table 5.2 Filter Parameters**

<b>Filter Parameter</b>	<b>Value</b>
$L_5$	13.5 mH
$C_5$	30 $\mu$ F
$L_7$	6.75 mH
$C_7$	30 $\mu$ F
$L_{rf}$	13.5 mH
$C_{rf}$	50 $\mu$ F

The power system may experience unbalanced load conditions sometimes. Thus, the behavior of the proposed control strategy is analyzed by simulating it under unbalanced loading conditions. Here an unbalanced load is created by connecting three single-phase uncontrolled rectifiers with capacitor and resistor in parallel on the DC side. The load values are given in Table – 5.3.

**Table 5.3 Load Values**

Phase	C	R
Phase a	2200 $\mu$ F	16.67 $\Omega$
Phase b	2200 $\mu$ F	25 $\Omega$
Phase c	2200 $\mu$ F	50 $\Omega$

The filter impedance should be less than the system impedance for effective filtering. The simulation is carried out under two conditions- with the actual system parameters and by increasing the impedance of the LC filter more than the source impedance.

### 5.1 With the Actual System Parameters

The proposed control strategy is simulated with actual system parameters given in Table-5.2, filter parameters given in Table-5.3 with unbalanced load values given in Table-5.4. Fig. 5.2 shows the source current waveform without any compensation. From the waveform, it is clear that there many harmonics present in the system. Fig.5.4 shows the source current waveform with a passive filter. Thus, to reduce these harmonics, APF is connected, and then the source current is changed as shown in Fig. 5.6. So it is clear from Fig. 5.6 that the three-phase source current is almost sinusoidal. Hence, the system performance is enhanced by connecting the APF under unbalanced load conditions.

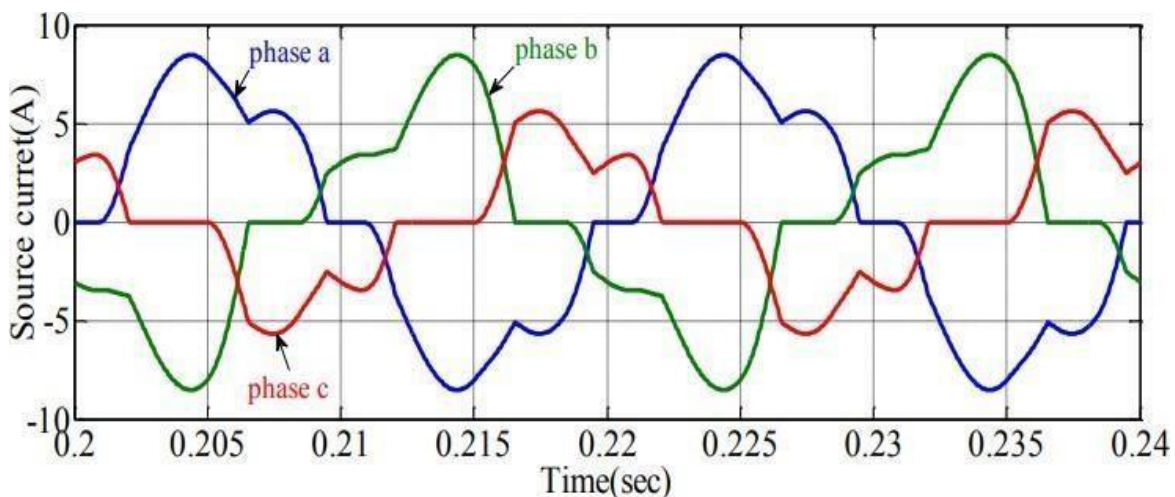


**Fig.-5.2 Source Current without any Compensation**

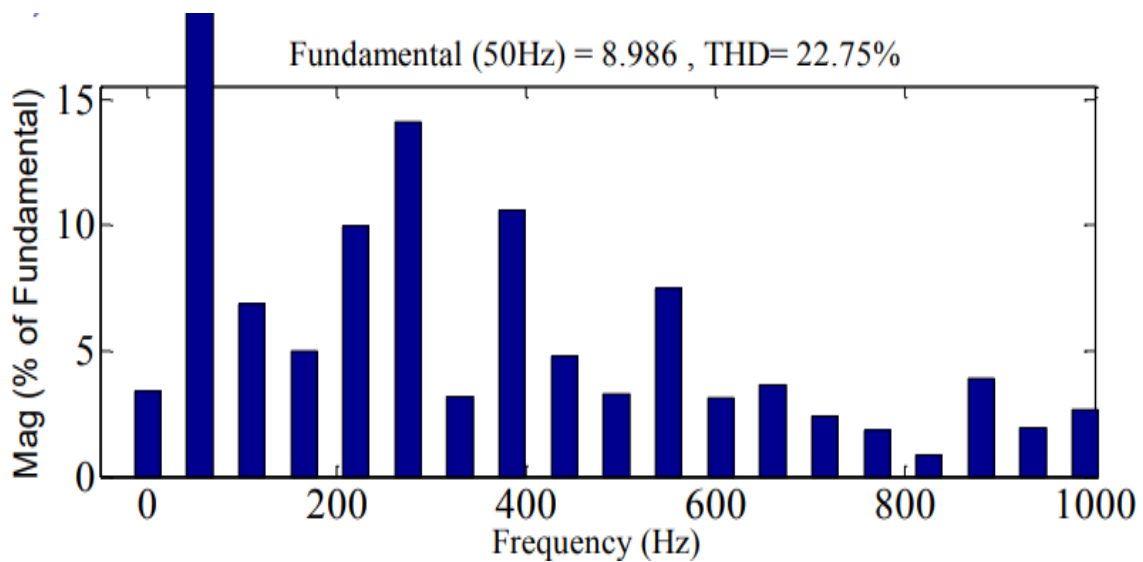


Fig.-5.3 THD of Source Current without any Compensation

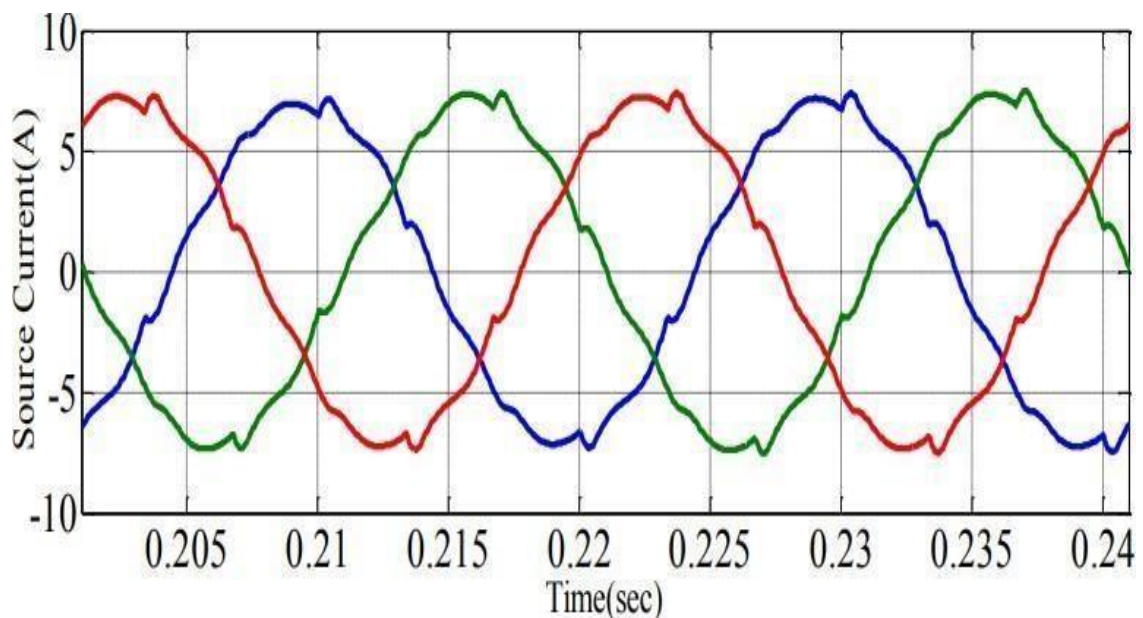


Fig.-5.4 Source Current with Passive filter

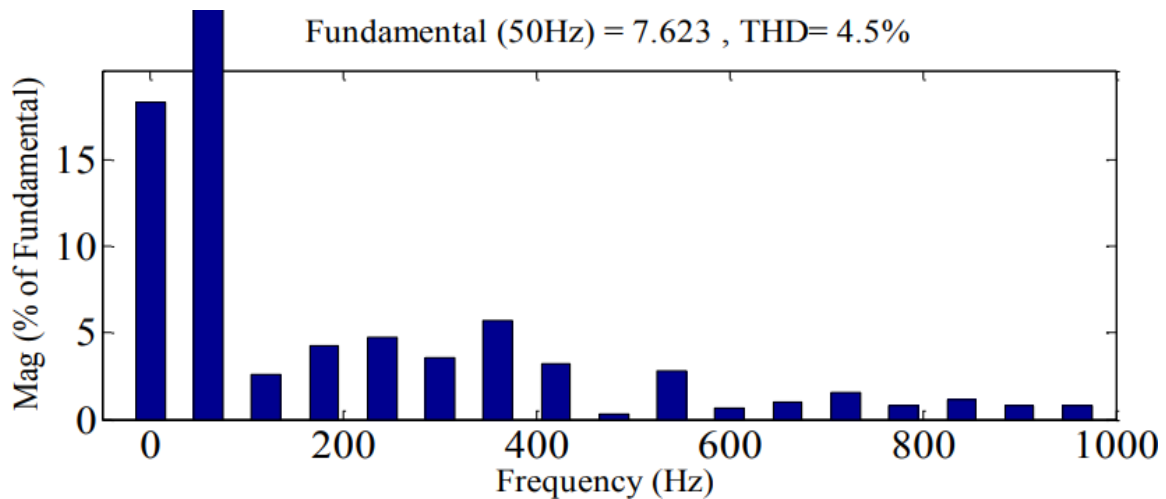


Fig.-5.5 THD of Source Current with Passive filter

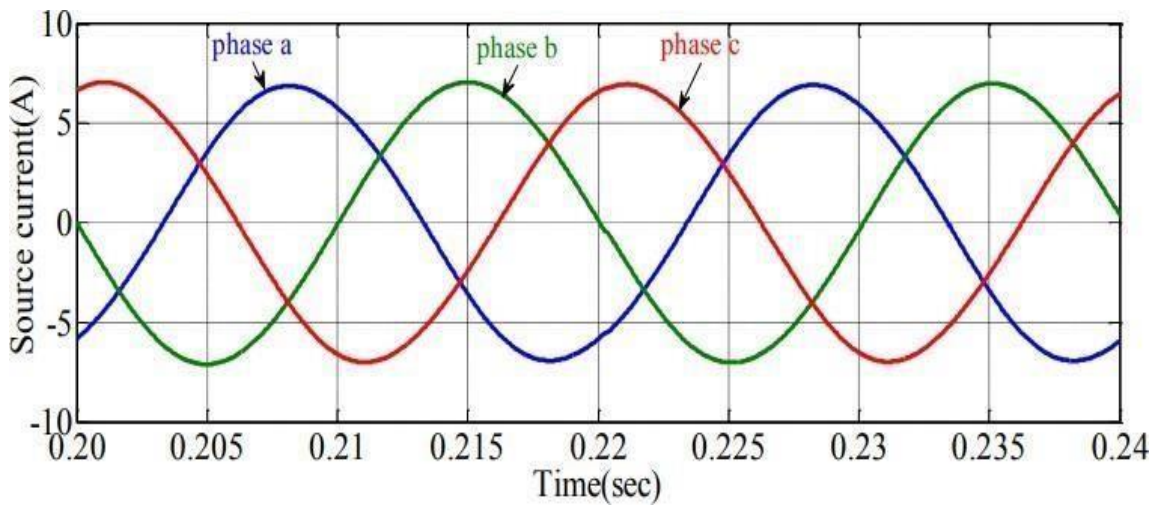


Fig.-5.6 Source Current with Hybrid filter

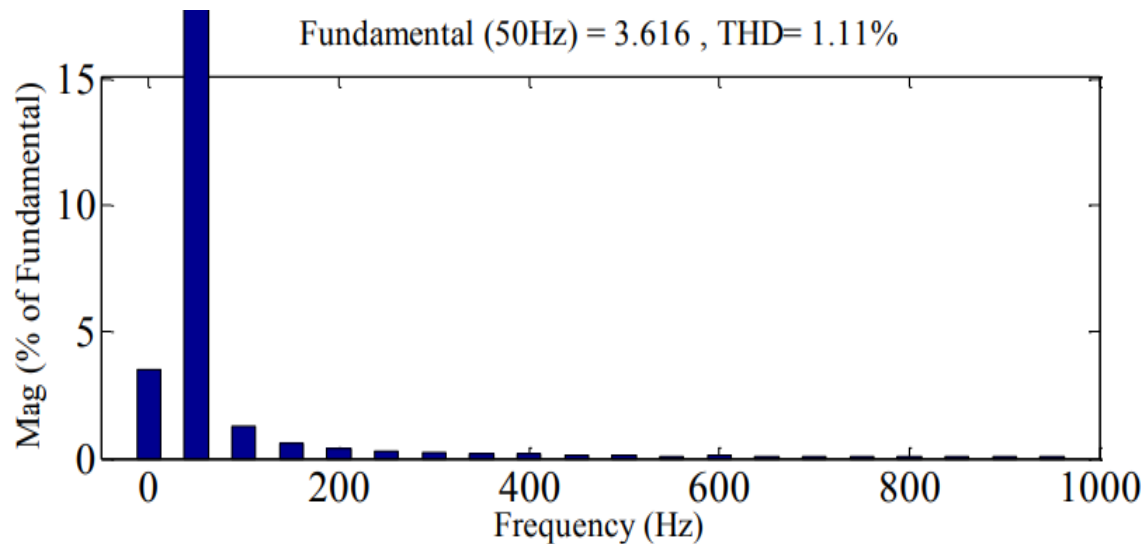


Fig.-5.7 THD of Source Current with Hybrid filter

### 5.2 When the Source Impedance is Changed

The source impedance of the system is reduced from its previous value given in Table-5.1 and the new values are- $L_s = 2.34 \text{ mH}$  and  $R_s = 1.3 \Omega$ . The simulation results are presented in Fig. 5.8. As in balanced load conditions, even under unbalance conditions the system behavior is affected if the source impedance is less than the filter impedance. So the filter design should be done in such a way that the filter impedance is always less than the source impedance.

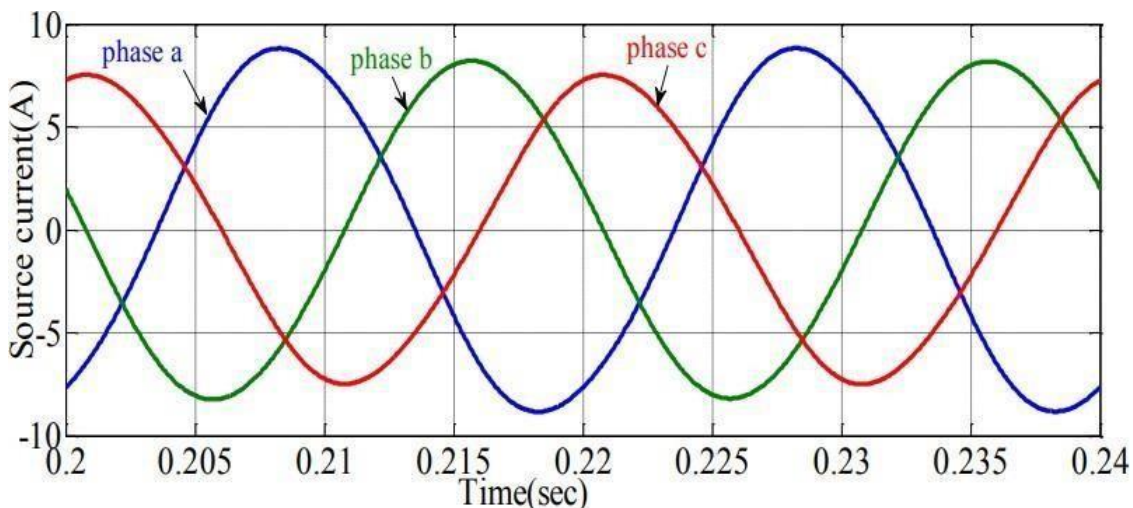
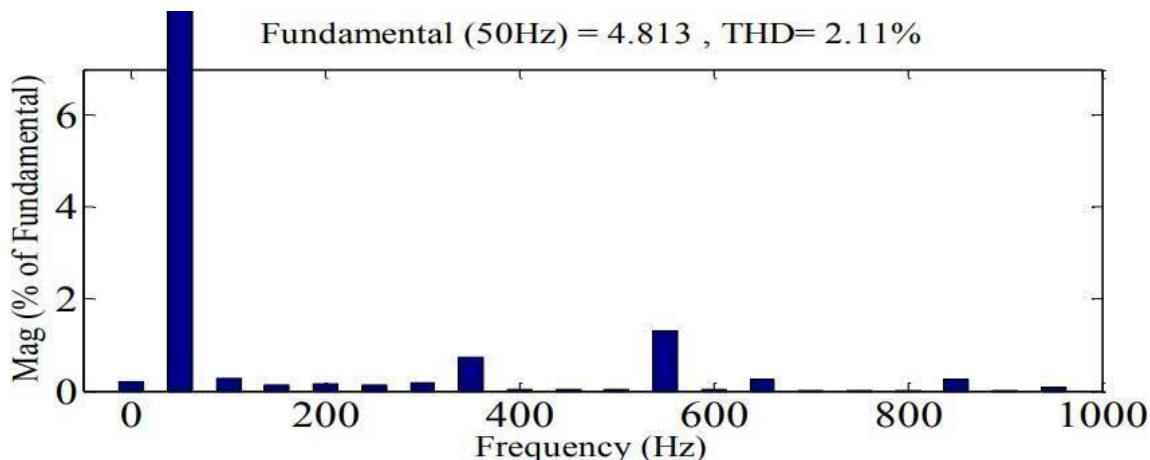


Fig.-5.8 Source Current with Hybrid filter when Source impedance is changed



**Fig.-5.9 THD of Source Current with Hybrid filter when Source impedance is changed**

### 5.3 Comparative Study under Unbalanced Load Condition

A comparative study of the three-phase source current THD during unbalanced load at various operating conditions, presented in Table-5.4. It is clear from these results that the proposed control strategy works optimally in almost all operating conditions and thus helps in improving the quality of electrical power delivered to the end-user.

**Table 5.4 Comparison of source current THD under unbalanced load**

CONDITIONS	THD			POWER FACTOR
	Phase a	Phase b	Phase c	
Source current without filter	22.75%	35.0%	37.6%	0.941
Source current with passive filter	4.5%	4.3%	5.1%	0.977
Source current with hybrid filter	1.4%	1.1%	1.3%	0.99
Source current with hybrid filter when source impedance is changed	1.8%	1.5%	2.1%	0.99

### References

- [1]. Awad, H.; Bollen, M. H J, "Power electronics for power quality improvements," Industrial Electronics, 2003. ISIE '03. 2003 IEEE International Symposium on, vol.2, no., pp.1129,1136 vol. 2, 9-11 June 2003 doi: 10.1109/ISIE.2003.1267983
- [2]. Singh, Bhim; Al-Haddad, K.; Chandra, A., "A review of active filters for power quality improvement," Industrial Electronics, IEEE Transactions on, vol.46, no.5, pp.960,971, Oct 1999 doi: 10.1109/41.793345
- [3]. Rivas, D.; Moran, L.; Dixon, J.W.; Espinoza, J.R., "Improving passive filter compensation performance with active techniques," Industrial Electronics, IEEE Transactions on, vol.50, no.1, pp.161,170, Feb. 2003 doi: 10.1109/TIE.2002.807658
- [4]. Herrera, R.S.; Salmeron, P., "Instantaneous Reactive Power Theory: A Comparative Evaluation of Different Formulations," Power Delivery, IEEE Transactions on, vol.22, no.1, pp.595,604, Jan. 2007 doi: 10.1109/TPWRD.2006.881468
- [5]. Salmeron, P.; Litran, S.P., "Improvement of the Electric Power Quality Using Series Active and Shunt Passive Filters," Power Delivery, IEEE Transactions, vol.25, no.2, pp.1058,1067, April 2010 doi: 10.1109/TPWRD.2009.2034902

- [6]. M H J Bollen, Understanding Power Quality Problems Voltage Sags and Interruptions, New York, IEEE Press, 1999.
- [7]. Axente, N. G. Jayanti, M. Basu, and M. F. Conlon, —A 12 kVA DSPcontrolled laboratory prototype UPQC capable of mitigating unbalance in source voltage and load current,|| IEEE Trans. Power Electron. , vol. 25, no. 6, pp. 1471–1479, Jun. 2010.
- [8]. H. Akagi, —Active harmonic filters,|| Proc. IEEE, vol. 93, no. 12, pp. 2128– 2141, Dec. 2005.
- [9]. B. Singh, K. Al-Haddad, and A. Chandra, —A review of active filters for power quality improvement,|| IEEE Trans. Ind. Electron., vol. 46, no. 5, pp. 960–971, Oct. 1999.
- [10]. J. W. Dixon, G. Venegas, and L. A. Moran, —A series active power filter based on a sinusoidal current-controlled voltage-source inverter,|| IEEE Trans. Ind. Electron., vol. 44, no. 5, pp. 612–620, Oct. 1997.
- [11]. H. Yang and S. Ren, —A practical series-shunt hybrid active power filter based on fundamental magnetic potential self-balance,|| IEEE Trans. Power Del., vol. 23, no. 4, pp. 2089–2096, Oct. 2008.
- [12]. A. Luo, Z. Shuai, W. Zhu, R. Fan, and C. Tu, —Development of hybrid active power filter based on the adaptive fuzzy dividing frequency-control method,|| IEEE Trans. Power Del., vol. 24, no. 1, pp. 424–432, Jan. 2009.
- [13]. Kneschke, T., "Distortion and power factor of nonlinear loads," Power Engineering Society Summer Meeting, 1999. IEEE, vol.1, no., pp.457,462 vol.1, 18-22 Jul 1999 doi: 10.1109/PESS.1999.784391
- [14]. F. Z. Peng and D. J. Adams, —Harmonics sources and filtering approaches,|| in Proc. Industry Applications Conf., Oct. 1999, vol. 1, pp. 448–455.
- [15]. H. Yang and S. Ren, —A practical series-shunt hybrid active power filter based on fundamental magnetic potential self-balance,|| IEEE Trans. Power Del., vol. 23, no. 4, pp. 2089–2096, Oct. 2008.
- [16]. A. Luo, Z. Shuai, W. Zhu, R. Fan, and C. Tu, —Development of hybrid active power filter based on the adaptive fuzzy dividing frequency-control method,|| IEEE Trans. Power Del., vol. 24, no. 1, pp. 424–432, Jan. 2009.
- [17]. F. Z. Peng, H. Akagi, and A. Nabae, —A new approach to harmonic compensation in power systems-a combined system of shunt passive and series active filters,|| IEEE Trans. Ind. Appl., vol. 26, no. 6, pp. 983–990, Nov./Dec. 1990.
- [18]. H. Zhong, P. Chen, Z. Lu, Z. Qian, and H. Ma, —Three phase fourwire series hybrid active power filter with fundamental current bypass channel,|| in Proc. Industrial Electronics Society (IECON), Nov. 2004, vol. 1, pp. 536– 539.
- [19]. G.-M. Lee, D.-C. Lee, and J.-K. Seok, —Control of series active power filters compensating for source voltage unbalance and current harmonics,|| IEEE Trans. Ind. Electron., vol. 51, no. 1, pp. 132–139, Feb. 2004.
- [20]. P. Salmerón, R. S. Herrera, and J. R. Vázquez, —Mapping matrices against vectorial frame in the instantaneous reactive power compensation,|| IET Elect. Power Appl., vol. 1, no. 5, pp. 727–736, Sep. 2007.
- [21]. H. Akagi, Y. Kanazawa, and A. Nabae, —Instantaneous reactive power compensators comprising switching devices without energy storage components,|| IEEE Trans. Ind. Appl., vol. IA-20, no. 3, pp. 625–630, May/Jun. 1984.
- [22]. A. Horn, L. A. Pittorino, and J. H. R. Enslin, —Evaluation of active power filter control algorithms under non-sinusoidal and unbalanced conditions,|| in Proc. 7th Int. Conf. Harmonics and Quality Power, Oct. 16– 18, 1996, pp. 217–224.
- [23]. J. K. Phipps, J.P. Nelson, P. K. Sen, —Power Quality and Harmonic Distortion on Distribution Systems,|| in IEEE Trans. on Ind. Appl., vol. 30, No 2, March/April 1994, pp. 176-184.
- [24]. H. Sasaki and T. Machida, —A new method to eliminate ac harmonic currents by magnetic compensation - consideration on basic design,|| IEEE Trans. Power Appl. Syst. 90 (5), 2009 2019 (1971).

# RENEWABLE ENERGY SOURCES – A REVIEW

ManMahendra Singh Daksh, Shubham Shahi, Vishal Yadav

**Abstract** - Renewable energy is energy that is collected from the sources that can be renewed, which are naturally replenished on a human timescale, such as sunlight, wind, rain, tides, waves, and geothermal heat. At the national level, at least 30 nations around the world already have renewable energy contributing more than 20 percent of energy supply. At least 47 nations around the world already have over 50 percent of electricity from renewable resources. Many renewable energy projects are large-scale, renewable technologies are also suited to rural and remote areas and developing countries, where energy is often crucial in human development. This paper includes the study of different types of renewable sources of India and the possibilities of fulfillment of nations' energy requirement in coming future from different types of renewable sources.

## 1. INTRODUCTION

The most efficient forms of renewable energy are geothermal, solar, wind, hydroelectricity and biomass. Biomass has the biggest contribution with 50% followed by hydroelectricity at 26% and wind power at 18%, solar at 4%, geothermal at 2%. Geothermal energy is generated by harnessing the Earth's natural heat. There is a tremendous amount stored in the planet with the conduction rate pegged at 44.2 terawatts. According to a report, the global industry is expected to produce around

18.4 giga watts by 2021. Wind energy make use of air flow to move massive wind turbines. The mechanical action generates electric power. Rows of windmills are usually constructed along coastal areas where there are no barriers to impede flow. This industry could make up 35% of US electrical production by 2050. By 2050, experts believe that solar energy could be supplying 25% of our energy needs. Biomass refers to wood, bio fuels, waste and other forms of organic matter which are burned to produce energy. The burning process releases carbon emissions but it is still considered renewable source of energy because the plants used can be re-grown.

Hydroelectric plants use the moving water to generate electricity. The conventional method is to build dams to control the flow. This requires massive investment but maintenance cost is quite low. The currently accounts for 7% of the total US energy production. The energy efficiency of different biogas systems, including single and co-digestion of multiple feedstock, different biogas utilization pathways, and waste-stream management strategies was evaluated.[1]

## 2. INDIA ENERGY SCENARIO

India is the seventh largest geography and ranks fourth among high energy consuming countries in the world with over 1.27 billion population. Total primary energy consumption has increased manifolds during the past three decades from 18 MTOE (in 1980) to 104 MTOE (2011) in India (EIA 2013; TEDDY 2013). Coal, natural gas, crude oil is the leading commercial sources of energy of the country in which most of the crude oil are being imported. Even though the industrial and commercial sectors make use of fossil fuel resources, the Indian domestic sector largely depends on non-commercial energy sources such as fuel wood, agricultural and horticultural residues, animal residues, biogas, and combustible waste. However, the commercial consumption of bio energy has decreased with switch over to fossil energy sources (coal, crude oil, natural gas, etc.) over the years. Rural population constitutes 70% in India and largely depends on bio resources for domestic energy. About 75% of the rural households depend on firewood, 10% on dung cake, 5% on LPG for cooking whereas, 22% of the urban households depend on firewood, 22% on kerosene, and 44% on LPG for cooking in the country. Some fraction of the urban households is also dependent on fuel wood for cooking, water heating, and space heating.[3-4]

**Table: 1. Plant load factor (PLF)**

Year	PLF	Sector-wise PLF (%)		
		%	Central	State
2009-10	77.5	85.5	70.9	83.9
2010-11	75.1	85.1	66.7	80.7
2011-12	73.3	82.1	68	69.5
2012-13	69.9	79.2	65.6	64.1

2013-14	65.6	76.1	59.1	62.1
2014-15	64.46	73.96	59.83	60.58
2015-16	62.29	72.52	55.41	60.49
2016-17	59.88	71.98	54.35	55.73
2017-18	60.67	72.35	56.83	55.32
2018-19	61.07	72.64	57.81	55.24
2019- 20*	60.96	67.55	58.46	58.07

\* Up to July 2019 (Provisional), Source: CEA

### 3. ECONOMIC AND TECHNICAL ANALYSIS OF RENEWABLE ENERGY

According to this an energy system can be transformed into a 100% renewable energy system by the following stages.

- Installation of small and large-scale heat pumps
- Reducing grid regulation requirements
- Adding flexible electricity demands and electric vehicles
- Producing synthetic methanol for transport
- Using synthetic gas to replace the remaining fossil fuels.

For each step, the economics and technical performance of the energy system is calculated. The results indicate that a 100% renewable energy system can provide the same end- user energy demands as today's energy system and at the same price [5].

Electricity will be the backbone of the energy system, but the flexibility in today's electricity sector will be transferred from the supply side of the demand side in the future.

These results are significant since they indicate that the transition to a 100% renewable energy system can begin today, without increasing the cost of energy in the short-or long-term, if the costs currently forecasted for 2050 become a reality.[3]

### 4. RENEWABLE ENERGY SOURCES IN INDIA

#### 4.1 Solar Energy

India is endowed with vast solar energy potential. About 5,000 trillion kWh per year energy is incident over India's land area with most parts receiving 4-7 kWh per sq. m per day. Hence both technology routes for conversion of solar radiation into heat and electricity, namely, solar thermal and solar photo voltaics, can effectively be harnessed providing huge scalability for solar in India. Solar also provides the ability to generate power on a distributed basis and enables rapid capacity addition with short lead times. Off-grid decentralized and low-temperature applications will be advantageous from a rural electrification perspective and meeting other energy needs for power and heating and cooling in both rural and urban areas. From an energy security perspective, solar is the most secure of all sources, since it is abundantly available. Theoretically, a small fraction of the total incident solar energy (if captured effectively) can meet the entire country's power requirements. It is also clear that given the large proportion of poor and energy un-served population in the country, every effort needs to be made to exploit the relatively abundant sources of energy available to the country. While, today, domestic coal based power generation is the cheapest electricity source, future scenarios suggest that this could well change [2].

**Table: 2. Installed solar power capacity**

Installed solar power capacity (MW) of India					
State	31-Mar-15	31-Mar-16	31-Mar-17	31-Dec-17	31-Mar-19
Telangana	167.05	527.84	1,286.98	2,990.07	3,592.09
Rajasthan	942.1	1,269.93	1,812.93	2,310.46	3,226.79
Andhra Pradesh	137.85	572.97	1,867.23	2,165.21	3,085.68
Tamil Nadu	142.58	1,061.82	1,691.83	1,819.42	2,575.22
Gujarat	1,000.05	1,119.17	1,249.37	1,344.69	2,440.13

The Potential for wind power generation for grid interaction has been estimated at about **1,02,788 MW** taking sites having wind power density greater than 200 W/sq. m at 80 m hub-height with 2% land availability in potential areas for setting up wind farms @ **9 MW/sq. km.**

An aggregate demonstration wind power capacity of 71 MW has been established at 33 locations in 9 states viz., Andhra Pradesh, Gujarat, Karnataka, Kerala, Madhya Pradesh, Maharashtra, Rajasthan, Tamil Nadu and West Bengal.

**Table: 3. Largest Wind farms in India**

<b>Largest wind farms in India</b>				
S.N.	Wind farm	Producer	State	Current capacity (MW)
1	Muppandal Wind Park	Muppandal Wind	T.N.	1,500
2	Jaisalmer Wind Park	Suzlon Energy	RJ	1,275
3	Brahmanvel windfarm	Parakh Agro Industries	MH	528
4	Dhalgaon wind farm	Gadre Marine Exports	MH	278
5	Chakala wind farm	Sujlon Energy	MH	217
6	Vankusawad Wind Park	Sujlon Energy	MH	189
7	Vaspet Wind farm	Renew Power	MH	144

A total capacity of 22,465 MW has been established up to December, 2014, mainly in Tamil Nadu, Gujarat, Maharashtra, Andhra Pradesh, Karnataka and Rajasthan. Wind electric generators of unit sizes between 225 kW and 2.1 MW have been deployed across the country. India now ranks 5th in the world after China, USA, Germany and Spain in grid connected wind power installations.

#### **4.3 Hydro Energy**

Hydro power projects are generally categorized in two segments i.e. small and large hydro. In India, hydro projects up to 25 MW station capacities have been categorized as Small Hydro Power (SHP) projects.

While Ministry of Power, Government of India is responsible for large hydro projects, the mandate for the subject small hydro power (up to 25 MW) is given to Ministry of New and Renewable Energy. Small hydro power projects are further classified as

**Table: 4. Type of Hydro Power Plant**

Class	Station Capacity in kW
Micro Hydro	Up to 100
Mini Hydro	101 to 2000
Small Hydro	200125000

An estimated potential of about 20,000 MW of small hydro power projects exists in India.

#### **4.4. Biomass Energy**

Biomass has always been an important energy source for the country considering the benefits it offers. It is renewable, widely available, carbon -neutral and has the potential to provide significant employment in the rural areas. Biomass is also capable of providing firm energy. About 32% of the total primary energy use in the country is still derived from biomass and more than 70% of the country's population depends upon it for its energy needs. Ministry of New and Renewable Energy has realized the potential and role of biomass energy in the Indian context and hence has initiated a number of programs for promotion of efficient technologies for its use in various sectors of the economy to ensure derivation of maximum benefits. Biomass power generation in India is an industry that attracts investments of over Rs.600 crores every year, generating more than 5000 million units of electricity and yearly employment of more than 10 million man-days in the rural areas. For efficient utilization of biomass, bagasse-based cogeneration in sugar mills and biomass power generation have been taken up under biomass power and cogeneration program.

Studies sponsored by the Ministry has estimated surplus biomass availability at about 120 – 150 million metric tonnes per annum covering agricultural and forestry residues corresponding to a potential of about 18,000 MW. This apart, about 5000 MW additional power could be generated through bagasse based cogeneration in the country's 550 Sugar mills, if these sugar mills were to adopt technically and economically optimal levels of cogeneration for extracting power from the bagasse produced by them.

**Table: 5. Biomass Power installed capacity**

<b>State Wise Biomass Power installed capacity</b>	
<b>State</b>	<b>Capacity (MW)</b>
Andhra Pradesh	389.75
Bihar	43.42
Chhattisgarh	264.9
Gujarat	55.9
Haryana	52.3
Karnataka	737.28
Madhya Pradesh	36
Maharashtra	1,112.78
Odisha	20
Punjab	140.5

Rajasthan	111.3
Tamil Nadu	662.3
Uttarakhand	30
Uttar Pradesh	936.7
West Bengal	26
<b>Total</b>	<b>4,761.00</b>

#### 4.5 Tidal Energy

Oceans cover 70 percent of the earth's surface and represent an enormous amount of energy in the form of wave, tidal, marine current and thermal gradient. A variety of different technologies are currently under development throughout the world to harness this energy in all its forms.

Total identified potential of Tidal Energy is about 12455 MW, with potential locations identified at Khambat & Kutch regions, and large backwaters, where barrage technology could be used [8].

The tidal cycle occurs every 12 hours due to the gravitational force of the moon. The difference in water height from low tide and high tide is potential energy. Similar to traditional hydropower generated from dams, tidal water can be captured in a barrage across an estuary during high tide and forced through a hydro-turbine during low tide. The capital cost for tidal energy power plants is very high due to high civil construction and high power purchase tariff. To capture sufficient power from the tidal energy potential, the height of high tide must be at least five meters (16 feet) greater than low tide. The Gulf of Cambay and the Gulf of Kutch in Gujarat on the west coast have the locations in the country where potential exist.

**Table: 6. Installed Tidal Power capacity**

Station	Capacity (MW)	Location	Year
Gulf of Kutch project & Khambat Project	12455	Gulf of Kutch and Khambat	2019

## REFERENCES

- [1] Sulaiman, and M. A. Irfan, —The techno-economic potential of Saudi Arabia’s solar industry,|| Renew Sustain. Energy Rev., vol. 55, pp. 697–702, 2016
- [2] State wise Estimated Solar Power Potential in the Country, -National Institute of Solar Energy Publication|. Available: <http://Statewise-Solar-Potential-NISE.pdf>. 2014.
- [3] R. K. kumawat, Seema Agrawal, Seemant Chourasiya, D.K. Paliwalia, —Modeling & Simulation of PV ARRAY with Single Phase Reduced Switch Count Five Level PWM Inverter for Renewable Energy Applications||, APGRES June, 2015.
- [4] C. S. Bhattacharyya, —An overview of problems and prospects for the Indian power sector,|| Energy, vol. 19, pp.795–803, 1999.
- [5] A. Kumar et al. / Renewable and Sustainable Energy Reviews 14 (2010) 2434–2442
- [6] Bhattacharyya, S. C. (2011). Energy Economics: Concepts, Issues, Markets and Governance: 31 Springer
- [7] MNRE: Renewable energy in India growth and targets, May 2019. <http://mnre.gov.in>.
- [8] CEA; Installed capacity; <http://cea.nic.in/enabling-technology>,|| Renewable and Sustainable Energy Reviews, vol. 30, pp. 748-764, 2014.
- [9] N. Golait, R. M. Moaril and P. S. Kulkarni, —Wind electric power in the world and perspective of its development in India,|| Renewable and Sustainable Energy Reviews, vol. 13, pp. 233-247, 2009.
- [10] P. Abhishek –India 2020: Utilities & Renewable,|| Deutsche Bank Markets Research. Available: <https://www.db.com/cr/en/docs/Deutsche-Bank-report-Make-way-for-the-Sun.pdf>. 2015.
- [11] B. Mehmet, O. Arif, B. Sahin and A. Kahraman, —An overview of renewable electric power capacity and progress in new technologies in the world,|| Renewable and Sustainable Energy Reviews, vol.49, pp. 323-334, 2015.
- [12] Borowitzka, Michael A., and Navid Reza Moheimani. "Open pond culture systems." In Algae for Biofuels and Energy, pp. 133-152. Springer Netherlands, 2013.

# **Effects of Marble Slurry and Granite Dust in the Manufacturing of Concrete**

**Shahnawaz Ansari, Sunil R Meena, Amit Kumwat**

**Abstract :** The basic objective of this research was to identify alternative source of good quality aggregates. Marble and Granite are important materials used in construction industry. Marble dust is produced from processing plants during sawing and polishing of marble blocks and about 20-25% processed marble is turned into powdered form. Granite dust is the stone waste generated from granite stone industries. Disposal of these wastes from the industries is one of the major environmental concerns worldwide. The present investigation was undertaken to study the effect of Marble dust and Granite dust on the mechanical properties of concrete. The main parameter investigated was the cube compressive strength. In this research, M-25 grade concrete mix was prepared using IS method of mix design. Cubic specimens of dimension (150 x 150 x 150) mm were casted for compressive strength test. Total of 24 cubes were casted, 6 specimens of nominal mix, 6 specimens with 20% marble inclusion, 6 specimens with 20% granite inclusion and 6 specimens with 10%-10% both marble and granite inclusion. Cubes were tested for 7 days and 28 days.

**IndexTerms –** **Marble slurry, Granite dust, Cube Compressive Strength, Mix design, Compressive strength test.**

## **I. Introduction**

Rapid urbanization in developing countries such as India is creating a shortage of adequate housing in cities. Using artificial aggregates for quality concrete is a natural step to mitigate this problem. To overcome the stress and demand for river fine aggregate, research sand practitioners in the construction industries have identified some alternative materials such as fly ash, slag, limestone powder and siliceous stone powder. In India attempts have been made to replace river sand with Marble dust and Granite dust. The successful utilization of Marble and Granite dust as fine aggregate would turn this waste materials that causes disposal problem into a valuable resource. This utilization will also reduce the strain on supply of natural fine aggregate, which will also reduce the cost of concrete. The main objective of this investigation was to evaluate the possibilities of using Marble and Granite dust as a replacement of fine aggregate. Present investigation was aimed to study the partial replacement of traditional Sand with Marble dust, Granite dust and both. Compressive strengths were found after 7 days and 28 days of curing.

## **II. LITERATURE REVIEW**

- Sakalkale et al. (2014) and Reddy et al. (2015) conducted strength tests by substituting Marble Dust in different proportions by weight of Sand (25%, 50%, 75%, 100%). The compressive strength of concrete was increased with addition of waste marble powder upto 50% and any further addition of waste marble powder decreases the compressive strength.
- Kalchuri et al. (2015) and Anwar et al. (2015) obtained the strength characteristics of concrete with and without Marble Dust in different proportions (0%, 10%, 20%, 30%, and 40%). The compressive strength of concrete is increased with addition of waste marble powder upto 20% by replacing Sand. Waste Marble Dust has cementitious properties and thus it can be used as a filler material. Sharma and Kumar (2015)
- Deepankar et al. (2013) used marble dust in M-30 concrete by partially replacing natural sand and cement in different proportions (0%, 10%, 15%, 20%, and 30%). Replacement of Sand by MD upto 15% increases Compressive strength but replacement of Cement by MD upto 15% decreases the strength. Durability of mix increases with reference to the control mix.

- Kumar and Rao (2017) used marble dust in M-25 concrete by partially replacing natural sand (0%, 5%, 10%, 15%, 20%, 25%, 30%, 35%, and 40%). They concluded that Sand can be replaced by MD upto 40% without affecting the target strength.
- Arivumangai et al. (2014) conducted a detailed experimental study on compressive strength by replacing sand by granite powder in 0, 25 and 50% and cement with silica fume, fly ash, slag and super plasticizer. He observed that granite powder concrete enhances the resistance and thus could improve the chemical resistance of concrete.
- Shehdeh et al. (2016) conducted an experimental investigation to explore the possibility of using the granite powder and iron powder as a partial replacement of sand in concrete. He concluded that granite powder and iron powder as partial replacement of sand showed good workability and fluidity similar to normal concrete mixes.

### **III. properties of material used**

#### **3.1 Cement**

Pozzolona Portland cement with conforming to BIS (IS: 455-1989) of grade 43 was used in the entire experimental study.

#### **3.2 Coarse Aggregate:**

Coarse Aggregate from Crushed Basalt rock confirming to BIS (IS 383:1970) was used in this experiment. The fractions from 20 mm to 10 mm were used.

#### **3.3 Fine Aggregate:**

River Sand and Crushed sand were used in combination as fine aggregate confirming to BIS (IS 383:1970). The fractions from 4.75 mm to 150 micron were used.

#### **3.4 MarbleDust:**

India is the third top most exporter of marble in the world. Every year million tons of marble waste from processing plants are released during sawing and polishing of marble blocks and about 20-25% processed marble is turned into powdered form. Locally available marble dust from Ashoka Marble Pvt. Ltd, Vishwakarma Industrial Area, Jaipur and M/S Khaitan Tiles Pvt. Ltd, Vishwakarma Industrial Area, Jaipur was used in this research project.

#### **3.5 Granite Dust:**

Indian Granite Stone industry produces around 17.8 million tons of solid granite wastes in form of cuttings, trimmings and granite slurry from processing and polishing units. Locally available marble dust from Ashoka Marble Pvt. Ltd, Vishwakarma Industrial Area, Jaipur and M/S Khaitan Tiles Pvt. Ltd, Vishwakarma Industrial Area, Jaipur was used in this research project.

#### **3.6 Admixture:**

Super plasticizer, *BS Futura PCX 107* was used in this project. It is a light brown liquid in ready to use form. It has to be introduced in the concrete mix along with the dosing water. It was obtained from Techno trade Associates, Lalkothi, Jaipur, Rajasthan.

### **IV. TEST PERFORMED ON CONCRETE**

Two tests were performed on the four types of concrete mix. Slump test was conducted for measurement of workability of concrete and compressive strength test was performed to determine compressive strength of the concrete mix.

#### **4.1 Slump test:**

Slump test is used to determine the workability of fresh concrete as per BIS (IS: 1199).

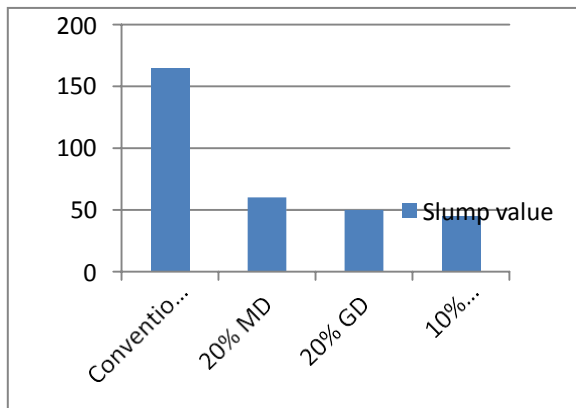


**Fig. 1 Bar Graph for Slump Value**

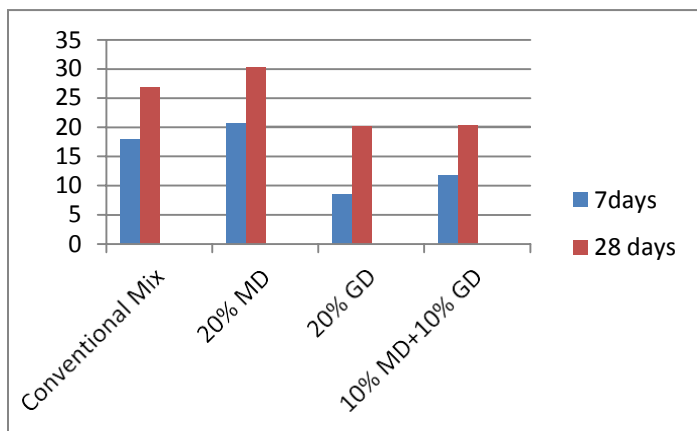


**Fig. 2 Bar Graph for Compressive strength test results**

#### 4.2 Compressive Strength Test:

Compressive strength of concrete cube test provides an idea about all the characteristics of concrete in accordance with BIS (IS: 516).

#### V. CONCLUSION

- In case of marble dust replacement, from the above investigation we conclude that at 20% inclusion of marble dust compressive strength of replaced concrete increases by 14.8 % at 7 day curing and 12.9% at 28 day curing.
- In case of granite dust replacement, from the above investigation we conclude that at 20% inclusion of granite dust compressive strength of replaced concrete decreases by 52% at 7 day curing and 25% at 28 day curing.
- In case of both marble and granite dust replacement, from the above investigation we conclude that at 10%+10% inclusion of both marble and granite dust compressive strength of replaced concrete decreases by 34.3% at 7 day curing and 24.5 % at 28 day curing.

- For granite dust replacement, from literature review we conclude that granite dust offers a considerable amount of increase in compressive strength when cement is also partially replaced with along with granite replacement. Only Granite replacement offers no such benefits.
- The compressive strength of concrete increases when natural river sand is replaced with 20% Marble dust powder.

## **REFERENCES**

- [1] Sakalkale, A. D., & Dhawale, G. D. (2014). Experimental study on use of waste marble dust in concrete. *International Journal of Engineering Research and Applications*, 4(10), 44-50.
- [2] Anwar, A., Ahmad, S., Husain, S. M. A., & Ahmad, S. A. (2015). Replacement Of Cement By Marble Dust And Ceramic Waste In Concrete For Sustainable Development. *International Journal of Innovative Science, Engineering & Technology (IJISET)*, 2(6), 496-503.
- [3] Kalchuri, B. S., & Chandak, R. (2015). Study On Concrete Using Marble Powder Waste As Partial Replacement Of Sand. *International Journal of Engineering Research and Applications*, 5(4), 87-89.
- [4] Sahu, C. (2016). Partial replacement of cement with marble dust powder. *Imperial Journal of Interdisciplinary Research*, 2(8).
- [5] Ashish, D. K., Verma, S. K., Kumar, R., & Sharma, N. (2016). Properties of concrete incorporating waste marble powder as partial substitute of cement and sand. In *Proceeding of The 2016 World Congress on The 2016 Structures Congress*.
- [6] Reddy, M. V. S., & Ashalatha, K. (2015). Effect of Various Replacement Levels of Waste Marble Dust In Place of Fine Aggregate to Study the Fresh and Hardened Properties of Concrete. *International Journal of Engineering Research and Applications*, 5(12), 73-77.
- [7] Vigneshpandian, G. V., Shruthi, E. A., Venkatasubramanian, C., & Muthu, D. (2017, July). Utilisation of Waste Marble Dust as Fine Aggregate in Concrete. In *IOP Conference Series: Earth and Environmental Science* (Vol. 80, No. 1, p. 012007). IOP Publishing.
- [8] Kumar, S.,& Rao,M.S (2017) Partial replacement of fine aggregate with marble dust in concrete. ANVESHANA'S INTERNATIONAL JOURNAL OF RESEARCH IN ENGINEERING AND APPLIED SCIENCES, VOLUME 2, ISSUE 2 (2017, FEB)
- [9] Sharma, N., & Kumar, R. (2015, April). Review on Use of Waste Marble Powder as Partial Replacement in Concrete Mix. In *EFES-2015 National Conference on Emerging Fields in Engineering and Science ISSN* (pp. 2349-0918).
- [10] Shirule, P. A., Rahman, A., & Gupta, R. D. (2012). Partial replacement of cement with marble dust powder. *International Journal of Advanced Engineering Research and Studies*, 1(3), 175-177.
- [11] Manasseh, J. O. E. L. (2010). Use of crushed granite fine as replacement to river sand in concrete production. *Leonardo electronics journal of practice and technologies*, 17, 85-96.
- [12] Arivumangai, A., & Felixkala, T. (2014). Strength and durability properties of granite powder concrete. *Journal of Civil Engineering Research*, 4(2A), 1-6.
- [13] Ghannam, S., Najm, H., & Vasconez, R. (2016). Experimental study of concrete made with granite and iron powders as partial replacement of sand. *Sustainable Materials and Technologies*, 9, 1-9.

# **STUDY OF PLASTICIZER ON THE PROPERTIES OF CONCRETE**

**Shiv Kumar ,S. Meharuddin Ahmad, Juber Khan**

**Abstract** -To improve the workability, strength, ability to control during work times and durability of cement concrete, engineers, chemists, manufacturers and others have helped the concrete by adding some additional substances known as admixtures. There are different kinds of admixtures available; and each admixture has its own specialty. This paper has been made an attempt to study the effect of plasticizer doses of 0.25, 0.30 and 0.35 percentage (by weight of cement) on performance of M15 concrete grade. The tests considered for study are slump test and compressive strength test. The results show that for the constant water cement ratio, increase of plasticizer dose in Concrete leads to gain of good workability. Moreover, there is also slightly increase in compressive strength than that of normal concrete mix.

**Keywords** - compressive strength test, plasticizer, workability, normal concrete

## **I. INTRODUCTION**

For developing infrastructures like commercial, industrial, residential, military structures etc., the concrete performance plays an important role. In order to improve its workability, strength, ability to control during work times and durability of cement concrete, engineers, chemists, manufacturers and others have helped the concrete by adding some additional substances known as admixtures[9]. Now a day's admixture became an essential component for concrete mix, because it provides an understanding for the variance between water and workability and performance of hardened concrete. There are different kinds of admixtures available; and each admixture has its own specialty. Some admixtures reduce the water content that means to increase the strength of concrete, some admixtures accelerates or retards the setting time of concrete, some admixtures increase the workability of concrete, some admixtures reduces the corrosion effect on reinforced concrete, some admixtures reduce the shrinkage of concrete and some reduces the alkali-silica reactivity. This research paper explains the effect of water reducing admixture on properties of concrete. Water reducing admixtures generally are of two types. (1) Plasticizers – which reduces the water requirement by 15% and these are based on Calcium ligno Sulphate, (2) Super-plasticizers – reduces the water requirement by 30% and these are based on sulphonated melamine formaldehyde condensate (SMF) and sulphonated naphthalene formaldehyde condensate (SNF)[8]. The general objective of this paper is to evaluate the performance of concrete without and with varying dosages of plasticizer. The main objective is the

influence of plasticizer on properties of concrete like workability and strength of concrete through slump and compressive strength tests.

## **II. MATERIALS USED AND PROPERTIES**

The materials used for this study are cement, fine aggregate, coarse aggregate and plasticizer. Few tests are conducted as per codal provisions on concrete materials to determine their properties and suitability for the tests under consideration.

### **A. CEMENT**

Cement is one of the most essential components of concrete because of its binding property. Various tests were conducted to determine the properties of Portland pozzolana cement (PPC) of 53 grade confirming to IS:1489 part – 1, such as fineness = 1.38%, standard consistency = 35%, specific gravity = 3.15, compressive strength at 7 days = 28.09 N/mm<sup>2</sup> and at 28 days = 64.66 N/mm<sup>2</sup>

### **B. FINE AND COARSE AGGREGATES**

The aggregates are important because of its strength. To determine the properties of aggregates following tests were conducted. Sieve analysis and specific gravity for fine and coarse aggregate, aggregate crushing strength and aggregate impact test for coarse aggregate. The tests results are obtained in laboratory for Specific gravity of FA = 2.65 and of CA = 2.76, aggregate crushing strength test = 33.6% and aggregate impact test = 17.28%.

### **C. PLASTICIZER**

It is a water-reducing admixture based on calcium ligno sulphate. It increases the workability of concrete and ultimately increases the strength of concrete. Three design mixes of M15 with same water cement ratio and varying doses of plasticizer of 0.25, 0.30 and 0.35% of cement content. The plasticizer is locally available.

## **III. CONCRETE MIX PROPORTION**

For the performance analysis, three design mix of M15 concrete grade with same water cement ratio 0.58 and with varying dosages of plasticizer of 0.25, 0.30 and 0.35% of cement content are prepared. Three mixes are casted in standard concrete cubes and tested in laboratory and these are named as B, C and D. The concrete with varying dosages of admixture are compared with the normal concrete abbreviated as A.

**Table 1**  
Mix proportions for trial mixes of M15 concrete grade

Trial mix	Proportion				
	water	cement	fine aggregate	coarse aggregate	Plasticizer(by weight of cement)
A	0.58	1.01	2.33	4.23	--
B	0.58	1.01	2.33	4.23	0.0025
C	0.58	1.01	2.33	4.23	0.003
D	0.58	1.01	2.33	4.23	0.0035

## **IV. EXPERIMENTAL RESULTS AND DISCUSSIONS**

The tests conducted on fresh concrete is slump, on hardened concrete is compressive strength test, and compressive strength test is tested at 7 and 28 days. The water used while mixing is of potable water or drinking water. After casting, the mix in cube mould for 24 hours then the same is cured in normal water of curing tank having room temperature.

### **A. WORKABILITY TEST**

The workability of fresh concrete is determined by various tests, but here workability is measured through slump test only. From table 2, it is noted that slump value of normal concrete is 60mm. By adding the admixture to the

concrete, the friction between the particles decreases and fluidity increases. If water reducing admixture or plasticizer content is increased, then its fluidity or workability also increases.

**Table 2**  
Workability test results for various concrete mixes

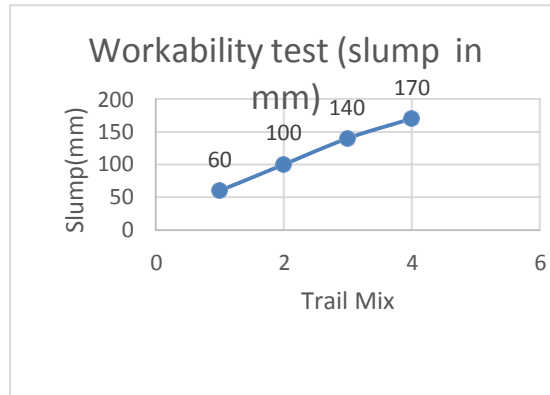


**Fig 1. Comparison of slump values of various mixes at 7 and 28 days**

#### B. COMPRESSIVE STRENGTH

For each concrete mix, three cubes are casted to know the average compressive strength of concrete cubes at 7 and 28 days of curing in the laboratory. From the table below, the compressive strength of B Trail mix increases at 7 and 28 days when compared to the normal concrete of trail mix A. The compressive strength of trail mixes C and D decreases at 7 and 28 days due to the excess content of plasticizer.

Table No 3

various days	Concrete mix	Percentage of plasticizer	Workability test (slump in mm)		Compressive strength of concrete mixes at 7 and 28
			7 Days	28 Days	
	A	--	60		
	B	0.25	100		
	C	0.3	140		
	D	0.35	170		

Trail Mix	Percentage of Plasticizer	Actual Compressive strength(MPa)		Avg. Compressive strength (MPa)	
		7 Days	28 Days	7 Days	28 Days
A	--	10.667	20.222	10.593	21.036

Avg. Compressive strength (Mpa)		10.444	22	12.74	22.222
			10.667		
B	0.25	13.555	21.555	12.74	22.222
		11.555	23.111		
		13.111	22		
		11.111	18.889		
C	0.3	10.889	17.333	11.037	18.147
		11.111	18.222		
		9.333	17.333		
D	0.35	10	16.222	9.852	16.666
		10.222	16.444		

days

Compressive strength of various mixes at 7 and 28 days

Fig 2.  
trial

## V. CONCLUSION

The general objective of this paper is to evaluate the workability and compressive strength of concrete mixes of different dosages of plasticizer at 7 and 28 days are

1. The workability of the concrete increases with the increase in dosages of water reducing admixture or plasticizer
2. The maximum compressive strength occurs in the concrete mix of 0.3% of plasticizer (by weight of cement)
3. By adding the plasticizer, the water content nearly reduces to 15% and it increases the compressive strength of the concrete for 0.3% of plasticizer (by weight of cement)

## ACKNOWLEDGEMENTS

The author would like to express gratitude to the faculty of Department of Civil Engineering for providing the facilities of conducting various tests in the laboratory. I would like to extend thanks to my colleagues and students of fourth year Civil Engineering for their continuous support during experimental work.

## REFERENCES

1. Rahul Singh, S.M. Gupta and Babita Saini, Effect of mineral and chemical admixtures on the properties of mortar and concrete – A review, The Indian Concrete Journal, March 2016.
2. S.M.Dumne,Effect of Superplasticizer on Fresh and Hardened Properties of Self-Compacting Concrete Containing Fly Ash, American Journal of Engineering Research (AJER), 3, No.3, 2014, 205-211.
3. IS 8112, Ordinary Portland Cement 43 grade, 1989, May 2006.
4. IS 383, Indian standard specification for coarse and fine aggregates from natural sources for concrete (second revision), Bureau of Indian Standards, Manak Bhavan, 9 Bahadur Shah Zafar Marg, New Delhi 110 002, 1970.
5. IS 10262, (Reaffirmed 1999), Recommended Guidelines for Concrete Mix Design, Bureau of Indian Standards, Manak Bhavan, 9 Bahadur Shah Zafar Marg, New Delhi 110 002, 1982.
6. SP 23, Handbook of concrete mixes (based on Indian standards), Bureau of Indian Standards, Manak Bhavan 9 Bahadur Shah Zafar Marg, New Delhi 110 002, 1982.

7. Saeed Ahmed, Attaullah Shah, Karamet Ali, Effect of Water Reducing Concrete Admixtures on The Properties of Concrete, Our World in Concrete and Structures, 2004.
8. M K Maroliya, Influence of chemical admixtures on density and slump loss of concrete, International Journal of Modern Engineering Research (IJMER), 2(6), 2012,4077-4079.

# Design and Development of a Drone with Video Recording and Weight Lifting Function

Rohit Saini, Sonu Saini, Prashant Kumar, Bhavana Mathur

**Abstract** This research paper explores the applications of quadcopters or drones in various scenarios, including search and rescue operations in remote areas, monitoring areas and boundaries, and aerial photography. The paper highlights the advantages of using drones in these contexts, such as their ability to provide a higher perspective for capturing landscapes and their potential for delivering assistance in emergency situations. The study focuses on the development of an unmanned aerial vehicle (UAV) using specific components, including the flight controller "KK2.1.5," electronic speed control units (ESC) of 30A, and 3 phase brushless motors (1000KV) capable of capturing and delivering images during flight. The component selection takes into consideration factors like weight, strength, and cost. Once a conceptual design is developed and the necessary materials are gathered, all the components are assembled in a frame to test the quadcopter's performance. The quadcopter focuses primarily on its functionality while considering future studies and development. The paper concludes by emphasizing the potential benefits of utilizing drones in search and rescue, surveillance, and aerial photography applications.

**Keywords**-Quadcopter Design, Dynamics, Motion, Paint Spray, Precise Marking

## 1. Introduction

A quadcopter is an aircraft that is heavier than air and capable of vertical take-off and landing. It is propelled by four motors positioned in the same plane parallel to the ground. Unlike traditional helicopters, a quadcopter utilizes fixed-pitch blades in its rotors and achieves motion through the air by adjusting the relative speed of each propeller. The first quadcopter, the Omnichen 2, was invented by Etienne Omnichen in 1920 and successfully completed 1000 flights with a recorded distance of 360 meters. Dr. George E. Bothezat designed a quadcopter based on a converted wings model in 1956. In the 21st century, there has been a remarkable evolution in quadcopter technology. Universities, students, and researchers are continuously working on developing robust controllers and modeling techniques to provide detailed and accurate representations of real-life quadrotors. This study focuses on the design and development of a quadcopter equipped with a paint spray mechanism for precise marking on the ground. The quadcopter has various potential applications including aerial surveying, security patrols, 3D building modeling, safety inspections, and more. Quadcopters are also being used for object detection through image processing in national border security. A quadcopter or drone can be useful for certain scenarios such as search and rescue operations in remote areas, monitoring areas and boundaries, aerial photography. In certain remote areas, in case of an emergency, there is often a limitation of human reach, in that case an unmanned aerial vehicle (U.A.V.) can be sent to such areas for appropriate help. These U.A.V.s could capture the images, deliver medical care and can even bring food. Quadcopters or drones can be used for surveillance of certain areas and boundaries for security purposes. We can easily monitor one area by sitting at another place. This could help deploy preventive measures in case of trespassing by an uncouth entity. In aerial photography, we have certain applications such as shooting of movies, sports, nature and wildlife and events. A. S. Vempati et al. (2014) described the design and construction of a lightweight quadrotor with enhanced on-board computational control and various functions. They provided a brief overview of the functionality of the hardware components used in the fabrication process. Parag Parihar et al. (2016) explained the component selection process for a quadcopter and analyzed it based on thrust requirements. The paper provided a detailed step-by-step process, including testing the previous model, performing calculations, designing the quadcopter, purchasing components, and assembling them to create the final product. Dr. Pran Kanai Saha (2019) focused on the design and simulation of the Roll  $Troll(s)$ , Pitch  $Tpitch(s)$ , and Yaw  $Tpitch(s)$  angle control system. The paper also discussed the integration of Android mobile devices, GPS, and 3G communication technologies to gather real-time audiovisual geolocation information. Vibha Kishor and Ms. Swati Singh (2017) designed and developed a quadcopter using an Arduino Uno board instead of a pre-programmed KK flight controller board. The quadcopter was equipped with a camera and GPS tracker for surveillance purposes in areas such as forests and coast guard applications. Anudeep M et al. (2014) presented the design and development of a quadcopter and performed modifications to the quadcopter frame to enhance its. In the paper by Anudeep M et al. (2014), the focus is on the design and development of a quadcopter. They made modifications to the quadcopter frame to enhance its load-bearing capacity, and a static analysis was conducted to evaluate the frame's performance. The results showed minimal deformation, which remained within acceptable limits. [2] In another study by Omkar Tatale et al. (2018), the design, construction, and testing procedure of a quadcopter were discussed. The design considerations were based on factors such as payload capacity and the weight of individual components, which influenced the selection of electronic components. [5]

## 2. Operational Principle

The quadcopter operates based on the principle of generating upward lift through increased air pressure. It achieves motion by adjusting the relative speed of its four propellers. The paper explains the quadcopter's motion and control, including yaw rotation, roll, pitch, and roll. It also discusses the hovering or static position of the quadcopter. The quadcopter's motion relies on two main phenomena: thrust and torque. The quadcopter utilizes four propellers connected to motors to generate thrust for lift. Its movement is

described by input values ( $x, y, z, \theta, \phi, \psi$ ) provided to the quadcopter. Out of the four propellers, two rotate clockwise (CW), while the other two rotate counterclockwise (CCW). The quadcopter's motion is primarily controlled by three movements:

**Yaw Rotation ( $\psi$ ):** Yaw refers to the quadcopter's left or right motion, controlled by the transmitter's throttle stick. It determines the direction of the quadcopter.

**Pitch Rotation ( $\theta$ ):** Pitch represents the quadcopter's forward or backward motion, controlled by the receiver's throttle. Moving the throttle forward propels the quadcopter forward, while moving it backward causes backward motion. [2]

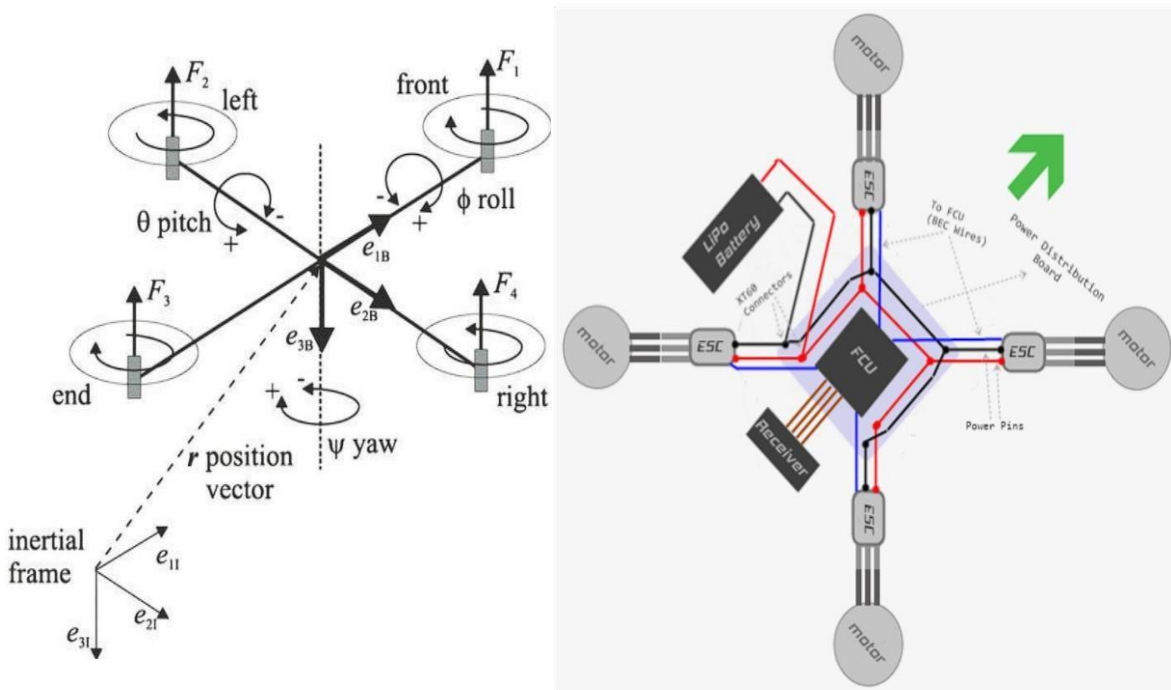


**Figure 2.1: Yaw, Pitch & Roll rotation and Basic Wire Diagram of the Quadcopter**

**Roll Rotation ( $\phi$ ):** Roll refers to the movement around the quadcopter's longitudinal axis. Left or right motion of the throttle stick results in corresponding movement towards the right or left. This parameter enables the quadcopter to fly in either direction. [2]

#### Take-off and Landing Mechanism:

Take-off involves the quadcopter lifting off from the ground to a hover position, while landing refers to descending from the hover position. Take-off and landing motions are controlled by adjusting the speed of all four rotors simultaneously, thereby altering the vertical motion.

#### Forward and Backward Motion:

Forward (backward) motion is controlled by increasing (decreasing) the speed of the rear (front) rotor. Changing the speed of the rear (front) rotor affects the pitch angle of the quadcopter.

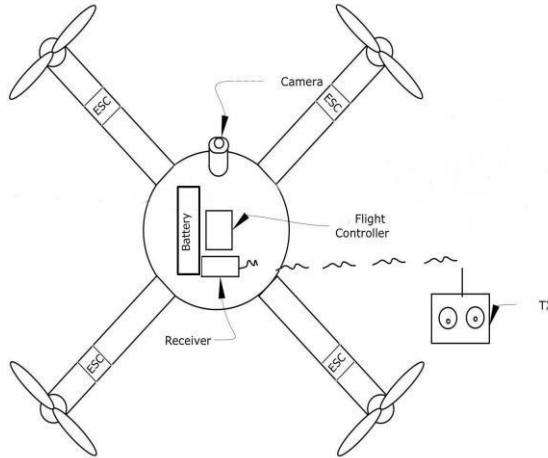


**Fig 2.2 Component Placement**

#### Left and Right Motion:

To achieve left or right motion, the yaw angle of the quadcopter is adjusted. This can be done by increasing (decreasing) the speed of the counterclockwise rotors while decreasing (increasing) the speed of the clockwise rotors.

#### Hovering or Static Position:

In the hovering or static position, two pairs of rotors rotate in opposite directions (clockwise and counterclockwise) with equal speeds. This configuration ensures that the total sum of reaction torque is zero, allowing the quadcopter to hover in place.

### 3. List of component.

Following components were used in development to the DRONE

**Table 1. list of component**

Components	Configuration
Flight Control Unit (FCU)	KK 2.1.5
Motor	BLDC 1000KV
Battery	LiPo 25C, 2200mAh, 11.1V
ESC	30A
Frame	Quad Arm
Transmitter & Receiver	FS-CT6B 2.4 GHZ, 6 Channel
Balanced Charger	3-Cell Charging
Propeller	Twin Blade

#### 3.1 Brushless Motor

Brushless DC motors utilize electric switches to achieve current commutation, enabling continuous rotation of the motor. These switches are typically arranged in an H-bridge structure for single-phase BLDC motors and a three-phase bridge structure for three-phase BLDC motors, as shown in Figure 2.3. Pulse-width modulation (PWM) is commonly used to control the high-side switches, converting a DC voltage into a modulated voltage. This method efficiently limits startup current, controls speed, and adjusts torque. It's important to note that increasing the switching frequency can lead to higher PWM losses, while reducing the frequency restricts the system's bandwidth and may cause destructive ripple current pulses that could shut down the BLDC motor driver. Among BLDC motors, three-phase motors are the most popular and widely used.

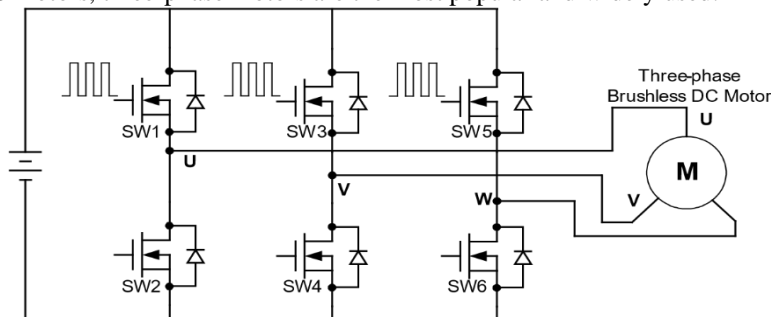


**Fig. 3.1: Three-phase Brushless DC Motor**

#### 3.2 Balanced Charger

In a multiple-celled battery pack, it is possible for the individual cells to develop differences in their charge levels. Since Lithium Polymer (LiPo) batteries are very sensitive to overcharging, it's important that their cells be kept at or very near equal levels when charging. A balanced charger (or balancer) does this by monitoring the individual cell voltages in a pack through a connector on the pack (called a balance connector) and adjusting their rate of charge accordingly. When such a balancer is built into a charger, the charger is known as a Balance Charger.



**Fig. 3.2 Balanced Charger**

To detect the rotor's position in a three-phase BLDC motor, three Hall sensors are required. The physical position of these Hall sensors results in two types of output: a 60° phase shift and a 120° phase shift. By combining the signals from these three Hall sensors, the exact communication sequence can be determined.

BLDC motors offer several advantages over brushed DC motors and induction motors, including:

- Better speed versus torque characteristics
- Faster dynamic response
- High efficiency
- Long operating life
- Noiseless operation
- Higher speed ranges

These advantages make BLDC motors well-suited for various applications in different industries.

### 3.3 Transmitter and Receiver

The transmitter enables the user to control the aircraft from a distance, using 2.4 gigahertz spread spectrum radio signals. Receivers are electric devices with built in antennas that intercept the radio signals from the transmitters, and convert them into alternating current pulses. The receiver then produces information and sends it to the Flight Control Board.

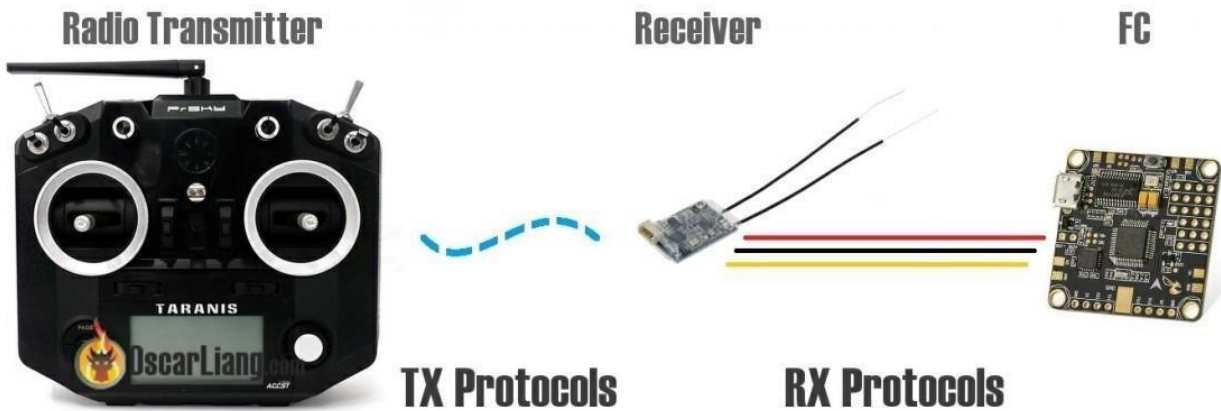


Fig. 3.3 A Tx & Rx Module

### 3.4 Propellers

To construct the quadcopter, propellers of size 1045 are utilized. These propellers create lifting force through high-speed rotation, and each rotation provides a pitch of 4.5 inches.



Fig. 3.4 Propellers

### 3.5 Electronic Speed Controller (ESC)

The ESCs receive PWM signals as commands, which are converted into appropriate motor speeds. They convert the 2-phase battery current into 3-phase power and regulate the speed of the brushless motors. The ESC rating is higher than the motor's ampere rating, typically ranging from 1.2 to 1.5 times the maximum motor rating.

### 3.6 Battery

Quadcopters use Lithium Polymer (LiPo) rechargeable batteries due to their high energy density and lightweight properties.

### 3.7 Motors

Brushless DC motors are commonly used in drone manufacturing. The motor's RPM can be controlled by adjusting the input current. The chosen motor, MOTOR KV1800, combined with the P1045 propeller, generates a maximum thrust of 1500 grams.

### 3.8 Power Distribution Board

The power distribution board is responsible for transferring power from the battery to the ESCs.

### 3.9 Flight Controller

The flight controller controls the drone's operations and includes auto altitude hold functionality. It processes signals from the

receiver using accelerometer and gyroscope sensors, and outputs the necessary commands to the ESCs. Additionally, it can measure altitude, attitude, and be used for autopilot functions with GPS support.

### 3.10 GPS

The GPS module enables navigation along preplanned waypoints and can be configured for return-to-home functionality. It communicates with the flight control board and navigational software to ensure precise path coverage.

### 3.11 Radio Transmitter and Receiver

The FlySky CT6B 2.4GHz 6CH transmitter and FS-R6B receiver are used, providing a range of approximately 1000 meters. This combination allows for up to 6 channels of control.

### 3.12 3DR Telemetry

Telemetry radios, such as the 3DR Telemetry, can establish a wireless MAVLink connection between a ground control station (e.g., mission planner) and the drone's flight control board. This connection enables real-time telemetry inspection, parameter tuning during flight, and on-the-fly mission changes.

### 3.13 Quadcopter Frame

The design of the quadcopter frame plays a crucial role in its overall design. A 650mm diagonal quadcopter frame made of carbon fiber material, specifically the 'X' configuration, is chosen for its stability and lightweight properties.

**Table 2. Weight of components used in development of Quadcopter**

Sr.no.	Component	Specification	Weight(gm)
1	Propeller	10x4.5	40
2	BL Motor	1800 kv	400
3	Battery	3S, 5200MAH	360
4	ESC	40A	136
5	Power Distribution Board		8
6	Flight Control Board	Pixhawk V2.4.8	40
7	GPS Module	M8N inbuilt Compass	33
8	3DR Telemetry Air Module	Range 2.5km, frequency 433 MHz	30
9	Remote Control Receiver	Receiver 6 Channels	20
10	R385 Pump with Air nozzle	DC 6-12V maximum flow rate of up to 1 3L/min	36
11	Motor Driver with SG90 Servo motor		30
12	Quadcopter Frame	650mm Carbon Fibre quadcopter Frame	620
13	Total Weight		1753

## 4. Methodology

The Quadcopter or 4 Armed Drone works on the same principle of Aviation as a Helicopter does. It has 4 equally spaced motors arranged and placed at four corners of the structure forming a (X) like shape. Multirotor like Quadcopters are unstable without Electronic Assistance. Therefore to Balance it in the midair, a Microcontroller board or a Flight Control Unit (FCU) is required. It Takes the inputs from the Receiver Elevator, Rudder, Aileron and Throttle and Instructs the Electronic Speed Control Units to drive the motors accordingly. The signals transmitted from the transmitter are received by the receiver inside the drone. The receiver sends the signals to the flight controller, which processes them using accelerometer. The signals can be transmitted from the Transmitter and received by the Receiver within the drone. From the receiver, the signal is sent to the Flight controller where it can be processed using accelerometer and gyroscope sensors. The processed signal is then sent to the ESC, which regulates the current supplied to the motor based on the received signal. The propellers are mechanically connected to the motors, causing them to rotate and generate thrust. The FPV camera is powered by the flight controller and records video footage, which is then processed by the transmitter and received on the ground. The pump draws power from the Li-Po battery and pressurizes the liquid from the storage tank. The pressurized liquid flows through the pipeline and exits through the nozzle, creating a spray. The pump's flow rate can be controlled by adjusting the input current, which is managed from the transmitter.



**Fig. 4.1 (a) Main Screen of the FCU KK 2.1.5 (b) Inside the PI Editor Menu and adjusting the Yaw Axis PI values for Stable Flight**

#### 4.1 CALCULATIONS

##### CALCULATIONS

After selecting components for constructing a drone, the mass can be approximated as 1 kg, which is equivalent to 1000 gm. Therefore, the weight of the drone can be calculated as follows(Pudke et al., 2021):

$$\text{Weight (W)} = \text{mass (m)} * \text{acceleration due to gravity (g)} = 2.753 * 9.81 = 27.00 \text{ N.}$$

##### A. Lift

To counteract the weight of 28.25 N and achieve takeoff, the lift force must exceed the weight. Since a quadcopter has 4 arms, this force can be divided into 4 parts. Hence, the lift required for each arm is:

$$L = 27 / 4 = 6.75 \text{ N.}$$

At this level of force, the UAV (Unmanned Aerial Vehicle) will hover. To accelerate the drone and increase its altitude, the lift force must be greater than 6.75 N. Therefore, we will consider a lift of 8 N for the structural analysis.

##### B. Motor calculations:

To achieve takeoff, the thrust generated must overcome the weight. When the thrust is equal to the weight, the UAV will hover and descend. The thrust required for takeoff is calculated as follows:

$$\text{Thrust} = 2 * \text{mass} = 2 * 2.753 = 5.50 \text{ kg or } 5500 \text{ g.}$$

The force required for takeoff will be twice the hover thrust and will allow for upward acceleration. Therefore, the motor should be selected to provide a minimum thrust of 5500 g.

##### Thrust Calculation

The thrust developed at 100% RPM can be three times greater than the total weight of the drone. This provides better maneuverability and enables the drone to climb to higher altitudes with a higher rate of climb.

Thrust produced by one propeller with one motor = 1500 grams.

Total thrust produced =  $4 \times 1500 = 6000$  grams.

Thrust-to-weight ratio = Thrust produced / total weight of the drone =  $6000 / 2753 = 2.18 : 1$ .

#### Conclusion

In this research, we have presented a design of a quadcopter incorporating a paint spraying mechanism for construction layout marking. This method reduces labor, time, cost, and risks associated with manual layout marking processes in the construction industry. The quadcopter can also be utilized for spraying disinfectant liquids over buildings, water bodies, and densely populated areas. If equipped with a camera, the quadcopter can perform additional management tasks such as security monitoring, site management, and visual inspections. The weight-lifting capacity of the quadcopter can be increased by adding more motors, increasing the propeller size, or raising the motor RPM. Enhanced weight-lifting capability would allow carrying more pesticide in the tank. Flight time can be extended by using higher-capacity batteries, although it should be considered that increased battery capacity also adds weight. In the current COVID-19 pandemic situation, the quadcopter can be employed for sanitizing large hotspot areas without the need for physical presence.

#### References

- [1]. S. Vempati, V. Choudhary, L. Behera, -Quadrotor: Design, Control and Vision Based Localization], Advances in Control and Optimization of Dynamical Systems (2014) 1104-1110.
- [2]. Anudeep M, G Diwakar, Ravi Katukam, (2014), -Design of A Quad Copter and Fabrication], International Journal of Innovations in Engineering and Technology Vol. 4 Issue 1 pp 59-65.
- [3]. Dr. Pran Kanai Saha , -Design and Development of Unmanned Aerial Vehicle ], Procedia Manufacturing 32 (2019) 564–571
- [4]. Omkar Tatale, Nitinkumar Anekar, Supriya Phatak, Suraj Sarkale (2018), -Quadcopter: Design, Construction and Testing], International Journal for Research in Engineering Application & Management Vol.04, Special Issue AMET-2018
- [5]. Parag Parihar, Priyanshu Bhawsar, Piyush Hargod, —Design & Development Analysis of Quadcopter], An international journal of advanced computer technology, 5 (6) , (2016), 2128-2133

# Design and Simulation of C2N based Solar Cell using SCAPS 1D

Vivek Bhojak, Lalit Kumar Lata, Praveen K Jain

**Abstract** Recently, a straightforward wet-chemical approach has been used to effectively synthesise the new nitrogenated holey two-dimensional material known as C2N. Scientists have given it a lot of consideration due to its benefits. To the best of our knowledge, however, only few recorded experiments used C2N as a photovoltaic material, and actual solar cells based on C2N have not been manufactured in a lab. In this study, we used Scaps-1D simulation to examine the effects of various factors on the C2N-based solar cell. We discovered that a large layer thickness of C2N, the ideal thickness of the window layer, and low ambient temperature were crucial to obtaining high-performance solar cells by adjusting the layer thickness and annealing the device at various temperatures. The efficiency of a C2N/SnO<sub>2</sub> based solar cell may reach above 17% with the right conditions. This research may provide insightful tips for future C2N-based solar cell design.

**Keywords-** C2N, two-dimensional material, thickness, efficiency, perovskites.

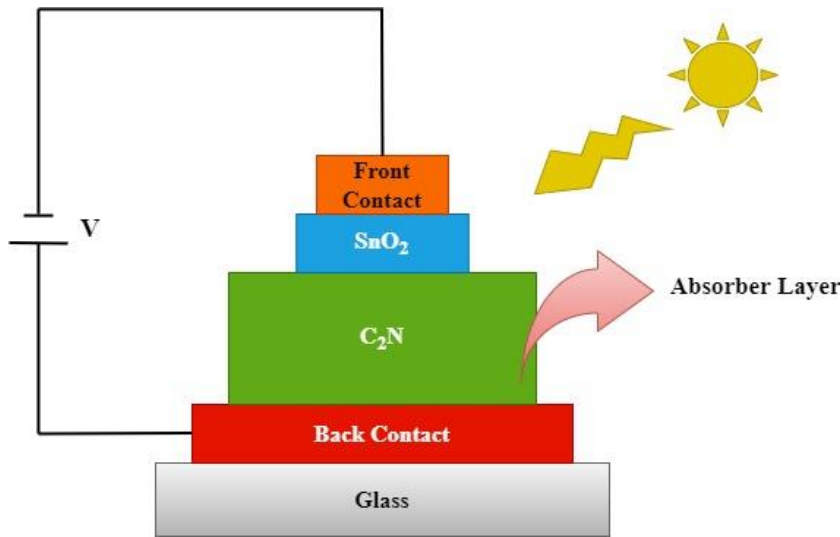
## 1. Introduction

In these days, because of the high demands for energy, continuous burning of fuel energy resources and their effect on the environment, the research on different environmental friendly sustainable energy resources have expanded. In all natural renewable energy resources, solar energy is very popular as an abundant and permanent source of energy [1,2]. In the last few years, the solar cells production created an enormous expansion in the field of materials fabrication [3]. Numbers of materials have been investigated, developed and implanted in solar cells as an absorber layer, such as perovskites [23-24], polymers and silicon [[4], [5], [6], [7], [8]]. And some of these materials gave high efficiencies, but have some disadvantages such as toxicity and instability, which limit their use in solar cell [[9], [10], [11]]. very recently, grapheme -like materials have attracted the attention as promising, economic, and environmental-friendly materials for photovoltaic applications. The nitrogenated holey two-dimensional (2D) material C2N is one of the recent discovered graphene-like structure [12]. It is a flat layered material with homogeneous holes and nitrogen atoms [13,14]. It exhibits a moderate energy band gap values in the range from 1.7 eV to 1.96 eV with a good structural stability [12]. Several theoretical calculations revealed that C2N might have extraordinary electronic and optical properties [[15], [16], [17]]. To best of our knowledge, the implantation of the C2N as a layer in the fabrication of the solar cells still not achieved yet, and most reports are confined on highlighting their basic physical properties. Simulation of solar cells is a necessary step toward fabricating solar cells in the laboratories. Utilizing the appropriate buffer layer in the solar cell is very important for the solar cell performance. The bands alignment between the buffer layer and the absorber layer is crucial in determining the performance trend in the solar cell. Minemoto et al. has reported that the coupling mechanism between the buffer layer and the absorber layer, and the type of the energy band produced at the interface between the two layers is vital in understanding the device operation mechanism [18]. Recent numerical calculation by using CdS as an electrons transport layer in C2N based solar cell has predicted an efficiency of 17% [19].

## 2. Methods

### Solar Cell Design-

This solar cell consists of several layers. Each layer has its specific role. C2N layer works as an absorber layer and SnO<sub>2</sub> works as a window layer. The main function of absorber layer is to absorb the maximum amount of light. The main role of window layer to allow the light to penetrate the structure and enter into absorber layer. The front and back contacts are used for biasing purpose. FTO works as a front electrode while gold work as a back electrode. The schematic of proposed solar cell is shown in figure below-



### 3. Numerical Modelling-

SCAPS 1D is used for the numerical simulation of the proposed solar cell. SCAPS (Solar Cell Capacitance Simulator) is a computer software tool used for the simulation of various aspects of solar cells. It is specifically designed for modeling the electrical behavior and characteristics of different types of solar cells, such as silicon-based solar cells, thin-film solar cells, and emerging photovoltaic technologies.

SCAPS utilizes a one-dimensional (1D) numerical model to simulate the electrical behavior of solar cells. It takes into account various parameters such as material properties, device structure, and external conditions to predict the performance of solar cells.

The software can simulate a wide range of solar cell characteristics, including current-voltage (I-V) characteristics, capacitance-voltage (C-V) characteristics, and internal quantum efficiency. It can also provide insights into carrier transport, recombination processes, and the influence of various design and process parameters on the performance of solar cells.

### 4. Material Parameter-

The AM 1.5 light setting is used for all simulations. Table 1 details the input parameters that were employed in our numerical study.

**Table 1: Materials parameters employed in simulation [20-22]**

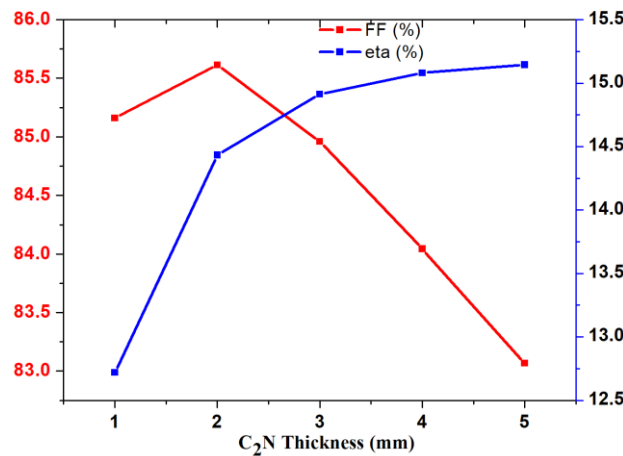
Parameters	C <sub>2</sub> N	SnO <sub>2</sub>
Thickness (μm)	Variable	Variable
Band-gap (Eg)	1.810	3.600
Electron Affinity (Ev)	4.420	4.500
Relative Dielectric Permittivity	4.500	9.000
Effective Density of States in VB((1/cm <sup>3</sup> )	1.000E+19	1.800E+19
Effective Density of States in CB (1/cm <sup>3</sup> )	1.000E+19	2.200E+18
Hole Thermal Velocity (cm/s)	1.000E+7	1.000E+7
Electron Thermal Velocity (cm/s)	1.000E+7	1.000E+7
Hole Mobility(cm <sup>2</sup> /Vs)	2.060E+1	2.500E+0
Electron Mobility (cm <sup>2</sup> /Vs)	1.300E+1	1.000E+0

Shallow Uniform Acceptor Density $N_A$ (1/cm <sup>3</sup> )	1.000E+18	0.000E+0
Shallow Uniform Donor Density $N_D$ (1/cm <sup>3</sup> )	0.000E+0	2.000E+19

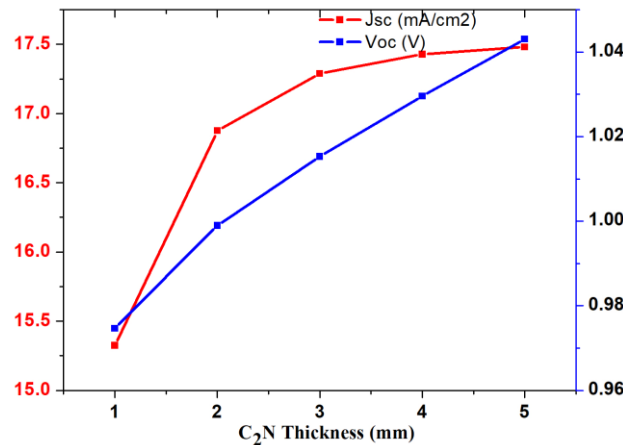
## 4. Results

### Effect of C2N absorber later thickness-

The efficiency of a solar cell is a measure of its ability to convert sunlight into electricity. The absorber layer plays a crucial role in absorbing photons from sunlight and generating electron-hole pairs. In general, thicker absorber layers can absorb more photons, resulting in a higher probability of generating electron-hole pairs and thus potentially increasing the overall efficiency of the solar cell. From figure 2 it is clear that when we increase the thickness of absorber layer efficiency increases and it is maximum when the thickness of absorber layer is maximum. The fill factor is a measure of how effectively a solar cell can convert absorbed light into electrical current. It is influenced by various factors, including the absorber layer thickness. A thicker absorber layer may lead to increased series resistance within the solar cell, which can lower the fill factor. Additionally, thicker absorber layers may also increase the recombination losses, which can further reduce the fill factor. The fill factor first increases and it is maximum when the thickness of absorber layer is 2 um and after this it starts decreasing. The fill factor is minimum when the thickness of absorber layer is 5 um.

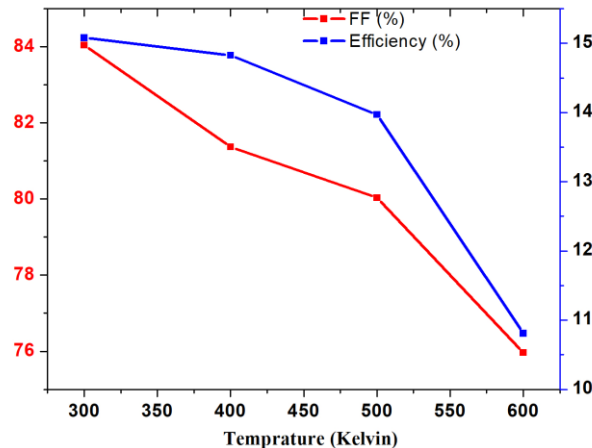


The open circuit voltage ( $V_{oc}$ ) of a solar cell is the maximum voltage it can produce when there is no external load connected. The absorber layer thickness can affect the open circuit voltage by influencing the carrier collection efficiency and recombination losses. Thicker absorber layers can enhance carrier collection, resulting in a higher open circuit voltage. However, excessively thick absorber layers can also lead to increased recombination losses, reducing the open circuit voltage. Therefore, there is an optimal absorber layer thickness that balances carrier collection and recombination losses to achieve the highest open circuit voltage. It is clear from figure 3 that open circuit voltage increases almost linearly when we increase the thickness of absorber layer. The short circuit current density ( $J_{sc}$ ) of a solar cell represents the maximum current that can be generated when the terminals are shorted. The absorber layer thickness affects the  $J_{sc}$  by influencing light absorption, carrier collection, and recombination losses. Thicker absorber layers can absorb more photons, resulting in a higher  $J_{sc}$ . However, excessively thick absorber layers may increase carrier recombination, reducing the  $J_{sc}$ . As with the other parameters, there is an optimal absorber layer thickness that maximizes the short circuit current density. The short circuit current density of proposed solar cell increases when we increase absorber layer thickness and it tends to saturate after 3 um thickness.

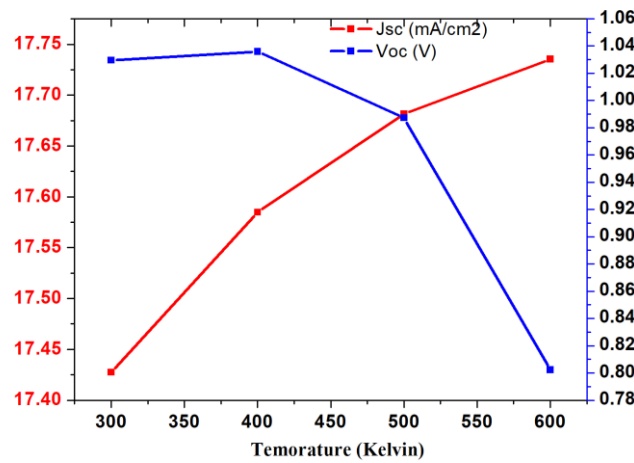


## Effect of Temperature-

The efficiency of a solar cell is inversely affected by temperature. As the temperature increases, the efficiency of the solar cells tends to decrease. This decrease is primarily due to the increase in thermalization losses, which refers to the loss of energy as heat instead of being converted into electricity. The increase in temperature can also lead to an increase in non-radiative recombination, further reducing the efficiency of the solar cell. The fill factor of a solar cell is also influenced by temperature. Higher temperatures generally lead to a decrease in the fill factor. This decrease can be attributed to several factors, including an increase in series resistance, an increase in recombination losses, and changes in the mobility and lifetime of charge carriers. These factors can limit the flow of current and reduce the fill factor. The variation of Fill factor and efficiency with respect to temperature is shown in figure 4 below.

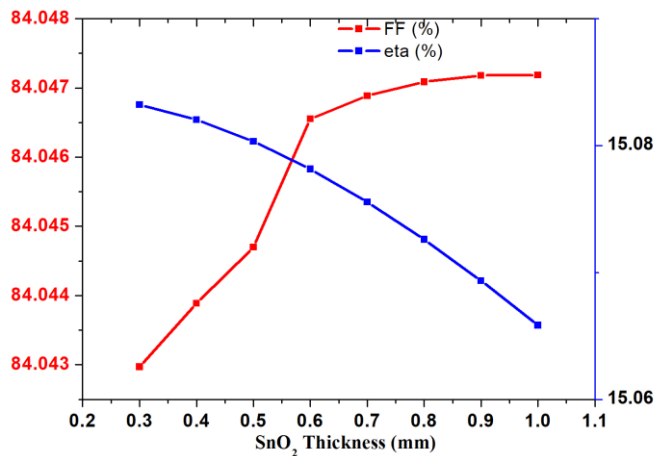


The open circuit voltage ( $V_{oc}$ ) of a solar cell decreases with increasing temperature. This decrease occurs primarily due to the increase in the intrinsic carrier concentration of the semiconductor material with temperature. As temperature rises, the increased thermal energy excites more electrons, leading to a higher population of charge carriers and reducing the open circuit voltage. The short circuit current density ( $J_{sc}$ ) of a solar cell tends to increase with temperature, up to a certain point. This increase is primarily due to the increase in the number of available charge carriers at higher temperatures. However, beyond a certain temperature threshold, the  $J_{sc}$  may start to decrease due to the increased recombination rate and reduced carrier lifetime. The variation of Fill  $V_{oc}$  and  $J_{sc}$  with respect to temperature is shown in figure 5 below.

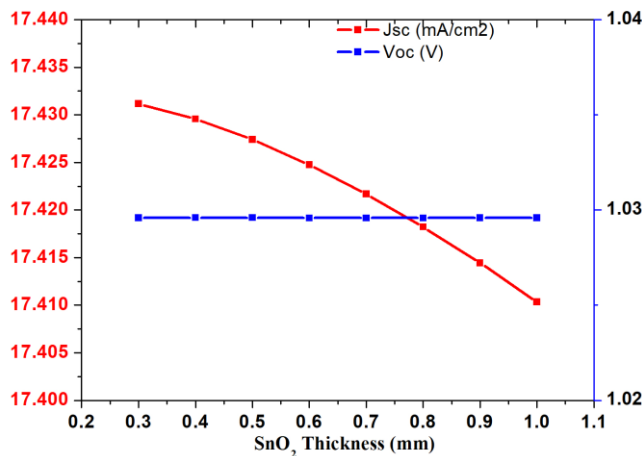


## Effect of thickness of SnO<sub>2</sub> Layer-

The efficiency of a solar cell can be influenced by the SnO<sub>2</sub> window layer thickness. The window layer serves to enhance the extraction of photo-generated carriers from the absorber layer and reduce surface recombination losses. Generally, a thin SnO<sub>2</sub> window layer is preferred to minimize optical losses and ensure efficient carrier extraction. However, if the SnO<sub>2</sub> layer is too thin, it may lead to increased electrical resistance, which can impede charge transport and reduce the overall efficiency of the solar cell. Therefore, there is an optimal thickness for the SnO<sub>2</sub> window layer that balances optical transmission and electrical conductivity to maximize efficiency. As shown in figure 6 efficiency is lesser for thicker window layer. The fill factor of a solar cell can also be affected by the SnO<sub>2</sub> window layer thickness. A thicker SnO<sub>2</sub> layer may lead to increased series resistance, which can hinder charge transport and reduce the fill factor. On the other hand, an excessively thin SnO<sub>2</sub> layer may result in increased surface recombination, leading to lower charge carrier collection efficiency and decreased fill factor. Hence, an optimal thickness for the SnO<sub>2</sub> window layer is desirable to minimize series resistance and surface recombination losses, thereby maximizing the fill factor. The variation of fill factor with respect to variation in thickness of SnO<sub>2</sub> layer is shown in figure 6 below.



The open circuit voltage ( $V_{oc}$ ) of a solar cell can be impacted by the  $\text{SnO}_2$  window layer thickness. It is clear from figure that the open circuit voltage is not impacted by variation in  $\text{SnO}_2$  layer thickness. There are very small variations in open circuit voltage with respect to  $\text{SnO}_2$  layer thickness as shown in figure 7. The short circuit current density ( $J_{sc}$ ) of a solar cell can also be influenced by the  $\text{SnO}_2$  window layer thickness. A thinner  $\text{SnO}_2$  layer allows for improved light transmission to the absorber layer, potentially leading to higher  $J_{sc}$  values. However, an excessively thin  $\text{SnO}_2$  layer may result in increased resistive losses and reduced charge carrier collection, thereby limiting the short circuit current density. Therefore, an optimal  $\text{SnO}_2$  window layer thickness is crucial to ensure sufficient light absorption and efficient charge carrier collection, maximizing the short circuit current density. The short circuit current density decreases when we increase the thickness of  $\text{SnO}_2$  layer. The variation of short circuit current density with respect to  $\text{SnO}_2$  layer thickness is shown in figure below.



## Acknowledgments

The author would like to extend her deepest gratitude and gratefulness to teachers for providing with the right ways of thinking and concepts of this research. The author wishes deeply thankful to her beloved parents and hubby who fulfill whatever she needs and gives her never-ending love and encouragement which have been helpful in my research to attain the destination without any trouble.

## References

- [1] M. Hosenzaman et al: Global prospects, progress, policies, and environmental impact of solar photovoltaic power generation., *Renew. Sustain. Energy Rev.* (2015).
- [2] A review on solar energy use in industries *Renew. Sustain. Energy Rev.* (2011)
- [3] B. Parida *et al.* A review of solar photovoltaic technologies *Renew. Sustain. Energy Rev.* (2011)
- [4] A. Blakers *et al.* High efficiency silicon solar cells *Energy Procedia* (2013).
- [5] S. Yasin *et al.* Design and simulation of high efficiency lead-free heterostructure perovskite solar cell using SCAPS-1D Optik - International Journal for Light and Electron Optics (2021)
- [6] T. Minemoto *et al.* Theoretical analysis on effect of band offsets in perovskite solar cells *Sol. Energy Mater. Sol. Cell.* (2015)
- [7] M. Burgelman *et al.* Modelling polycrystalline semiconductor solar cells *Thin Solid Films* (2000)
- [8] A.D. Adewoyin *et al.* Development of CZTGS/CZTS tandem thin film solar cell using SCAPS-1D Optik - International Journal for Light and Electron Optics (2019)
- [9] J. Madan *et al.* Device simulation of 17.3% efficient lead-free all-perovskite tandem solar cell *Sol. Energy* (2020)
- [10] T. Ouslimane *et al.* Impact of absorber layer thickness, defect density, and operating temperature on the performance of MAPbI<sub>3</sub> solar cells based on ZnO electron transporting material *Heliyon* (2021)
- [11] W. Eisele *et al.* XPS, TEM and NRA investigations of Zn(Se,OH)/Zn(OH)<sub>2</sub> films on Cu(In, Ga)(S, Se)2 substrates for highly efficient solar cells *Sol. Energy Mater. Sol. Cell.* (2003)
- [12] M. Taguchi *et al.* 24.7% record efficiency HIT solar cell on thin silicon wafer *IEEE J. Photovolt.* (2014)
- [13] G. Li *et al.* Polymer solar cells *Nat. Photonics* (2012)
- [14] R.P. Singh *et al.* Polymer solar cells: an overview *Macromol. Symp.* (2013)
- [15] Y. Jia *et al.* Effect of Sr substitution on the property and stability of CH<sub>3</sub>NH<sub>3</sub>SnI<sub>3</sub> perovskite: a first-principles investigation *Int. J. Energy Res.* (2020)
- [16] H.J. Du *et al.* Device simulation of lead-free CH<sub>3</sub>NH<sub>3</sub>SnI<sub>3</sub> perovskite solar cells with high efficiency *Chin. Phys. B* (2016)
- [17] A. Gusain *et al.* Polymer solar cells—interfacial processes related to performance issues *Front. Chem.* (2019)
- [18] J. Mahmood *et al.* Nitrogenated holey two-dimensional structures *Nat. Commun.* (2015)
- [19] Z. Chen *et al.* The contacts of the monolayer semiconductor C<sub>2</sub>N with 2D metal electrodes *Adv. Theory Simul.* (2019).
- [20] Shoewu O, Anuforonini G and Duduyemi O 2016 Simulation of the performance of CdTe/CdS/ZnO Multi-junction thin film solar cell *Review of Information Engg. Appl.* 3 1–10
- [21] Zhou, X., & Han, J. (2020). Design and simulation of C<sub>2</sub>N based solar cell by SCAPS-1D software. *Materials Research Express*, 7(12), 126303.
- [22] Green, M.A.: General temperature dependence of solar cell performance and implications for device modeling. *Prog. Photovolt. Res. Appl.* 11(5), 333-340 (2003)
- [23] Bhojak, V.; Bhatia, D.; Jain, P.K. Investigation of photocurrent efficiency of Cs<sub>2</sub>TiBr<sub>6</sub> double perovskite solar cell. *Mater. Today Proc.* 2022, 66, 3692–3697
- [24] Bhojak, V.; Bhatia, D.; Jain, P.K., Shashi Kant Dargar , Michał Jasinski, Radomir Gono and Zbigniew Leonowicz : Numerical Investigation of Power Conversion Efficiency of Sustainable Perovskite Solar Cells, *Electronics MDPI* 2023, 12, 1762. (2023)



**ANAND**  
INTERNATIONAL COLLEGE  
OF ENGINEERING



# Recent Developments in Engineering & Technology-II

---

Edited by Dr. Praveen Agarwal, Dr. Ruzana Pskhu & Dr. Bhavana Mathur.

**ISBN 978-81-953996-5-9**



**ANAND**  
INTERNATIONAL COLLEGE  
OF ENGINEERING

Near Kanota, Agra Road, Jaipur-303012, Rajasthan, India  
Tel.: 9928755552, 53 | [www.anandice.ac.in](http://www.anandice.ac.in)